International Journal of Photoenergy

Hybrid Solar Technology for Power Polygeneration and Energy Saving

Guest Editors: T. T. Chow, G. N. Tiwari, and Christophe Menezo

Hybrid Solar Technology for Power Polygeneration and Energy Saving

International Journal of Photoenergy

Hybrid Solar Technology for Power Polygeneration and Energy Saving

Guest Editors: T. T. Chow, G. N. Tiwari, and Christophe Menezo

Editorial Board

Contents

Hindawi Publishing Corporation
International Journal of Photoenergy
Volume 2012, Article ID 957425, 2 pages
doi:10.1155/2012/957425

Editorial

Hybrid Solar Technology for Power Polygeneration and Energy Saving

T. T. Chow,[1] G. N. Tiwari,[2] and Christophe Menezo[3]

[1] *Building Energy and Environmental Technology Research Unit, Division of Building Science and Technology, City University of Hong Kong, Tat Chee Avenue, Hong Kong*
[2] *Centre for Energy Studies, Indian Institute of Technology Delhi, Hauz Khas, New Delhi 110 016, India*
[3] *CETHIL UMR 5008, Domaine Scientifique de La Doua, 9 rue de la Physique, INSA de Lyon, 69621 Villeurbanne Cedex, France*

Correspondence should be addressed to T. T. Chow, bsttchow@cityu.edu.hk

Received 4 December 2012; Accepted 4 December 2012

Global climate change and fuel supply security have led to the fast development in renewable energy applications. In the building sector, the limited space available for solar panels has driven a demand on the use of hybrid solar technology for polygeneration of active power and/or passive solar devices. The importance is growing with the worldwide trend of constructing low-energy and zero-carbon buildings. This special issue is for the collection of contemporary research and review papers in addressing the state-of-the-art.

The progression on flat-plate collector technology so far has dominated the combined photovoltaic/thermal (PVT) research. While the forced airflow type is a simple low-cost design, the water flow type receives more attention because of the better heat transfer capability and the flexibility in applications. The effectiveness of different absorber designs for forced or natural flow, free-stand or building integration has been widely investigated. The two papers presented by J.-H. Kim and J.-T. Kim discussed and compared the energy performance of the glazed and unglazed water-flow thermosyphon PVT collector systems, and further for the unglazed option, the performances of the sheet-and-tube and the rectangular-box-channel thermal absorber designs were compared. The performance of the building-integrated water flow option (BiPVT/w) was discussed in T. Matuska's paper, where two types of fin configurations were compared with the corresponding BiPV installation using polycrystalline silicon cells. In his study, two different European climates, namely, Athens and Prague, and both roof and façade applications were evaluated. The paper of T.-T. Chow and J. Ji introduced the life cycle assessment of a rectangular-box-channel PVT/w collector system in terms of economic, energy, and greenhouse-gas payback time; both free-stand and building-integrated performances were addressed, confirming the merits of the hybrid solar design over the plaint PV option.

For the production of hot water at high temperature, either heat pump integration or concentrator PVT (c-PVT) design can be adopted. Y. Bai et al. presented a case study of using PVT/w collectors as the water preheating device of a solar assisted heat pump system. The energy and economic performances of the same system in cities of different climates, including Hong Kong and three other cities in France, were compared. The paper of X. Ji et al. presented the development of simulation model of an experimental trough c-PVT system; the quality of the numerical work was demonstrated by experimental validation. With this, they found that the trough c-PVT system performance can be optimized by improving the mirror reflectivity and the thermal solar radiation absorptivity of the lighting plate, and by pursuing a suitable focal line with uniform light intensity distribution. The L. Zhang et al. paper gave a general review of c-PVT technology and then proposed a PV system with integrated compound parabolic collector plate that adopts a low precision solar tracking method; the performance was shown better than the fixed installation or the case with periodic adjustment in months.

While silicon-based PV technology has many physical barriers, it is expected that the future PVT developments will be closely linked to the breakthroughs in solar cell technology. The next-generation solar cells such as polymer,

nanocrystalline, and dye-sensitized solar cells will be less expensive, flexible, compact, lightweight, and efficient. The paper of L.-T. Yan et al. addressed the use of hybrid ZnO/TiO_2 photoanodes for utilizing the high electron transport rate of ZnO and the high electron injection efficiency as well as the stability of TiO_2 materials. Developments in the balance of system are also important. The paper of C.-L. Shen and J.-C. Su covered the improvements in power quality and power factor in PV inverter design. On the other hand, the improvements in power supply stability with power conditioner and better integration of renewable energy sources onto utility grid have been other key research areas, as discussed in the paper of D. Amorndechaphon et al. Finally, the review paper given by us included a broad overview of the published works. It comes to us, despite the sharp increase in academic activities in the last decade, that the developments of commercial PVT products and their real system applications are still very limited. More efforts must be on the identification of robust product designs, suitable product materials, manufacturing techniques, testing and training requirements, operation and maintenance needs, potential customers, market strength, and so on.

T. T. Chow
G. N. Tiwari
Christophe Menezo

Hindawi Publishing Corporation
International Journal of Photoenergy
Volume 2012, Article ID 307287, 17 pages
doi:10.1155/2012/307287

Review Article

Hybrid Solar: A Review on Photovoltaic and Thermal Power Integration

T. T. Chow,[1] G. N. Tiwari,[2] and C. Menezo[3]

[1] *Building Energy and Environmental Technology Research Unit, Division of Building Science and Technology, City University of Hong Kong, Tat Chee Avenue, Hong Kong*
[2] *Centre for Energy Studies, Indian Institute of Technology Delhi, Hauz Khas, New Delhi 11 00 16, India*
[3] *CETHIL UMR 5008, Domaine Scientifique de La Doua, INSA de Lyon, 9 Rue de la Physique, 69621 Villeurbanne Cedex, France*

Correspondence should be addressed to T. T. Chow, bsttchow@cityu.edu.hk

Received 23 August 2012; Accepted 9 November 2012

Academic Editor: Mark van Der Auweraer

The market of solar thermal and photovoltaic electricity generation is growing rapidly. New ideas on hybrid solar technology evolve for a wide range of applications, such as in buildings, processing plants, and agriculture. In the building sector in particular, the limited building space for the accommodation of solar devices has driven a demand on the use of hybrid solar technology for the multigeneration of active power and/or passive solar devices. The importance is escalating with the worldwide trend on the development of low-carbon/zero-energy buildings. Hybrid photovoltaic/thermal (PVT) collector systems had been studied theoretically, numerically, and experimentally in depth in the past decades. Together with alternative means, a range of innovative products and systems has been put forward. The final success of the integrative technologies relies on the coexistence of robust product design/construction and reliable system operation/maintenance in the long run to satisfy the user needs. This paper gives a broad review on the published academic works, with an emphasis placed on the research and development activities in the last decade.

1. Introduction

In the past 3-4 decades, the market of solar thermal and photovoltaic (PV) electricity generation has been growing rapidly. So were the technological developments in hybrid solar photovoltaic/thermal (PVT) collectors and the associated systems. Generally speaking, a PVT system integrates photovoltaic and solar thermal systems for the co-generation of electrical and thermal power from solar energy. A range of methods are available such as the choices of monocrystalline/polycrystalline/amorphous silicon (c-Si/pc-Si/a-Si) or thin-film solar cells, air/liquid/evaporative collectors, flat-plate/concentrator types, glazed/unglazed designs, natural/forced fluid flow, and stand-alone/building-integrated features. Accordingly, the systems are ranging from PVT air and/or water heating system to hot-water supply through PV-integrated heat pump/pipe or combined heating and cooling and to actively cooled PV concentrator through the use of lens/reflectors. Engineering considerations can be on the selection of heat removal fluid, the collector type, the balance of system, the thermal to electrical yield ratio, the solar fraction, and so on. These all have determining effects on the system operating mode, working temperature, and energy performance.

Theoretical and experimental studies of PVT were documented as early as in mid 1970s [1–3]. Despite the fact that the technical validity was early concluded, only in recent years that it has gained wide attention. The amount of publications grows rapidly. The following gives an overview of the development of the technology, placing emphasis on the research and development activities in the last decade. Readers may refer to Chow [4] for a better understanding of the early developments.

2. PVT Developments in the Twentieth Century

2.1. Early Works on Collector Design. The early research works were mainly on flat-plate collectors [5, 6]. Garg and

his coworkers carried out mathematical and experimental studies on PVT systems [7–9]. Sopian et al. developed steady-state models, for comparing the performance of single- and doublepass PVT/a collectors [10, 11]. Through transient analysis, Prakash [12] pointed out that the air collector (PVT/a) design is lower in thermal efficiency than the water collector (PVT/w), because of the inferior heat transfer between the thermal absorber and the airflow stream. Bergene and Løvvik [13] derived a detailed physical model of a flat-plate PVT/w collector, through which the total efficiency was evaluated.

de Vries [14] investigated the performance of several PVT collector designs. The single-glazed design was found better than the unglazed (of which the thermal efficiency is unfavorable) or the double-glazed design (of which the electrical efficiency is unfavorable). Nevertheless, exergy analysis performed by Fujisawa and Tani [15] indicated that the exergy output density of the unglazed design is slightly higher than the single-glazed option, taking the fact that the thermal energy contains more unavailable energy. For low temperature water heating applications like for swimming pool-water heating, the unglazed PVT/w system is recommended. In cold winter days, antifreeze liquid can be used but then the summer performance will be affected [16].

Rockendorf et al. [17] compared the performance of a thermoelectric collector (first generating heat and subsequently electricity) and a PVT/w collector (in sheet-and-tube design); the electrical output of the PVT/w collector was found significantly higher than the thermoelectric collector.

In the above mathematical and experimental studies, the reported thermal efficiency of practical PVT/liquid systems is generally in the range of 45 to 70% for unglazed to glazed collector designs. For flat-plate PVT/a systems, the optimal thermal efficiency can be up to 55%.

2.2. Developments towards Complex Systems. In the 1990s, the initiative of PVT research was apparently a response to the global environmental deterioration and the growing interest in building-integrated photovoltaic (BiPV) designs. Comparing with the separated PV systems, the building integration of PV modules improves the overall performance and durability of the building facade. Nevertheless, building integration may bring the cell temperatures up to 20°C above the normal working temperature [18]. Other than the benefits of cooling, PVT collectors provide aesthetical uniformity than the side-by-side arrays of PV and solar thermal collectors. Alternative cooling schemes of the BiPV systems were examined [19–21]. Hollick [22] assessed the improvement in the system energy efficiency when solar cells were added onto the solar thermal metallic cladding panels on vertical facades.

Continued successfulness on concentrator-type (c-PVT) systems began to take shape. Akbarzadeh and Wadowski [23] studied a heat-pipe-based coolant design which is a linear, trough-like system. Luque et al. [24] successfully developed a concentrating array using reflecting optics and one-axis tracking. By that time, facing the conflicting roles of water heating and PV cooling, the design temperature of water that leaves a PVT/w collector is not high. Combining PVT and solar-assisted heat pump (SAHP) technology was then seen as a good alternative. Ito et al. [25] constructed a PVT-SAHP system with pc-Si aluminum roll-bond solar panels.

Generally speaking, in the 20th century the PVT research works had been mostly focused on improving the cost-performance ratio as compared to the solar thermal and PV systems installed side by side. For real-building projects the PVT/a systems were more readily adopted in Europe and North America, though the higher efficiency of the PVT/w system has been confirmed by that time. Solar houses with PVT/w provision were once sold in Japan in late 1990s. Unfortunately such innovative housing was in lack of demand in the commercial market [26]. A summary of the PVT technology in the period, including the marketing potentials, was reported by the Swiss Federal Office [27] and the International Energy Agency (IEA) [28].

3. Recent Developments in Flat-Plate PVT

3.1. PVT Air Collector Systems

3.1.1. Collector Design and Performance. The PVT air collectors, either glazed or unglazed, provide simple and economical solution to PV cooling. The air can be heated to different temperature levels through forced or natural flow. Forced circulation is more effective than natural circulation owing to better thermal convective and conductive behavior, but the fan power consumption reduces the net electricity output. Their use is mostly to meet the demands on industrial hot air, indoor space heating, and/or agricultural dehydration.

Hegazy investigated the thermal, electrical, hydrodynamic, and overall performance of four types of flat-plate PVT/a collectors [29]. These included channel above PV as Mode 1, channel below PV as Mode 2, PV between single-pass channels as Mode 3, and finally the double-pass design as Mode 4. The numerical analysis showed that while Mode 1 has the lowest performance, the other three have comparable energy outputs. On the whole, Mode 3 requires the least fan power.

Tripanagnostopoulos et al. carried out outdoors tests on different PVT/a and PVT/w collector configurations in Patra, Greece [30]. It was suggested to place the collectors in parallel rows and keeping a distance between adjacent rows to avoid shading. Diffuse reflectors then were placed between the adjacent rows to enlarge the received radiation at collector surfaces. Their experimental tests at noon hour gave a range of thermal efficiency from 38% to 75% for PVT/a collectors and 55% to 80% for PVT/w designs, depending on whether the reflectors were in place. The research team [31] further studied numerically the effect of adding suspended metal sheet at the middle of the air channel and the finned arrangements at the opposite wall of the air channel. It was found that such low cost improvements are more relevant to small collector length and can be readily applied to BiPVT/a installations. They [32] also introduced a PVT/bi-fluid collector incorporated with improvements identified in their previous work.

Tiwari et al. explored the overall efficiency performance and optimal designs of an unglazed PVT/a collector [33]. Energy matrices were derived considering the embodied energy at different processing stages in India [34]. Raman and Tiwari [35] then studied the annual thermal and exergy efficiencies of their proposed PVT/a collector for five different climate zones. The exergy efficiency was found unfavorable under strong solar radiation. Also the double-pass design shows better performance than the single-pass option; this echoes the findings of Sopian et al. [10] and Hegazy [29]. Furthermore, the life cycle analysis showed that the energy payback time (EPBT) in India is about 2 years. Also evaluated were the effect of fill factor [36] and the integrated performance with an earth air heat exchanger system [37]. Further, Dubey et al. [38] compared different configurations of glass-to-glass and glass-to-tedlar PV modules in Delhi. Experiments found that the glass-to-glass module is able to achieve higher supply air temperature and electrical efficiency. Their study extended to derive the analytical expressions for multiple PVT/a collectors connected in series, including the testing procedures [39, 40].

Assoa et al. in France introduced a PVT/bi-fluid collector that integrates preheating and domestic hot-water production [41]. The design includes alternate positioning of the solar thermal collector section and the PV section. The higher fluid temperature output allows the flexibility such as coupling with solar cooling devices during summer and facilitates a direct domestic hot-water system without adding auxiliary heating device. Parametric studies showed that the thermal efficiency could reach 80% under favorable collector length and mass flow rate conditions.

Sukamongkol et al. [42] studied the dynamic performance of a condenser desiccant for air conditioning energy reduction with the use of double-pass PVT/a collector. The thermal energy generated by the system was able to produce warm dry air as high as 53°C and 23% relative humidity. Electricity of about 6% of the daily total solar radiation can be obtained. Moreover, together with the heat recovery from the condenser to regenerate the desiccant for dehumidification, around 18% of the air conditioning energy can be saved.

Ali et al. [43] investigated the characteristics of convective heat transfer and fluid flow inside a PVT/a channel with the provision of a single row of oblique plates array. These plates arrays were positioned obliquely to the flow direction with variable oblique angles and with separations that avoid the partial shading of solar cells. The study was initiated taking the fact that the entrance region of a heated fluid flow channel is characterized by differentiating thermal and hydrodynamics boundary layers; the convective heat-transfer coefficient is then substantially larger than that at downstream locations. Thus, using oblique (interrupted) plates in a duct, or a channel, to prevent fully developed flow formation has the advantage of obtaining enhanced heat-transfer characteristics.

Kumar and Rosen [44] investigated the effect of adding vertical fins to the lower air channel of a double-pass PVT/a collector. The extended fin area was found able to reduce the cell temperature significantly.

3.1.2. Building-Integrated Options (BiPVT/a). In conventional BiPV systems, an air gap is often provided at the rear of the PV arrays for the air cooling of modules by natural convection. The heat recovery from the air stream for a meaningful use constitutes a BiPVT/a system. From a holistic viewpoint, Bazilian and Prasad [45] summarized its potential applications. The multifunctional façade or roof was ideal for PVT integration that produces heat, light, and electricity simultaneously, in addition to the building shelter functionality.

(1) Works in Europe. In UK, the Brockstill Environment Centre in Leicester opened in 2001 was equipped with a roof-mounted PVT/a system [46]. To assess the performance of various operational and control modes, a combined simulation approach was adopted with the use of two popular thermal simulation tools: ESP-r and TRNSYS. Monitored actual energy use data of the building shows very positive results.

Mei et al. [47] studied the dynamic performance of a BiPVT/a collector system constructed in the 90s at the Mataro Library in Spain. Their TRNSYS model was validated against experimental data from a pc-Si PV facade. The heating and cooling loads for various European buildings with and without such a ventilated facade were then evaluated. The simulation results showed that more winter heating energy can be saved for the use of the preheated ventilation in a building located in Barcelona, but less is for Stuttgart in Germany and Loughborough in UK. The higher latitude locations therefore need a higher percentage of solar air collectors in the combined system. Further, Infield et al. [48] explored different approaches to estimate the thermal performance of BiPVT/a facades, including a design methodology based on an extension of the familiar heat loss and radiation gain factors.

The main difficulty in analyzing BiPVT/a performance lies in the prediction of its thermal behavior. When the temperature profile and the sun shading situation are known, the electrical performance can be readily determined. This is not the case for thermal computation. The estimation of the convective heat-transfer coefficients, for example, is far from direct. The actual processes may involve a mix of forced and natural convection, laminar and turbulent flow, and, simultaneously, the developing flow at the air entrance. The external wind load on the panels further complicates the situation. For a semitransparent facade, thermal energy enters and transmits through the air cavity both directly (for glazing transmission) and indirectly (through convection and radiation exchange). The heat transfer to the ventilating stream is probably most complex, particularly for buoyant flow.

Sandberg and Moshfegh derived analytical expressions for the coolant flow rate, velocity, and temperature rise along the length of the vertical channel behind the PV panels [49]. Their experimental results were well matching the theoretical predictions for constrained flow, but were less accurate for ducts with opened ends. For the latter, Mittelman et al. developed a generalized correlation for the average channel Nusselt number for the combined convective-radiative

cooling [50]. Their solution of the governing equations and boundary conditions was computed through CFD analysis. Gan also studied the effect of channel size on the PV performance through CFD analysis [51]. To reduce possible overheating or hot spot formation, the required minimum air gaps were determined. Experimental works on a PVT façade were undertaken by Zogou and Stapountzis [52] for better understanding of the flow and turbulence with natural and forced convection modes. Supported by CFD modeling, the results show that the selection of flow rate and the heat-transfer characteristics of the back sheet are critical.

(2) Works in North America. In Canada, Chen et al. [53, 54] introduced a BiPVT/a system to a near net-zero energy solar house in Eastman Quebec. The solar house, built in 2007, featured with ventilated concrete slabs (VCSs). A VCS is a type of forced-air thermoactive building systems in which the concrete slabs exchange thermal energy with the air passage through its internal hollow voids. The BiPVT system is designed to cover one continuous roof surface to enhance aesthetic appeal and water proofing. Outdoor air is drawn by a variable speed fan with supervisory control to achieve the desired supply temperature. On a sunny winter day, the typical air temperature rise was measured 30–35°C. The typical thermal efficiency was at least 20% based on the gross roof area. Analysis of the monitored data showed that the VCS was able to accumulate thermal energy during a series of clear sunny days without overheating the slab surface or the living space.

Athienitis et al. [55] presents a design concept with transpired collector. This was applied to a full-scale office building demonstration project in Montreal. The experimental prototype was constructed with UTC (open-loop unglazed transpired collector) of which 70% surface area was covered with black-frame PV modules specially designed to enhance solar energy absorption and heat recovery. The system was compared side by side with a UTC of the same area under outdoor sunny conditions with low wind. This project was considered a near optimal application in an urban location in view of the highly favorable system design. While the thermal efficiency of the UTC system was found higher than the BiPVT/a combined thermal plus electrical efficiency, the equivalent thermal efficiency of the BiPVT/a system (assuming that electricity can be converted to four times as much heat) can be 7–17% higher.

Pantic et al. [56] compared 3 different open-loop systems via mathematical models. These include Configuration 1: unglazed BiPVT roof, Configuration 2: unglazed BiPVT roof connected to a glazed solar air collector, and Configuration 3: glazed BiPVT. It was pointed out that air flow in the BiPVT cavity should be selected as a function of desired outlet temperatures and fan energy consumption. Cavity depths, air velocity in the air cavity, and wind speed were found having significant effect on the unglazed BiPVT system energy performance. Development of efficient fan control strategies has been suggested an important step. Configurations 2 and 3 may be utilized to significantly increase thermal efficiency and air outlet temperature. In contrast, Configuration 3 significantly reduces electricity production and may lead to excessive cell temperatures and is thus not recommended unless effective means for heat removal are in place. The unglazed BIPVT system linked to a short vertical solar air collector is suitable for a connection with a rock bed thermal storage.

(3) Works in Asia Pacific. For warm climate applications, the ventilated BiPV designs are found better than the PVT/a designs with heat recovery. Crawford et al. [57] compared the EPBT of a conventional c-Si BiPV system in Sydney with two BiPVT/a systems with c-Si and a-Si solar cells, respectively. They found that the EPBT of the above three installations are in the range of 12–16.5 years, 4–9 years, and 6–14 years, respectively. The two BiPVT/a options reduce the EPBT to nearly one-half.

Agrawal and Tiwari [58, 59] studied a BiPVT/a system on the rooftop of a building, under the cold climatic conditions of India. It is concluded that for a constant mass flow rate of air, the series connected collectors are more suitable for the building fitted with the BIPVT/a system as rooftop. For a constant velocity of air flow, the parallel combination is then the better choice. While the c-Si BiPVT/a systems have higher energy and exergy efficiencies, the a-Si BiPVT systems are the better options from the economic point of view.

Jie et al. [60] studied numerically the energy performance of a ventilated BiPV façade in Hong Kong. It was found that the free airflow gap affects little the electrical performance, but is able to reduce the heat transmission through the PV façade. Yang et al. [61] carried out a similar study based on the weather conditions of three cities in China: Hong Kong, Shanghai, and Beijing. It was found that on typical days the ratio of space cooling load reduction owing to the ventilated PV facade is 33–52%.

Chow et al. [62] investigated the BiPVT/a options of a hotel building in Macau, with the PVT facade associated with a 24-hour air-conditioned room. The effectiveness of PV cooling by means of natural airflow was investigated with two options: free openings at all sides of the air gap as Case 1 and in Case 2 the enclosed air gap that behaves as a solar chimney for air preheating. These were also compared with the conventional BiPV without ventilation. The ESP-r simulation results showed an insignificant difference in electricity output from the three options. This was caused by a reverse down flow at the air gap at night, owing to the cooling effect of a 24-hour air-conditioned room located behind the PVT facade. It was concluded that both the climate condition and system operating mode affect significantly the PV productivity.

In China, Ji et al. [63] studied theoretically and experimentally the performance of a photovoltaic-Trombe wall, which was constructed at an outdoor environmental chamber. This south-facing façade in Hefei was composed of a PV glazing (with pc-Si cells) at the outside and an insulation wall at the inside with top and bottom vent openings. This leaves a natural flow air channel in between for space heating purpose. The results confirmed its dual benefits—improving the room thermal condition (with 5–7°C air temperature rise in winter) and generating electricity (with cell efficiency at 10.4% on average).

(4) Works on Window Systems. In Sweden, a multifunction PVT hybrid solar window was proposed by Fieber et al. [64]. The solar window is composed of thermal absorbers on which PV cells are laminated. The absorbers are building integrated into the inside of a standard window, thus saving frames and glazing and also the construction cost. Reflectors are placed behind the absorbers for reducing the quantity of cells. Via computer simulation, the annual electrical output shows the important role of diffuse radiation, which accounts for about 40% of the total electricity generation. Compared to a flat PV module on vertical wall, this solar window produces about 35% more electrical energy per unit cell area.

Vertical collectors and windows are more energy efficient at high-latitude locations, considering the sun path. Davidsson et al. [65] studied the performance of the above hybrid solar window in Lund, Sweden (55.44°N). Also a full-scale system combining four of these solar windows was constructed in a single family home in Alvkarleo, Sweden (60.57°N). The solar window system was equipped with a PV-driven DC pump. The projected solar altitude is high in summer, and accordingly a large portion of the solar beam falls directly onto the absorber with a minor contribution from the reflector. This is the ideal operating mode of the solar window, with the reflector partly opened and the window delivers heat, electricity, and light altogether. Effects of different control strategies for the position of the rotatable reflector were also studied, so was the performance comparison with roof collector [66].

A ventilated PV glazing consists of a PV outer glazing and a clear inner glazing. The different combinations of vent openings allow different modes of ventilating flow, which can be buoyant/induced or mechanical/driven. The space heating mode belongs to the BiPVT/a category. Besides the popularly used opaque c-Si solar cells on glass, the see-through a-Si solar window can also be used. Chow et al. [67] analyzed its application in the office environment of Hong Kong. The surface transmissions were found dominated by the inner glass properties. The overall heat transfer however is affected by both the outer and inner glass properties. Experimental comparisons were made between the use of PV glazing and absorptive glazing [68]. The comparative study on single, double, and double-ventilated cases showed that the ventilated PV glazing is able to reduce the direct solar gain and glare effectively. The savings on air-conditioning electricity consumption are 26% for the single-glazing case and 82% for the ventilated double-glazing case. Further, via a validated ESP-r simulation model [69], the natural-ventilated PV technology was found reducing the air-conditioning power consumption by 28%, comparing with the conventional single absorptive glazing system. With daylight control, additional saving in artificial lighting can be enhanced [70].

3.2. PVT Liquid Collector Systems

3.2.1. PVT/w Collectors

(1) Collector Design and Applications. Zondag et al. compared the energy performance of different PVT/w collector design configurations [71, 72]. The efficiency curves of nine collector configurations were obtained through computer analysis. At zero reduced temperature, the thermal efficiencies of the unglazed and single-glazed sheet-and-tube collectors were found 52% and 58%, respectively, and that of the channel-above-PV design is 65%. Also compared were the annual yields when these collectors were assumed to serve a DHW system. The channel-below-PV (transparent) configuration was found having the highest overall efficiency. Nevertheless, the more economical single-glazed sheet-and-tube design was recommended for DHW production since its efficiency was found only 2% less. For low-temperature water heating, the unglazed PVT/w collector is recommended.

Sandnes and Rekstad developed a PVT/w collector with c-Si solar cells pasted on polymer thermal absorber [73]. Square-shape box-type absorber channels were filled with ceramic granulates. This improves heat transfer to flowing water. The opposite surface was in black color which allows it to serve as a solar thermal collector when turned up-side-down. The analysis showed that the presence of solar cells reduces the heat absorption by about 10% of the incident radiation, and the glazing (if exists) reduces the optical efficiency by around 5%. It was expected to serve well in low-temperature water-heating system.

Chow introduced an explicit dynamic model for analyzing transient performance of single-glazed sheet-and-tube collector [74]. Through the multinodal finite different scheme, the dynamic influences of intermittent solar irradiance and autocontrol device operation can be readily investigated. The appropriateness of the nodal scheme was evaluated through sensitivity tests. The study also reveals the importance of having good thermal contact between the water tubing and the thermal absorber, as well as between the absorber and the encapsulated solar cells.

Zakharchenko et al. also pointed out the importance of good thermal contact between solar cells and thermal absorber [75]. So the direct use of commercial PV module in PVT collectors is not recommended. They introduced a substrate material with 2 mm aluminum plate covered by 2 μm insulating film, of which the thermal conductivity was only 15% less than that of aluminum. They also pointed out that the solar cell area should be smaller than the size of the absorber and should be at the portion of the collector where the coolant enters. As an echo to this last point, Dubey and Tiwari [76] examined the performance of a self-sustained single-glazed PVT/w collector system with a partial coverage of PV module (packing factor = 0.25) in Delhi. The electricity generated from the PV module positioned at the water inlet end was used to drive a DC pump.

Kalogirou [77] developed a TRNSYS model of a pump-operated domestic PVT/w system complete with water tank, power storage and conversion, and temperature differential control. Further, Kalogirou and Tripanagnostopoulos [78] examined domestic PVT/w applications working with either thermosyphon or pump circulation modes. Their simulation study covered 12 cases with pc-Si and a-Si PV modules, and in three cities: Athens in Greece, Nicosia in Cyprus, and Madison in USA. The results showed that the economical advantage is more obvious for Nicosia and Athens where the

availability of solar radiation is higher. Similar conclusions can be reached when comparing comparable applications at an industrial scale [79]. Also in Cyprus, Erdil et al. [80] carried out experimental measurements on an open-loop PVT/w domestic water-preheating system. Water flowed by gravity into a channel-above-PV type collector. The CPBT was estimated around 1.7 years.

Vokas et al. [81] performed a theoretical analysis of PVT/w application in domestic heating and cooling systems in three cities that belong to different climate zones, namely, Athens, Heraklion, and Thessaloniki. The thermal efficiency was found around 9% lower than the conventional solar thermal collector. Hence the interpolation of the PV laminate only affects slightly the thermal efficiency. The difference between the mentioned two systems in the percentage of domestic heating and cooling load coverage is only around 7%.

The effect of reflectors on PVT/w collector equipped with c-Si solar cells was studied by Kostić et al. [82]. Both numerical computation and experimental measurements arrived at the same optimal angle positions of the bottom reflector. The results show the positive effect of reflectors made of aluminum sheet and, considering the additional cost of about 10% for the reflectors, there is an energy gain in the range of 20.5–35.7% in summer.

Saitoh et al. [83] carried out the experimental study of a single-glazed sheet-and-tube PVT collector using brine (propylene glycol) solution as the coolant. Field measurements at a low energy house in Hokkaido were also observed. With a solar fraction of 46.3%, the system electrical efficiency was 8-9% and thermal efficiency 25–28%. When compared with the conventional system, the payback periods were found 2.1 years for energy, 0.9 years for GHG emission, and 35.2 years for cash flow, respectively.

The use of optimized working fluid (like nanofluid) was proposed through a numerical study by Zhao et al. [84]. The system consists of a PV module using c-Si solar cell and a thermal unit based on the direct absorption collector (DAC) concept. First the working fluid of the thermal unit absorbs the solar infrared radiation. Then, the remaining visible light is transmitted and converted into electricity by the solar cell. The arrangement prevents the excessive heating of the solar cell. The system works for both nonconcentrated and concentrated solar radiation. The optical properties of the working fluid were optimized to maximize the transmittance and the absorptance of the thermal unit in the visible and infrared part of the spectrum, respectively.

Chow et al. compared the performance of glazed and unglazed sheet-and-tube thermosyphon PVT/w collector systems in Hong Kong through theoretical models as well as experimental tests [85]. The evaluation indicates that the glazed design is always suitable if either the thermal or the overall energy output is to be maximized, but the exergy analysis supports the use of unglazed design if the increase of PV cell efficiency, packing factor, ratio of water mass to collector area, and wind velocity are seen as the desirable factors. Similar experimental work was done by J. H. Kim and J. T. Kim in Korea [86]; the results show that the thermal efficiency of the glazed collector is 14% higher than the unglazed alternative, but the unglazed one had electrical efficiency 1.4% higher than the glazed design. Further for the unglazed option, they compared the performance of the conventional sheet-and-tube thermal absorber with the rectangular-box-channel design, which was made of aluminum. At zero reduced temperature, the thermal and electrical efficiencies were found 66% and 14%, respectively, whereas those of the box-channel configuration were 70% and 15%, respectively [87].

Dubey and Tiwari [88] analyzed the thermal energy, exergy, and electrical energy yield of PVT/w sheet-and-tube collectors in India. Based on a theoretical model, the number of collectors in use, their series/parallel connection patterns, and the weather conditions were examined. For enhancing economical/environmental benefits, the optimum hot-water withdrawal rate was evaluated [89]. Optimum PVT/w system configuration was also evaluated by Naewngerndee et al. [90] via CFD employing the finite element method.

Rosa-Clot et al. [91] suggested a PVT configuration with water flow in polycarbonate box above the PV panel. The water layer absorbs the infrared radiation leaving the visible part almost unaffected. Efficiencies were evaluated and in particular the effects of temperature and irradiance mismatching on PV outputs were discussed.

(2) Absorber Materials. In view of the limitations on the fin performance of a sheet-and-tube PVT/w collector [74], an aluminum-alloy box-channel PVT/w collector was developed through the collaborative efforts of the City University of Hong Kong and the University of Science and Technology of China. Several generations of the collector prototypes were produced and tested under the subtropical Hong Kong and temperate Hefei climatic conditions [92–95]. The thermosyphon system was found working well in both locations. Dynamic simulations showed that better convective heat transfer between the coolant and the channel wall can be achieved by reducing the channel depth and increasing the number of channels per unit width [95]. Sensitivity tests in Hefei showed that the daily cell efficiency reaches 10.2%, daily primary energy saving efficiency reaches 65% with a packing factor of 0.63 [96]. In Hong Kong, the CPBT was found to be 12 years which is comparable to the more bulky side-by-side arrangement and is much better than the 52 years for plain PV module operation [97].

Affolter et al. [98] pointed out that the typical solar performances of PVT/liquid collectors are similar to those of nonselective-type solar thermal absorbers. Observations showed that the stagnation temperature (i.e., the elevated panel temperature in the absence of water flow) of the absorber of a solar thermal collector with a state of-the art spectrally selective coating may reach 220°C. Since a PVT absorber generally has higher solar reflectance and higher infrared emission than a solar thermal absorber, the stagnation temperature may be lowered to 150°C. But this is still higher than 135°C; that is, the temperature that the common encapsulation materials like EVA (ethylene vinyl acetate) resin may withstand [99]. EVA oxidizes rapidly at above 135°C.

Charalambous et al. [100] carried out a mathematical analysis on the optimum copper absorber plate configuration having the least material content and thus cost, whilst maintaining high collector efficiency. Both header-and-riser arrangement and serpentine arrangement were studied. It was found that light weight collector design can be achieved using very thin fins and small tubes.

The possible use of copolymer absorber to replace the commonly used metallic sheet-and-tube absorber had been examined extensively [101, 102]. This replacement offers several advantages:

(i) the weight reduction leads to less material utilization and easier installation;

(ii) the manufacturing process is simplified since fewer components are involved;

(iii) the above leads to a reduction in production costs.

However, there are disadvantages such as low thermal conductivity, large thermal expansion, and limited service temperature. On the other hand, the copolymer in use has to be good in physical strength, UV light protected, and chemically stable.

Huang et al. studied a PVT/w collector system complete with DC circulating pump and storage tank [103]. The collector was fabricated by the attachment of commercial PV modules on a corrugated polycarbonate absorber plate with square-shaped box channels.

Cristofari et al. studied the performance of a PVT/w collector with polycarbonate absorber and pc-Si PV modules carrying top and bottom glass sheets [104]. Water in forced flow passed through parallel square channels at very low flow rate and so with negligible pumping power. The system design capacity was based on the hot-water demands for the inhabitants at Ajaccio in France. With the use of a mathematical model, the annual averaged efficiencies of 55.5% for thermal, 12.7% for PV, 68.2% for overall, and 88.8% for energy saving were obtained. The maximum stagnation temperature at the absorber was found 116.2°C, which is acceptable. They further developed a collector with copolymer material that reduces the weight by more than half in comparison with the conventional metallic one [105].

Fraisse et al. suggested that PVT/liquid system is very suitable for the low temperature operation of Direct Solar Floor (DSF) system [106]. An application example in the Macon area of France was evaluated with the use of a glazed collector system. With propylene glycol as the coolant, the TRNSYS simulation results gave the annual c-Si cell efficiency as 6.8%, that is, a 28% drop as compared to a conventional nonintegrated PV module. Without the front glazing, the cell efficiency was increased to 10% as a result of efficient cooling. It was also found that, in the case of a glazed collector with a conventional control system for DSF, the maximum temperature at the PV modules was above 100°C in summer. At this temperature level, the use of EVA in PV modules will be subject to strong risks of degradation. The use of either a-Si cells or unglazed collector was recommended.

(3) PVT Collector Design. Santbergen et al. [107] carried out a numerical study on a forced-flow PVT/w system. Single-glazed sheet-and-tube flat-plate PVT collectors were employed and designed for grid-connected PV system with c-Si PUM cells. Both the annual electrical and thermal efficiencies were found around 15% lower, when compared to separate conventional PV and conventional solar thermal collector systems. It was suggested that both the electrical and the thermal efficiency can be improved through the use of antireflective coatings. Alternatively, the thermal efficiency can be improved by the application of low-e coating, but at the expenses of the electrical efficiency.

Since long wavelength irradiance with photon energies below the bandgap energy is hardly absorbed at all, the solar absorptance of the solar cells is significantly lower than that of a black absorber (with absorptance = 0.95). Santbergen and van Zolingen [108] also suggested two methods to increase long wavelength absorption:

(i) to use semitransparent solar cells followed by a second absorber and

(ii) to increase the amount of long wavelength irradiance absorption in the back contact of the solar cell.

Computer analysis showed that these two methods are able to achieve an overall absorption of 0.87 and 0.85, respectively.

Dupeyrat et al. [109] developed a PV cell lamination with Fluorinated Ethylene Propylene (FEP) at the front. This results in an alternative encapsulation with a lower refractive index than glass pane and a lower UV absorbing layer than conventional EVA material. Experimental tests showed an increase of more than 2 mA/cm^2 in generated current density for the PVT module. Finally the developments led to a new covered PVT collector for domestic hot-water application [110]. The c-Si PV cells were directly laminated on an optimized aluminium heat exchanger. The thermal efficiency at zero-reduced temperature was measured 79% with a corresponding electrical efficiency of 8.8%, leading to a high overall efficiency of almost 88%. This PVT collector in the standard conditions is therefore reaching the highest efficiency level reported in the literature.

Employing a bifacial PV module having two active surfaces can to generate more electric power than the traditional one-surface module. The optical properties of water allow its absorption of light mainly in the infrared region. This is compatible with PV modules using shorter wavelengths in the solar spectra for its electricity conversion. The water absorption only slightly affects the working region of a-Si PV cell (decrease of water transparency at around 950 nm), but it strongly absorbs the light with wavelengths above 1100 nm (the "thermal part" of the solar spectrum). Therefore, a PVT/w collector system with Si bifacial solar PV module can be advantageous. In Mexico, Robles-Ocampo et al. [111] carried out experimental test on a PVT/w system with c-Si bifacial PV module in Queretaro. The transparent flat collector was fabricated with a 15 mm channel underneath a glass cover, which was found better than the plastic cover in terms of service life. Stainless steel mirror reflectors (to

prevent oxidation in the outdoor environment) were used for illuminating the rear face of the solar cells. Measurements found that the glass water-filled flat collector placed above the PV module reduces the front face efficiency by 10%. When considering the radiation flux incident directly onto the active elements of the hybrid system, the system is able to achieve an electrical efficiency around 16% and an equivalent thermal efficiency around 50%.

3.2.2. Building-Integrated Systems (BiPVT/w). The research works on BiPVT/w systems have been less popular than the BiPVT/a systems. Ji et al. carried out a numerical study of the annual performance of a BiPVT/w collector system for use in the residential buildings of Hong Kong [112]. Pump energy was neglected. Assuming perfect bonding of PV encapsulation and copper tubing onto the absorber, the annual thermal efficiencies on the west-facing facade were found 47.6% and 43.2% for film cells and c-Si cells, respectively, and the cell efficiencies were 4.3% and 10.3%. The reductions in space heat gain were estimated 53.0% and 59.2%, respectively.

Chow et al. studied a BiPVT/w system applicable to multistory apartment building in Hong Kong [113]. The TRNSYS system simulation program was used. They also constructed an experimental BiPVT/w system at a rooftop environmental chamber [114]. The energy efficiencies of thermosyphon and pump circulation modes were compared across the subtropical summer and winter periods. The results show the better energy performance of the thermosyphon operation, with thermal efficiency reaches 39% at zero-reduced temperature and the corresponding cell efficiency 8.6%. The space cooling load is reduced by 50% in peak summer. Ji et al. [115] further carried out an optimization study on this type of installation. The appropriate water flow rate, packing factor and connecting pipe diameter were determined.

Based on the above-measured data, Chow et al. also developed an explicit dynamic thermal model of the BiPVT/w collector system [116]. Its annual system performance in Hong Kong reconfirmed the better performance of the natural circulation mode. This is because of the elimination of the pumping power and hence better cost saving [117]. The CPBT was 13.8 years, which is comparable to the stand-alone box channel PVT/w collector system. This BiPVT/w application is able to shorten the CPBT to one-third of the plain BiPV application. The corresponding energy payback time (EPBT) and greenhouse-gas payback time (GPBT) were found 3.8 years and 4.0 years [118]; these are much more favorable than CPBT.

Anderson et al. analyzed the design of a roof-mounted BiPVT/w system [119]. Their BiPVT/w collector prototype was integrated to the standing seam or toughed sheet roof, on which passageways were added to the trough for liquid coolant flow. Their modified Hottel-Whillier model was validated experimentally. The results showed that the key design parameters, like fin efficiency, lamination requirements, and thermal conductivity between the PV module and the supporting structure, affect significantly the electrical and thermal efficiencies. They also suggested that a lower cost material like precoated steel can replace copper or aluminum for thermal absorption since this does not significantly reduce the efficiencies. Another suggestion was to integrate the system "into" (rather than "onto") the roof structure, as the rear air space in the attic can provide a high level of thermal insulation. The effect of nonuniform water flow distribution on electrical conversion performance of BiPVT/w collector of various size was studied by Ghani et al. [120]. The numerical work identified the important role of the array geometry.

Eicker and Dalibard [121] studied the provision of both electrical and cooling energy for buildings. The cooling energy can be used for the direct cooling of activated floors or ceilings. Experimental works with uncovered PVT collector prototypes were carried out to validate a simulation model, which then calculated the night radiative heat exchange with the sky. Large PVT frameless modules were then developed and implemented in a residential zero energy building and tested.

Matuska compared the performance of two types of fin configurations of BiPVT/w collector systems with the BiPV installation using pc-Si cells [122]. Two different European climates and for roof/façade applications were evaluated by computer simulation. Better energy production potential of the BiPVT/w collector systems was confirmed—the results show 15–25% increase in electricity production in warm climate (Athens) and 8–15% increase in moderate climate (Prague). The heat production by steady flow forced convection can be up to 10 times higher than the electricity production.

Corbin and Zhai [123] monitored a prototype full-scale BiPVT/w collector installed on the roof of a residential dwelling. Measured performance was used to develop a CFD model which was subsequently used in a parametric study to assess the collector performance under a variety of operating conditions. Water temperature observed during testing reaches 57.4°C at an ambient temperature of 35.3°C. The proposed BiPVT/w collector shows a potential for providing the increased electrical efficiency of up to 5.3% above a naturally ventilated BiPV roof.

3.3. PVT Refrigeration

3.3.1. Heat-Pump Integration (PVT/Heat Pump). Conventional air-to-air heat pumps cannot function efficiently in cold winter with extreme low outdoor air temperatures. Bakker et al. [124] introduced a space and tap-water heating system with the use of roof-sized PVT/w array combined with a ground coupled heat pump. The system performance, as applied to one-family Dutch dwelling, was evaluated through TRNSYS simulation. The results showed that the system is able to satisfy all heating demands, and at the same time, to meet nearly all of its electricity consumption, and to keep the long-term average ground temperature constant. The PVT system also requires less roof space and offers architectural uniformity while the required investment is comparable to those of the conventional provisions.

Bai et al. [125] presented a simulation study of using PVT/w collectors as water preheating devices of a solar-assisted heat pump (SAHP) system. The system was for application in sports center for swimming pool heating and also for bathroom services. The energy performances of the same system under different climatic conditions, that included Hong Kong and three other cities in France, were analyzed and compared. Economic implications were also determined. The results show that although the system performance in Hong Kong is better than the cities in France, the cost payback period is the longest in Hong Kong since there was no government tax reduction.

Extensive research on PVT/heat pump system with variable pump speed has been conducted in China. Experimental investigations were performed on unglazed PVT evaporator system prototype [126, 127]. Mathematical models based on the distributed parameters approach were developed and validated [128, 129]. The simulation results show that its performance can be better than the conventional SAHP system. With R-134a as the refrigerant, the PV-SAHP system is able to achieve an annual average COP of 5.93 and PV efficiency 12.1% [130].

In the warm seasons, glazed PVT collector may not serve well as PVT evaporator. In cold winter however, the outdoor temperature can be much lower than the evaporating temperature of the refrigeration cycle. Then the heat loss at the PV evaporator is no longer negligible. The front cover would be able to improve both the photothermic efficiency and the system COP. Pei et al. concluded that for winter operation, the overall PVT exergy efficiency as well as the COP can be improved in the presence of the glass cover [131]. This is beneficial since the space heating demand is higher in winter.

3.3.2. PVT-Integrated Heat Pipe. These works were basically done in China. Based on the concept of integrating heat pipes and a PVT flat-plate collector into a single unit, Pei et al. [132, 133] designed and constructed an experimental rig of heat-pipe PVT (HP-PVT) collector system. The HP-PVT collector can be used in cold regions without freezing, and corrosion can be reduced as well. The evaporator section of the heat pipes is connected to the back of the aluminum absorber plate, and the condenser section is inserted into a water box above the absorber plate. The PV cells are laminated onto the surface of the aluminum plate. Detailed simulation models were developed and validated by the experimental findings. Through these, parametric analyses as well as annual system performance for use in three typical climatic areas in China were predicted. The results show that for the HP-PVT system without auxiliary heating equipment, in Hong Kong there are 172 days a year that the hot water can be heated to more than 45°C using solar energy. In Lhasa and Beijing, the results are 178 days and 158 days for the same system operation.

In order to solve the nonuniform cooling of solar PV cells and control the operating temperature of solar PV cells conveniently, Wu et al. [134] developed a heat-pipe PVT hybrid system by selecting a wick heat pipe to absorb isothermally the excessive heat from solar cells. The PV modules were in a rectangular arrangement, and below which the wick heat-pipe evaporator section is closely attached. The thermal-electric conversion performance was theoretically investigated.

3.3.3. PVT Trigeneration. Calise et al. [135] studied the possible integration of medium-temperature and high-temperature PVT collectors with solar heating and cooling technology, and hence a polygeneration system that produces electricity, space heating and cooling, and domestic hot water. A case study was performed with PVT collectors, single-stage absorption chiller, storage tanks, and auxiliary heaters as the main system components. The system performance was analyzed from both energetic and economic points of view. The economic results show that the system under investigation in Italy can be profitable, provided that an appropriate funding policy is available.

4. Recent Developments in Concentrator-Type Design

The use of concentrator-type PVT (or c-PVT) collector can to increase the intensity of solar radiation on the PV cells than the flat-plate collector. The c-PVT collectors are generally classified into three groups: single cells, linear geometry, and densely packed modules. Higher efficiency solar cells that handle higher current can be used, although they are more expensive than the flat-plate module cells. The complex sun tracking driving mechanism also incurs additional costs [136]. But the benefit is that a considerable portion of the cell surfaces can be replaced by low-cost reflector surfaces. Connecting the solar cells in series can to increase the output voltage and decrease the current at a given power output. This reduces the ohmic losses. During operation, nonuniform temperature can exist across the cells. The cell at the highest temperature will limit the efficiency of the whole string [137]. Hence the c-PVT coolant circuit should be designed to keep the cell temperature uniform and relatively low. A precise shape of the reflector surface and an accurate alignment is also essential, particularly when the concentration ratio is high. A precise tracking system is also important.

Refractive lenses and reflector surfaces are commonly in use in c-PVT. Comparatively, lens is lower in weight and material costs. For systems designed for higher concentration, more concentrator material per unit cell/absorber area is in need. Then the use of lenses is more appropriate. However, concentrator systems that utilize lenses are unable to focus scattered light. This limits their usage to places with mostly clear weather. On the other hand, using liquid as the coolant is more effective than using air to obtain better electrical output. These make reflector-type c-PVT systems good for medium- to high-temperature hot-water systems that are required for cooling, desalination, or other industrial processes. At lower operating temperatures, a flat-plate collector may have higher efficiency than the c-PVT collector when both are directly facing the sun. But at

higher temperature differential, the large exposed surface of a flat-plate collector leads to more thermal loss. So the performance gap between the two will diminish when the working temperature gradually increases.

Rosell et al. in Spain constructed a low-concentrating PVT prototype with the combination of flat-plate channel-below-PV (opaque) collector and linear Fresnel concentrator that worked on two-axis tracking system [138]. The total efficiency was found above 60% when the concentration ratio was above 6x. Their theoretical analysis reconfirms the importance of the cell-absorber thermal conduction.

Experimental trough c-PVT systems with energy flux ratio in the range of 10–20 were developed and tested in China by Li et al. [139]. Performances of arrays with the use of different solar cells types were compared. Ji et al. [140] also developed steady models of the system and validated them by the measured data. They found that the system performance can be optimized by improving the mirror reflectivity and the thermal solar radiation absorptivity of the lighting plate and by pursuing a suitable focal line with uniform light intensity distribution. Also as a China-UK joint research effort, a CPC-based PVT system with a U-pipe was investigated [141]. CPC stands for compound parabolic concentrator. The U-pipe avoids the temperature gradient on the whole absorber and on every block cell and simultaneously produces electricity using the same temperatures. More recently, Zhang et al. [142] proposed a PV system with integrated CPC plate that adopts a low precision solar tracking method; the performance can be better than the fixed installation or the case with periodic adjustment only in several months.

Coventry developed a combined heat and power solar (CHAPS) collector system in Australia [143]. This was a linear trough system designed for single tracking. The c-Si solar cells (at 20% standard conversion efficiency) in row were bonded to an aluminum receiver and were cooled by water with antifreeze and anticorrosive additives flowing in an internally finned aluminum pipe. Light was focused onto the cells through the use of glass-on-metal parabolic reflectors (92% reflectance) and at high concentration ratio (37x). Under typical operating conditions the measurements gave a thermal efficiency around 58%, electrical efficiency around 11%, and a combined efficiency around 69%.

Kribus et al. [144] developed a miniature concentrating PV system that can be installed on any rooftop. The design is based on a small parabolic dish which is similar to a satellite dish. The system equipments are relatively easy to deliver and handle without the use of special tools. By concentrating sunlight about 500 times, the solar cell area is greatly reduced.

In high-latitude countries like Sweden, the solar radiation is asymmetric over the year because of the high cloud coverage during winter, and thus concentrated to a small angular interval of high irradiation. This makes the use of economical stationary reflectors or concentrators attractive. Cost reduction can be realized by laminating thin aluminum foil on steel substrate. Nilsson et al. [145] carried out experimental tests on an asymmetric compound parabolic reflector system, with two different truncated parabolic reflectors made of anodized aluminum and aluminum laminated steel, respectively. Their measurements confirmed that changing the back reflector from anodized aluminum to aluminum laminated steel does not change the energy output. They also found that the optimal cell position is to face the front reflector, assuming no space restriction. This will result in the lowest cost for electricity generation. For cases with limited roof space, they suggested to place the solar cells on both sides of the absorber. This considers that, once a trough with cells on one side of the absorber is constructed, the cost of adding cells to the other side is relatively low.

A two-stage hybrid device was theoretically studied by Vorobiev et al. [146, 147], with solar cells incorporated on energy flux concentrator and heat-to-electric/mechanic energy converter. Two option cases were investigated:

(i) system with the separation of "thermal solar radiation", and

(ii) system without solar spectrum division and solar cell operating at high temperature.

The first case allows the solar cell to operate at a low ambient temperature, but then requires the production of a new kind of solar cell which does not absorb or dissipate solar radiation as infrared. The calculations showed that with a concentration as high as 1500x, the total conversion efficiency could reach 35–40%. The solar cell in the second option is subject to concentrated sunlight. It was found that with the use of GaAs-based single-junction cell having room temperature efficiency at 24% and a concentrator at 50x, the total conversion efficiency is around 25–30%. If a higher concentration is used, the efficiency can be even higher.

Jiang et al. [148] introduced a two-stage parabolic trough concentrating PVT system, which contains a concentrator, a spectral beam splitting filter, an evacuated collector tube, and the solar cell components. The nondimensional optical model with the focal length of the concentrator as the characteristic length has been developed to analyze the properties of the concentrating system using the beam splitting filter. The geometry concentration ratio and the size of solar image at different structure parameters have been obtained. It is shown that using the filter the heat load of the cell can be reduced by 20.7%. Up to 10.5% of the total incident solar energy can be recovered by the receiver, and the overall optical efficiency in theory is about 0.764.

Kostic et al. [149] studied the influence of reflectance from flat-plate solar radiation concentrators made of aluminum sheet and aluminum foil on energy efficiency of PVT collector. The total reflectance from concentrators made of aluminum sheet and aluminum foil is almost the same, but specular reflectance (which is bigger in concentrators made of aluminum foil) results in an increase of solar radiation intensity concentration factor. The total energy generated by c-PVT collector made of aluminum foil in optimal position is higher than the total energy generated by those made of aluminum sheet.

The basic feature of an STPV (solar thermophotovoltaic) is in the use of high temperature emitter as an intermediate element that absorbs concentrated solar light and emits photonic energy to solar cells through which the thermal

radiation energy is converted to electricity. Compared with the solar cells, the STPV system can utilize the concentrated solar energy sufficiently. It conveniently adjusts the spectral feature of photons released from the emitter corresponding to the bandgaps of solar cells in the system by controlling the emitter temperature and/or installing the spectral filter. Xuan et al. [150] established the design and optimization method of STPV systems by taking into account the energy transport and/or conversion processes among the solar concentrator, the emitter, the spectral filter, the solar cells, and the cooling subsystem. The effects of the nonparallelism of sun rays, aperture ratios, and the tracking error on concentration capacity were investigated. The emitters made of different materials and with different configurations were numerically analyzed. The effects of concentration ratio, spectral characteristic of the filter, series and shunt resistance of the cell, and the performance of the cooling system on the STPV systems were discussed. Compared with the one-dimensional photonic filer, the optimized nonperiodic filter has a better performance. A high-performance cooling system is required to keep the cell temperature below 50°C.

As an attempt to improve the system efficiency of concentrating photovoltaics (CPVs), an investigation has been done by Kosmadakis et al. [151] into the technical aspects as well as the cost analysis, by combining the technologies of the CPV and the organic Rankine cycles (ORCs). The heat rejected from the CPV is recovered from the ORC, in order to increase the total electric power output. The findings constitute evidence that the CPV-ORC system can be an alternative for recovering the heat from concentrating PVs. Nevertheless, the mechanical power produced from the expander of the ORC can be used in other applications as well.

Huang et al. [152] suggested a PVT system based on organic photovoltaics (OPVs). The OPV cells were fabricated onto one-half of a tubular light pipe inside which the silicone oil was flowed. This allows solar energy in the visible wavelengths to be effectively converted into electricity by photocell while simultaneously the silicone oil captures the infrared radiation part of the spectrum as heat energy. The oil filled tube acts as a passive optical element that concentrates the light into the PV and thereby increases its overall efficiency.

While silicon-based PV technology has many physical barriers, it is expected that the future PVT developments will be closely linked to the breakthroughs in solar cell technology. The next generation solar cells such as polymer, nanocrystalline, and dye-sensitized solar cells will be less expensive, flexible, compact, lightweight, and efficient. Take dye-sensitized solar cells (DSSCs) as an example, the operation does not need the p-n junction but mimics the principle of natural photosynthesis. It is composed of a porous layer of titanium dioxide nanoparticles, covered with a molecular dye that absorbs sunlight, like the chlorophyll in green leaves. The DSSCs today convert about 11 to 12% of the sunlight into electricity. The use of hybrid ZnO/TiO_2 photoanodes will be able to utilize the high electron transport rate of ZnO and the high electron injection efficiency and stability of TiO2 materials [153].

5. Miscellaneous Developments in Recent Years

5.1. Autonomous Applications. Desalination is a process to produce the distilled water from brackish/saline water by means of solar still. Solar distillation of brackish water is a good option to obtain fresh water in view of its simple technology and low energy operation. A proposed design of PVT-integrated active solar still was tested in India by Kumar and Tiwari [154–156]. This PVT active solar still is self-sustainable and can be used in remote areas. Compared with a passive solar still, the daily distillate yield was found 3.5 times higher, and 43% of the pumping power can be saved. Based on 0.05 m water depth, the range of CPBT can be shortened from 3.3–23.9 years to 1.1–6.2 years (depending on the selling price of distilled water) and the EPBT from 4.7 years to 2.9 years. The hybrid active solar still is able to provide higher electrical and overall thermal efficiency, which is about 20% higher than the passive solar still. On the other hand, Gaur and Tiwari [157] conducted a numerical study to optimize the number of collectors for PVT/w hybrid active solar still. The number of PVT collectors connected in series has been integrated with the basin of a solar still.

Another potential application lies in crop drying, which is the process of removing excess moisture from crop produced through evaporation, either by natural or forced convection mode. Tiwari et al. developed a PVT mixed mode dryer together with an analytical model for performance analysis [158]. The experimental tests were executed for the forced convection mode under no load conditions. The annual gains for different Indian cities were evaluated and the results show that Jodhpur is the best place for the installation of this type of PVT dryer.

5.2. High Temperature Applications. Mittelman et al. [159] studied the application of c-PVT system in a LiBr absorption chiller designed for single effect. In the theoretical analysis, the desorber inlet temperature was set in the range of 65–120°C and without thermal storage. The PV module was based on triple-junction cells with a nominal conversion efficiency of 37%. A typical dish concentrator with an 85% optical efficiency was used. The results showed that the loss in cell efficiency owing to the increase in operation temperature was insignificant. Under a reasonably range of economic conditions, the c-PVT cooling system can be comparable to, and sometimes even better than, a conventional cooling system.

A c-PVT water desalination system was also proposed by Mittelman et al. [160], in which a c-PVT collector field was to couple to a large-scale multiple-effect evaporation thermal desalination system. Small dish concentrator type was used in the numerical analysis. The vapor formed in each evaporator condenses in the next (lower temperature) effect and thus provides the heat source for further evaporation. Additional feed preheating is to be provided by vapor process bleeding from each effect. The range of top brine temperature is from 60 to 80°C. Through numerical analysis, this approach was found competitive relative to other solar-driven desalination systems and even relative to the conventional reverse-osmosis desalination. Because of the higher ratio of electricity to heat

generation, the high concentration option with the use of advanced solar cells can be advantageous.

5.3. Commercial Aspects. The commercial markets for both solar thermal and photovoltaic are growing rapidly. It is expected that the PVT products, once become mature, would experience a similar trend of growth. In future, the market share might be even larger than that for solar thermal collectors. The higher energy output characteristics of the PVT collector suit better the increasing demands on low-energy or even zero-carbon buildings. Nevertheless, although there are plenty reported literatures on the theoretical and experimental findings of PVT collector systems, those reporting on full-scale application and long-term monitoring have been scarce [161]. The number of commercial systems in practical services remains small. The majority involves flat-plate collectors but only with limited service life. The operating experiences are scattered. In the inventory of IEA Solar Heating and Cooling Task 35, over 50 PVT projects have been identified in the past 20 years. Less than twenty of these projects belong to the PVT/w category which is supposed to have better application potential. On the other hand, while most projects were in Europe such as UK and Netherlands, there have been projects realized in Thailand, in which large-scale glazed a-Si PVT/w systems were installed at hospital and government buildings [162]. It is important to have full documentation of the initial testing and commissioning, as well as the long-term monitoring of the real systems performance, including the operating experiences and the problems encountered. Developments in the balance of system are also important—for example the improvement works in power quality and power factor in PV inverter design [163]. The improvements in power supply stability with power conditioner and better integration of renewable energy sources on to utility grid have been other key research areas [164].

Standard testing procedures for PVT commercial products are so far incomplete. In essence, the performance of PVT commercial products can be tested either outdoor or indoor. The outdoor test needs to be executed in steady conditions of fine weather, which should be around noon hours and preferably with clear sky and no wind. This can be infrequent; say for Northern Europe, it may take six months to acquire the efficiency curve [165]. Indoor test can be quicker and provides repeatable results. To make available an internationally accepted testing standard is one important step for promoting the PVT products.

Although there have been an obvious increase in academic publications in hybrid PVT technology in recent years, many key issues related to the commercialization of PVT products are still not resolved. The lack of economic viability, public awareness, product standardization, warranties and performance certification, installation training, and experiences are the barriers. It is important for the reliability of the technology to be thoroughly assessed.

6. Conclusion

Global climate change and fuel supply security have led to the fast development in renewable technology, including solar energy applications. The installations of solar thermal and PV electricity generation devices are growing rapidly and these lead to an increase in the demand of PVT collector system. PVT products have much shorter CPBT than the PV counterpart. Hence PVT (rather than PV) as a renewable energy technology is expected to first become competitive with the conventional power generating systems.

In the past decades, the performance of various PVT collector types had been studied theoretically, numerically, and experimentally. This paper serves to review the endeavor in the past years. While in the early works the research efforts were on the consolidation of the conceptual ideas and the feasibility study on basic PVT collector designs, the PVT studies from the 90s onward have been more related to the collector design improvement and economical/environmental performance evaluation. There were more rigorous numerical analyses of the energy and fluid flow phenomena on conventional collectors with an experimental validation. The ideas of building-integrated design emerged and the demonstration projects were reported. Since the turn of century, the focus has been generally shifted towards the development of complimentary products, innovative systems, testing procedures, and design optimization. The marketing potential and justification on various collector designs and system applications have been evaluated through user feedback, life cycle cost, and/or embodied energy evaluations. The computational analyses become more comprehensive with the use of powerful analytical tools. There have been increased uses of explicit dynamic modeling techniques and also public domain simulation programs, including CFD codes. The evaluation has been extended to geographical comparison of long-term performance based on typical year round weather data on one hand and the second-law thermodynamic assessment on the other. International research collaborations and related activities have been increasing.

Despite the sharp increase in academic activities, the developments of commercial products and real system applications are still limited. The issues of investment costs and product reliability are to be fully attended. More efforts must be on the identification of suitable product materials, manufacturing techniques, testing and training requirements, potential customers, market strength, and so on.

Acknowledgment

The research work described in this paper was fully supported by the France/Hong Kong Joint Research Scheme (project no. F_HK05/11T).

References

[1] M. Wolf, "Performance analyses of combined heating and photovoltaic power systems for residences," *Energy Conversion*, vol. 16, no. 1-2, pp. 79–90, 1976.

[2] E. C. Kern and M. C. Russell, "Combined photovoltaic and thermal hybrid collector systems," in *Proceedings of the 13th IEEE Photovoltaic Specialists*, pp. 1153–1157, Washington DC, USA, June 1978.

[3] L. W. Florschuetz, "Extension of the Hottel-Whillier model to the analysis of combined photovoltaic/thermal flat plate collectors," *Solar Energy*, vol. 22, no. 4, pp. 361–366, 1979.

[4] T. T. Chow, "A review on photovoltaic/thermal hybrid solar technology," *Applied Energy*, vol. 87, no. 2, pp. 365–379, 2010.

[5] C. H. Cox III and P. Raghuraman, "Design considerations for flat-plate-photovoltaic/thermal collectors," *Solar Energy*, vol. 35, no. 3, pp. 227–241, 1985.

[6] B. Lalović, Z. Kiss, and H. Weakliem, "A hybrid amorphous silicon photovoltaic and thermal solar collector," *Solar Cells*, vol. 19, no. 2, pp. 131–138, 1986.

[7] H. P. Garg and R. S. Adhikari, "Conventional hybrid photovoltaic/thermal (PV/T) air heating collectors: steady-state simulation," *Renewable Energy*, vol. 11, no. 3, pp. 363–385, 1997.

[8] H. P. Garg and R. S. Adhikari, "Optical design calculations for CPCS," *Energy*, vol. 23, no. 10, pp. 907–909, 1998.

[9] H. P. Garg and R. S. Adhikari, "Performance analysis of a hybrid photovoltaic/thermal (PV/T) collector with integrated CPC troughs," *International Journal of Energy Research*, vol. 23, no. 15, pp. 1295–1304, 1999.

[10] K. Sopian, K. S. Yigit, H. T. Liu, S. Kakaç, and T. N. Veziroglu, "Performance analysis of photovoltaic thermal air heaters," *Energy Conversion and Management*, vol. 37, no. 11, pp. 1657–1670, 1996.

[11] K. Sopian, H. T. Liu, S. Kakac, and T. N. Veziroglu, "Performance of a double pass photovoltaic thermal solar collector suitable for solar drying systems," *Energy Conversion and Management*, vol. 41, no. 4, pp. 353–365, 2000.

[12] J. Prakash, "Transient analysis of a photovoltaic-thermal solar collector for co-generation of electricity and hot air/water," *Energy Conversion and Management*, vol. 35, no. 11, pp. 967–972, 1994.

[13] T. Bergene and O. M. Løvvik, "Model calculations on a flat-plate solar heat collector with integrated solar cells," *Solar Energy*, vol. 55, no. 6, pp. 453–462, 1995.

[14] D. W. de Vries, *Design of a photovoltaic/thermal combi-panel [Ph.D. thesis]*, Eindhoven Technical University, Eindhoven, The Netherlands, 1998.

[15] T. Fujisawa and T. Tani, "Annual exergy evaluation on photovoltaic-thermal hybrid collector," *Solar Energy Materials and Solar Cells*, vol. 47, no. 1–4, pp. 135–148, 1997.

[16] B. Norton and J. E. J. Edmonds, "Aqueous propylene-glycol concentrations for the freeze protection of thermosyphon solar energy water heaters," *Solar Energy*, vol. 47, no. 5, pp. 375–382, 1991.

[17] G. Rockendorf, R. Sillmann, L. Podlowski, and B. Litzenburger, "PV-hybrid and thermoelectric collectors," *Solar Energy*, vol. 67, no. 4–6, pp. 227–237, 1999.

[18] M. W. Davis, A. H. Fanney, and B. P. Dougherty, "Prediction of building integrated photovoltaic cell temperatures," *Journal of Solar Energy Engineering*, vol. 123, no. 3, pp. 200–210, 2001.

[19] B. Moshfegh and M. Sandberg, "Flow and heat transfer in the air gap behind photovoltaic panels," *Renewable and Sustainable Energy Reviews*, vol. 2, no. 3, pp. 287–301, 1998.

[20] J. A. Clarke, J. W. Hand, C. M. Johnstone, N. Kelly, and P. A. Strachan, "Photovoltaic-integrated building facades," *Renewable Energy*, vol. 8, no. 1–4, pp. 475–479, 1996.

[21] B. J. Brinkworth, R. H. Marshall, and Z. Ibarahim, "A validated model of naturally ventilated PV cladding," *Solar Energy*, vol. 69, no. 1, pp. 67–81, 2000.

[22] J. C. Hollick, "Solar cogeneration panels," *Renewable Energy*, vol. 15, no. 1, pp. 195–200, 1998.

[23] A. Akbarzadeh and T. Wadowski, "Heat pipe-based cooling systems for photovoltaic cells under concentrated solar radiation," *Applied Thermal Engineering*, vol. 16, no. 1, pp. 81–87, 1996.

[24] A. Luque, G. Sala, J. C. Arboiro, T. Bruton, D. Cunningham, and N. Mason, "Some results of the EUCLIDES photovoltaic concentrator prototype," *Progress in Photovoltaics: Research and Applications*, vol. 5, no. 3, pp. 195–212, 1997.

[25] S. Ito, N. Miura, and K. Wang, "Performance of a heat pump using direct expansion solar collectors," *Solar Energy*, vol. 65, no. 3, pp. 189–196, 1999.

[26] S. Ito and N. Miura, "Photovoitaic and thermal hybrid systems," in *Proceedings of the Asia-Pacific Conference of International Solar Energy Society*, pp. 73–78, Gwangju, South Korea, October 2004.

[27] P. Affolter, D. Ruoss, P. Toggweiler, and B. A. Haller, "New Generation of Hybrid Solar Collectors," Final Report DIS 56360/16868, Swiss Federal Office for Energy, 2000.

[28] IEA, "Photovoltaic/thermal solar energy systems: status of the technology and roadmap for future development," Task 7 Report, International Energy Agency, PVPS T7-10, 2002.

[29] A. A. Hegazy, "Comparative study of the performances of four photovoltaic/thermal solar air collectors," *Energy Conversion and Management*, vol. 41, no. 8, pp. 861–881, 2000.

[30] Y. Tripanagnostopoulos, T. Nousia, M. Souliotis, and P. Yianoulis, "Hybrid photovoltaic/thermal solar systems," *Solar Energy*, vol. 72, no. 3, pp. 217–234, 2002.

[31] J. K. Tonui and Y. Tripanagnostopoulos, "Air-cooled PV/T solar collectors with low cost performance improvements," *Solar Energy*, vol. 81, no. 4, pp. 498–511, 2007.

[32] Y. Tripanagnostopoulos, "Aspects and improvements of hybrid photovoltaic/thermal solar energy systems," *Solar Energy*, vol. 81, no. 9, pp. 1117–1131, 2007.

[33] A. Tiwari, M. S. Sodha, A. Chandra, and J. C. Joshi, "Performance evaluation of photovoltaic thermal solar air collector for composite climate of India," *Solar Energy Materials and Solar Cells*, vol. 90, no. 2, pp. 175–189, 2006.

[34] A. Tiwari, P. Barnwal, G. S. Sandhu, and M. S. Sodha, "Energy metrics analysis of hybrid—photovoltaic (PV) modules," *Applied Energy*, vol. 86, no. 12, pp. 2615–2625, 2009.

[35] V. Raman and G. N. Tiwari, "A comparison study of energy and exergy performance of a hybrid photovoltaic double-pass and single-pass air collector," *International Journal of Energy Research*, vol. 33, no. 6, pp. 605–617, 2009.

[36] A. S. Joshi, I. Dincer, and B. V. Reddy, "Thermodynamic assessment of photovoltaic systems," *Solar Energy*, vol. 83, no. 8, pp. 1139–1149, 2009.

[37] S. Nayak and G. N. Tiwari, "Energy metrics of photovoltaic/thermal and earth air heat exchanger integrated greenhouse for different climatic conditions of India," *Applied Energy*, vol. 87, no. 10, pp. 2984–2993, 2010.

[38] S. Dubey, G. S. Sandhu, and G. N. Tiwari, "Analytical expression for electrical efficiency of PV/T hybrid air collector," *Applied Energy*, vol. 86, no. 5, pp. 697–705, 2009.

[39] S. Dubey, S. C. Solanki, and A. Tiwari, "Energy and exergy analysis of PV/T air collectors connected in series," *Energy and Buildings*, vol. 41, no. 8, pp. 863–870, 2009.

[40] S. C. Solanki, S. Dubey, and A. Tiwari, "Indoor simulation and testing of photovoltaic thermal (PV/T) air collectors," *Applied Energy*, vol. 86, no. 11, pp. 2421–2428, 2009.

[41] Y. B. Assoa, C. Menezo, G. Fraisse, R. Yezou, and J. Brau, "Study of a new concept of photovoltaic-thermal hybrid collector," *Solar Energy*, vol. 81, no. 9, pp. 1132–1143, 2007.

[42] Y. Sukamongkol, S. Chungpaibulpatana, B. Limmeechokchai, and P. Sripadungtham, "Condenser heat recovery with a PV/T air heating collector to regenerate desiccant for reducing energy use of an air conditioning room," *Energy and Buildings*, vol. 42, no. 3, pp. 315–325, 2010.

[43] A. H. H. Ali, M. Ahmed, and M. S. Youssef, "Characteristics of heat transfer and fluid flow in a channel with single-row plates array oblique to flow direction for photovoltaic/thermal system," *Energy*, vol. 35, no. 9, pp. 3524–3534, 2010.

[44] R. Kumar and M. A. Rosen, "Performance evaluation of a double pass PV/T solar air heater with and without fins," *Applied Thermal Engineering*, vol. 31, no. 8-9, pp. 1402–1410, 2011.

[45] M. D. Bazilian and D. Prasad, "Modelling of a photovoltaic heat recovery system and its role in a design decision support tool for building professionals," *Renewable Energy*, vol. 27, no. 1, pp. 57–68, 2002.

[46] B. P. Cartmell, N. J. Shankland, D. Fiala, and V. Hanby, "A multi-operational ventilated photovoltaic and solar air collector: application, simulation and initial monitoring feedback," *Solar Energy*, vol. 76, no. 1–3, pp. 45–53, 2004.

[47] L. Mei, D. Infield, U. Eicker, and V. Fux, "Thermal modelling of a building with an integrated ventilated PV façade," *Energy and Buildings*, vol. 35, no. 6, pp. 605–617, 2003.

[48] D. Infield, L. Mei, and U. Eicker, "Thermal performance estimation for ventilated PV facades," *Solar Energy*, vol. 76, no. 1–3, pp. 93–98, 2004.

[49] M. Sandberg and B. Moshfegh, "Buoyancy-induced air flow in photovoltaic facades effect of geometry of the air gap and location of solar cell modules," *Building and Environment*, vol. 37, no. 3, pp. 211–218, 2002.

[50] G. Mittelman, A. Alshare, and J. H. Davidson, "A model and heat transfer correlation for rooftop integrated photovoltaics with a passive air cooling channel," *Solar Energy*, vol. 83, no. 8, pp. 1150–1160, 2009.

[51] G. Gan, "Effect of air gap on the performance of building-integrated photovoltaics," *Energy*, vol. 34, no. 7, pp. 913–921, 2009.

[52] O. Zogou and H. Stapountzis, "Flow and heat transfer inside a PV/T collector for building application," *Applied Energy*, vol. 91, no. 1, pp. 103–115, 2012.

[53] Y. Chen, A. K. Athienitis, and K. Galal, "Modeling, design and thermal performance of a BIPV/T system thermally coupled with a ventilated concrete slab in a low energy solar house: part 1, BIPV/T system and house energy concept," *Solar Energy*, vol. 84, no. 11, pp. 1892–1907, 2010.

[54] Y. Chen, K. Galal, and A. K. Athienitis, "Modeling, design and thermal performance of a BIPV/T system thermally coupled with a ventilated concrete slab in a low energy solar house: part 2, ventilated concrete slab," *Solar Energy*, vol. 84, no. 11, pp. 1908–1919, 2010.

[55] A. K. Athienitis, J. Bambara, B. O'Neill, and J. Faille, "A prototype photovoltaic/thermal system integrated with transpired collector," *Solar Energy*, vol. 85, no. 1, pp. 139–153, 2011.

[56] S. Pantic, L. Candanedo, and A. K. Athienitis, "Modeling of energy performance of a house with three configurations of building-integrated photovoltaic/thermal systems," *Energy and Buildings*, vol. 42, no. 10, pp. 1779–1789, 2010.

[57] R. H. Crawford, G. J. Treloar, R. J. Fuller, and M. Bazilian, "Life-cycle energy analysis of building integrated photovoltaic systems (BiPVs) with heat recovery unit," *Renewable and Sustainable Energy Reviews*, vol. 10, no. 6, pp. 559–575, 2006.

[58] B. Agrawal and G. N. Tiwari, "Optimizing the energy and exergy of building integrated photovoltaic thermal (BIPVT) systems under cold climatic conditions," *Applied Energy*, vol. 87, no. 2, pp. 417–426, 2010.

[59] B. Agrawal and G. N. Tiwari, "Life cycle cost assessment of building integrated photovoltaic thermal (BIPVT) systems," *Energy and Buildings*, vol. 42, no. 9, pp. 1472–1481, 2010.

[60] J. Jie, H. Wei, and H. N. Lam, "The annual analysis of the power output and heat gain of a PV-wall with different integration mode in Hong Kong," *Solar Energy Materials and Solar Cells*, vol. 71, no. 4, pp. 435–448, 2002.

[61] H. Yang, J. Burnett, and Z. Zhu, "Building-integrated photovoltaics: effect on the cooling load component of building façades," *Building Services Engineering Research and Technology*, vol. 22, no. 3, pp. 157–165, 2001.

[62] T. T. Chow, J. W. Hand, and P. A. Strachan, "Building-integrated photovoltaic and thermal applications in a sub-tropical hotel building," *Applied Thermal Engineering*, vol. 23, no. 16, pp. 2035–2049, 2003.

[63] J. Ji, B. Jiang, H. Yi, T. T. Chow, W. He, and G. Pei, "An experimental and mathematical study of efforts of a novel photovoltaic-Trombe wall on a test room," *International Journal of Energy Research*, vol. 32, no. 6, pp. 531–542, 2008.

[64] A. Fieber, H. Gajbert, H. Hakansson, J. Nilsson, T. Rosencrantz, and B. Karlsson, "Design, building integration and performance of a hybrid solar wall element," in *Proceedings of the ISES Solar World Congress*, Gothenburg, Sweden, 2003.

[65] H. Davidsson, B. Perers, and B. Karlsson, "Performance of a multifunctional PV/T hybrid solar window," *Solar Energy*, vol. 84, no. 3, pp. 365–372, 2010.

[66] H. Davidsson, B. Perers, and B. Karlsson, "System analysis of a multifunctional PV/T hybrid solar window," *Solar Energy*, vol. 86, no. 3, pp. 903–910, 2012.

[67] T. T. Chow, K. F. Fong, W. He, Z. Lin, and A. L. S. Chan, "Performance evaluation of a PV ventilated window applying to office building of Hong Kong," *Energy and Buildings*, vol. 39, no. 6, pp. 643–650, 2007.

[68] T. T. Chow, G. Pei, L. S. Chan, Z. Lin, and K. F. Fong, "A comparative study of PV glazing performance in warm climate," *Indoor and Built Environment*, vol. 18, no. 1, pp. 32–40, 2009.

[69] T. T. Chow, Z. Qiu, and C. Li, "Potential application of "see-through" solar cells in ventilated glazing in Hong Kong," *Solar Energy Materials and Solar Cells*, vol. 93, no. 2, pp. 230–238, 2009.

[70] T. T. Chow, Z. Qiu, and C. Li, "Performance evaluation of PV ventilated glazing," in *Proceedings of the Building Simulation 2009, 11th International Building Performance Simulation Association Conference*, Glasgow, UK, July 2009.

[71] H. A. Zondag, D. W. de Vries, W. G. J. van Helden, R. J. C. van Zolingen, and A. A. van Steenhoven, "The thermal and electrical yield of a PV-thermal collector," *Solar Energy*, vol. 72, no. 2, pp. 113–128, 2002.

[72] H. A. Zondag, D. W. de Vries, W. G. J. van Helden, R. J. C. van Zolingen, and A. A. van Steenhoven, "The yield of different combined PV-thermal collector designs," *Solar Energy*, vol. 74, no. 3, pp. 253–269, 2003.

[73] B. Sandnes and J. Rekstad, "A photovoltaic/thermal (PV/T) collector with a polymer absorber plate. Experimental study and analytical model," *Solar Energy*, vol. 72, no. 1, pp. 63–73, 2002.

[74] T. T. Chow, "Performance analysis of photovoltaic-thermal collector by explicit dynamic model," *Solar Energy*, vol. 75, no. 2, pp. 143–152, 2003.

[75] R. Zakharchenko, L. Licea-Jiménez, S. A. Pérez-García et al., "Photovoltaic solar panel for a hybrid PV/Thermal system," *Solar Energy Materials and Solar Cells*, vol. 82, no. 1-2, pp. 253–261, 2004.

[76] S. Dubey and G. N. Tiwari, "Thermal modeling of a combined system of photovoltaic thermal (PV/T) solar water heater," *Solar Energy*, vol. 82, no. 7, pp. 602–612, 2008.

[77] S. A. Kalogirou, "Use a TRNSYS for modelling and simulation of a hybrid pv-thermal solar system for Cyprus," *Renewable Energy*, vol. 23, no. 2, pp. 247–260, 2001.

[78] S. A. Kalogirou and Y. Tripanagnostopoulos, "Hybrid PV/T solar systems for domestic hot water and electricity production," *Energy Conversion and Management*, vol. 47, no. 18-19, pp. 3368–3382, 2006.

[79] S. A. Kalogirou and Y. Tripanagnostopoulos, "Industrial application of PV/T solar energy systems," *Applied Thermal Engineering*, vol. 27, no. 8-9, pp. 1259–1270, 2007.

[80] E. Erdil, M. Ilkan, and F. Egelioglu, "An experimental study on energy generation with a photovoltaic (PV)-solar thermal hybrid system," *Energy*, vol. 33, no. 8, pp. 1241–1245, 2008.

[81] G. Vokas, N. Christandonis, and F. Skittides, "Hybrid photovoltaic-thermal systems for domestic heating and cooling—a theoretical approach," *Solar Energy*, vol. 80, no. 5, pp. 607–615, 2006.

[82] L. T. Kostić, T. M. Pavlović, and Z. T. Pavlović, "Optimal design of orientation of PV/T collector with reflectors," *Applied Energy*, vol. 87, no. 10, pp. 3023–3029, 2010.

[83] H. Saitoh, Y. Hamada, H. Kubota et al., "Field experiments and analyses on a hybrid solar collector," *Applied Thermal Engineering*, vol. 23, no. 16, pp. 2089–2105, 2003.

[84] J. Zhao, Y. Song, W. H. Lam et al., "Solar radiation transfer and performance analysis of an optimum photovoltaic/thermal system," *Energy Conversion and Management*, vol. 52, no. 2, pp. 1343–1353, 2011.

[85] T. T. Chow, G. Pei, K. F. Fong, Z. Lin, A. L. S. Chan, and J. Ji, "Energy and exergy analysis of photovoltaic-thermal collector with and without glass cover," *Applied Energy*, vol. 86, no. 3, pp. 310–316, 2009.

[86] J. H. Kim and J. T. Kim, "Comparison of electrical and thermal performances of glazed and unglazed PVT collectors," *International Journal of Photoenergy*, vol. 2012, Article ID 957847, 7 pages, 2012.

[87] J. H. Kim and J. T. Kim, "The experimental performance of an unglazed PVT collector with two different absorber types," *International Journal of Photoenergy*, vol. 2012, Article ID 312168, 6 pages, 2012.

[88] S. Dubey and G. N. Tiwari, "Analysis of PV/T flat plate water collectors connected in series," *Solar Energy*, vol. 83, no. 9, pp. 1485–1498, 2009.

[89] A. Tiwari, S. Dubey, G. S. Sandhu, M. S. Sodha, and S. I. Anwar, "Exergy analysis of integrated photovoltaic thermal solar water heater under constant flow rate and constant collection temperature modes," *Applied Energy*, vol. 86, no. 12, pp. 2592–2597, 2009.

[90] R. Naewngerndee, E. Hattha, K. Chumpolrat, T. Sangkapes, J. Phongsitong, and S. Jaikla, "Finite element method for computational fluid dynamics to design photovoltaic thermal (PV/T) system configuration," *Solar Energy Materials and Solar Cells*, vol. 95, no. 1, pp. 390–393, 2011.

[91] M. Rosa-Clot, P. Rosa-Clot, and G. M. Tina, "TESPI: thermal electric solar panel integration," *Solar Energy*, vol. 85, no. 10, pp. 2433–2442, 2011.

[92] T. T. Chow, W. He, and J. Ji, "Hybrid photovoltaic-thermosyphon water heating system for residential application," *Solar Energy*, vol. 80, no. 3, pp. 298–306, 2006.

[93] T. T. Chow, J. Ji, and W. He, "Photovoltaic-thermal collector system for domestic application," *Journal of Solar Energy Engineering*, vol. 129, no. 2, pp. 205–209, 2007.

[94] W. He, T. T. Chow, J. Ji, J. Lu, G. Pei, and L. S. Chan, "Hybrid photovoltaic and thermal solar-collector designed for natural circulation of water," *Applied Energy*, vol. 83, no. 3, pp. 199–210, 2006.

[95] J. Ji, J. Han, T. T. Chow, C. Han, J. Lu, and W. He, "Effect of flow channel dimensions on the performance of a box-frame photovoltaic/thermal collector," *Proceedings of the Institution of Mechanical Engineers A*, vol. 220, no. 7, pp. 681–688, 2006.

[96] J. Ji, J. P. Lu, T. T. Chow, W. He, and G. Pei, "A sensitivity study of a hybrid photovoltaic/thermal water-heating system with natural circulation," *Applied Energy*, vol. 84, no. 2, pp. 222–237, 2007.

[97] T. T. Chow, W. He, J. Ji, and A. L. S. Chan, "Performance evaluation of photovoltaic-thermosyphon system for subtropical climate application," *Solar Energy*, vol. 81, no. 1, pp. 123–130, 2007.

[98] P. Affolter, W. Eisenmann, H. Fechner et al., *PVT Roadmap: A European Guide for the Development and Market Introduction of PV-Thermal Technology*, ECN, 2007.

[99] H. A. Zondag and W. G. J. van Helden, "Stagnation temperature in PVT collector," Report ECN-RX-02-045, 2002, http://www.ecn.nl/library/reports/2002/rx02045.html.

[100] P. G. Charalambous, S. A. Kalogirou, G. G. Maidment, and K. Yiakoumetti, "Optimization of the photovoltaic thermal (PV/T) collector absorber," *Solar Energy*, vol. 85, no. 5, pp. 871–880, 2011.

[101] M. Meir and J. Rekstad, "Der solarnor kunststoffkollektor—the development of a polymer collector with glazing," in *Proceedings of the Polymeric Solar Material, Erstes Leobener Symposium "Solartechnik—Neue moglichkeiten fur die Kunststoffbranche"*, pp. II. 1–II. 8., Polymer Competence Center Leoben, Leoben, Austria, October 2003.

[102] P. Papillon, G. Wallner, and M. Kohl, "Polymeric materials in solar thermal applications," Solar Heating and Cooling Program, Task 39, International Energy Agency, http://www.iea-shc.org/task39.

[103] B. J. Huang, T. H. Lin, W. C. Hung, and F. S. Sun, "Performance evaluation of solar photovoltaic/thermal systems," *Solar Energy*, vol. 70, no. 5, pp. 443–448, 2001.

[104] C. Cristofari, G. Notton, and J. L. Canaletti, "Thermal behavior of a copolymer PV/Th solar system in low flow rate conditions," *Solar Energy*, vol. 83, no. 8, pp. 1123–1138, 2009.

[105] C. Cristofari, J. L. Canaletti, G. Notton, and C. Darras, "Innovative patented PV/TH solar collector: optimization and performance evaluation," *Energy Procedia*, vol. 14, pp. 235–240, 2012.

[106] G. Fraisse, C. Ménézo, and K. Johannes, "Energy performance of water hybrid PV/T collectors applied to combisystems of direct solar floor type," *Solar Energy*, vol. 81, no. 11, pp. 1426–1438, 2007.

[107] R. Santbergen, C. C. M. Rindt, H. A. Zondag, and R. J. C. van Zolingen, "Detailed analysis of the energy yield of systems with covered sheet-and-tube PVT collectors," *Solar Energy*, vol. 84, no. 5, pp. 867–878, 2010.

[108] R. Santbergen and R. J. C. van Zolingen, "Modeling the thermal absorption factor of photovoltaic/thermal combi-panels," *Energy Conversion and Management*, vol. 47, no. 20, pp. 3572–3581, 2006.

[109] P. Dupeyrat, C. Ménézo, H. Wirth, and M. Rommel, "Improvement of PV module optical properties for PV-thermal hybrid collector application," *Solar Energy Materials and Solar Cells*, vol. 95, no. 8, pp. 2028–2036, 2011.

[110] P. Dupeyrat, C. Ménézo, M. Rommel, and H. M. Henning, "Efficient single glazed flat plate photovoltaic-thermal hybrid collector for domestic hot water system," *Solar Energy*, vol. 85, no. 7, pp. 1457–1468, 2011.

[111] B. Robles-Ocampo, E. Ruíz-Vasquez, H. Canseco-Sánchez et al., "Photovoltaic/thermal solar hybrid system with bifacial PV module and transparent plane collector," *Solar Energy Materials and Solar Cells*, vol. 91, no. 20, pp. 1966–1971, 2007.

[112] J. Ji, T. T. Chow, and W. He, "Dynamic performance of hybrid photovoltaic/thermal collector wall in Hong Kong," *Building and Environment*, vol. 38, no. 11, pp. 1327–1334, 2003.

[113] T. T. Chow, A. L. S. Chan, K. F. Fong, W. C. Lo, and C. L. Song, "Energy performance of a solar hybrid collector system in a multistory apartment building," *Proceedings of the Institution of Mechanical Engineers A*, vol. 219, no. 1, pp. 1–11, 2005.

[114] T. T. Chow, W. He, and J. Ji, "An experimental study of façade-integrated photovoltaic/water-heating system," *Applied Thermal Engineering*, vol. 27, no. 1, pp. 37–45, 2007.

[115] J. Ji, J. Han, T. T. Chow et al., "Effect of fluid flow and packing factor on energy performance of a wall-mounted hybrid photovoltaic/water-heating collector system," *Energy and Buildings*, vol. 38, no. 12, pp. 1380–1387, 2006.

[116] T. T. Chow, W. He, A. L. S. Chan, K. F. Fong, Z. Lin, and J. Ji, "Computer modeling and experimental validation of a building-integrated photovoltaic and water heating system," *Applied Thermal Engineering*, vol. 28, no. 11-12, pp. 1356–1364, 2008.

[117] T. T. Chow, A. L. S. Chan, K. F. Fong, Z. Lin, W. He, and J. Ji, "Annual performance of building-integrated photovoltaic/water-heating system for warm climate application," *Applied Energy*, vol. 86, no. 5, pp. 689–696, 2009.

[118] T. T. Chow and J. Ji, "Environmental life-cycle analysis of hybrid solar photovoltaic/thermal systems for use in Hong Kong," *International Journal of Photoenergy*, vol. 2012, Article ID 101968, 9 pages, 2012.

[119] T. N. Anderson, M. Duke, G. L. Morrison, and J. K. Carson, "Performance of a building integrated photovoltaic/thermal (BIPVT) solar collector," *Solar Energy*, vol. 83, no. 4, pp. 445–455, 2009.

[120] F. Ghani, M. Duke, and J. K. Carson, "Effect of flow distribution on the photovoltaic performance of a building integrated photovoltaic/thermal (BIPV/T) collector," *Solar Energy*, vol. 86, no. 5, pp. 1518–1530, 2012.

[121] U. Eicker and A. Dalibard, "Photovoltaic-thermal collectors for night radiative cooling of buildings," *Solar Energy*, vol. 85, no. 7, pp. 1322–1335, 2011.

[122] T. Matuska, "Simulation study of building integrated solar liquid PV-T collectors," *International Journal of Photoenergy*, vol. 2012, Article ID 686393, 8 pages, 2012.

[123] C. D. Corbin and Z. J. Zhai, "Experimental and numerical investigation on thermal and electrical performance of a building integrated photovoltaic-thermal collector system," *Energy and Buildings*, vol. 42, no. 1, pp. 76–82, 2010.

[124] M. Bakker, H. A. Zondag, M. J. Elswijk, K. J. Strootman, and M. J. M. Jong, "Performance and costs of a roof-sized PV/thermal array combined with a ground coupled heat pump," *Solar Energy*, vol. 78, no. 2, pp. 331–339, 2005.

[125] Y. Bai, T. T. Chow, C. Ménézo, and P. Dupeyrat, "Analysis of a hybrid PV/thermal solar-assisted heat pump system for sports center water heating application," *International Journal of Photoenergy*, vol. 2012, Article ID 265838, 13 pages, 2012.

[126] J. Ji, K. Liu, T. T. Chow, G. Pei, W. He, and H. He, "Performance analysis of a photovoltaic heat pump," *Applied Energy*, vol. 85, no. 8, pp. 680–693, 2008.

[127] J. Ji, G. Pei, T. T. Chow et al., "Experimental study of photovoltaic solar assisted heat pump system," *Solar Energy*, vol. 82, no. 1, pp. 43–52, 2008.

[128] J. Ji, K. Liu, T. T. Chow, G. Pei, and H. He, "Thermal analysis of PV/T evaporator of a solar-assisted heat pump," *International Journal of Energy Research*, vol. 31, no. 5, pp. 525–545, 2007.

[129] J. Ji, H. He, T. T. Chow, G. Pei, W. He, and K. Liu, "Distributed dynamic modeling and experimental study of PV evaporator in a PV/T solar-assisted heat pump," *International Journal of Heat and Mass Transfer*, vol. 52, no. 5-6, pp. 1365–1373, 2009.

[130] T. T. Chow, K. F. Fong, G. Pei, J. Ji, and M. He, "Potential use of photovoltaic-integrated solar heat pump system in Hong Kong," *Applied Thermal Engineering*, vol. 30, no. 8-9, pp. 1066–1072, 2010.

[131] G. Pei, J. Ji, T. T. Chow, H. He, K. Liu, and H. Yi, "Performance of the photovoltaic solar-assisted heat pump system with and without glass cover in winter: a comparative analysis," *Proceedings of the Institution of Mechanical Engineers A*, vol. 222, no. 2, pp. 179–187, 2008.

[132] G. Pei, H. Fu, H. Zhu, and J. Ji, "Performance study and parametric analysis of a novel heat pipe PV/T system," *Energy*, vol. 37, no. 1, pp. 384–395, 2012.

[133] G. Pei, H. Fu, J. Ji, T. T. Chow, and T. Zhang, "Annual analysis of heat pipe PV/T systems for domestic hot water and electricity production," *Energy Conversion and Management*, vol. 56, pp. 8–21, 2012.

[134] S. Y. Wu, Q. L. Zhang, L. Xiao, and F. H. Guo, "A heat pipe photovoltaic/thermal (PV/T) hybrid system and its performance evaluation," *Energy Build*, vol. 43, no. 12, pp. 3558–3567, 2011.

[135] F. Calise, M. D. d'Accadia, and L. Vanoli, "Design and dynamic simulation of a novel solar trigeneration system based on hybrid photovoltaic/thermal collectors (PVT)," *Energy Conversion and Management*, vol. 60, pp. 214–225, 2012.

[136] A. Segal, M. Epstein, and A. Yogev, "Hybrid concentrated photovoltaic and thermal power conversion at different spectral bands," *Solar Energy*, vol. 76, no. 5, pp. 591–601, 2004.

[137] A. Royne, C. J. Dey, and D. R. Mills, "Cooling of photovoltaic cells under concentrated illumination: a critical review," *Solar Energy Materials and Solar Cells*, vol. 86, no. 4, pp. 451–483, 2005.

[138] J. I. Rosell, X. Vallverdu, M. A. Lechon, and M. Ibanez, "Design and simulation of a low concentrating photovoltaic/thermal system," *Energy Conversion and Management*, vol. 46, no. 18-19, pp. 3034–3046, 2005.

[139] M. Li, G. L. Li, X. Ji, F. Yin, and L. Xu, "The performance analysis of the trough concentrating solar photovoltaic/thermal system," *Energy Conversion and Management*, vol. 52, no. 6, pp. 2378–2383, 2011.

[140] X. Ji, M. Li, W. Lin, W. Wang, L. Wang, and X. Luo, "Modeling and characteristic parameters analysis of a trough concentrating photovoltaic/thermal system with GaAs and super cell arrays," *International Journal of Photoenergy*, vol. 2012, Article ID 782560, 10 pages, 2012.

[141] G. Li, G. Pei, S. Yuehong, X. Zhou, and J. Ji, "Preliminary study based on building-integrated compound parabolic concentrators (CPC) PV/thermal technology," *Energy Procedia*, vol. 14, pp. 343–350, 2012.

[142] L. Zhang, D. Jing, L. Zhao, J. Wei, and L. Guo, "Concentrating PV/T hybrid system for simultaneous electricity and usable heat generation: a review," *International Journal of Photoenergy*, vol. 2012, Article ID 869753, 8 pages, 2012.

[143] J. S. Coventry, "Performance of a concentrating photovoltaic/thermal solar collector," *Solar Energy*, vol. 78, no. 2, pp. 211–222, 2005.

[144] A. Kribus, D. Kaftori, G. Mittelman, A. Hirshfeld, Y. Flitsanov, and A. Dayan, "A miniature concentrating photovoltaic and thermal system," *Energy Conversion and Management*, vol. 47, no. 20, pp. 3582–3590, 2006.

[145] J. Nilsson, H. Håkansson, and B. Karlsson, "Electrical and thermal characterization of a PV-CPC hybrid," *Solar Energy*, vol. 81, no. 7, pp. 917–928, 2007.

[146] Y. Vorobiev, J. González-Hernández, P. Vorobiev, and L. Bulat, "Thermal-photovoltaic solar hybrid system for efficient solar energy conversion," *Solar Energy*, vol. 80, no. 2, pp. 170–176, 2006.

[147] Y. V. Vorobiev, J. González-Hernández, and A. Kribus, "Analysis of potential conversion efficiency of a solar hybrid system with high-temperature stage," *Journal of Solar Energy Engineering*, vol. 128, no. 2, pp. 258–260, 2006.

[148] S. Jiang, P. Hu, S. Mo, and Z. Chen, "Optical modeling for a two-stage parabolic trough concentrating photovoltaic/thermal system using spectral beam splitting technology," *Solar Energy Materials and Solar Cells*, vol. 94, no. 10, pp. 1686–1696, 2010.

[149] L. T. Kostic, T. M. Pavlovic, and Z. T. Pavlovic, "Influence of reflectance from flat aluminum concentrators on energy efficiency of PV/Thermal collector," *Applied Energy*, vol. 87, no. 2, pp. 410–416, 2010.

[150] Y. Xuan, X. Chen, and Y. Han, "Design and analysis of solar thermophotovoltaic systems," *Renewable Energy*, vol. 36, no. 1, pp. 374–387, 2011.

[151] G. Kosmadakis, D. Manolakos, and G. Papadakis, "Simulation and economic analysis of a CPV/thermal system coupled with an organic Rankine cycle for increased power generation," *Solar Energy*, vol. 85, no. 2, pp. 308–324, 2011.

[152] H. Huang, Y. Li, M. Wang et al., "Photovoltaic-thermal solar energy collectors based on optical tubes," *Solar Energy*, vol. 85, no. 3, pp. 450–454, 2011.

[153] L. T. Yan, F. L. Wu, L. Peng et al., "Photoanode of dye-sensitized solar cells based on a ZnO/TiO_2 composite film," *International Journal of Photoenergy*, vol. 2012, Article ID 613969, 4 pages, 2012.

[154] S. Kumar and A. Tiwari, "An experimental study of hybrid photovoltaic thermal (PV/T)-active solar still," *International Journal of Energy Research*, vol. 32, no. 9, pp. 847–858, 2008.

[155] S. Kumar and G. N. Tiwari, "Life cycle cost analysis of single slope hybrid (PV/T) active solar still," *Applied Energy*, vol. 86, no. 10, pp. 1995–2004, 2009.

[156] S. Kumar and A. Tiwari, "Design, fabrication and performance of a hybrid photovoltaic/thermal (PV/T) active solar still," *Energy Conversion and Management*, vol. 51, no. 6, pp. 1219–1229, 2010.

[157] M. K. Gaur and G. N. Tiwari, "Optimization of number of collectors for integrated PV/T hybrid active solar still," *Applied Energy*, vol. 87, no. 5, pp. 1763–1772, 2010.

[158] G. N. Tiwari, S. Nayak, S. Dubey, S. C. Solanki, and R. D. Singh, "Performance analysis of a conventional PV/T mixed mode dryer under no load condition," *International Journal of Energy Research*, vol. 33, no. 10, pp. 919–930, 2009.

[159] G. Mittelman, A. Kribus, and A. Dayan, "Solar cooling with concentrating photovoltaic/thermal (CPVT) systems," *Energy Conversion and Management*, vol. 48, no. 9, pp. 2481–2490, 2007.

[160] G. Mittelman, A. Kribus, O. Mouchtar, and A. Dayan, "Water desalination with concentrating photovoltaic/thermal (CPVT) systems," *Solar Energy*, vol. 83, no. 8, pp. 1322–1334, 2009.

[161] H. Zondag, J. Bystrom, and J. Hansen, "PV-thermal collectors going commercial," IEA SHC Task 35 paper, 2008.

[162] J. Hansen, H. Sørensen, J. Byström, M. Collins, and B. Karlsson, "Market, modelling, testing and demonstration in the framewrk of IEA SHC Task 35 on PV/thermal solar systems," in *Proceedings of the 22nd European Photovoltaic Solar Energy Conference and Exhibition*, DE2-5, Milan, Italy, September 2007.

[163] C. L. Shen and J. C. Su, "Grid-connection half-bridge PV inverter system for power flow controlling and active power filtering," *International Journal of Photoenergy*, vol. 2012, Article ID 760791, 8 pages, 2012.

[164] D. Amorndechaphon, S. Premrudeepreechacharn, K. Higuchi, and X. Roboam, "Modified grid-connected CSI for hybrid PV/wind power generation system," *International Journal of Photoenergy*, vol. 2012, Article ID 381016, 12 pages, 2012.

[165] M. J. Elswijk, H. A. Zondag, and W. G. J. van Helden, "Indoor test facility PVT-panels—a feasibility study," Energy Research Centre of the Netherlands, ECN-I-02-005, 2002.

Hindawi Publishing Corporation
International Journal of Photoenergy
Volume 2012, Article ID 782560, 10 pages
doi:10.1155/2012/782560

Research Article

Modeling and Characteristic Parameters Analysis of a Trough Concentrating Photovoltaic/Thermal System with GaAs and Super Cell Arrays

Xu Ji,[1] Ming Li,[1] Weidong Lin,[1] Wenbo Wang,[2] Liuling Wang,[2] and Xi Luo[1]

[1] *Solar Energy Research Institute, Yunnan Normal University, Kunming 650092, China*
[2] *School of Physics and Electronic Information, Yunnan Normal University, Kunming 650092, China*

Correspondence should be addressed to Ming Li, liming@ynnu.edu.cn

Received 5 April 2012; Revised 4 July 2012; Accepted 11 July 2012

Academic Editor: G. N. Tiwari

The paper established the one-dimension steady models of a trough concentrating photovoltaic/thermal system with a super cell array and a GaAs cell array, respectively, and verified the models by experiments. The gaps between calculation results and experimental results were less than 5%. Utilizing the models, the paper analyzed the influences of the characteristic parameters on the performances of the TCPV/T system with a super cell array and a GaAs cell array, respectively. The reflectivity of the parabolic mirror in the TCPV/T system was an important factor to determine the utilizing efficiency of solar energy. The performances of the TCPV/T system can be optimized by improving the mirror reflectivity and the thermal solar radiation absorptivity of the lighting plate and pursuing a suitable focal line with uniform light intensity distribution. All these works will benefit to the utilization of the trough concentrating system and the combined heat/power supply.

1. Introduction

The solar concentrating photovoltaic/thermal (CPV/T) system combines the solar cells to the low-cost concentrating collector. The solar energy flux intensity is increased by concentration and tracking sun to improve the output power of solar cells, and meanwhile the forced-circulated cooling water is utilized to ensure photovoltaic cells working normally in concentrating irradiance. The electrical power and the thermal energy are obtained simultaneously from the system. The replacement of the expensive solar cells by the trough parabolic mirrors would result into the reduction of the cost of PV power generation. The combined CPV/T system improves the comprehensive utilization of solar energy.

In 2004, the Renewable Research Institute of Australia National University performed a detailed study on a trough concentrating photovoltaic/thermal (TCPV/T) system. The efficiency of the solar cell array reached 22%, and the cost of electricity generation was reduced by 40% compared with the traditional PV system [1–3]. Mittelman et al. [4] investigated the performances and cost of a CPV/T system with single-effect absorption cooling in detail. Kribus et al. [5] presented the evaluation and design approach on a miniature concentrating PV (MCPV) system and analyzed the heat transport subsystem, the electrical and thermal performances, the manufacturing cost, and the resulting cost of energy. Tyagi et al. [6] evaluated the exergetic performance of a concentrating solar collector and studied the related parameters based on hourly solar radiation. Shanghai Jiao Tong University also investigated a CPV/T system using Fresnel lens in China, established the one-dimensional steady heat transfer model, and calculated the thermal, electrical, and exergy efficiency [7]. Southeast University of China also developed a one-dimensional steady heat transfer model for a CPVT system with fins and analyzed the effects of air mass flow rate, incident solar intensity, and wind velocity on air temperature and efficiency of air collector [8].

Our research group began to investigate the TCPV/T system in 2005. The performances of some solar cell arrays in our TCPV/T system and of the TCPV/T system with flat-plate PV module were reported in [9–12]. Based on

the previous works, this paper focuses on the establishment of mathematical models of the TCPV/T system with a super cell array and a GaAs cell array, models validation by experiments, and utilizing the models to analyze the influences of the characteristic parameters on the performances of the system. Some theoretic calculation and some experiments were performed in the work, and the corresponding results were presented. All these works are helpful to the further study on the trough concentrating system.

2. Working Principle of the TCPV/T System

Figure 1 shows the configuration of the TCPV/T system. It consists of the parabolic trough concentrator, the receiver, the sun tracking system, the electrical power output system, and the system. The solar cell arrays are pasted on the lighting plate of the receiver with thermally conductive tape, and generate electricity when the sunlight is concentrated on them. With increase of the temperature of the solar cells arrays, the electrical performance of the solar cells arrays will deteriorate. So the forced-circulated cooling water flowing in the inner cavity of the receiver is necessary to reduce the temperature of the solar cells arrays. The heated water is guided and stored in water tank for use. In order to minimize the thermal loss, the inner cavity is encased using the thermal insulation material. The solar energy collected by the system will be converted to electric power and thermal energy via the solar cell arrays and the heated cavity. When the system works, the solar concentrator tracks the sun to collect the direct radiation. The system tracks the solar altitude angle by adjusting the push rod in single-axis east-west tracking mode (trough concentrator north-south oriented).

3. Mathematical Model of the TCPV/T System

3.1. The Energy Balance Equations of the TCPV/T System. According to the configuration of TCPV/T system on Figure 2(a), the thermal network of the system is shown on Figure 2(b). The thermal network is used to describe energy flow in the TCPV/T system. The one-dimensional heat transfer model of the system is established in this paper. In order to simplify the calculation, it is assumed that

(1) the heat transfer model is a steady-state model;

(2) all of the thermal physical properties and optical parameters of the materials such as the tube, solar cell array, heat sinking tape, plate, and insulation cover are constants;

(3) The heat conductions of different components along the flowing direction are neglected. The energy flowing balance equations of the TCPV/T system are established as follows.

(a) The solar cell array absorbs and converts the solar direct radiant energy, dissipates heat to the surroundings and conducts heat to the thermally conductive tape, respectively, simultaneously generates electrical power as follows:

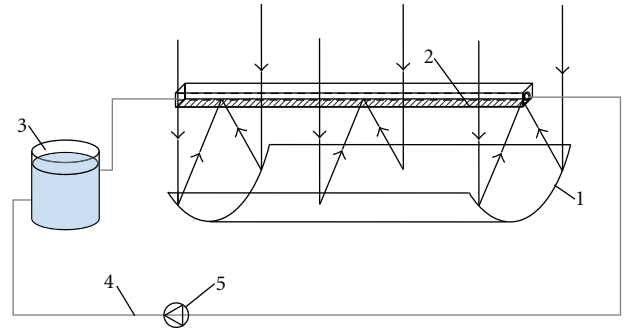

Figure 1: The configuration of the TCPV/T system. (1) Trough concentrator, (2) receiver, (3) storage tank, (4) pipe, and (5) pump.

$$\left(\frac{T_p - T_a}{R_{\text{cpa}}} + \frac{T_p - T_a}{R_{\text{rpa}}}\right) + \frac{T_p - T_B}{R_{\text{kpB}}} = Q_p - P_{\max} t, \quad (1)$$

where T_p is the average working temperature of solar cell array, °C; T_a is the ambient temperature, °C; T_B is the average temperature of the thermally conductive tape, °C; R_{cpa}, R_{rpa} are the convective and radiative heat transfer thermal resistances between solar cell array and the surroundings, respectively, Ω; R_{kpB} is the heat-conductive thermal resistance between solar cell array and the thermally conductive tape, Ω; Q_P is the solar direct radiant energy on the solar cell array, kJ; $P_{\max}$ is the maximum electrical power output, W; t is the operating time, s.

(b) The thermally conductive tape absorbs thermal energy from solar cell array and conducts heat to the aluminum-alloy plate as follows:

$$\frac{T_B - T_p}{R_{\text{kpB}}} + \frac{T_B - T_{\text{plate}}}{R_{\text{kBpl}}} = 0, \quad (2)$$

where T_{plate} is the temperature of the aluminum-alloy plate, °C; R_{kBpl} is the heat-conductive thermal resistance between the thermally conductive tape and the aluminum-alloy plate, Ω.

(c) The aluminum-alloy plate absorbs the energy from solar direct radiation and the thermally conductive tape, transfers it to the thermally insulating layer, the conduit, and radiates to the surroundings, respectively

$$\frac{T_B - T_{\text{plate}}}{R_{\text{kBpl}}} + Q_{p1} = \frac{T_{\text{plate}} - T_{\text{cover}}}{R_{\text{kplc}}} + \frac{T_{\text{plate}} - T_t}{R_{\text{kplt}}} + \left(\frac{T_{\text{plate}} - T_a}{R_{\text{rpla}}} + \frac{T_{\text{plate}} - T_a}{R_{\text{cpla}}}\right), \quad (3)$$

where Q_{P1} is the concentrating solar direct radiant energy on the aluminum alloy plate, kJ;

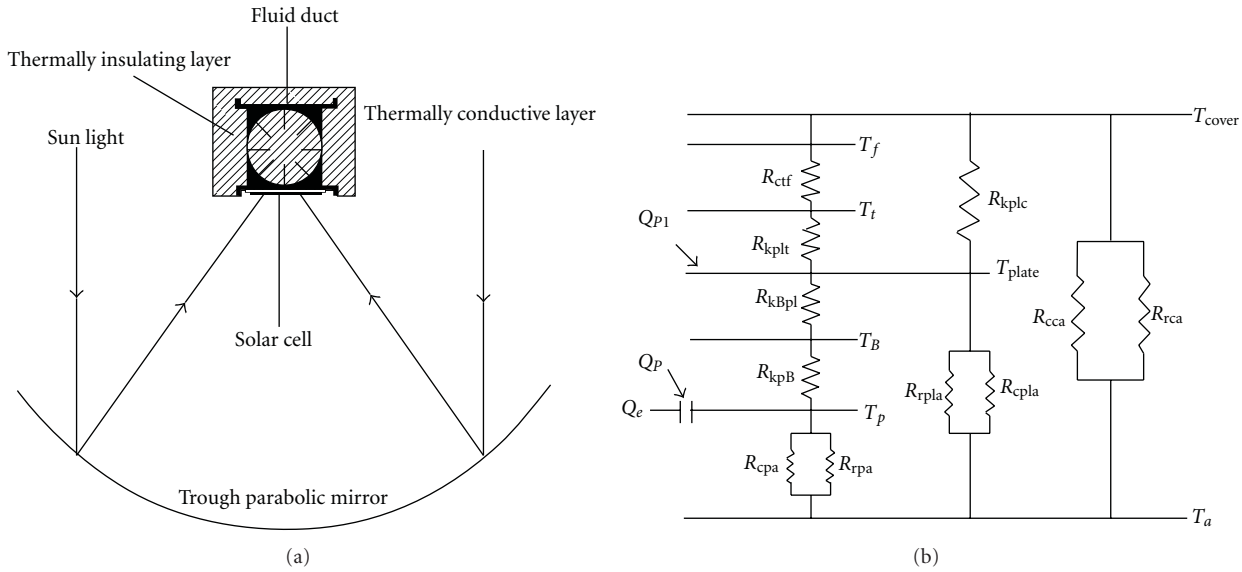

Figure 2: The thermal network describing the TCPV/T system.

T_{cover} is the average temperature of the thermally insulating layer, °C; T_t is the temperature of the conduit, °C; R_{kplc} is the heat-conductive thermal resistance between aluminum-alloy plate and the thermally insulating layer, Ω; R_{kplt} is the heat-conductive thermal resistance between aluminum-alloy plate and the conduit, Ω; R_{rpla} and R_{cpla} are the convective and radiative heat transfer thermal resistances between the aluminum-alloy plate and the surroundings, respectively, Ω.

(d) The conduit absorbs the thermal energy from the aluminum-alloy plate and transmits to the cooling fluid (water) as follows:

$$\frac{T_{plate} - T_t}{R_{kplt}} = mc_{p,f}(T_{out} - T_{in}), \tag{4}$$

where m is the fluid mass, kg; $c_{p,f}$ is the specific heat-capacity, kJ/(kg·°C); T_{out} and T_{in} are the outlet and inlet fluid temperatures, °C.

(e) The relationship between the temperature of the conduit and the inlet and outlet fluid temperatures

$$\frac{T_t - T_{out}}{T_t - T_{in}} = \exp\left(-\frac{mc_{p,f}}{A_t h_{t-f}}\right), \tag{5}$$

where A_t is internal surface area of the conduit, m^2; h_{t-f} is the convective heat transfer coefficient between the conduit and the fluid, W·m^{-2}°C^{-1}.

(f) The thermally insulating layer absorbs the thermal energy from aluminum-alloy plate and radiates heat to the surroundings as follows:

$$\frac{T_{plate} - T_{cover}}{R_{kplc}} = \left(\frac{T_{cover} - T_a}{R_{rca}} + \frac{T_{cover} - T_a}{R_{cca}}\right), \tag{6}$$

R_{rca} and R_{cca} are the radiative and convective heat transfer thermal resistance between the thermally insulating layer and the surroundings, respectively, Ω.

In above equations, the output characteristics and the average working temperature of the solar cell array will be obtained by an iterative approach. By assuming the average working temperature of the solar cell array firstly, and adding the electrical power output to calculate the maximum electrical power output, then substitute them into the thermal balance equations. The approach is repeated to get more accurate working temperature and the maximum electrical power output of solar cell array.

3.2. The Electrical Performance of the Solar Cell Array. The current equation of the solar cell is defined as follows:

$$I = I_L - I_0\left\{\exp\left[\frac{q(V + IR_s)}{AkT_p}\right] - 1\right\}, \tag{7}$$

where I_L is the photocurrent, A; I_0 is the reverse saturation current of the diode, A; q is the elementary charge, C; V is the load voltage, V; R_s is the series resistance, Ω; A is the quality factor of the diode; k is the Boltzmann's constant; T_p is the average working temperature of solar cell array, °C.

The solar cells are connected in series to constitute the solar cell array. The amount of the solar cell is n, the quality factor of the PN junction, the series resistances and the open-circuit voltage of the cell array all increase to n times by those of each solar cell. So the electrical power output of the solar cell array is defined as

$$P = I\left[\frac{nAkT_p}{q}\ln\left(\frac{I_L - I}{I_0} + 1\right) - nIR_s\right]. \tag{8}$$

As for a triple-junction GaAs solar cell array, it is hard to calculate the specific values for each junction

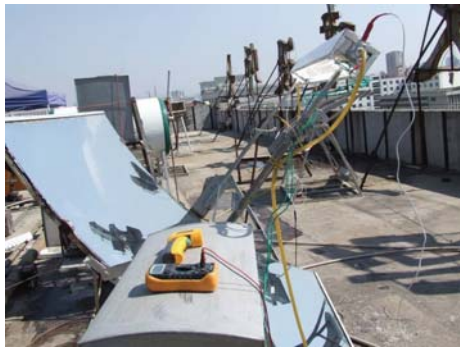

Figure 3: The setup of the TCPV/T system.

according to the current (7). But we can get the fitted empirical formula on the basis of experiments. The electrical efficiency corresponding to the maximum electrical power of photovoltaic power generation appears linear with the temperatures of the solar cell array.

$$\eta_{\text{mp}} = \eta_{\text{mp,ref}} - \mu_{p,\text{mp}}\left(T_p - T_{\text{ref}}\right), \tag{9}$$

η_{mp} is the electrical efficiency of solar cell array, %; $\eta_{\text{mp,ref}}$ is the reference efficiency obtained at reference temperature, %; $\mu_{p,\text{mp}}$ is the related coefficient between the electrical efficiency of the solar cell array and the temperature, %/°C; T_{ref} is the reference temperature 25°C.

The electrical power output of the triple-junction GaAs solar cell array is defined as

$$P_{\max} = \frac{\eta_{\text{mp}} Q_p}{t}, \tag{10}$$

where $P_{\max}$ is the maximum electrical power output, W; Q_P is the solar direct radiant energy on the solar cell array, kJ; t is the working time, s.

3.3. The Evaluation of the TCPV/T System. The TCPV/T system can produce electrical power and thermal power simultaneously. Many researchers use the total efficiency η_0, the sum of the electrical efficiency η_e and the thermal efficiency η_t to evaluate the performance of the PV/T system [13–15]. The thermal efficiency η_t and the electrical efficiency η_e of the TCPV/T system are given by

$$\eta_t = \frac{mc_{p,f}(T_{\text{out}} - T_{\text{in}})}{I_d A_m}, \qquad \eta_e = \frac{P_{\max}}{I_d A_m}, \tag{11}$$

where I_d is the solar direct radiation, W/m^2; A_m is the effective area of the reflecting mirror, m^2.

It is obviously unreasonable to use the total efficiency for evaluating the performance of the TCPV/T system because electrical energy and thermal energy have different energy quality. The reference [14] uses the quantity of economizing primary energy source to evaluate the performance of the PV/T system. Although electrical energy and thermal energy are distinguished to some extent, the difference of the energy quality is still not considered. It is clear that using available energy (exergy) as a performance assessment standard is a reasonable method. The exergy efficiency η_{exergy} of the TCPV/T system is shown as follows [2, 14]:

$$\eta_{\text{exergy}} = \frac{\eta_e I_d A_m + mc_{p,f}\{[h - (T_a + 273.15)\text{s}]_{\text{out}} - [h - (T_a + 273.15)s]_{\text{in}}\}}{I_d \times (1 - (T_a + 273.15)/5777)}, \tag{12}$$

where h is the specific enthalpy, kJ/kg; s is the specific entropy, kJ/(kg·°C).

4. Validation of the Model by Experiments

The experimental setup of the TCPV/T system with a geometric concentration ratio of 16.92 is shown in Figure 3. The effective aperture area of the trough parabolic mirror is 1.95 m^2, and the mirror reflectivity is 0.69 (tested by ultraviolet spectrophotometer UV3600). The focal length and focal spot width are 1.20 m and 0.10 m, respectively. The energy flux concentration ratio of the system is 10.27 tested by the laser power instrument MODEL460-1A from EG&G Gamma Scientific San Diego, CA. The laser power meter can measure the intensities of different wavelength. Averaging the intensities, then divided by the direct solar radiation, we can obtain the energy flux concentration ratio. The length, width, and height of the receiver are 1.50 m, 0.12 m, and 0.09 m, respectively. Insider diameter of the conduit is 0.03 m. The related parameters of all materials are shown in Table 1.

The total radiation is measured using the pyranometer TBQ-2 with an accuracy of ±2%. The direct radiation is measured with the pyrheliometer TBS2-2 with an accuracy of ±2%. The current and voltage of the solar cell arrays are measured with a digital multimeter (Fluke 17B) with an accuracy of ±1.5%. The working temperature of solar cells is measured with a thermometer (Fluke 63) with an accuracy of ±1°C. The inlet and outlet temperatures of the cooling fluid are measured using the thermocouple temperature probe PT100 with an accuracy of ±0.1°C. The mass flow is measured by a glass rotameter with an accuracy of ±0.0014 kg/s. The calculation results based on the theoretical model are verified with the following experimental results.

4.1. The Electrical Performance of the Super Cell Array Based on the TCPV/T System. The super cell array shown in

Table 1: Parameters of structure materials of the system.

	Super cell array					GaAs cell array				
	Cell array	Thermally conductive tape	Aluminum alloy plate	Conduit	Thermally insulating layer	Cell array	Thermally conductive tape	Aluminum alloy plate	Conduit	Thermally insulating layer
Thermal conductivity coefficient λ ($W \cdot m^2/^\circ C$)	150.0	0.42	107.0	107.0	0.04	55.0	0.42	107.0	107.0	0.04
Absorptivity a	0.80	0.30	0.60	—	0.20	0.85	0.30	0.60	—	0.20
Emissivity p	0.35	—	0.10	—	0.20	0.30	—	0.10	—	0.20
Thickness d (mm)	0.30	0.40	5.00	4.00	42.50	0.70	0.40	5.00	4.00	42.50

Figure 4: The photograph of the super cell array.

Figure 4 is a mono-Si solar cell from the USA, named after the solar cell used for space power. The specification of each cell is 6.2 cm × 7.1 cm. The open-circuit voltage and the short-circuit current of each cell are 0.55 V and 1.45 A, respectively, with the radiation of 1000 W/m^2 and the cell temperature of 25°C. The super cell array composed of 16 pieces cell with series connection is tested on the TCPV/T system. The experimental results and simulation results are shown in Figure 5. We can see the simulating curves approximately approach to the experimental testing curves. In concentrating irradiance, the *I-V* curves approximate linear and the output performances become poor due to its high series resistance.

4.2. The Electrical Performance of a Triple-Junction GaAs Cell Array Based on the TCPV/T System. The GaAs cell shown in Figure 6 is a triple-junction solar cell, which is made in Shanghai of China, the specification of each cell is 3.0 cm × 4.0 cm. In nonconcentrating condition, the open-circuit voltage and the short-circuit current of each cell are 2.58 V and 0.17 A, respectively, with the radiation of 1000 W/m^2 and the cell temperature of 25°C. The GaAs cell array composed of 40 pieces series-connected cells is tested on the TCPV/T system. According to the experimental testing results, we get the fitted empirical formula of the GaAs solar cell array electrical efficiency which working in concentrating irradiance shown as follows:

$$\eta_{\mathrm{mp}} = 26.06\% - 0.0886\%\left(T_p - T_{\mathrm{ref}}\right). \quad (13)$$

4.3. The Electrical Performances and Thermal Performances of the TCPV/T System. The electrical performances and thermal performances of the TCPV/T system with a super cell array and a GaAs cell array are characterized, respectively. All results were achieved with the concentrated irradiance, and the concentration ration was 10.27. Theoretical calculation results and experimental results are shown in Table 2. The gaps between the theoretical calculation results and experimental results are less than 5%. The model can accurately elucidate the performance characterization of the TCPV/T system. From (13), the maximum efficiency of 26.06% for the GaAs solar cell array is achieved at the reference temperature of 25°C. However, the maximum efficiency in our experiments is around 5.8%. This is because the cell temperature rises significantly with the concentrated irradiance, so the cells are hardly to reach their optimal working temperature.

Although the single-diode equation was applied for the super cell array and the empirical linear equation was applied for the temperature dependence in case of the GaAs module, the electrical efficiencies from the theoretical calculations agree with the measured results well for both cases of cells in Table 2. Comparing with the super cell, the GaAs cell has better high temperature characteristics. In the concentrated irradiance scope of our experiments, the characteristic of the GaAs cell still kept linear, so the empirical linear equation for the GaAs module is appropriate. However, the empirical linear equation for the super cell maybe inappropriate in such concentrated irradiance. The single-diode model could usually improve the model response/accuracy with respect the empirical equation, and the single-diode equation could illustrate the super cell well in our case.

5. Analysis on Characteristic Parameters of the TCPV/T System with a Super Cell Array and a GaAs Cell Array

Based on the model, we analyze the influences of the related characteristic parameters on the performance of the TCPV/T system with a super cell array and a GaAs cell array, respectively. The related characteristic parameters include mirror reflectivity, width of focal spot, thermal absorptivity

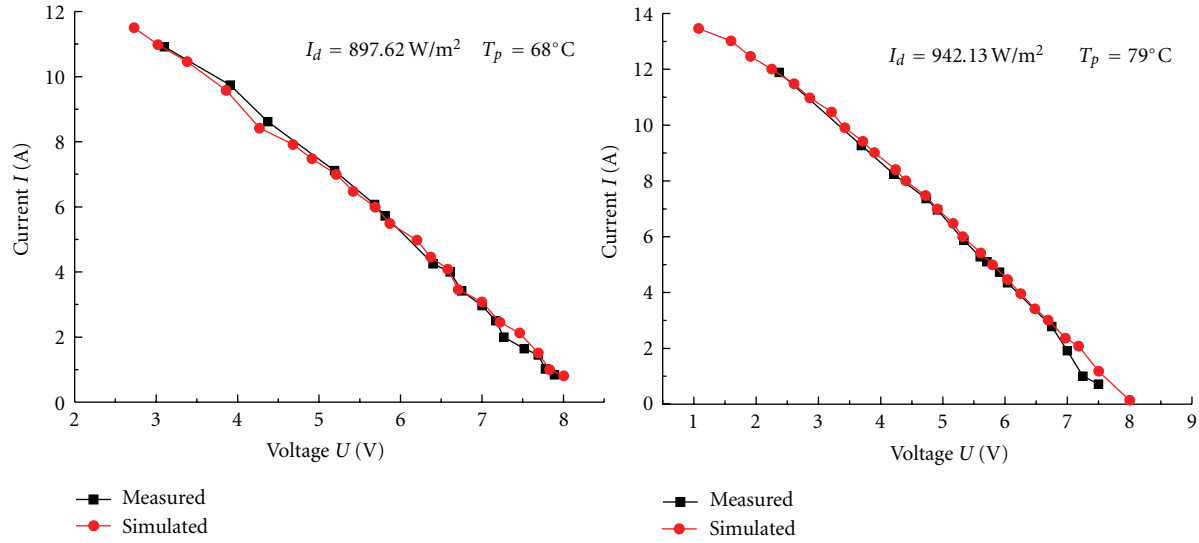

Figure 5: The I-V characteristics of the super cell array comparisons between experiments and simulations.

Table 2: The theoretical calculation results and the experimental results of the TCPV/T system.

(a)

	I_d (W/m^2)	m (kg)	T_{in} (°C)	T_a (°C)	v_w (m/s^1)	T_{out} (°C)		T_p/(°C)	
	—	—	—	—	—	M	S	M	S
Super cell array	905.1	0.0050	22.6	16.7	1.7	50.1	50.5	83.2	84.40
	953.7	0.0111	24.1	16.4	3.5	39.0	38.6	57.6	56.26
GaAs cell array	902.1	0.008	20.1	19.9	1.0	39.1	38.6	61.4	60.20
	894.2	0.008	19.8	20.2	2.0	38.2	37.8	59.4	58.3

(b)

	P_{max} (W)		η_t (%)		η_e (%)		η_0 (%)	
	M	S	M	S	M	S	M	S
Super cell array	34.11	33.44	32.56	33.04	1.93	1.89	34.50	34.93
	41.33	42.19	37.17	36.18	2.22	2.27	39.40	38.44
GaAs cell array	100.80	101.94	36.12	35.17	5.73	5.80	41.85	40.96
	101.92	102.71	35.29	34.52	5.85	5.89	41.13	40.41

(I_d—direct radiation, m—fluid mass, T_{in}—inlet temperature of fluid, T_a—ambient temperature, v_w—wind speed, T_{out}—outlet temperature of fluid, T_p—temperature of solar cell array, P_{max}—the maximum power output of system, η_0—total efficiency; M—measured, S—simulated).

Figure 6: The photograph of the GaAs solar cell array.

of the lighting plate, and solar direct radiation. In order to conveniently calculate and compare, it is supposed that the water mass flow is 0.008 kg/s, the inlet temperature of fluid is 20.0°C, solar direct radiation is 900 W/m^2, and the ambient temperature and wind speed are 20.0°C and 1.0 m/s, respectively, in the calculation.

5.1. The Effect of the Mirror Reflectivity. The TCPV/T system reflects and concentrates the solar radiation to the focal spot by using the trough parabolic mirrors. The light intensity can be improved to a high level. It is clearly to see from Figure 7 that with increasing of mirror reflectivity from 0.5 to 0.95, the electrical efficiency, the thermal efficiency, and the exergy efficiency increase by 0.02 times, 0.94 times, 0.62 times (for the TCPV/T system with a super cell array) and 0.65 times, 0.90 times, 0.93 times (for the TCPV/T system with a GaAs cell array). The electrical efficiency of the super cell array TCPV/T system increases firstly and then drops slightly, that is, due to the concentration ratio of 8.46 is preferred for the optimum output performance of the super cell array (from [16], we can get the conclusion that the parabolic mirror reflectivity of the TCPV/T

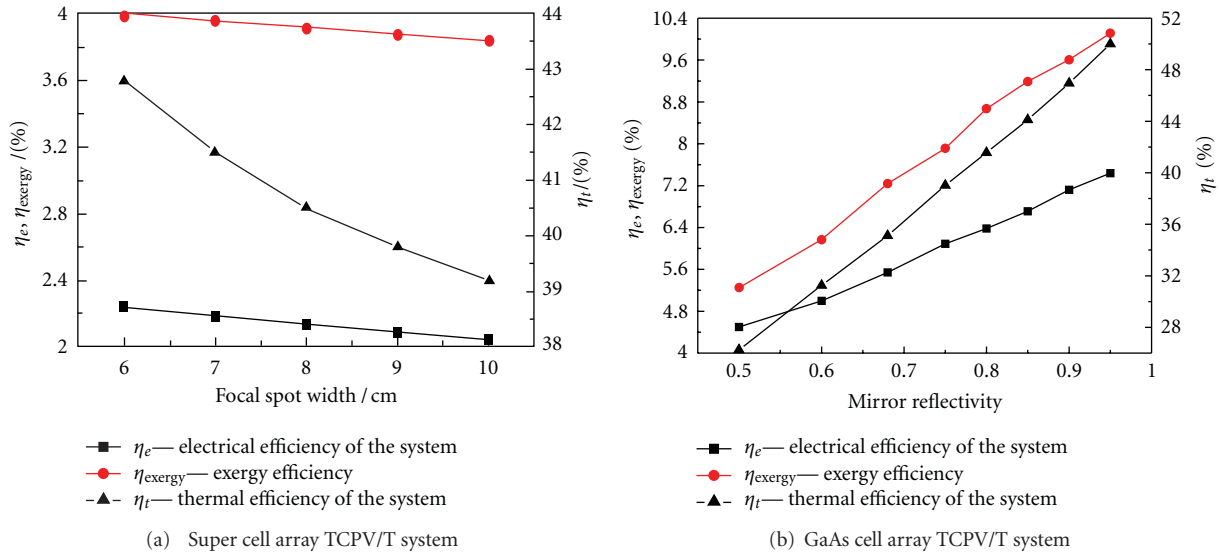

(a) Super cell array TCPV/T system (b) GaAs cell array TCPV/T system

Figure 7: The influences of mirror reflectivity on the system performances.

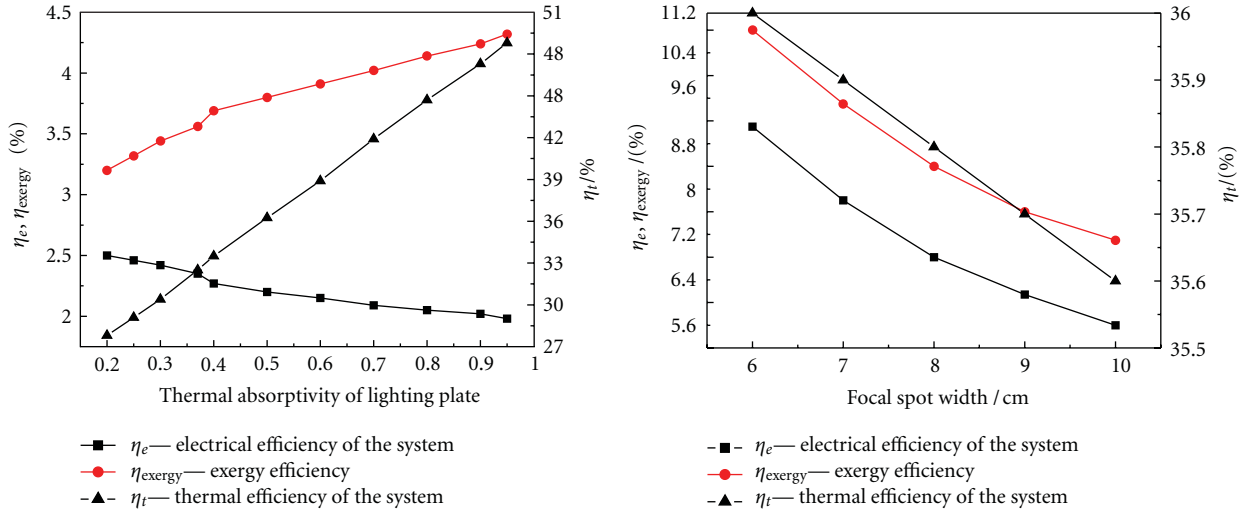

(a) Super cell array TCPV/T system (b) GaAs cell array TCPV/T system

Figure 8: The influences of focal spot widths on the system performances.

system is an important factor to determine the utilizing efficiency of solar energy. So it is an effective way to improve the mirror reflectivity for optimizing the TCPV/T system.

5.2. The Effect of the Focal Line Width. The sunlight is concentrated on the focal line which has high-energy flux density. With the same parabolic mirror, the narrower focal line has a higher energy flux density. From Figure 8, we can see the electrical efficiency, the thermal efficiency, and the exergy efficiency all drops with increasing of focal line widths. The widths of the Super cell array and GaAs cell array are 6.2 cm and 4.0 cm, respectively. When the focal line width is larger than the width of solar cell array, parts of solar energy will be wasted. So a suitable focal line with uniform light intensity distribution indicates a high utilizing efficiency of solar energy.

5.3. The Effect of the Thermal Absorptivity of the Lighting Plate. From Figure 9, although the high thermal absorptivity results in a high-operating temperature of solar cell arrays and a lower electrical efficiency, the thermal efficiency, and exergy efficiency increase by 0.75 times, 0.35 times (for super cell array TCPV/T system) and 1.38 times, 0.14 times (for GaAs cell array TCPV/T system) with the thermal absorptivity of the lighting plate increasing from 0.2 to 0.9.

5.4. The Effect of Solar Direct Radiations. For the concentrating system, only the solar direct radiation can be utilized,

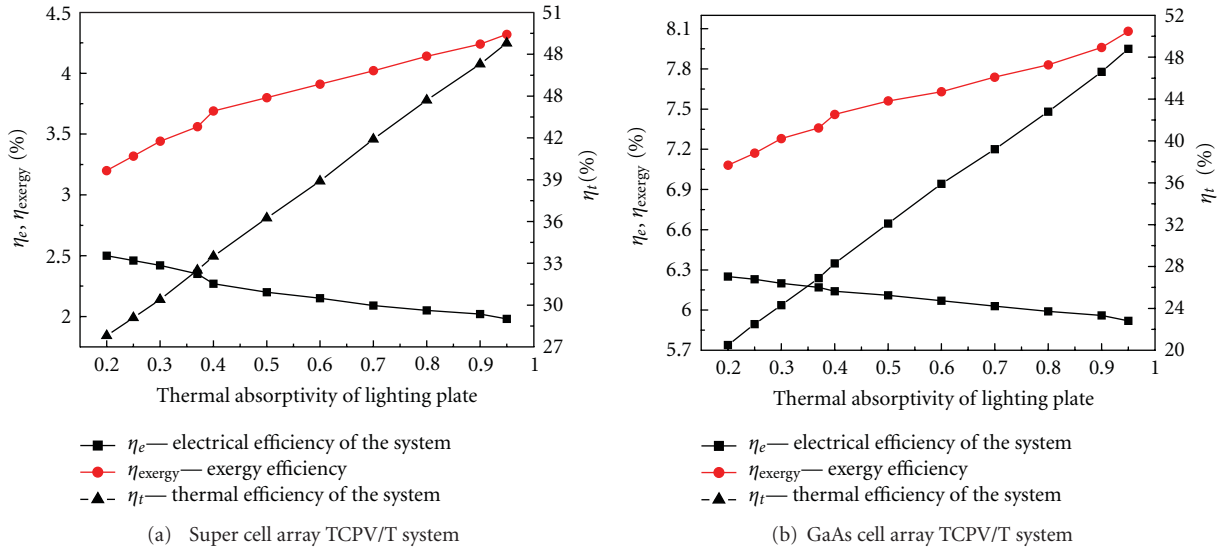

(a) Super cell array TCPV/T system

(b) GaAs cell array TCPV/T system

Figure 9: The influences of thermal absorptivity of lighting plate on the system performances.

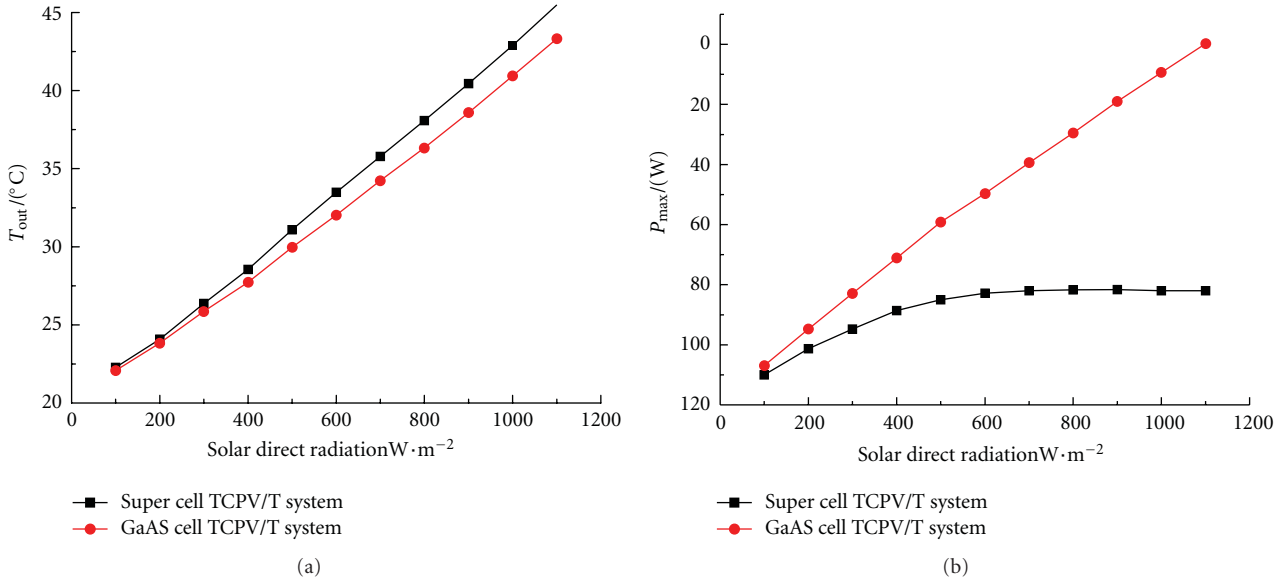

(a)

(b)

Figure 10: The influences of solar direct radiation on the system performances.

it contributes to the input energy, directly influences the maximum electrical power output of solar cell array and outlet temperature of fluid directly, so the effect of solar direct radiation to the performances of TCPV/T system should be discussed.

Figure 10 shows that the outlet fluid temperatures of the TCPV/T systems with super cell array and GaAs cell array increase linearly with the rising of solar direct radiation. With the rising of solar direct radiation, the maximum electrical power output of the GaAs cell array TCPV/T system increases linearly, but that of the super cell array TCPV/T system increases firstly and then tends to be steady. We can see from Figure 10 that the optimum solar direct radiation for the super cell array TCPV/T system is 700 W/m^2.

6. Conclusions

(1) The energy flow balance equations of the CPV/T system are deduced, and the one-dimension steady models of a trough concentrating photovoltaic/thermal system with a Super cell array and a GaAs cell array are established, respectively.

(2) In our validation experiments using a 2 m^2 TCPV/T system, the gaps between the theoretical calculation results based on the above models and the experimental results are less than 5%, which indicate that the models are valid.

(3) Based on the model, we analyze the influences of the related characteristic parameters such as mirror

reflectivity, width of focal spot, thermal absorptivity of the lighting plate, and solar direct radiation on the performances of the TCPV/T system with a super cell array and a GaAs cell array, respectively. The parabolic mirror reflectivity of the TCPV/T system is an important factor to determine the utilizing efficiency of solar energy. We can optimize the TCPV/T system by improving the mirror reflectivity and thermal absorptivity of the lighting plate, pursuing a suitable focal line with uniform light intensity distribution.

Nomenclature

A : Quality factor of the diode
A_m: Effective area of the reflecting mirror (m^2)
A_t: Internal surface area of the conduit (m^2)
$c_{p,f}$: Specific heat capacity (kJ/(kg·°C))
h: The specific enthalpy (kJ/kg)
h_{t-f}: Convective heat transfer coefficient between the conduit and the fluid ($W/(m^2 °C^1)$)
I: Current (A)
I_0: Reverse saturation current of the diode (A)
I_d: Solar direct radiation (W/m^2)
I_L: Photocurrent (A)
k: Boltzmann' constant
m: Fluid mass (kg)
n: Pieces of solar cell
η_{mp}: Electrical efficiency of solar cell array (%)
$\eta_{mp,ref}$: Reference efficiency (%)
η_t: Thermal efficiency of system (%)
η_e: Electrical efficiency of system (%)
η_{exergy}: Exergy efficiency (%)
P_{max}: Maximum electrical power output (W)
q: Elementary charge (C)
Q_P: Solar direct radiant energy on the solar cell array (kJ)
Q_{P1}: Concentrating solar direct radiant energy on the aluminum alloy plate (kJ)
R_s: Series resistance (Ω)
R_{cpa}: Convective heat transfer thermal resistances between solar cell array and the surroundings (Ω)
R_{rpa}: Radiative heat transfer thermal resistances between solar cell array and the surroundings (Ω)
R_{kpB}: Heat-conductive thermal resistance between solar cell array and the thermally conductive tape (Ω)
R_{kBpl}: Heat-conductive thermal resistance between the thermally conductive tape and the aluminum alloy plate (Ω)
R_{kplc}: Heat-conductive thermal resistance between aluminum alloy plate and the thermally insulating layer (Ω)
R_{kplt}: Heat-conductive thermal resistance between aluminum alloy plate and the conduit (Ω)
R_{rpla}: Convective heat transfer thermal resistances between the aluminum alloy plate and the surroundings (Ω)
R_{cpla}: Radiative heat transfer thermal resistances between the aluminum alloy plate and the surroundings (Ω)
R_{rca}: Radiative heat transfer thermal resistance between the thermally insulating layer and the surroundings (Ω)
R_{cca}: Convective heat transfer thermal resistance between the thermally insulating layer and the surroundings (Ω)
s: The specific entropy (kJ/(kg·°C))
t: Operating time (s)
T_a: Ambient temperature (°C)
T_B: Temperature of the thermally conductive tape (°C)
T_{cover}: Average temperature of the thermally insulating layer (°C)
T_p: Working temperature of solar cell array (°C)
T_{plate}: Temperature of the aluminum alloy plate (°C)
T_t: Temperature of the conduit (°C)
T_{out}: Outlet temperature of fluid (°C)
T_{in}: Inlet temperature of fluid (°C)
T_{ref}: The reference temperature (°C)
$\mu_{p,mp}$: Related coefficient between the electrical efficiency of the solar cell array and the temperature (%/°C)
V: Load voltage (V).

Acknowledgments

The present study was supported by National Natural Science Foundation, China (Grant nos. 50966004, 51106134, and U1137605), the program of Changjiang Scholars and Innovative Research Team in Ministry of Education, China.

References

[1] J. S. Coventry, "Performance of a concentrating photovoltaic/thermal solar collector," *Solar Energy*, vol. 78, no. 2, pp. 211–222, 2005.
[2] J. S. Coventry and K. Lovegrove, "Development of an approach to compare the 'value' of electrical and thermal output from a domestic PV/thermal system," *Solar Energy*, vol. 75, no. 1, pp. 63–72, 2003.
[3] J. Conventry, E. Franklin, and A. Blakers, "Thermal and electrical performance of a concentrating PV/Thermal collector: results from the ANU CHAPS collector," in *Proceedings of the 40th Conference of the Australia and New Zealand Solar Energy Society (ANZSES '02)*, Newcastle, Australia, 2002.
[4] G. Mittelman, A. Kribus, and A. Dayan, "Solar cooling with concentrating photovoltaic/thermal (CPVT) systems," *Energy Conversion and Management*, vol. 48, no. 9, pp. 2481–2490, 2007.
[5] A. Kribus, D. Kaftori, G. Mittelman, A. Hirshfeld, Y. Flitsanov, and A. Dayan, "A miniature concentrating photovoltaic and thermal system," *Energy Conversion and Management*, vol. 47, no. 20, pp. 3582–3590, 2006.
[6] S. K. Tyagi, S. W. Wang, M. K. Singhal, S. C. Kaushik, and S. R. Park, "Exergy analysis and parametric study of concentrating type solar collectors," *International Journal of Thermal Sciences*, vol. 46, no. 12, pp. 1304–1310, 2007.
[7] H. Zhai, Y. J. Dai, and J. Y. Wu, "Investigation of concentrating solar photovoltaic/thermal system performance based on Fresnel lens," *Journal of Engineering Thermophysics*, vol. 28, no. 5, pp. 725–728, 2007.
[8] J. Sun and M. H. Shi, "Energy and exergy efficiency analysis of a solar concentrating PV/T air heating collector," *Journal*

of Engineering Thermophysics, vol. 30, no. 11, pp. 1929–1932, 2009.

[9] M. Li, G. L. Li, X. Ji, F. Yin, and L. Xu, "The performance analysis of the Trough Concentrating Solar Photovoltaic/Thermal system," *Energy Conversion and Management*, vol. 52, no. 6, pp. 2378–2383, 2011.

[10] L. Ming, J. Xu, L. Guo-liang et al., "Performance investigation and optimization of the Trough Concentrating Photovoltaic/Thermal system," *Solar Energy*, vol. 85, no. 5, pp. 1028–1034, 2011.

[11] M. Xiang, M. Li, L. L. Wang et al., "Investigation of performance on Trough Concentrating Solar Photovoltaic/Thermal System based on super cells," *Acta Optica Sinica*, vol. 29, no. 2, pp. 482–489, 2009.

[12] Y. F. Wang, M. Li, W. X. Lin et al., "Performance analysis on solar cell modules of flat-plate and Trough Concentrating Photovoltaic System," *Acta Optica Sinica*, vol. 29, no. 8, pp. 2287–2292, 2009.

[13] J. Ji, J. P. Lu, T. T. Chow, W. He, and G. Pei, "A sensitivity study of a hybrid photovoltaic/thermal water-heating system with natural circulation," *Applied Energy*, vol. 84, no. 2, pp. 222–237, 2007.

[14] T. Bergene and O. M. Løvvik, "Model calculations on a flat-plate solar heat collector with integrated solar cells," *Solar Energy*, vol. 55, no. 6, pp. 453–462, 1995.

[15] B. J. Huang, W. C. Hung, and F. S. Sun, "Performance evaluation of solar photovoltaic/thermal systems," *Solar Energy*, vol. 70, no. 5, pp. 443–448, 2001.

[16] Y. F. Xu, M. Li, L. L. Wang et al., "The effect of concentrated light intensity on output performance of solar cell arrays," *Acta Physica Sinica*, vol. 58, no. 11, pp. 8067–8076, 2009.

Hindawi Publishing Corporation
International Journal of Photoenergy
Volume 2012, Article ID 101968, 9 pages
doi:10.1155/2012/101968

Research Article

Environmental Life-Cycle Analysis of Hybrid Solar Photovoltaic/Thermal Systems for Use in Hong Kong

Tin-Tai Chow[1] and Jie Ji[2]

[1] *BEETRU, Division of Building Science and Technology, City University of Hong Kong, Kowloon, Hong Kong*
[2] *Department of Thermal Science and Energy Engineering, University of Science and Technology of China, Hefei 230026, China*

Correspondence should be addressed to Tin-Tai Chow, bsttchow@cityu.edu.hk

Received 4 May 2012; Accepted 15 August 2012

Academic Editor: Christophe Menezo

While sheet-and-tube absorber is generally recommended for flat-plate photovoltaic/thermal (PV/T) collector design because of the simplicity and promising performance, the use of rectangular-channel absorber is also tested to be a good alternative. Before a new energy technology, like PV/T, is fully implemented, its environmental superiority over the competing options should be assessed, for instance, by evaluating its consumption levels throughout its production and service life. Although there have been a plenty of environmental life-cycle assessments on the domestic solar hot water systems and PV systems, the related works on hybrid solar PV/T systems have been very few. So far there is no reported work on the assessment of PV/T collector with channel-type absorber design. This paper reports an evaluation of the energy payback time and the greenhouse gas payback time of free-standing and building-integrated PV/T systems in Hong Kong. This is based on two case studies of PV/T collectors with modular channel-type aluminium absorbers. The results confirm the long-term environmental benefits of PV/T applications.

1. Introduction

A photovoltaic/thermal (PV/T) system is a combination of photovoltaic (PV) and solar thermal devices that generate both electricity and heat energy from one integrated system. With solar cells as (part of) the thermal absorber, the hybrid design is able to maximize the energy output from an allocated space reserved for solar application. Air and/or water can be used as the heat removal fluid(s) to lower the solar cell working temperature and to improve the electricity conversion efficiency. Comparatively, the water-type product design provides more effective cooling than the air-type counterpart because of the favorable thermal properties. Those with flat plate collectors meet well the low temperature water heating system requirements. They are also ideal for preheating purposes when hot water at higher temperature is required.

While sheet-and-tube absorber is one common feature in flat-plate collectors, the use of rectangular-channel absorbers also has been examined extensively [1–3]. An aluminum water-in-channel-type PV/T collector design is recommended by the authors, with the prototypes well-tested under both free-standing and building-integrated manners [4, 5]. Through the adoption of the channel absorber design, the potential problem of low fin efficiency can be readily improved. Based on the thermosyphon working principle, the collector performance is found to have geographical dependence and working well at the warmer climate zones. In the Asia Pacific region, most large cities are dominated by air-conditioned buildings where space cooling demands are high. In these buildings, the exposed facades provide very good opportunity for accommodating the building integrated systems, hence, the BiPV/T. When a part of the solar radiation that falls on the building façade is directly converted to useful thermal and electric power, the portion of solar energy transmitted through the external facade is reduced. Hence, the space cooling load is reduced. Through dynamic simulation with the use of experimentally validated system models and the typical meteorological year (TMY) data of Hong Kong, the cost payback time (CPBT) of free-standing and building-integrated PV/T systems were found 12.1 and 13.8 years, respectively [6, 7]. The assessments were taken, respectively, at their best tilted and vertical collector positions for maximizing their system outputs. It is expected

that these CPBT will be gradually shortened as the PV technology is in progressive advancement. In this paper, the environmental life-cycle analysis (LCA) of such hybrid solar systems as applied in Hong Kong is reported.

2. Environmental Life-Cycle Analysis

LCA is a technique for assessing various aspects associated with development of a product and its potential impact throughout a product's life [8]. Before a new energy technology is fully implemented, the environmental superiority over competing options can be asserted by evaluating its consumption levels (such as cost investments, energy uses, and GHG emissions) throughout its entire production and service life. In terms of economic analysis, a simplified approach is to ignore the time element so the cost payback time (CPBT) can be used. This is by adding together the cash inflows from successive years until the cumulative cash inflow is the same as the required investment. In analogy to the economical evaluation, two environmental cost-benefit parameters, the energy payback time (EPBT) and greenhouse gas payback time (GPBT), can be used to evaluate the time period after which the real environmental benefit starts [9]. EPBT is the period that a system has to be in operation in order to save the amount of primary energy that has been spent for production, operation, and maintenance of the system. It is the ratio of embodied energy to annual net energy output. In a BiPV/T system, for example,

$$\text{EPBT} = \frac{\sum_{\text{pvt}} + \sum_{\text{bos}} - \sum_{\text{mtl}}}{E_{\text{pv}} + E_t + E_{\text{ac}} - E_{\text{om}}}, \quad (1)$$

where $\sum_{\text{pvt}}$, $\sum_{\text{bos}}$ and $\sum_{\text{mtl}}$, are, respectively, the embodied energy of the PV/T collectors, of the balance of system (BOS), and of the replaced building materials; E_{pv} is the annual useful electricity output, E_t the annual useful heat gain (equivalent), E_{ac} the annual electricity saving of the HVAC system due to the space thermal load reduction, and E_{om} is the annual electricity consumed in system operation and maintenance activities. $\sum_{\text{mtl}}$ and E_{ac} can be omitted in free-stand PV/T system evaluation. Hence,

$$\text{EPBT} = \frac{\sum_{\text{pvt}} + \sum_{\text{bos}}}{E_{\text{pv}} + E_t - E_{\text{om}}}. \quad (2)$$

Similarly, in terms of greenhouse gas (GHG) emission, for BiPV/T

$$\text{GPBT} = \frac{\Omega_{\text{pvt}} + \Omega_{\text{bos}} - \Omega_{\text{mtl}}}{Z_{\text{pv}} + Z_t + Z_{\text{ac}}}, \quad (3)$$

where Ω stands for the embodied GHG (or carbon dioxide equivalent) emission and Z the reduction of annual GHG emission from the local power plant owing to the BiPV/T operation. And for the free-stand system,

$$\text{GPBT} = \frac{\Omega_{\text{pvt}} + \Omega_{\text{bos}}}{Z_{\text{pv}} + Z_t}. \quad (4)$$

Thus EPBT and GPBT are functions of the related energy system performance and their environmental impacts, like those of the power utilities, the building systems, local and overseas manufacturing, and transportation and on-site handling of PV/T collector system as a whole.

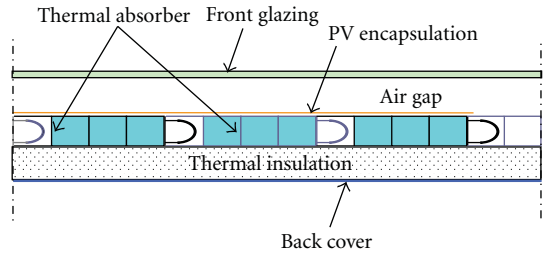

Figure 1: Cross-sectional view of the PV/T collector showing several absorber modules in integration (N.T.S).

Figure 2: Front view of free-stand PV/T collector system.

3. Aluminum Rectangular-Channel PV/T Systems

The sectional view of an aluminum rectangular-channel PV/T collector developed by the authors is shown in Figure 1. It is composed of the following layers: (i) front low-iron glass cover, (ii) crystalline silicon (c-Si) PV encapsulation, (iii) metallic thermal absorber constructed from extruded aluminum, (iv) thermal insulation layer with glass wool, and (v) back-cover steel sheet. The PV encapsulation includes TPT (tedlar-polyester-tedlar) and EVA (ethylene-vinyl acetate) layers at both sides of the solar cells. The rectangular-channel design strengthens the heat transfer and structural durability.

In a free-stand thermosyphon system, the PV/T collector carries a water tank with the natural water circulation via inter-connecting pipes. Figure 2 shows the external view. Water enters the collector at the lower header and leaves via the upper header. Table 1 lists the technical data of this PV/T collector for free-stand applications.

Figure 3: Front view of BiPV/T system with water tank at top of wall.

A BiPV/T system, on the other hand, is composed of an array of PV/T collectors that are integrated to the external wall of an air-conditioned building. See Figure 3 for reference. The water tank is located at the roof-top and the water circulation is again by means of thermosyphon. Table 2 lists the technical data of the BiPV/T wall system in our study.

4. Review of Previous Works on Flat Plate Collector Systems

4.1. Solar Hot Water Systems. The LCA works on domestic solar hot water (DSHW) systems in majority were from EU countries [10–13]. Streicher et al. [10] evaluated the EPBT of solar thermal systems by dividing the system into components. The cumulative energy demand was obtained by multiplying the weight of the main components with their respective cumulative energy demand values. They estimated that in Germany the DSHW systems have EPBT from 1.3 to 2.3 years. In their study, construction credit was given to the collector system in integrated roof-mounting mode. This is for the savings in building materials, transportation, and construction works. The collector itself accounts for 89% and 85% of the total embodied energy in the roof-integrated and open-stand systems, respectively. Tsilingiridis et al. [11] found that in Greece the materials used, including steel and copper, have the major contribution to the environmental impacts. Ardente et al. [12] found that in Italy the indirect emissions (related to production of raw materials) are about 80–90% of the overall GHG releases. Kalogirou [13] worked on a thermosyphon DSHW system in Cyprus. The system thermal performance was evaluated by dynamic simulation program. The LCA determined that 77% of the embodied energy goes to the collector panels, 15% goes to the steel frame, 5% goes to piping, and the remaining accounts for less than 3% of the total. Considerable amounts of GHG can be saved. The EPBT was estimated around 1.1 year.

Outside Europe, the study of Crawford et al. [14] in Australia showed that although the CPBT of DSHW systems can be 10 years or more, the corresponding GPBT can be only around 2.5–5 years. In their study, a conversion factor of 60 kg CO_2 eq/GJ was used to determine the GHG emission from the cumulative energy of the entire system. Arif [15] evaluated the environmental performance of DSHW systems in India. Based on the 100 litre-per-day and steady year-round usage, the EPBT was estimated 1.6–2.6 years, all depending on the local climates and also the collector materials in use. In the LCA work of Hang et al. [16] on a range of solar hot water systems in USA; dynamic thermal simulation was again applied.

4.2. PV Systems. In the last decades, plenty of works have been reported on life cycle performance of PV systems in both free-stand and building-integrated manners. The

Table 1: Collector and technical design data of free-stand PV/T system.

Design parameters	Data
Glazing (low-iron glass)	
Thickness	0.004 m
Emissivity	0.88
Extinction coefficient	26/m
Refraction index	1.526
Depth of air gap underneath	0.025 m
PV encapsulation (TPT + EVA + solar cell + EVA + TPT + silicon gel)	
Solar cell type	single-crystalline silicon
Cell area	1.11 m^2
Cell electrical efficiency at STC	13%
Solar cell temperature coefficient	0.005/K
Emissivity	0.8
Absorptivity	0.8
Packing factor (wrt glazing)	63%
Thermal absorber (Aluminum)	
No. of flat-box absorber module	15
Absorber module size	0.105 × 1.38 × 0.012 m
No. of header	2
Header size	1.575 × 0.025 (dia.) × 0.002 (thick) m
Thermal insulation layer (glass wool)	
Thickness	0.03 m
Back cover (galvanized iron)	
Thickness	0.001 m
Water tank and connecting pipes	
Water storage capacity	155 kg
Tank length	1.2 m
Tank diameter	0.21 m
Pipe diameter	0.015 m
Thickness of insulation layer at tank	0.025 m
Thickness of insulation layer on pipe	0.02 m

Table 2: Collector and technical design data of BiPV/T system.

Design parameters	Data
Front glazing (low-iron glass)	
Thickness	0.004 m
Surface area	1.61 m^2
Depth of air gap underneath	0.025 m
PV encapsulation (TPT + EVA + solar cell + EVA + TPT + silicon gel)	
Solar cell type	single-crystalline silicon
Cell area	0.81 m^2
Cell electrical efficiency at STC	13%
Solar cell temperature coefficient	0.005/K
Emissivity	0.8
Absorptivity	0.8
Packing factor (wrt glazing)	50%
Thermal absorber (aluminum alloy)	
Thermal capacity	903 kJ/(kg·K)
Density	2702 kg/m^3
Thermal conductivity	237 W/(m·K)
Emissivity	0.8
Absorptivity	0.9
Insulation material (glass wool)	
Thickness	0.03 m
Air gap between insulation layer and building wall	0.02 m
Building wall (brick)	
Thickness	0.15 m
Density	1600 kg/m^3
Thermal capacity	880 J/(kg·K)
Thermal conductivity	1.0 W/(m·K)
Water tank (steel) and connecting pipes (copper)	
Water storage capacity	0.46 m^3
Tank length	1.5 m
Tank diameter	0.54 m
Pipe diameter	0.055 m
Thickness of insulation layer at tank	0.025 m
Thickness of insulation layer on pipe	0.02 m

estimations of EPBT and GPBT have been kept on revising owing to the advancements in PV technology.

The production of a PV module includes the following processes:

(i) silicon purification and processing,

(ii) silicon ingot slicing, and

(iii) PV module fabrication.

Silica is first melted and manufactured into metallurgical-grade silicon (MG-Si), then into electronic silicon (EG-Si) through the Siemen's process or into solar-grade silicon (SoG-Si) through the modified Siemens process [17]. Finally, after the Czochralski process (for sc-Si) or other production process, silicon is made available for the solar cell production. The silicon ingot is needed to be sliced into wafer. The technologies of cell production include etching, doping, screen printing, and coating. The solar cells are then tested, packed, and interconnected with other components to form PV modules.

Alsema [18] studied the EPBT and the GHG emissions of grid-connected PV systems. The cumulative energy demands of sc-Si and mc-Si frameless modules were evaluated as 5700 and 4200 MJ/m^2. Further, it was pointed out that with the implementation of new manufacturing technologies, the above data could be as low as 3200 and 2600 MJ/m^2. Later on, Alsema et al. [19, 20] reviewed the important options that were available for further reduce energy consumption and environment impacts of the PV module production processes. As for BOS, Alsema and Nieuwlaar [21] presented that because of the less use of aluminum in supporting structure, the energy requirement for array support of ground-mounted PV system was about 1800 MJ/m^2, but this could be only 700 MJ/m^2 for rooftop installation; hence rooftop systems should have better potentials for EPBT reduction than ground-mounted systems.

Mason et al. [22] studied the energy contents of the BOS components used in a 3.5 MWp mc-Si PV plant. By integrating the weight of the PV modules with the supports, the embodied energy of the BOS components was found as low as 542 MJ/m^2—a sharp reduction from the previous estimations. Fthenakis and Kim [23] showed that in Japan the primary energy demand for sc-Si PV module was in the range of 4160–15520 MJ/m^2, and the life-cycle GHG emissions rate for PV systems in the United States were from 22 to 49 g CO_2-eq/kWh_e.

In Singapore, Kannan et al. studied a 2.7 kWp distributed PV system with sc-Si modules [24]. Specific energy consumptions for the PV modules and the inverters were estimated 16 and 0.17 MWh_e/kWp respectively. The manufacturing of solar PV modules accounted for 81% of the life cycle energy use. The aluminium supporting structure accounted for about 10%, and the recycling of aluminium accounted for another 7%. The EPBT was estimated to be 6.74 years. It was claimed that this can be reduced to 3.5 years if the primary energy use on PV module production is reduced by 50%.

In India, Nawaz and Tiwari [25] calculated EPBT by evaluating the energy requirement for manufacturing a sc-Si PV system for open field and rooftop conditions with BOS. Mitigation of CO_2 emissions at macrolevel (where lifetime of battery and PV system are the same) and microlevel of the PV system has also been studied. For a 1 m^2 sc-Si PV system, their estimations give an embodied energy of 666 kWh for silicon purification and processing, 120 kWh for cell fabrication, and 190 kWh for subsequent PV module production. Hence without BOS, the embodied energy was estimated 976 kWh/m^2 and the GHG emission was 27.23 kg/m^2.

In Hong Kong Lu and Yang [26] investigated the EPBT and GPBT of a roof-mounted 22 kW BiPV system. It was found that 71% of the embodied energy on the whole is from the embodied energy of the PV modules, whereas the remaining 29% is from the embodied energy of BOS. The

EPBT of the PV system was then calculated as 7.3 years. Considering the fuel mixture composition of local power stations, the corresponding GPBT is 5.2 years. Further, it was predicted that the possible range of EPBT of BiPV installations in Hong Kong is from 7.1 years (for optimal orientation) to 20 years (for west-facing vertical façade).

Bankier and Gale [27] gave a review of EPBT of roof mounted PV systems reported in the 10-year period (1996–2005). A large range of discrepancy was found. They pointed out that the limitations to the accuracy of the assessments came from the difficulties in determining realistic energy conversion factors, and in determining realistic energy values for human labor. According to their estimation, the appropriate range of EPBT for mc-Si PV module installations should be between 2–8 years. A more recent review was done by Sherwani et al. [28]. The EPBT for sc-Si, mc-Si, and a-Si PV systems have been estimated in the ranges of 3.2–15.5, 1.5–5.7, and 2.5–3.2, years, respectively. Similarly, GHG emissions are 44–280, 9.4–104, and 15.6–50 g CO_2-eq/kWh.

4.3. PV/T Systems. While there have been plenty studies of EPBT and GPBT on solar thermal and PV systems, our literature review shows that those on PV/T systems have been very few. In particular, there is so far no reported work on the assessment of PV/T collectors with channel-type absorber design.

Battisti and Corrado [29] made evaluation based on a conventional mc-Si building-integrated system located in Rome, Italy. An experimental PV/T system with heat recovery for DSHW application was examined. Evaluations were made for alternative heat recovery to replace either natural gas or electricity. Their results give the EPBT and GPBT of PV system as 3.3 and 4.1 years. On the other hand, those of the PV/T systems designed for natural gas replacement are 2.3 and 2.4 years.

Also in Italy, Tripanagnostopoulos et al. [30] evaluated the energy and environmental performance of their modified 3 kWp mc-Si PV and experimental water-cooled PV/T sheet-and-tube collector systems designed for horizontal-roof (free-stand) and tilted-roof (building integrated) installations. The application advantage of the glazed/unglazed PV/T over the PV options was demonstrated through the better LCA performances. The EPBT of the PV and BiPV system were found to be 2.9 and 3.2 years, whereas the GPBT were 2.7 and 3.1 years, respectively. For PV/T system with 35°C operating temperature, the EPBT of the PV/T and BiPV/T options were both 1.6 years, and the GPBT were 1.9 and 2.0 years respectively. The study showed that nearly the whole of the environmental impacts are due to PV module production, aluminium parts (reflectors and heat-recovery-unit) as well as copper parts (for heat-recovery-unit and hydraulic circuit), with barely significant contributions from the other system components, such as support structures or electrical/electronic devices. The disposal phase contribution is again almost negligible.

Dubey and Tiwari [31] carried out an environmental impact analysis of a hybrid PV/T solar water heater for use in the Delhi climate of India. With a glazed sheet-and-tube flat plate collector system designed for pump operation, the EPBT was found 1.3 years.

5. Environmental Analysis of Aluminum Rectangular-Channel PV/T Systems

5.1. EPBT of Free-Stand System. Skillful lamination of solar cell onto thermal absorber with layers of EVA and TPT is needed for PV/T collector production. Aluminum thermal absorber parts are made available by raw material mining and extraction, ingot melting, mechanical extrusion, machining, and assembling into whole piece. The major-component production and assembly processes include front glass (low iron), PV-laminated absorber, insulation material and aluminum frame. The supply was from the mainland. As for the BOS, the electrical BOS components include inverters, electrical wirings, and electronic devices. The mechanical BOS include water storage tank, pipe work, supporting structure, and accessories. The embodied energy to be considered in the LCA include the above during production, plus those related to the required transportation from factory to installation site, construction and testing, decommissioning and disposal, and any other end-of-life energy requirements.

Table 3 summarizes the materials used and cumulative energy of the free-stand PV/T collector system. The cumulative energy intensity of sc-Si PV module was estimated as 976 kWh/m^2, making references to [25, 26]. That of the inverter and electrical parts was taken as 5% of the PV module. The other values of cumulative energy intensity in MJ/unit was obtained from the Hong Kong government EMSD (Electrical and Mechanical Services Department) database that covers the specific (per unit quantity) impact profile due to consumption of materials in the "Cradle-to-As-built" stage [32]. The total cumulative energy comes up to 3041.8 kWh or 1728 kWh/m^2 for this free-stand system. Table 4 shows the distribution of the embodied energy in this case. It can be seen that the hybrid PV/T collector itself accounts for around 80% of the embodied energy. For the BOS, the water tank accounts for 11.4%, the other mechanical components accounts for 7%, whereas the electrical accessories accounts for only 1.8%. $\sum_{\text{pvt}}$ and $\sum_{\text{bos}}$ are then 2429 and 613 kWh, respectively.

With the installation of this PV/T system, two kinds of energy saving are involved: thermal energy for water heating and electrical energy. This will be no air-conditioning saving. A thermal energy saving of 2650 MJ/year and electricity saving of 473 MJ/year give an E_t of 736 kWh/year and an E_{pv} of 398 kWh/year. In the computation, a heat-to-electricity conversion factor of 0.33 has been used. Mainly labor costs were considered in E_{om}. This is estimated as 41 kWh/year and is therefore not significant. With (2), the EPBT is found 2.8 years. This is much shorter than the expected CPBT of 12.1 years reported in our previous work [6]. Assuming that the working life of PV/T system is similar to PV system, that is, 15–30 years in general [29], then it can be concluded that

Table 3: Cumulative energy in free-stand PV/T system.

Materials	Quantity consumed (kg)	Cumulative energy intensity (MJ/unit)	Cumulative energy (kWh)
PV/T collector			
Front glazing			
Low-iron glass (1.76 m^2)	19.7	19.7	107.9
Thermal insulation			
Glass wool	1.69	31.7	14.9
Thermal absorber			
Aluminum absorber	18.3	219	1114.7
Frame and back cover			
Aluminum	1.78	219	108.0
PV Encapsulation			
PV Module	1.11 m^2	976	1083.4
BOS			
Water tank			
Stainless steel tank	4.20	82.2	273.0
Tank insulation (Glass wool)	1.58	31.7	13.9
Aluminum Cladding	0.966	219	58.8
Connecting pipe			
Copper piping (15 mm dia.)	2.4 m	6.33	4.2
Pipe insulation (Glass wool)	0.0627	31.7	0.6
Structural support and accessories			
Steel stand	14.2	29.2	115.2
Pipe fittings and structural joints	7.19	140.0	93.3
Inverter + electric wiring	5% of PV module		54.2
		Total:	3041.8

Table 4: Distribution of embodied energy in PV/T collector systems.

System component description		Free-stand	BiPV/T
PV/T Collector	Mechanical components	44.2	51.8
	Electrical components	35.6	37.7
BOS	Water tank	11.4	4.9
	Pipe and structural supports	7.0	3.8
	Electrical components	1.8	1.9

the EPBT in this case study is an order of magnitude lower than its expected working life.

5.2. BiPV/T System. Table 5 summarizes the materials used and the cumulative energy in the 9.66 m^2 BiPV/T case. Accordingly, the values of Z_{pvt} and Z_{bos} are, respectively,

Table 5: Cumulative energy in BiPV/T system.

Materials	Quantity consumed (kg)	Cumulative energy intensity (MJ/unit)	Cumulative energy (kWh)
PV/T collector			
Front glazing			
Low-iron glass (1.61 m^2 × 6)	99.6	19.7	545.0
Thermal insulation			
Glass wool	9.50	31.7	83.7
Thermal absorber			
Aluminum absorber	86.7	219	5273.8
Frame and back cover			
Aluminum	10.1	219	611.8
PV Encapsulation			
PV Module	4.86 m^2	976	4743.4
BOS			
Water tank			
Stainless steel tank	19.9	82.2	454.0
Insulation (Glass wool)	2.14	31.7	18.8
Aluminum Cladding	1.53	219	93.0
Connecting pipe			
Copper piping (55 mm dia.)	7 m	40.1	77.9
Pipe insulation (Glass wool)	1.07	31.7	9.4
Structural support and accessories			
Pipe fittings and structural parts	5.25	140.0	68.1
Inverter + electric wiring	5% of PV module		237.2
		Total	12585.2

11258 and 1328 kWh. Z_{mtl} is estimated as 594 kWh, making reference to the work of Streicher et al. [10] and adjusted by the cost of living. Taking the advantage of building material replacement, the cumulative energy intensity reduces to 1241 kWh/m^2. The embodied energy distribution of this BiPV/T system is also given in Table 4. It can be seen that for this building integrated case the portion of the collector increases to 89%. For the BOS, the water tank accounts for 4.9%, the pipe and supporting components account for 3.8%, and the electrical components remain at less than 2%.

With the installation of this BiPVW system, the annual energy savings include the following:

(i) thermal energy: 2258 kWh (E_t);

(ii) electrical energy: 323 kWh;

(iii) space cooling load: 206 kWh.

By taking the COP of air-conditioning plant as 3.0, E_{pv} and E_{ac} are then 979 and 208 kWh/year, respectively. In this case E_{om} is 246 kWh/year, by estimation. By (1), the EPBT is 3.8 years, which is much shorter than its CPBT of

13.8 years. A longer period of EPBT in this BiPV/T than in the free-stand case is mainly because of its vertical collector position as compared to the best angle of tilt, and also the differences in collector size and solar cell packing factor. A shorter EPBT is expected if ms-Si cell modules were used in the analyses because of the lower energy consumption during the manufacturing process. As a matter of fact, this 3.8 years for vertical-mounted BiPV/T is advantageous as compared to the 7.1 years [26] for an optimal-oriented roof-top BiPV system in Hong Kong.

5.3. GHG Emission Analysis. In our analysis, the thermal energy saving was taken as a save of town gas consumed in the building. The electrical energy saving was taken as a save in purchased electricity from the utilities. Based on the data provided by the Hong Kong government, the territory-wide emission factor of GHG coming from utility power generation is 0.7 kg CO_2-eq/kWh$_e$ including the transmission losses [33]. As for town gas, the emission factors for CO_2, CH_4, and N_2O are, respectively, 2.815 kg/unit, 0.0446 g/unit and 0.0099 g/unit, where 1 unit of town gas is equivalent to 48 MJ consumed. For the free-stand case, the above information gives an annual reduction in GHG emission of 285 kg CO_2-eq. The PV/T system itself does not produce polluting emissions during their daily operation. And in these days, most of the manufacturing activities of products consumed in Hong Kong are taking place in the Mainland, so the emission factor of China can be used in our embodied GHG assessment. In China, the primary energy consumption for power generation is 12.01 MJ/kWh$_e$ and the CO_2 emission rate for coal-fired power plant is 24.7 g CO_2-eq/MJ [34], the embodied GHG intensity of the PV/T collector in this case is therefore 0.297 kg CO_2-eq/kWh cumulative energy. The local emission factor was used for the BOS part since local acquisition was assumed. Accordingly, with (4) this approximation gives a GPBT of 3.2 years for the free-stand system.

Similarly, for the BiPVT system the saving in air-conditioning energy is converted as electricity saving based on a system COP (coefficient of performance) of 3.0. With (3) this gives a GPBT of 4.0 years. The result is again lower than the previously estimated GPBT of 5.2 years for the general performance of BiPV systems in Hong Kong [26].

For completeness, Table 6 shows the technical data in the evaluation of their CPBT. Comparing with the free-stand PV/T case, the BiPV/T system had a lower investment cost on unit collector area basis. This is because on one hand there were building materials saving and there was no requirement on the steel stands which is essential for tilt-mounting of the free-stand PV/T collector. On the other hand, it was benefitted by the economy of scale for mass handling of the system components. During operation, however, the vertical collector position of the BiPV/T system made it disadvantageous in the quantity of year-round solar radiation received by the collector surface. At the same time, there would be greater transmission loss for a centralized energy system. The simulation results showed that the annual useful heat gains of the free-stand and the building integrated cases are 418 kWh/m^2 and 233 kWh/m^2, respectively, on unit glazing area basis. And the electrical energy gains are 118 kWh/m^2 and 66.4 kWh/m^2 on unit PV cell area basis. These came out with the CPBT of 12.1 years for the free-stand case and 13.8 years for the building integrated case.

Table 6: Evaluation of cost payback time.

Investment: HK$	Free-stand PV/T [6]	BiPV/T [7]
Water storage tank	400	750
Collector frame and support	400	1800
Modular thermal absorber	600	2700
Solar cells and encapsulation	4000	17500
Inverter	700	1000
Piping, wiring and accessories	300	900
Installation costs	1500	3000
Total system costs (HK$)	7900	27650
Useful energy savings	MJ (kWh)	MJ (kWh)
Thermal energy	2650.4 (736.2)	8127.5 (2257.6)
Electrical energy	473.2 (131.4)	1162.4 (322.9)
Space cooling load	—	742.6 (206.3)
Cost savings: HK$		
Gaseous fuel at HK$0.2/MJ	530.1	1625.5
Electricity at HK$0.95/kWh	124.9	372.0
Annual saving	655.0	1997.5
Cost payback time (CPBT)	12.1 years	13.8 years

Note: USD1 is equivalent to HK$7.8.

Our above findings are generally in line with the estimations by other researchers based on their own collector designs and local applications. Nevertheless, it should be noted that the above picture is not static. It is expected that the continuing improvements in material and energy utilization and recycling will change the current environmental profiles. On the other hand, the progression in solar cell performance will also lead to better EPBT and GPBT.

6. Conclusion

An environmental life-cycle assessment has been done to evaluate the energy and environmental profiles of two cases of PV/T system application in Hong Kong. In both cases, aluminum rectangular-channel absorber in association with sc-Si PV encapsulation was adopted in the single-glazed flat-plate PV/T collector design. In our analysis, the cumulative energy inputs and the embodied GHG emissions were determined by established methodology and technical data making reference to reported research works as well as local government publications. The annual thermal and electrical energy outputs were from results of dynamic simulation based on the TMY dataset of Hong Kong and validated PV/T system models. Our estimation shows that the EPBT of the free-stand PV/T system at the best angle of tilt is around 2.8 years, which is an order of magnitude lower than the expected system working life. In the vertical-mounted BiPV/T case, this is 3.8 years which is again considerably better than the general performance of roof-top BiPV system

in Hong Kong. The corresponding GPBT of 3.2 and 4.0 years as a result demonstrate the environmental superiority of this PV/T option over many other competing renewable energy systems.

Acknowledgment

The work described in this paper was supported by a Grant from the Research Grants Council of the Hong Kong Special Administrative Region, China (Project no. CityU112009).

References

[1] B. Sandnes and J. Rekstad, "A photovoltaic/thermal (PV/T) collector with a polymer absorber plate. Experimental study and analytical model," *Solar Energy*, vol. 72, no. 1, pp. 63–73, 2002.

[2] C. Cristofari, G. Notton, P. Poggi, and A. Louche, "Modelling and performance of a copolymer solar water heating collector," *Solar Energy*, vol. 72, no. 2, pp. 99–112, 2002.

[3] Y. Tripanagnostopoulos, T. Nousia, M. Souliotis, and P. Yianoulis, "Hybrid photovoltaic/thermal solar systems," *Solar Energy*, vol. 72, no. 3, pp. 217–234, 2002.

[4] T. T. Chow, J. Ji, and W. He, "Photovoltaic-thermal collector system for domestic application," *Journal of Solar Energy Engineering, Transactions of the ASME*, vol. 129, no. 2, pp. 205–209, 2007.

[5] T. T. Chow, W. He, A. L. S. Chan, K. F. Fong, Z. Lin, and J. Ji, "Computer modeling and experimental validation of a building-integrated photovoltaic and water heating system," *Applied Thermal Engineering*, vol. 28, no. 11-12, pp. 1356–1364, 2008.

[6] T. T. Chow, W. He, J. Ji, and A. L. S. Chan, "Performance evaluation of photovoltaic-thermosyphon system for subtropical climate application," *Solar Energy*, vol. 81, no. 1, pp. 123–130, 2007.

[7] T. T. Chow, A. L. S. Chan, K. F. Fong, Z. Lin, W. He, and J. Ji, "Annual performance of building-integrated photovoltaic/water-heating system for warm climate application," *Applied Energy*, vol. 86, no. 5, pp. 689–696, 2009.

[8] ISO, (International Organization for Standardization) 14040 Standard, Environmental Management-Life cycle Assessment-Principles and Framework, 1997.

[9] G. N. Tiwari and R. K. Mishra, *Advanced Renewable Energy Sources*, RSC Publishing, Cambridge, UK, 2012.

[10] E. Streicher, W. Heidemann, and H. Müller-Steinhagen, "Energy payback time—a key number for the assessment of thermal solar systems," in *Proceedings of EuroSun*, pp. 20–23, Freiburg, Germany, June 2004.

[11] G. Tsilingiridis, G. Martinopoulos, and N. Kyriakis, "Life cycle environmental impact of a thermosyphonic domestic solar hot water system in comparison with electrical and gas water heating," *Renewable Energy*, vol. 29, no. 8, pp. 1277–1288, 2004.

[12] F. Ardente, G. Beccali, M. Cellura, and V. Lo Brano, "Life cycle assessment of a solar thermal collector," *Renewable Energy*, vol. 30, no. 7, pp. 1031–1054, 2005.

[13] S. Kalogirou, "Thermal performance, economic and environmental life cycle analysis of thermosiphon solar water heaters," *Solar Energy*, vol. 83, no. 1, pp. 39–48, 2009.

[14] R. H. Crawford, G. J. Treloar, B. D. Ilozor, and P. E. D. Love, "Comparative greenhouse emissions analysis of domestic solar hot water systems," *Building Research and Information*, vol. 31, no. 1, pp. 34–47, 2003.

[15] M. Arif, "Life cycle analysis and carbon credit earned by solar water heating system," *International Journal of Research in Engineering and Applied Sciences*, vol. 2, no. 2, pp. 1884–1905, 2012.

[16] Y. Hang, M. Qu, and F. Zhao, "Economic and environmental life cycle analysis of solar hot water systems in the United States," *Energy and Buildings*, vol. 45, pp. 181–188, 2012.

[17] N. Jungbluth, "Life cycle assessment of crystalline photovoltaics in the Swiss ecoinvent database," *Progress in Photovoltaics: Research and Applications*, vol. 13, no. 5, pp. 429–446, 2005.

[18] E. A. Alsema, "Energy pay-back time and CO_2 emissions of PV systems," *Progress in Photovoltaics Research and Applications*, vol. 8, pp. 17–25, 2000.

[19] E. A. Alsema, M. J. de Wild-Scholten, and V. M. Fthenakis, "Environmental impacts of PV electricity generation, a critical comparison of energy supply options," in *Proceedings of 21st European Photovoltaic Solar Energy Conference*, Dresden, Germany, 2006.

[20] E. A. Alsema and M. J. de Wild-Scholten, "Reduction of the environmental impacts in crystalline silicon module manufacturing," in *Proceedings of the 22nd European Photovoltaic Solar Energy Conference*, Milan, Italy, 2007.

[21] E. A. Alsema and E. Nieuwlaar, "Energy viability of photovoltaic systems," *Energy Policy*, vol. 28, no. 14, pp. 999–1010, 2000.

[22] J. E. Mason, V. M. Fthenakis, T. Hansen, and H. C. Kim, "Energy payback and life-cycle CO_2 emissions of the BOS in an optimized 3.5MW PV installation," *Progress in Photovoltaics: Research and Applications*, vol. 14, no. 2, pp. 179–190, 2006.

[23] V. M. Fthenakis and H. C. Kim, "Greenhouse-gas emissions from solar electric- and nuclear power: a life-cycle study," *Energy Policy*, vol. 35, no. 4, pp. 2549–2557, 2007.

[24] R. Kannan, K. C. Leong, R. Osman, H. K. Ho, and C. P. Tso, "Life cycle assessment study of solar PV systems: an example of a 2.7 kWp distributed solar PV system in Singapore," *Solar Energy*, vol. 80, no. 5, pp. 555–563, 2006.

[25] I. Nawaz and G. N. Tiwari, "Embodied energy analysis of photovoltaic (PV) system based on macro- and micro-level," *Energy Policy*, vol. 34, no. 17, pp. 3144–3152, 2006.

[26] L. Lu and H. X. Yang, "Environmental payback time analysis of a roof-mounted building-integrated photovoltaic (BIPV) system in Hong Kong," *Applied Energy*, vol. 87, no. 12, pp. 3625–3631, 2010.

[27] C. Bankier and S. Gale, "Energy payback of roof mounted photovoltaic cells," *The Environmental Engineer*, vol. 7, no. 4, pp. 11–14, 2006.

[28] A. F. Sherwani, J. A. Usmani, and Varun, "Life cycle assessment of solar PV based electricity generation systems: a review," *Renewable and Sustainable Energy Reviews*, vol. 14, no. 1, pp. 540–544, 2010.

[29] R. Battisti and A. Corrado, "Evaluation of technical improvements of photovoltaic systems through life cycle assessment methodology," *Energy*, vol. 30, no. 7, pp. 952–967, 2005.

[30] Y. Tripanagnostopoulos, M. Souliotis, R. Battisti, and A. Corrado, "Energy, cost and LCA results of PV and hybrid PV/T solar systems," *Progress in Photovoltaics: Research and Applications*, vol. 13, no. 3, pp. 235–250, 2005.

[31] S. Dubey and G. N. Tiwari, "Life cycle cost analysis and carbon credit earned by PV/T solar water heater for Delhi climatic conditions," *Open Environmental Sciences*, vol. 2, pp. 15–25, 2008.

[32] Hong Kong Government, Life Cycle Assessment (LCA) and Life Cycle Costing (LCC) Tool for Commercial Building Developments in Hong Kong: User Manual, EMSD, Hong Kong SAR Government publication, 2005.

[33] "Hong Kong Government," Guidelines to Account for and Report on Greenhouse Gas Emission and Removals for Buildings (Commercial, Residential or Institutional Purposes) in Hong Kong, EMSD and EPD, Hong Kong SAR Government publication, 2008.

[34] M. Ito, K. Kato, K. Komoto, T. Kichimi, and K. Kurokawa, "A comparative study on cost and life-cycle analysis for 100 MW very large-scale PV (VLS-PV) systems in deserts using m-Si, a-Si, CdTe, and CIS modules," *Progress in Photovoltaics: Research and Applications*, vol. 16, no. 1, pp. 17–30, 2008.

Hindawi Publishing Corporation
International Journal of Photoenergy
Volume 2012, Article ID 957847, 7 pages
doi:10.1155/2012/957847

Research Article

Comparison of Electrical and Thermal Performances of Glazed and Unglazed PVT Collectors

Jin-Hee Kim[1] and Jun-Tae Kim[2]

[1] *Green Home Energy Technology Research Center, Kongju National University, 275 Budae-Dong, Chungnam, Cheonan 330-717, Republic of Korea*
[2] *Department of Architectural Engineering, Kongju National University, 275 Budae-Dong, Chungnam, Cheonan 330-717, Republic of Korea*

Correspondence should be addressed to Jun-Tae Kim, jtkim@kongju.ac.kr

Received 4 April 2012; Accepted 15 August 2012

Academic Editor: Christophe Menezo

Photovoltaic-thermal (PVT) collectors combine photovoltaic modules and solar thermal collectors, forming a single device that receives solar radiation and produces electricity and heat simultaneously. PVT collectors can produce more energy per unit surface area than side-by-side PV modules and solar thermal collectors. There are two types of liquid-type flat-plate PVT collectors, depending on the existence of glass cover over PV module: glass-covered (glazed) PVT collectors, which produce relatively more thermal energy but have lower electrical yield, and uncovered (unglazed) PVT collectors, which have relatively lower thermal energy with somewhat higher electrical performance. In this paper, the experimental performance of two types of liquid-type PVT collectors, glazed and unglazed, was analyzed. The electrical and thermal performances of the PVT collectors were measured in outdoor conditions, and the results were compared. The results show that the thermal efficiency of the glazed PVT collector is higher than that of the unglazed PVT collector, but the unglazed collector had higher electrical efficiency than the glazed collector. The overall energy performance of the collectors was compared by combining the values of the average thermal and electrical efficiency.

1. Introduction

The overall efficiency of a PV system, which has relatively lower efficiency among renewable energy systems, depends on the efficiency of the solar cells and the PV modules themselves. Today, in general, silicon-based PV modules have an electrical efficiency of about 12∼16% under standard test condition (STC: air mass 1.5, irradiation intensity 1000 W/m^2, and cell temperature 25°C). Furthermore, the efficiency of PV modules of a Building-Integrated Photovoltaic (BIPV) System can be lowered due to the increase of the PV module temperature.

The photovoltaic/thermal (PVT) concept offers an opportunity to increase overall efficiency by the use of waste heat generated in the PV module of the BIPV system. It is well known that PVT systems enhance PV efficiency by PV cooling, where PV cooling may be achieved by circulating a colder fluid, water, or air, at the underside of the PV module.

Among the various types of PVT systems, liquid-type PVT collectors combine a photovoltaic module and a solar thermal collector, forming a single device that converts solar energy into electricity and heat simultaneously. The heat from PV modules can be removed in order to enhance the electrical performance of the PV module; this heat can be converted into useful thermal energy. As a result, PVT collectors can generate more solar energy per unit surface area than can side-by-side photovoltaic modules and solar thermal collectors.

Since the early 1970s, much progress has been achieved in the research and development of PVT systems. In a study focused on a liquid type PVT collector, Wolf [1] analyzed the heating performance in a US residence using a liquid-type flat-plate PVT collector and concluded that it was technically feasible. Kern and Russell eliminated heat on the roof or wall of a BIPV, thus initiating theoretical and experimental research using air or water [2]. This approach

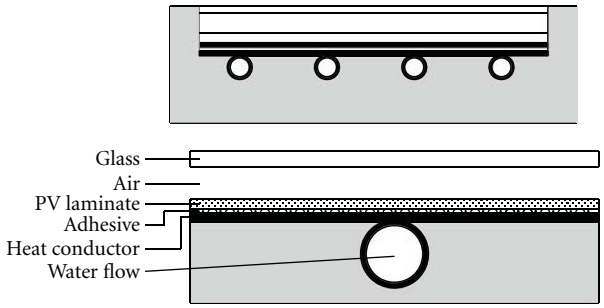

Figure 1: Sectional view of a glazed PVT collector.

began with technical and construction issues derived from a BIPV system combined with a roof-integrated collector. In addition, other studies [3] presented a theoretical model of a PVT system utilizing then-current solar collectors. Building on these studies, Raghuraman [4], Cox III and Raghuraman [5], Braunstein and Kornfeld [6], and Lalović et al. [7] carried out studies of PVT systems based on flat-type collectors.

Bergene and Løvvik [8] thoroughly analyzed the electrical and thermal efficiencies of a liquid-type PVT system and the energy conversion between different factors. Sopian et al. [9] compared the performances under normal conditions of single- and double-PVT collectors. They concluded that the double-pass-type-PVT collector showed better performance regarding the cooling effect of a solar cell. In another study [10, 11], experimental and theoretical performances were examined with respect to a liquid-type flat-plate PVT collector. Fujisawa and Tani [12] evaluated the effective energy of a PVT collector depending on the existence of a glass cover. One study [13] involved PVT collectors with various designs, such as the absence of a glass cover, use of a single cover, and incorporation of a double cover; these were designed and their long-term performance was calculated under normal conditions. Various types of liquid PVT collectors have also been suggested, such as a channel-type PVT collector [14], a PVT collector with polymer absorbers [15], and thermosyphon PVT collectors [16–18]. Glazed and unglazed PVT collectors were compared by Tripanagnostopoulos et al. [19].

Various designs of liquid type PVT systems have since been proposed, and the theoretical and experimental performances of PVT systems have been evaluated. In addition, research has been actively carried out on PVT systems linked to conventional heating and cooling facilities. Moreover, economic feasibility studies have been presented, including a calculation of the payback period and the effectiveness of PVT systems.

In general, in the case of liquid type PVT collectors, two types can be distinguished: glazed PVT collectors (Figure 1), which produce more heat but have slightly lower electrical yield, and unglazed PVT collectors (Figure 2), which produce relatively less thermal energy but show somewhat higher electrical performance.

Glazed PVT collectors are very similar in appearance to flat-plate solar thermal collectors, consisting of a PV-covered absorber in an insulated collector box with a glass cover. This

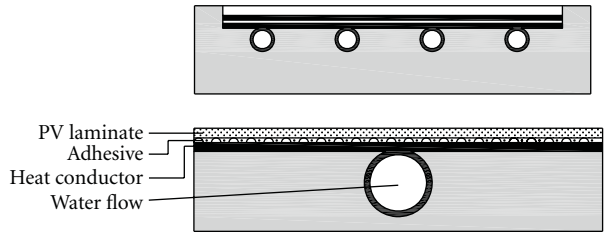

Figure 2: Sectional view of an unglazed PVT collector.

Figure 3: Glazed PVT collector.

glass-covered insulation leads to high thermal efficiency with some reduction of electrical efficiency due to solar radiation reflection and the increase in the PV module temperature introduced by the glass cover. On the other hand, unglazed PVT collectors are more similar to regular PV panels. They consist of a PV-covered absorber with no additional glass cover. The configuration without a glass cover results in lower thermal efficiency; hence, unglazed PVT collectors deliver relatively low thermal energy with higher electrical efficiency due to the PV module cooling effect. The electrical efficiency of an unglazed PVT collector is higher than that of a glazed PVT collector and is even higher than that of regular PV panels due to the PV cooling effect. However, the thermal efficiency of the unglazed type is lower than that of the glazed PVT collector due to higher heat loss from the collector surfaces.

The aim of this study is to compare the electrical and thermal performances of glazed (Figure 1) and unglazed collectors (Figure 2). In this paper, two different types of liquid-type PVT collectors were fabricated, and the thermal and electrical performance levels of these prototypes were measured outdoors. The results were then compared.

2. PVT Collector Design and Manufacture

The liquid-type flat plate PVT collectors used for this study are shown in Figures 3 and 4. The PVT collectors consist of PV modules in combination with water heat extraction units made from copper sheet and tube. The glazed PVT collector has a low-iron glazing cover of 4 mm thickness with air space of 20 mm and is thermally protected with 70 mm glass-wool thermal insulation. A copper sheet and tube absorber was attached at the PV module back side by thermal conduction adhesive. The PV modules used for the collectors are 200 W_p pc-si PV modules and have electrical efficiency of 14% under STC. The specifications are shown

Table 1: PV module specifications.

Cell type	Polycrystalline silicon
Maximum power	200 W
Maximum voltage	25.8 V
Maximum current	7.75 A
Shot current	8.65 A
Open voltage	33.21 V
Size	1454 ∗ 974 ∗ 38 mm

Figure 4: Unglazed PVT collector.

in Table 1. The configuration of unglazed PVT collector was the same as that of the glazed PVT collector except for the incorporation of the glass cover in the latter.

3. Experiment

The two different types of PVT collector were tested at solar radiation above 790 W/m^2 and a flow rate of 0.02 kg/sm^2, based on ASHRAE standard 93-77 [20] and PVT performance measurement guidelines of ECN (Energy Research Centre of The Netherlands) [21]. The electrical and thermal performance measurements were carried out under a quasi-stationary condition in an outdoor environment (Figure 5).

Several experimental devices were installed to measure the data related to the thermal and electrical performances of the PVT collector.

The PVT collector was tested at steady state conditions to determine its electrical and thermal performances for various inlet operating temperatures. Inlet and outlet temperatures of PVT collector were monitored and measured using a RTD-type thermocouple with a measurement error of ±0.1% at 0°C. The inlet temperature of PVT collector was controlled by set temperature equipment and the inlet temperature remained constant, while an outlet temperature varied. Also, the ambient temperature was measured by a T-type thermocouple with measurement error of ±0.2°C. Antifreezing liquid was supplied to the PVT collector at a uniform flow rate of 0.02 kg/sm^2 from a pump. The mass flow rate at the inlet pipe of the PVT collector was measured by an electronic flow meter. The normal quantity of solar radiation on the PVT collector surface was measured by Eppley pyranometer installed parallel to the collector plane.

Electrical loading resistors and a power meter were installed in order to measure the electrical performance (DC current—voltage and power) of the PVT. All of data related to the thermal and electrical performances of the PVT collector were monitored and recorded at 10 s intervals through a data acquisition system.

4. Results and Discussion

With the results of the outdoor test of the PVT collectors, the thermal and electrical performances were analyzed and the experimental results for the two different types of PVT collector were compared.

4.1. Thermal Performance. The thermal efficiency is determined as a function of the solar radiation (G), the input fluid temperature (T_i), and the ambient temperature (T_a). The steady state efficiency is calculated by the following equation:

$$\eta_{\text{th}} = \frac{\dot{m}C_p(T_o - T_i)}{(A_{\text{PVT}}G)}, \tag{1}$$

where η_{th} is the thermal efficiency [—]; A_{PVT} is the collector area [m^2]; T_o is the collector outlet temperature [°C]; T_i is the collector inlet temperature [°C]; $\dot{m}$ is the mass flow rate [kg/s]; C_p is the specific heat [J/kg K]; G is the irradiance on the collector surface [W/m^2].

The thermal efficiency (η_{th}) of the PVT collectors was conventionally calculated as a function of the ratio $\Delta T/G$ where $\Delta T = T_i - T_a$.

Here, T_i and T_a are the PVT collector inlet temperature and the ambient temperature, respectively, and G is the solar radiation in the collector plane. Hence, ΔT is a measurement of the temperature difference between the collector and its surroundings, relative to the solar radiation. The thermal efficiency η_{th} is then expressed as

$$\eta_{\text{th}} = \eta_0 - \alpha_1\left(\frac{\Delta T}{G}\right), \tag{2}$$

where η_0 is the thermal efficiency at zero-reduced temperature, and α_1 is the heat loss coefficient.

With the measurement results of the two different types of PVT collector, the thermal performance can be expressed as presented in Figure 6. Thermal efficiencies of the glazed and unglazed PVT collectors can be expressed with the relational expressions $\eta_{\text{th}} = 0.51 - 5.36(\Delta T/G)$ and $\eta_{\text{th}} = 0.45 - 10.15(\Delta T/G)$, respectively. Thus, the thermal efficiencies (η_0) at zero-reduced temperature are 0.51 and 0.45, respectively, thus showing that the glazed PVT collector efficiency is higher than that of the unglazed PVT collector. Also, the heat loss coefficient (α_1) is −5.36 W/m^2 °C and −10.15 W/m^2 °C, respectively: the unglazed PVT collector provided approximately twofold better performance than the glazed PVT collector. The average thermal efficiency of the glazed and unglazed PVT collectors is about 38% and 24%, respectively, at the same outdoor conditions.

4.2. Electrical Performance. The electrical efficiency depends mainly on the incoming solar radiation and the temperature

(a) (b)

Figure 5: View of PVT collector (a) evaluated in the experiment and performance measurement equipment for the PVT collector (b).

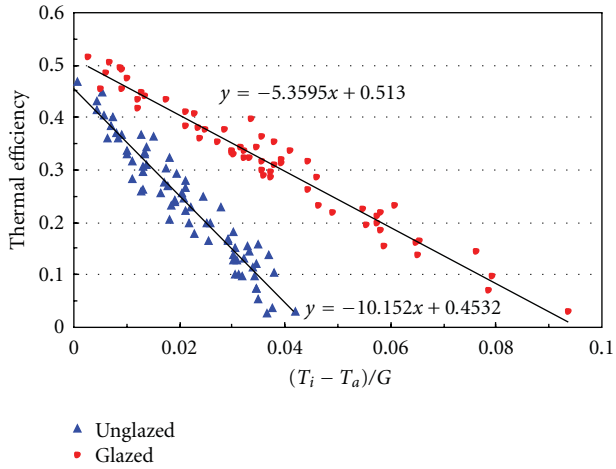

Figure 6: Glazed and unglazed PVT collectors thermal efficiency.

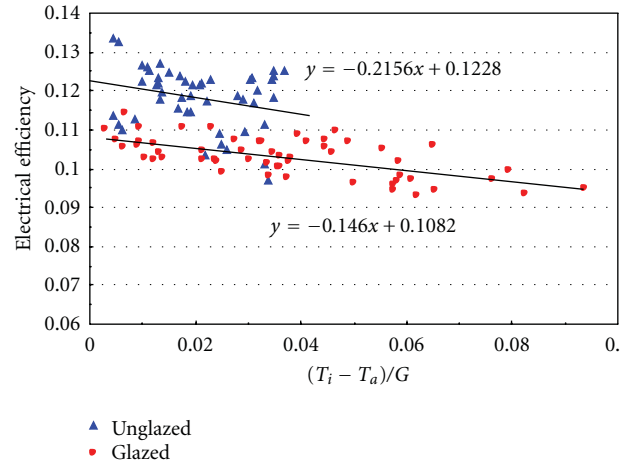

Figure 7: Glazed and unglazed PVT collectors electrical efficiency.

of PV module that was used in the tested PVT collectors and is calculated with the following:

$$\eta_{\text{el}} = \frac{I_m V_m}{A_{\text{PVT}} G}, \tag{3}$$

where I_m and V_m are the current and the voltage of the PV module operating at maximum power.

The electrical efficiencies of the glazed and unglazed PVT collector at the outdoor conditions are shown in Figure 7. The performance of the glazed and unglazed PVT collector can be expressed with the relational expressions $\eta_{\text{el}} = 0.108 - 0.15(\Delta T/G)$ and $\eta_{\text{el}} = 0.123 - 0.22(\Delta T/G)$, respectively. Thus, the electrical efficiency (η_0) at zero reduced temperature is 0.108 and 0.123, respectively, and the electricity loss coefficient is −0.22 and −0.15, respectively. From these results, it was analyzed that the unglazed PVT collector presents about 14% higher electrical efficiency, compared to the glazed PVT collector. This difference appears to be significant as about it reflects roughly a 1.5% difference in the PV modules' electrical efficiency. It is obvious that while the unglazed PVT collector displayed poorer thermal performance at zero reduced temperature, it performs better in terms of generating electricity. The average electrical efficiencies of the glazed and unglazed PVT collectors are about 10.3% and 11.8%, respectively.

The PV module temperature depends on the cooling effects of the PV module by the fluid in the PVT collectors. The electrical performance was analyzed as a function of the PVT inlet fluid temperature and solar radiation. The DC power generation of the PVT collectors as a function of solar radiation and inlet fluid temperature is shown in Figures 8 and 9.

For the glazed PVT collector, the DC power increased according to an increase of solar radiation, and the DC power generation improved with lower inlet fluid temperature. These results indicate that the inlet fluid temperature of the PVT collector affected the PV module temperature. In the case of unglazed PVT collector, the same result was also found. However, the DC power generation of the unglazed collector appears to be less influenced by solar radiation, compared to the glazed PVT.

Furthermore, the electrical performance was analyzed and compared as a function of each PVT inlet fluid temperature and solar radiation.

In Figures 10 and 11, the DC power generation and electrical efficiency of the PVT collectors as a function of

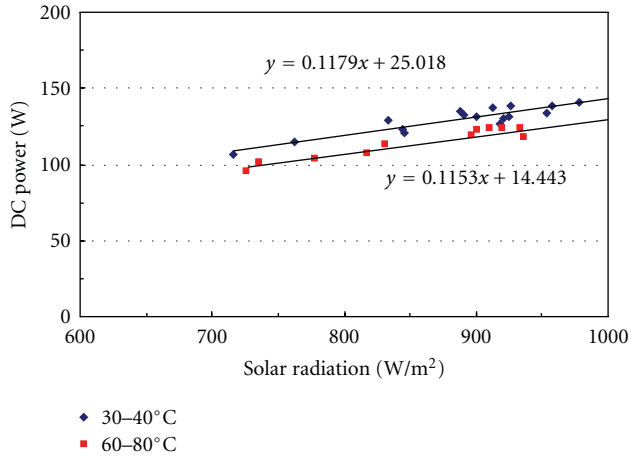

Figure 8: Electrical power of the glazed PVT collector as a function of solar radiation and fluid temperature.

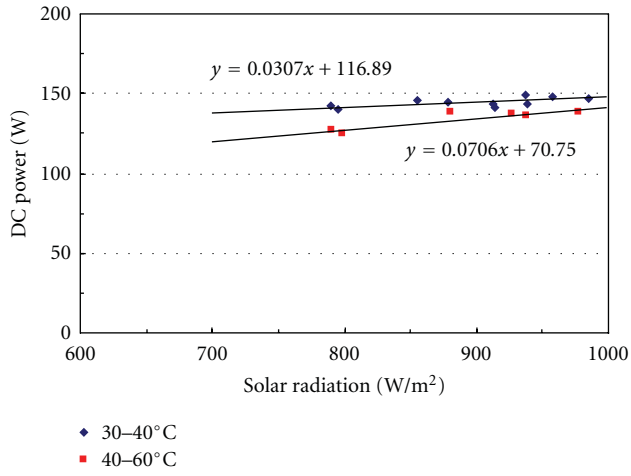

Figure 9: Electrical power of the unglazed PVT collector as a function of solar radiation and temperature.

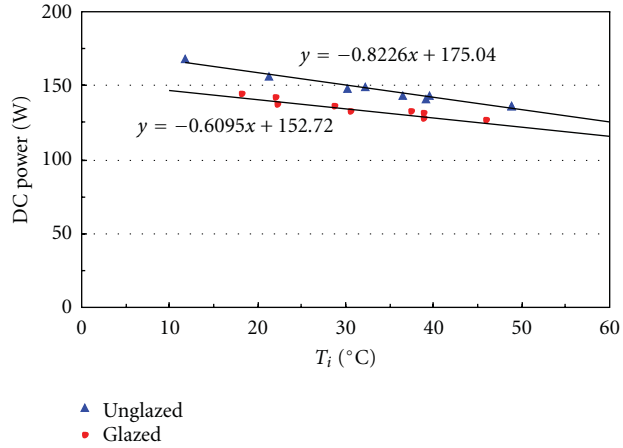

Figure 10: Electrical power of the glazed and unglazed PVT collectors as a function of temperature (solar radiation 950 W/m^2).

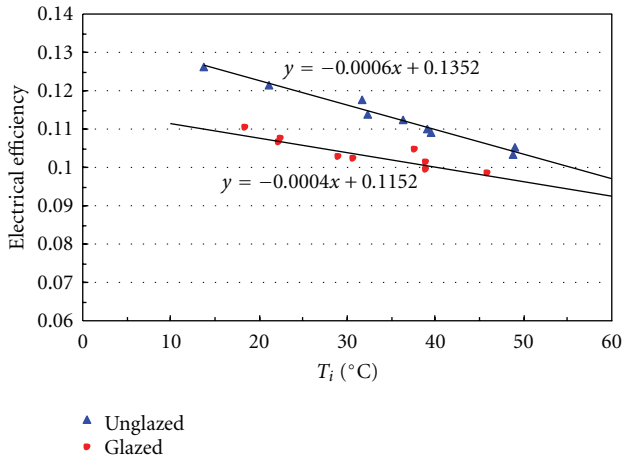

Figure 11: Electrical efficiency of the glazed and unglazed PVT collectors as a function of fluid inlet temperature (solar radiation 950 W/m^2).

the inlet fluid temperature are shown. For the glazed and unglazed PVT collectors, the electrical efficiency decreased according to increased inlet fluid temperature in both cases. The unglazed PVT collector presents higher electrical efficiency compared to the glazed PVT collector at the same inlet temperature condition of the PVT collector. The glazed type tends to lose less heat due to the incorporation of the glass cover as compared to the unglazed type. Therefore, the glazed type can maintain higher temperature of the fluid coming into the collector, which affects the PV module temperature.

In addition, in the case of the glazed collector, reflection and absorption losses of solar radiation at the glass cover reduce its electrical performance. As a result, the unglazed PVT collector provides better electrical performance than that of the glazed PVT collector.

The DC power generation and electrical efficiency of the PVT collectors as a function of solar radiation are shown in Figures 12 and 13. For the glazed and unglazed PVT collectors, the DC power increased in both cases according to increased solar radiation; on the other hand, their electrical efficiency decreased. These results may be due to increased PV module temperature.

5. Conclusion

This paper analyzed the thermal and electrical performance of two types of PVT collectors, a liquid-glazed type and -unglazed type. The results show that the thermal efficiency of the Glazed PVT collector is 14% higher than that of the unglazed collector, and the unglazed PVT collector had, on average, approximately 1.4% higher electrical efficiency than the glazed PVT collector.

The overall energy performance of the collectors can be compared by combining the values of the average thermal and electrical efficiencies: the glazed PVT collector presents a value of 48.4% and the unglazed PVT collector gives a value of 35.8%. Even though the overall performance of the

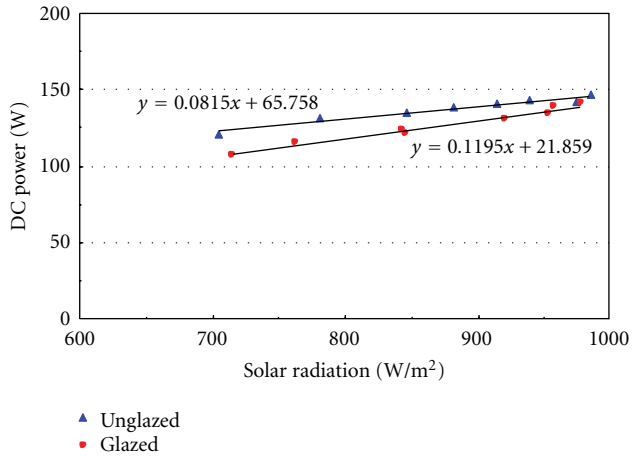

Figure 12: Electrical power of the glazed and unglazed PVT collectors as a function of solar radiation ($T_i = 40^\circ$C).

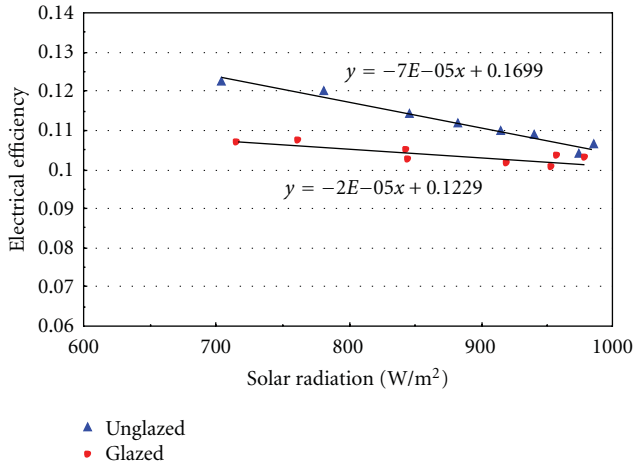

Figure 13: Electrical efficiency of the glazed and unglazed PVT collectors as a function of solar radiation ($T_i = 40^\circ$C).

glazed is 12.6% higher than that of the unglazed collector, it cannot be concluded that the former is superior to the latter: the selection of an optimal configuration will depend on the overall cost efficiency and energy balance of the systems. Also, it is clear that the electrical performance of PVT collectors depends on the cooling effect of the PV module from the PVT inlet fluid temperature and solar radiation.

Acknowledgments

This work was supported by the Priority Research Centers Program through the National Research Foundation of Korea (NRF) funded by the Ministry of Education, Science and Technology (no. 2009-0093825) and a Human Resources Development of the Korea Institute of Energy Technology Evaluation and Planning Grant (no. 20114010203040) funded by the Korean Ministry of Knowledge Economy.

References

[1] M. Wolf, "Performance analyses of combined heating and photovoltaic power systems for residences," *Energy Conversion*, vol. 16, no. 1-2, pp. 79–90, 1976.

[2] Y. Tripanagnostopoulos, T. Nousia, M. Souliotis, and P. Yianoulis, "Hybrid photovoltaic/thermal solar systems," *Solar Energy*, vol. 72, no. 3, pp. 217–234, 2002.

[3] S. D. Hendrid, "Evaluation of combined photovoltaic/thermal collectors," in *Proceedings of the ISES International Congress*, pp. 1865–1869, Atlanta, Ga, USA, March, 1979.

[4] P. Raghuraman, "Analytical predictions of liquid and air photovoltaic/thermal, flat-plate collector performance," *Journal of Solar Energy Engineering*, vol. 103, no. 4, pp. 291–298, 1981.

[5] C. H. Cox III and P. Raghuraman, "Design considerations for flat-plate-photovoltaic/thermal collectors," *Solar Energy*, vol. 35, no. 3, pp. 227–241, 1985.

[6] A. Braunstein and A. Kornfeld, "On the development of the solar photovoltaic and thermal (pvt) collector," *IEEE Transactions on Energy Conversion*, vol. EC-1, no. 4, pp. 31–33, 1986.

[7] B. Lalović, Z. Kiss, and H. Weakliem, "A hybrid amorphous silicon photovoltaic and thermal solar collector," *Solar Cells*, vol. 19, no. 2, pp. 131–138, 1986.

[8] T. Bergene and O. M. Løvvik, "Model calculations on a flat-plate solar heat collector with integrated solar cells," *Solar Energy*, vol. 55, no. 6, pp. 453–462, 1995.

[9] K. Sopian, K. S. Yigit, H. T. Liu, S. Kakaç, and T. N. Veziroglu, "Performance analysis of photovoltaic thermal air heaters," *Energy Conversion and Management*, vol. 37, no. 11, pp. 1657–1670, 1996.

[10] H. P. Garg, R. K. Agarwal, and J. C. Joshi, "Experimental study on a hybrid photovoltaic-thermal solar water heater and its performance predictions," *Energy Conversion and Management*, vol. 35, no. 7, pp. 621–633, 1994.

[11] H. P. Garg and R. K. Agarwal, "Some aspects of a PV/T collector/forced circulation flat plate solar water heater with solar cells," *Energy Conversion and Management*, vol. 36, no. 2, pp. 87–99, 1995.

[12] T. Fujisawa and T. Tani, "Annual exergy evaluation on photovoltaic-thermal hybrid collector," *Solar Energy Materials and Solar Cells*, vol. 47, no. 1–4, pp. 135–148, 1997.

[13] D. W. Vries, *Design of a photovoltaic/thermal combi-panel [Ph.D. thesis]*, Eindhoven Technical University, 1998.

[14] H. A. Zondag, D. W. de Vries, W. G. J. van Helden, R. J. C. van Zolingen, and A. A. van Steenhoven, "The yield of different combined PV-thermal collector designs," *Solar Energy*, vol. 74, no. 3, pp. 253–269, 2003.

[15] B. Sandnes and J. Rekstad, "A photovoltaic/thermal (PV/T) collector with a polymer absorber plate. Experimental study and analytical model," *Solar Energy*, vol. 72, no. 1, pp. 63–73, 2002.

[16] H. P. Garg, R. K. Agarwal, and J. C. Joshi, "Experimental study on a hybrid photovoltaic-thermal solar water heater and its performance predictions," *Energy Conversion and Management*, vol. 35, no. 7, pp. 621–633, 1994.

[17] T. T. Chow, A. L. S. Chan, K. F. Fong, W. C. Lo, and C. L. Song, "Energy performance of a solar hybrid collector system in a multistory apartment building," *Proceedings of the Institution of Mechanical Engineers A*, vol. 219, no. 1, pp. 1–11, 2005.

[18] T. T. Chow, W. He, J. Ji, and A. L. S. Chan, "Performance evaluation of photovoltaic-thermosyphon system for subtropical climate application," *Solar Energy*, vol. 81, no. 1, pp. 123–130, 2007.

[19] Y. Tripanagnostopoulos, T. Nousia, M. Souliotis, and P. Yianoulis, "Hybrid photovoltaic/thermal solar systems," *Solar Energy*, vol. 72, no. 3, pp. 217–234, 2002.

[20] American Society of Heating, Refrigerating and Air Conditioning Engineers (ASHRAE), *Methods of Testing To Determine the Thermal Performance of Solar Collectors*, ASHRAE, 1991.

[21] H. Zondag, N. Borg, and W. Eisenmann, *D8-6: PVT Performance Measurement Guidelines*, ECN Editor, Petten, The Netherlands, 2005.

Hindawi Publishing Corporation
International Journal of Photoenergy
Volume 2012, Article ID 381016, 12 pages
doi:10.1155/2012/381016

Research Article

Modified Grid-Connected CSI for Hybrid PV/Wind Power Generation System

D. Amorndechaphon,[1] S. Premrudeepreechacharn,[1] K. Higuchi,[2] and X. Roboam[3]

[1] *Department of Electrical Engineering, Chiangmai University, Suthep, Muang, Chiangmai 50200, Thailand*
[2] *Department of Electronics Engineering, University of Electro-Communications, 1-5-1 Chofugaoaka, Chofu, Tokyo 182-8585, Japan*
[3] *Laboratoire Plasma et Conversion d'Energie (LAPLACE), Institut National Polytechnique de Toulouse, 31071 Toulouse, France*

Correspondence should be addressed to D. Amorndechaphon, a_damrong@hotmail.com

Received 8 April 2012; Revised 15 August 2012; Accepted 24 August 2012

Academic Editor: Christophe Menezo

The principle of a power conditioning unit for hybrid PV/wind power generation system is proposed. The proposed power conditioner is based on the current source inverter (CSI) topology. All energy sources are connected in parallel with a DC-bus through the modified wave-shaping circuits. To achieve the unity power factor at the utility grid, the DC-link current can be controlled via the wave-shaping circuits with the sinusoidal PWM scheme. In this work, the carrier-based PWM scheme is also proposed to minimize the utility current THD. The power rating of the proposed system can be increased by connecting more PV/wind modules through their wave-shaping circuits in parallel with the other modules. The details of the operating principles, the system configurations, and the design considerations are described. The effectiveness of the proposed CSI is demonstrated by simulation results.

1. Introduction

The steadily increasing energy consumption for the conventional energy sources like a fossil-energy-based fuel has created much interest in the alternative energy sources. Many renewable energy sources are now developed and being widely used. These energy sources can be integrated to form a hybrid system which is an excellent option for distributed energy product. In general, the hybrid systems have better potential to provide higher quality and more reliable power than the single source systems. Recently, the solar and wind energy are the most commonly used renewable energy sources in a hybrid system due to the high efficiency and reliability to supply the continuous power to the load or the utility grid. The typical hybrid power generation system is shown in Figure 1(a). This system includes the energy sources, DC-DC converters, a DC-AC inverter, and the utility grid. All energy sources are connected in parallel to a common DC-AC inverter through their individual DC-DC converters.

Several configurations of hybrid PV/wind power generation systems, applying the various static converter topologies, have been proposed in the literatures [1, 2]. Previous approaches of the hybrid PV/wind power converters were mainly based on voltage source inverter (VSI) topology. One of the commonly used VSI for hybrid PV/wind is shown in Figure 1(b). In this topology, all energy sources are connected to a common DC-bus through the individual DC-DC boost converters. The DC-DC converters are responsible for tracking the maximum power of the wind and PV sources under all operating conditions. The outputs of both DC-DC converters are then connected to a single-phase DC-AC inverter. The DC-link voltage will be regulated by the DC-AC inverter with the current-regulated PWM control to achieve the unity power factor at the utility grid. Nowadays VSI has received a lot of attention but the high switching losses of the switching devices in both conversion stages are still a major drawback of this topology. To overcome this problem, several power converters based on the current source inverter (CSI) topology have been developed [3–8]. Compared with the VSI topology, CSI topology has the ability to boost the output voltage without an additional boost converter [4, 9]. Therefore, CSI is strongly suggested for the grid-connected systems which the magnitude of the DC input voltage is lower than the peak

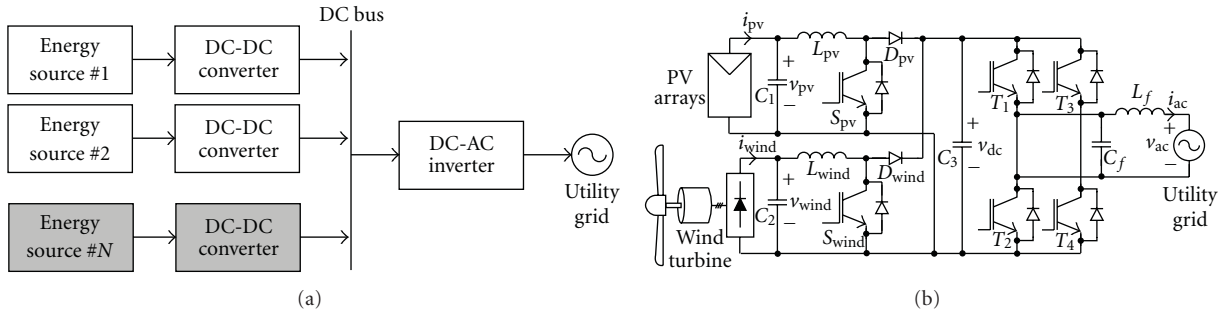

Figure 1: Hybrid PV/wind generation system—(a) general structure of typical hybrid system and (b) hybrid system based on VSI topology.

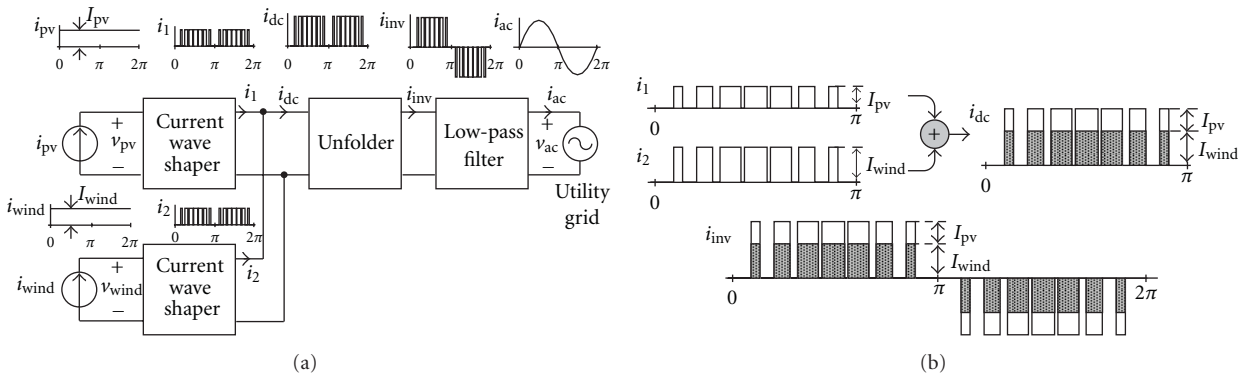

Figure 2: Conceptual expression of the proposed current sharing technique—(a) simplified block diagram and (b) current waveforms for showing the part shared by each energy source.

of utility voltage. In addition, CSI generally features simple converter structure and reliable short-circuit protection. Furthermore, the application of CSI for hybrid PV/wind grid-connected system has not been reported in the previous publications.

In this paper, a modified grid-connected CSI for hybrid renewable energy systems consisting of PV and wind is proposed. The details of the operation principle and the system configuration are also discussed. The simulation setup has been carried out to verify the system performance of the proposed ideas under the different scenarios.

2. Operating Principles

2.1. Overview Concept of the Proposed System with DC-Link Current Sharing Technique. In this section, the overview of the proposed hybrid PV/wind power generation system as shown in Figure 2 can be introduced. The proposed system consists of two constant current sources i_{pv} and i_{wind}, two current wave-shaping circuits (can be named as DC-DC chopper), an unfolding circuit, and a low-pass filter. Two constant current sources are connected in parallel to a common DC-bus through their own current wave-shaping circuits. Both wave shaping circuits, operating in the same switching frequency, are used to perform the PWM output currents i_1 and i_2 at a DC-bus. In order to supply active power to the utility grid, the DC-link current i_{dc} is controlled to be in phase with the utility voltage v_{ac}. Therefore, the unity power factor can be achieved. The unfolding circuit is used to produce a unipolar pulse-width modulation (PWM) current i_{inv} by setting the direction of a PWM current i_{dc} at a DC link. At the last stage, low-pass filter is connected to eliminate the high-frequency harmonic components in a unipolar PWM current i_{inv} before injected to the utility grid.

In Figure 2(b), the waveforms of i_1, i_2, i_{dc}, and i_{inv} in the block diagram in Figure 2(a) are shown. According to Kirchhoff's current law (KCL), it can be seen that the PWM current at a DC-bus i_{dc} is the sum of output currents from the two wave-shaping circuits i_1 and i_2, respectively. Hence, the instantaneous DC-link current i_{dc} can be determined by $i_{dc} = i_1 + i_2$. In addition, the magnitude of i_{dc} can be found by summing the magnitude of i_1 and i_2 ($I_{dc} = I_{pv} + I_{wind}$), respectively. As a result, the magnitude of i_{dc} can be independently controlled by two constant current sources i_{pv} and i_{wind}, respectively.

2.2. Circuit Configuration and Control Strategy. Figure 3(a) shows the circuit topology of the proposed grid-connected CSI for hybrid PV/wind power generation. The circuit diagram differs from that of a VSI in Figure 1(b) by the absence of a DC-link capacitor C_3. The proposed circuit is composed of two wave-shaping circuits, a thyristor-based H-bridge inverter, and *CL* low-pass filter. Input renewable energy sources, PV and wind, are connected to a common DC-bus through their own wave-shaping circuits. The proposed system control scheme is also illustrated in Figure 3(b).

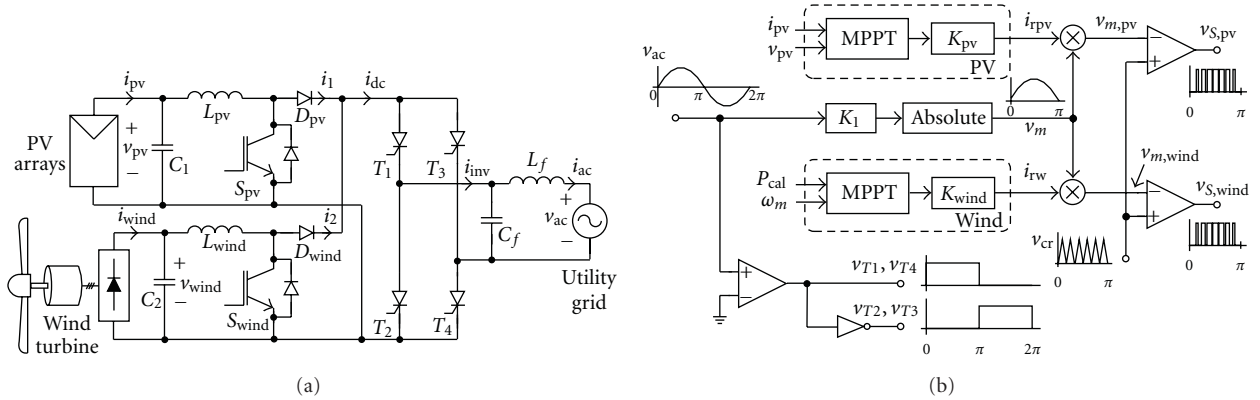

Figure 3: Proposed grid-connected CSI for hybrid PV/wind power generation—(a) power converter scheme and (b) system control scheme.

On the DC-side of the inverter, the DC chokes L_{pv} and L_{wind} are required to provide the smooth and continuous DC currents i_{pv} and i_{wind}, respectively. Chopper switches S_{pv} and S_{wind} can be controlled to shape the constant input DC current i_{pv} and i_{wind} to be the PWM currents i_1 and i_2, respectively, at a DC-bus. To achieve the unity power factor at the utility grid, the utility current i_{ac} is required to be sinusoidal and in phase with the utility voltage v_{ac}. Thus the voltage v_{ac} will be rectified to establish a full-wave rectified sinusoidal signal v_m, where K_1 is an absolute gain. In the same time, the maximum power point tracker (MPPT) can be used for tracking the maximum power of PV and wind by multiplying the reference signal v_m with the MPPT reference of each energy source i_{rpv} and i_{rw} to produce the modulating signal $v_{m,pv}$ and $v_{m,wind}$, respectively. In PV array, an MPPT algorithm is used to determine the optimal operating point i_{rpv}. The optimal current i_{rpv} is calculated and tracked from measured valued of PV voltage v_{pv} and PV current i_{pv}. Similarly, for the wind turbine, the extracted power of the wind turbine P_{cal} and wind speed ω_m are measured. The optimal point i_{rw} can be provided by the MPPT controller. In both energy sources, K_{pv} and K_{wind} are the constant gain of the MPPT controller of PV and wind, respectively.

To obtain the control signal of chopper switches $v_{S,pv}$ and $v_{S,wind}$, the modulating signals $v_{m,pv}$ and $v_{m,wind}$ are compared with a triangular-shaped carrier waveform v_{cr} of the switching frequency f_{sw}. The instantaneous DC-link current i_{dc} can be obtained by the summation of i_1 and i_2. The H-bridge inverter operates in synchronism with the utility grid and is controlled to provide a unipolar PWM current i_{inv}. The zero-crossing circuit is used to generate the control signal of H-bridge inverter v_{T1}, v_{T2}, v_{T3}, and v_{T4}. Switches T_1 and T_4 are turned on in the positive half-cycle of the grid voltage v_{ac}, whereas T_2 and T_3 are turned on in the negative half cycle. It can be observed that the inverter current i_{inv} is obtained by unfolding the DC-link current i_{dc}. At the last stage, C_f and L_f form the low-pass filter which attenuates the high frequency components in the inverter output current i_{inv}.

The principle of the PWM scheme for the proposed CSI is illustrated in Figure 4. For the proposed modulation scheme, two modulating waves $v_{m,pv}$ and $v_{m,wind}$ are required. Both modulating waves are of the same frequency and synchronize with the utility grid but the magnitudes $V_{m,pv}$ and $v_{m,wind}$ are different. The modulating waves $v_{m,pv}$ and $v_{m,wind}$ are compared with a common triangular carrier wave v_{cr}, generating two gating signals $v_{S,pv}$ and $v_{S,wind}$ for chopper switches S_{pv} and S_{wind}, respectively. It should be noted that the fundamental-frequency component of the inverter current i_{inv} can be expressed as i_{inv1} as shown in Figure 4.

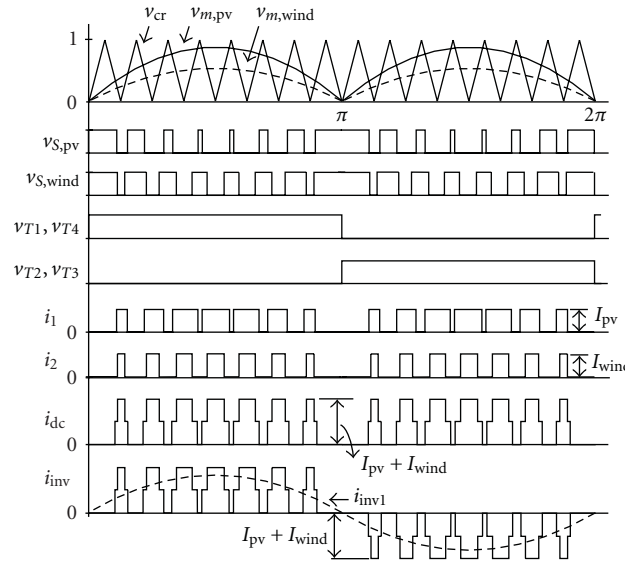

Figure 4: Steady-state waveforms of the proposed grid-connected CSI for hybrid PV/wind system.

2.3. Inverter Mode of Operation. In order to understand the operation details of the proposed grid-connected CSI in Figure 3(a), the equivalent circuit is illustrated in Figure 5. This circuit can be subdivided into two configurations, the input DC-side and the output AC-side, respectively.

For a simplify analysis in each interval of the circuit, the following conditions are assumed.

(I) The input voltage sources v_{pv} and v_{wind} and DC chokes L_{pv} and L_{wind} can be considered and modeled

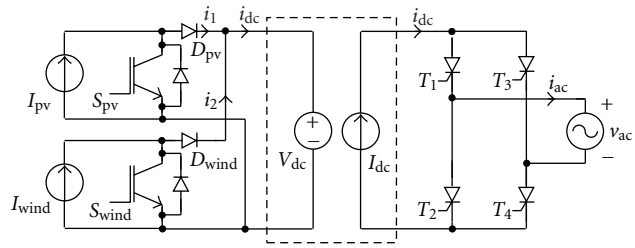

Figure 5: Simplified equivalent circuit of the proposed system.

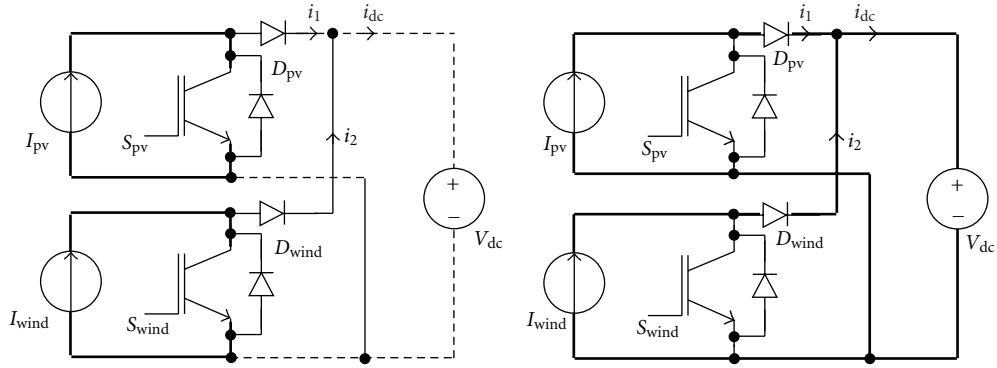

Figure 6: DC-side operation—(a) $v_m < v_{cr}$ and (b) $v_m > v_{cr}$.

as the constant current sources I_{pv} and I_{wind}, respectively.

(II) The output voltage at the DC-side can be assumed to be a constant DC voltage source V_{dc}.

(III) The input current at the AC-side can be assumed to be a constant DC current source I_{dc}.

(IV) All semiconductor switches in the DC-side and the AC-side are operated at the switching frequency (f_{sw}) and the grid frequency (f_{line}), respectively.

2.3.1. DC-Side Operation. For the one switching period, the operation of the converter in the DC-side can be divided into two stages. The equivalent circuit for each stage is shown in Figure 6 and its key waveforms are depicted in Figure 4. Assuming that the modulating signals for energy sources can be defined as $v_{m,pv} = v_{m,wind} = v_m$. The operation processes of the DC-side are specified as follows.

Stage 1 ($v_m < v_{cr}$). When $v_m < v_{cr}$, chopper switches S_{pv} and S_{wind} are on, chopper diodes D_{pv} and D_{wind} are off, the input DC currents I_{pv} and I_{wind} flow through S_{pv} and S_{wind}, respectively. The current I_{pv} and I_{wind} cannot flow through the diodes D_{pv} and D_{wind}, leading to $i_1 = i_2 = 0$. According to KCL, the DC-link current i_{dc} can be considered as consisting of the sum of diode currents i_1 and i_2. That is,

$$i_{dc}(t) = 0. \tag{1}$$

Stage 2 ($v_m > v_{cr}$). When $v_m > v_{cr}$, chopper switches S_{pv} and S_{wind} are off, chopper diodes D_{pv} and D_{wind} are on, the input DC currents I_{pv} and I_{wind} flow to the load through D_{pv} and D_{wind}, respectively, resulting in $i_1 = I_{pv}$ and $i_2 = I_{wind}$. Similar to the first stage, the DC-link current i_{dc} is obtained as

$$i_{dc}(t) = I_{pv} + I_{wind}. \tag{2}$$

The DC-link current i_{dc} for all stages can be rewritten in term of the switching states as follows:

$$i_{dc}(t) = I_{pv}\left[1 - d_{pv}\right] + I_{wind}[1 - d_{wind}], \tag{3}$$

where d_{pv} and d_{wind} are the switching states of the chopper switches S_{pv} and S_{wind}, respectively. The switching states $d_{pv} = 1$ and $d_{wind} = 1$ if $v_m < v_{cr}$ (in stage 1); otherwise 0 (in stage 2).

2.3.2. AC-Side Operation. In Figure 7, the equivalent circuit in the AC-side is shown. The AC utility voltage can be expressed by $v_{ac} = V_{ac} \cdot \sin(\omega t)$, where V_{ac} is the peak of utility voltage. The operation of this side consists of two stages during the switching cycle. The operation can be described as follows.

Stage 1 ($v_{ac} > 0$). When $v_{ac} > 0$, the inverter switches T_1 and T_4 are on, T_2 and T_3 are off, the input DC current I_{dc} flows to the grid through T_1 and T_4, respectively. Then the AC utility current i_{ac} equals to I_{dc}.

Stage 2 ($v_{ac} < 0$). The inverter switches T_1 and T_4 are off, T_2 and T_3 are on, when $v_{ac} < 0$. The DC current I_{dc} flows to the grid through T_2 and T_3, respectively, resulting in the utility current i_{ac} to be equal to $-I_{dc}$.

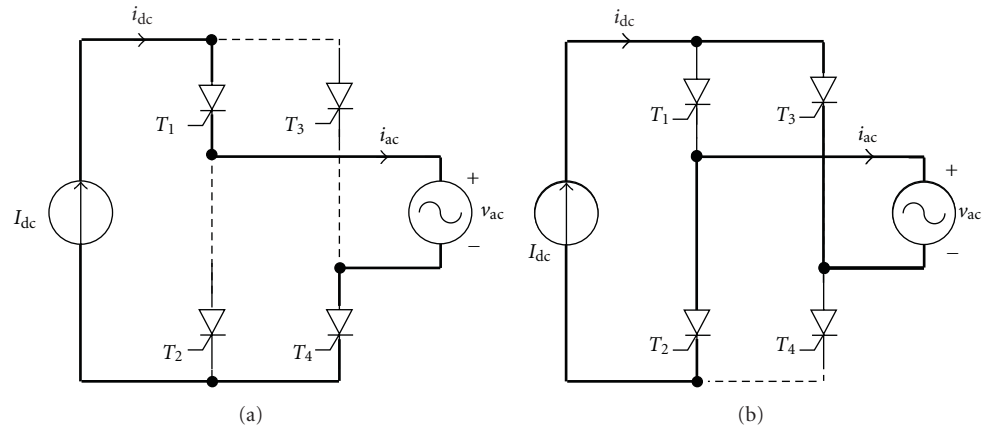

FIGURE 7: AC-side operation—(a) $v_{ac} > 0$ and (b) $v_{ac} < 0$.

Therefore, the utility current i_{ac} can be defined as

$$i_{ac}(t) = \begin{cases} i_{dc}(t); & \sin(\omega t) \geq 0 \\ -i_{dc}(t); & \sin(\omega t) < 0. \end{cases} \tag{4}$$

It should be noted that the low-pass filter is not considered in this analysis. Hence, the PWM output current i_{inv} is equal to the utility current i_{ac} ($i_{inv} = i_{ac}$).

2.4. PWM Current Analysis. From the PWM scheme in Section 2.2, the analysis of harmonic components in the proposed CSI can be performed. The mathematical expression of the PWM currents i_1 and i_2 can generally be expressed as follows [3]:

$$\begin{aligned} i_1(t) &= \frac{m_{pv} I_{pv}}{2} \cdot |\sin(\omega t)| \\ &\quad + \sum_{k=1}^{\infty} \frac{I_{pv}}{\pi k} \cdot \sin\left[k\pi m_{pv} |\sin(\omega t)|\right] \cdot \cos(k\omega_s t). \\ i_2(t) &= \frac{m_{wind} I_{wind}}{2} \cdot |\sin(\omega t)| \\ &\quad + \sum_{k=1}^{\infty} \frac{I_{wind}}{\pi k} \cdot \sin[k\pi m_{wind} |\sin(\omega t)|] \cdot \cos(k\omega_s t), \end{aligned} \tag{5}$$

where k = the number of kth harmonic component; $\omega \ll \omega_s$; $\omega = 2\pi f_{line}$ and $\omega_s = 2\pi f_{sw}$; $m_{pv} = V_{m,pv}/V_{cr}$ and $m_{wind} = V_{m,wind}/V_{cr}$; m_{pv} and m_{wind} are the modulation index of PV and wind sources, respectively; $V_{m,pv}$ and $V_{m,wind}$ are the peaks of modulating signals for PV and wind sources $v_{m,pv}$ and $v_{m,wind}$, respectively; V_{cr} is the peak of the triangular carrier waveform v_{cr}. Equations (5) are valid to $0 \leq m_{pv} \leq 1$ and $0 \leq m_{wind} \leq 1$, respectively.

The DC-link current i_{dc} can be found from

$$i_{dc}(t) = i_1(t) + i_2(t). \tag{6}$$

Thus,

$$\begin{aligned} i_{dc}(t) &= \frac{1}{2}\left(m_{pv} I_{pv} + m_{wind} I_{wind}\right) \cdot |\sin(\omega t)| \\ &\quad + \sum_{k=1}^{\infty} \frac{I_{pv}}{\pi k} \cdot \sin\left[k\pi m_{pv} |\sin(\omega t)|\right] \cdot \cos(k\omega_s t) \\ &\quad + \sum_{k=1}^{\infty} \frac{I_{wind}}{\pi k} \cdot \sin[k\pi m_{wind} |\sin(\omega t)|] \cdot \cos(k\omega_s t). \end{aligned} \tag{7}$$

According to (4) the inverter output current i_{inv} can be obtained by the operating of the unfolding circuit. Hence, the inverter output current i_{inv} can be expressed in terms of its harmonic components as

$$\begin{aligned} i_{inv}(t) &= \frac{1}{2}\left(m_{pv} I_{pv} + m_{wind} I_{wind}\right) \cdot \sin(\omega t) \\ &\quad + \sum_{k=1}^{\infty} \frac{I_{pv}}{\pi k} \cdot \sin\left[k\pi m_{pv} \sin(\omega t)\right] \cdot \cos(k\omega_s t) \\ &\quad + \sum_{k=1}^{\infty} \frac{I_{wind}}{\pi k} \cdot \sin[k\pi m_{wind} \sin(\omega t)] \cdot \cos(k\omega_s t). \end{aligned} \tag{8}$$

Under the conditions of $I_{pv} = I_{wind}$ and $m_{pv} \neq m_{wind}$, the waveform of the inverter output current i_{inv} and its harmonic contents in (8) can be shown in Figure 8. It can be observed that the waveform of the inverter current i_{inv} is close to a unipolar PWM waveform. We can consider at the conditions of $I_{pv} = I_{wind} = I$ and $m_{pv} = m_{wind} = m$, the current i_{inv} simplified as follows:

$$\begin{aligned} i_{inv}(t) &= mI \cdot \sin(\omega t) \\ &\quad + \sum_{k=1}^{\infty} \frac{2I}{\pi k} \cdot \sin[k\pi m \sin(\omega t)] \cdot \cos(k\omega_s t). \end{aligned} \tag{9}$$

From this result, the PWM inverter current i_{inv} can be shown in Figure 9(a). This waveform is similar to a unipolar PWM waveform. Figure 9(b) shows the harmonic spectrum of the inverter current i_{inv}. It can be seen that the current has

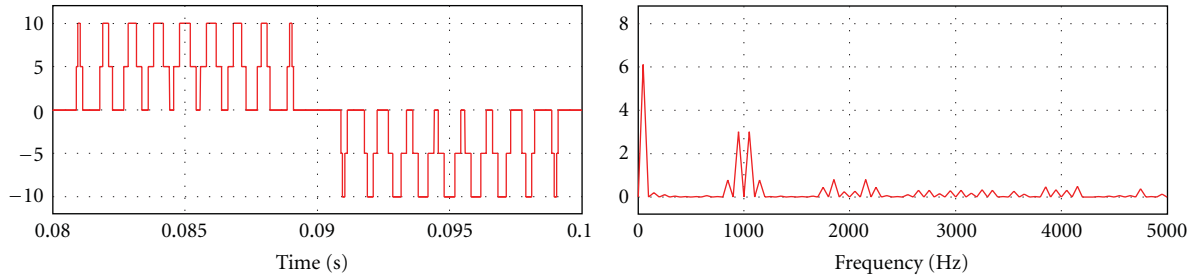

Figure 8: PWM output current waveform i_{inv} and harmonic content of the proposed circuit operating at $m_{pv} \neq m_{wind}$, $I_{pv} = I_{wind}$, $f_{line} = 50$ Hz and $f_{sw} = 1$ kHz.

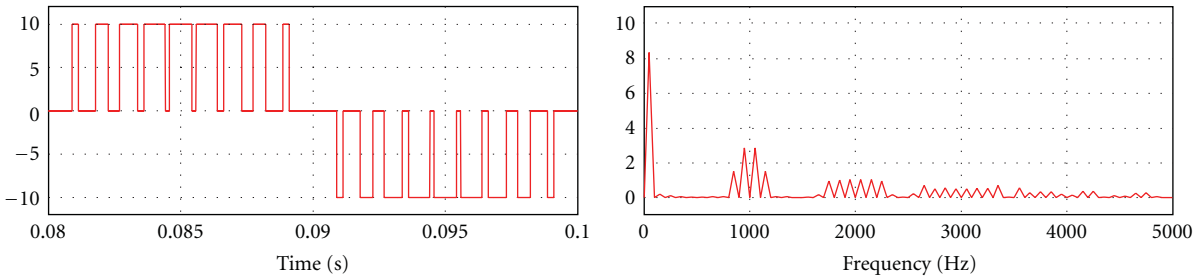

Figure 9: PWM output current waveform i_{inv} and harmonic content of the proposed circuit operating at $m_{pv} = m_{wind}$, $I_{pv} = I_{wind}$, $f_{line} = 50$ Hz, and $f_{sw} = 1$ kHz.

harmonics at the multiples of the switching frequency, that is, at f_{sw}, $2f_{sw}$, and so on. The harmonics of significant magnitudes also appear in the side bands of the switching frequency and its multiples.

2.5. Carrier-Based PWM Scheme. In order to reduce the harmonic distortion in the inverter output current i_{inv}, a carrier-based PWM scheme can be proposed. In general, this scheme can be classified into two categories: phase-shifted and level-shifted modulations. In this paper, a phase-shifted modulation is only studied and applied to the proposed hybrid PV/wind power systems. Normally, the hybrid PV/wind system may be connected in parallel more than two energy sources. The n energy sources require n triangular carrier signals. For the phase-shifted multicarrier modulation, the carrier waves for each module $v_{cr,pv}$ and $v_{cr,wind}$ are of same amplitude and frequency, but there is a phase shift ϕ_{cr} between any the adjacent carrier waves, given by

$$\phi_{cr} = \frac{360^\circ}{n}. \tag{10}$$

For the proposed hybrid PV/wind system as shown in the Figure 3(a), there are two energy sources for system. The modulating signals $v_{m,pv}$ and $v_{m,wind}$ have the same frequency but the amplitude is different depending on the MPPT signals of each module. According to (10), the phase shift ϕ_{cr} between each carrier wave $v_{cr,pv}$ and $v_{cr,wind}$ is 180°. The gate signals $v_{S,pv}$ and $v_{S,wind}$ are generated by comparing

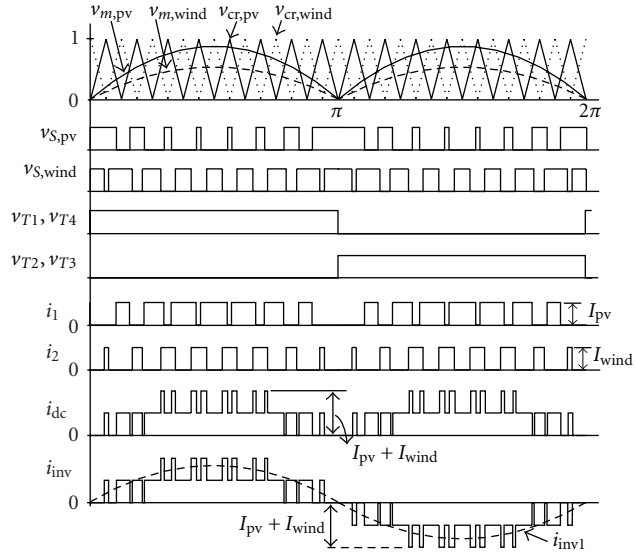

Figure 10: The steady-state waveforms of the proposed phase-shifted PWM multicarrier modulation.

the modulating wave $v_{m,pv}$ and $v_{m,wind}$ with the carrier waves $v_{cr,pv}$ and $v_{cr,wind}$, respectively. The principle of the proposed phase-shifted modulation for the hybrid PV/wind system can be shown in Figure 10. The inverter operates under the conditions of $I_{pv} = I_{wind} = I$ and $m_{pv} = m_{wind} = m$.

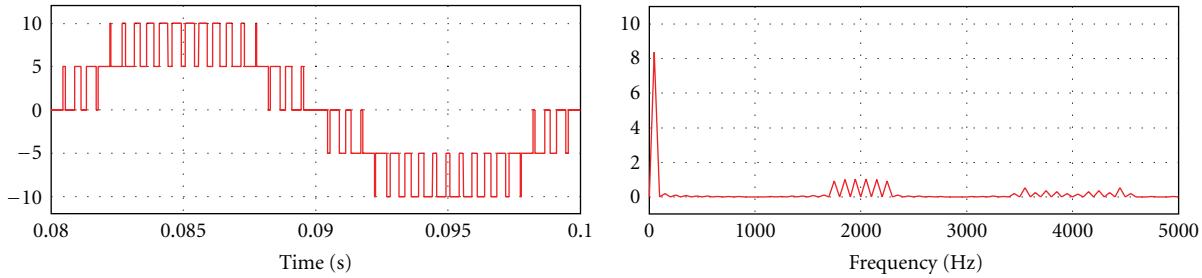

Figure 11: PWM output current waveform i_{inv} and harmonic content of the proposed circuit with phase-shifted modulation operating at $I_{pv} = I_{wind}$, $m_{pv} = m_{wind}$, $f_{line} = 50$ Hz, and $f_{sw} = 1$ kHz.

The inverter PWM current i_{inv} can be expressed in terms of Fourier series as [3]

$$i_{inv}(t) = mI \cdot \sin(\omega t) + \sum_{\text{even } k} \frac{2I}{\pi k} \cdot \sin[k\pi m \sin(\omega t)] \cdot \cos(k\omega_s t). \quad (11)$$

The inverter output current waveform i_{inv} based on phase-shifted multicarrier modulation is shown in Figure 11(a), and its spectrum is also illustrated in Figure 11(b). The operating conditions are $I_{pv} = I_{wind} = I$, $m_{pv} = m_{wind} = m$, $f_{line} = 50$ Hz, and $f_{sw} = 1$ kHz. The inverter current has harmonics and sidebands at the multiple of the twice switching frequency, that is, $2f_{sw}$, $4f_{sw}$, and so on. It is clear that the current waveform is formed by five current steps: $2I$, I, 0, $-I$, and $-2I$, resulting in a further reduction in THD.

3. Design Consideration

3.1. Input DC Choke Design. Large inductors L_{pv} and L_{wind} are used in the DC-side of the inverter, which make the input voltage sources v_{pv} and v_{wind} appear as the constant DC current sources I_{pv} and I_{wind}. When the chopper switch is turned on, the inductor current rises and the energy is stored in the inductor. If switch is turned off, the energy stored in the inductor is transferred to the AC-side through the diode and the inductor current falls. To design the value of this inductor, the inductor stored energy must be considered. When the switch is turned on, the energy stored in the inductor is

$$E_L = \frac{1}{2}LI^2 = P_{dc}T_{on}, \quad (12)$$

where L = choke inductance, P_{dc} = average input power at DC-side, T = switching period, $T_{on} = T/2$ = turn-on time, and I = average input current. The choke inductance can be expressed as

$$L = \frac{P_{ac}}{\eta I^2 f_{sw}}, \quad (13)$$

where η = converter efficiency, $P_{ac} = \eta \cdot P_{dc}$ = average output power at AC-side, and f_{sw} = switching frequency.

Table 1: Simulation parameters.

Output-rated power	$P_{ac} = 1000$ W
PV source current	$I_{pv} = 5$ A
Wind source current	$I_{wind} = 5$ A
Utility grid voltage	$v_{ac} = 220$ V_{rms}
Utility grid frequency	$f_{line} = 50$ Hz
Chopper switching frequency	$f_{sw} = 3$ kHz
Input inductor for PV converter	$L_{pv} = 13$ mH
Input inductor for wind converter	$L_{wind} = 13$ mH
Low-pass filter inductor	$L_f = 4$ mH
Low-pass filter capacitor	$C_f = 2\,\mu$F

3.2. Output Low-Pass Filter Design. In order to reduce the high-frequency harmonics in the PWM output current i_{inv} of the grid-connected inverter, a low-pass filter is needed. Passive low-pass filters are normally used as L, LC, CL, and LCL filters. In this paper, a simple CL low-pass filter is chosen. A detailed analysis is not considered in this paper. Following the design procedure of [10], the inductor L_f and capacitor C_f can be found through the following equations:

$$L_f = \frac{V_{ac}}{P_{ac} 2\pi f_{sw}}, \qquad C_f = \frac{0.33}{2\pi f_{sw} L_f}, \quad (14)$$

where V_{ac} is the amplitude of the grid voltage v_{ac}.

4. Results and Discussion

To verify the proposed grid-connected CSI for hybrid PV/wind system with a simple current-sharing technique, the simulation setup has been designed and carried out with PSIM. It should be noted that the MPPT operating for PV and wind energy is not studied in this paper. The circuit parameters are shown in Table 1. The PV and wind energy sources v_{pv} and v_{wind} and input DC chokes L_{pv} and L_{wind} are modeled by DC current sources I_{pv} and I_{wind}, respectively.

Figure 12 confirms the principle of PWM strategy for the proposed CSI operating under the condition of $m_{pv} = 0.9$ and $m_{wind} = 0.4$. The gate signals for all switches in CSI $v_{S,pv}$,

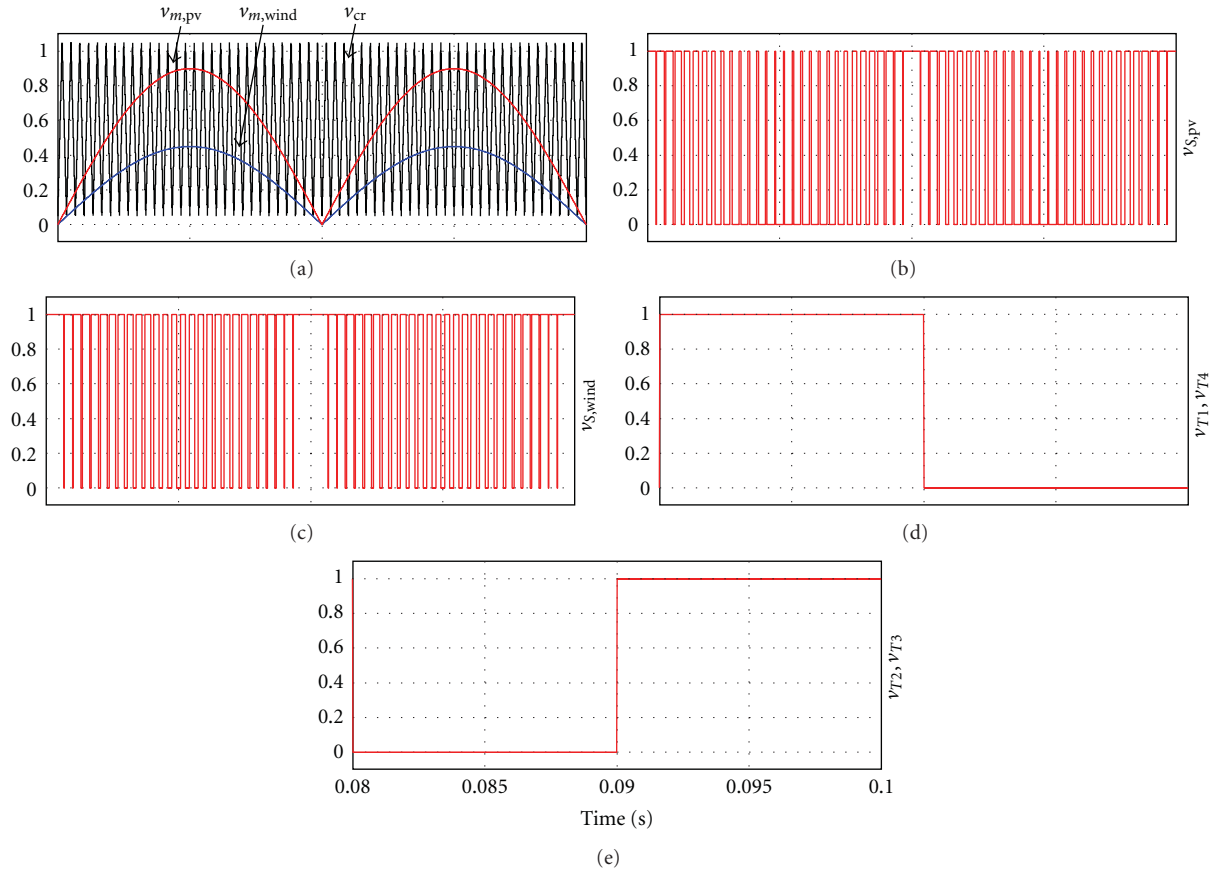

FIGURE 12: PWM switching strategy (top to bottom) $v_{m,pv}$, $v_{m,wind}$, v_{cr}, $v_{S,pv}$, $v_{S,wind}$, v_{T1}, v_{T4}, v_{T2}, and v_{T3}.

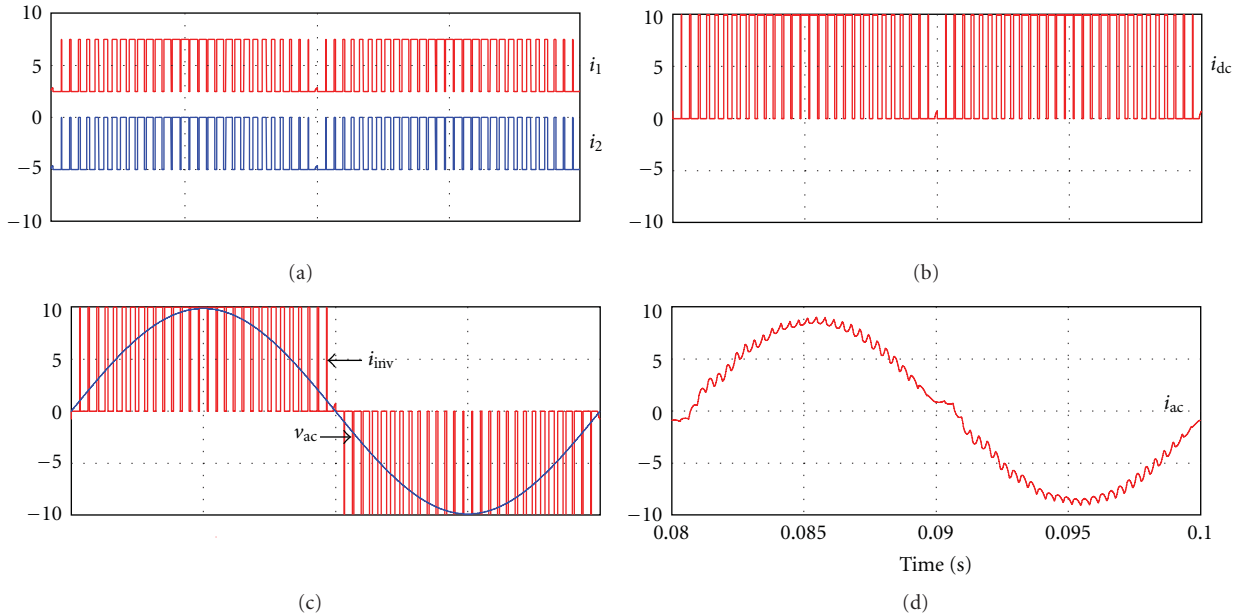

FIGURE 13: Operation of the system under the conditions of $m_{pv} = m_{wind}$, $I_{pv} = I_{wind}$, $f_{line} = 50$ Hz and $f_{sw} = 3$ kHz (top to bottom) i_1, i_2, i_{dc}, i_{inv}, v_{ac}, and i_{ac}.

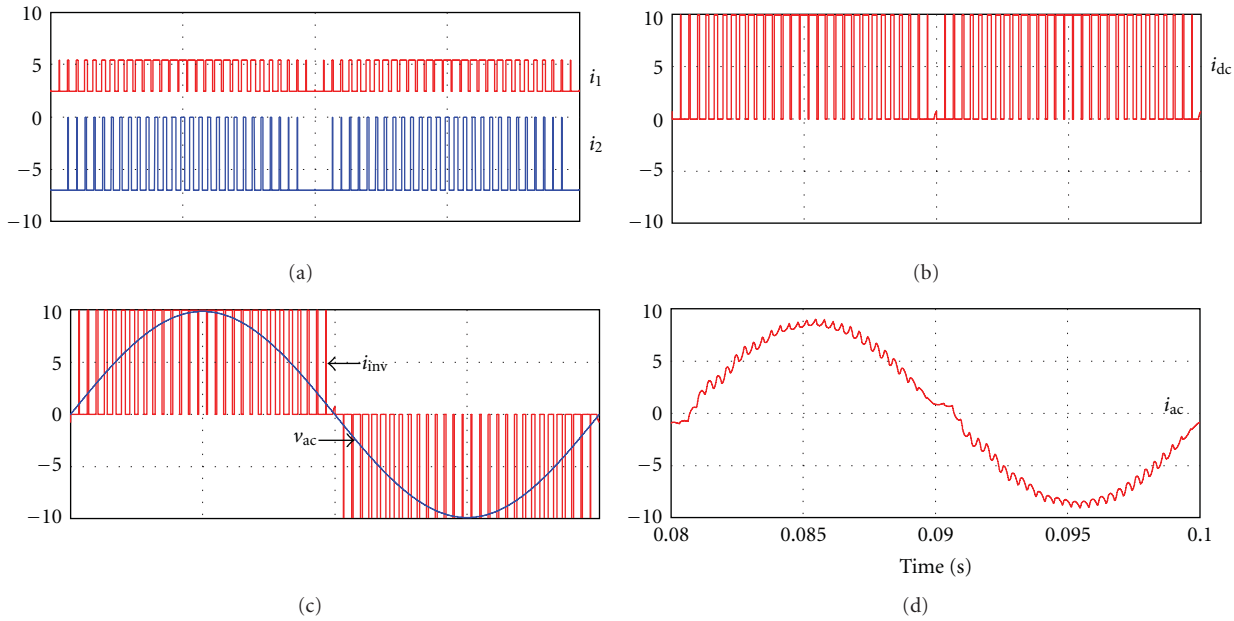

FIGURE 14: Operation of the system under the conditions of $m_{pv} = m_{wind}$, $I_{pv} < I_{wind}$, $f_{line} = 50$ Hz and $f_{sw} = 3$ kHz (top to bottom) i_1, i_2, i_{dc}, i_{inv}, v_{ac}, and i_{ac}.

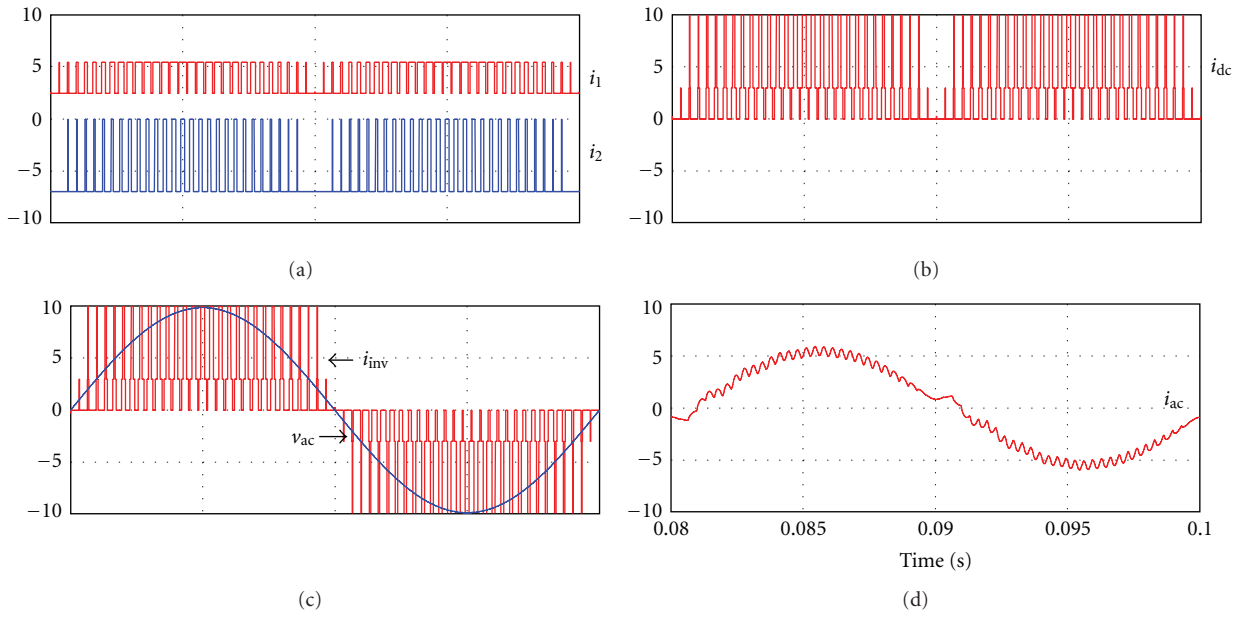

FIGURE 15: Operation of the system under the conditions of $m_{pv} > m_{wind}$, $I_{pv} < I_{wind}$, $f_{line} = 50$ Hz and $f_{sw} = 3$ kHz (top to bottom) i_1, i_2, i_{dc}, i_{inv}, v_{ac}, and i_{ac}.

$v_{S,wind}$, v_{T1}, v_{T2}, v_{T3}, and v_{T4} are also shown in Figure 12. Figures 13, 14 and 15 show the simulated waveform for the proposed CSI, operating under the different conditions, (a) $m_{pv} = m_{wind}$ and $I_{pv} = I_{wind}$; (b) $m_{pv} = m_{wind}$ and $I_{pv} < I_{wind}$; (c) $m_{pv} > m_{wind}$ and $I_{pv} < I_{wind}$. The following can be observed.

(a) The two different currents i_1 and i_2 can be combined to produce the current i_{dc} at a DC-bus.

(b) The amplitude of i_{dc} can be determined by $I_{DC} = I_{pv} + I_{wind}$. The magnitude of i_1 and i_2 can be independently controlled by the output power of each energy source.

(c) The unfolding circuit has two complementary switch pairs (T_1, T_4 and T_2, T_3) switching at line frequency 50 Hz. The unipolar PWM current i_{inv} is performed by unfolding the DC-link current i_{dc}.

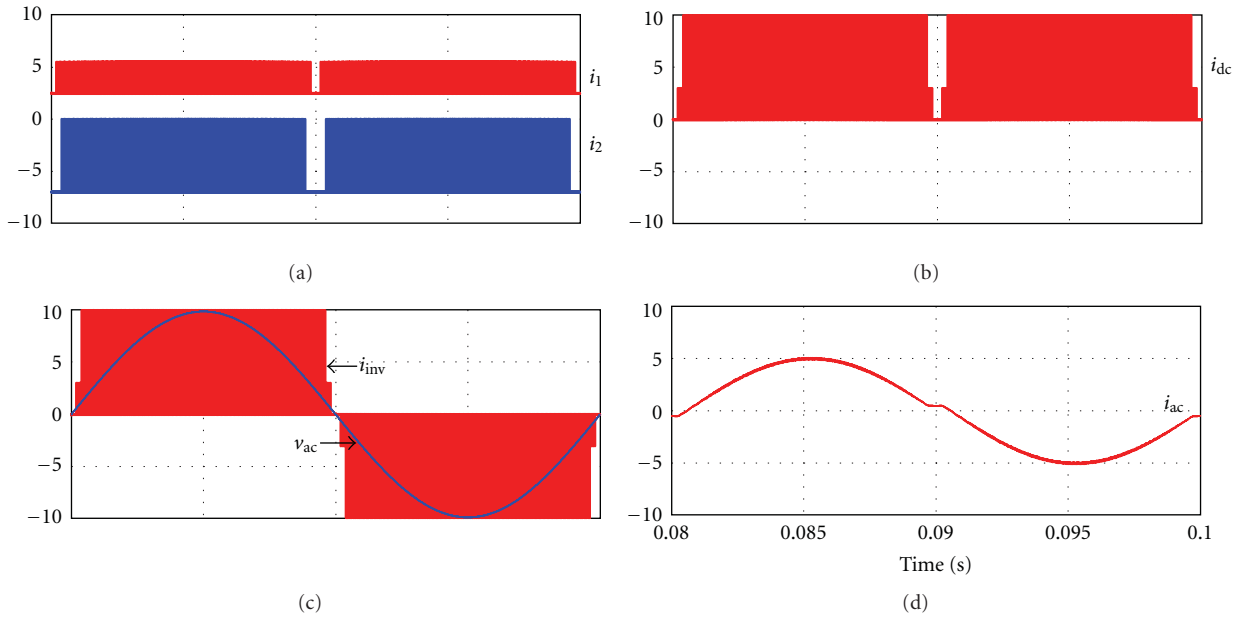

FIGURE 16: Operation of the system under the conditions of $m_{pv} > m_{wind}$, $I_{pv} < I_{wind}$, $f_{line} = 50$ Hz and $f_{sw} = 20$ kHz (top to bottom) i_1, i_2, i_{dc}, i_{inv}, and i_{ac}.

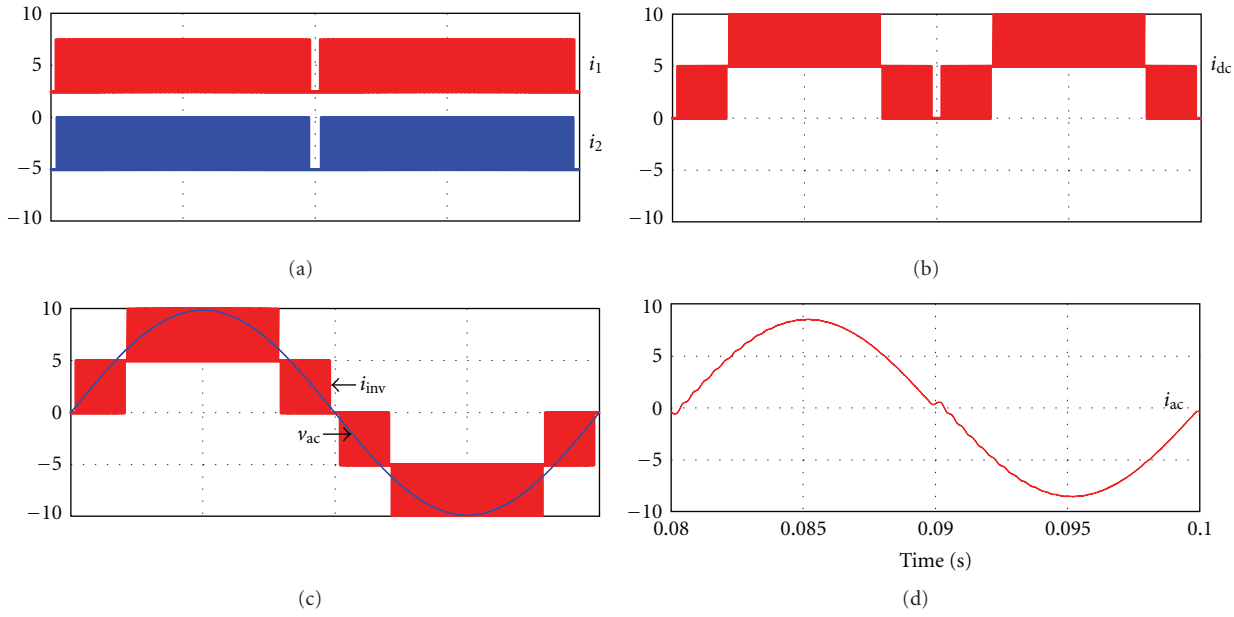

FIGURE 17: Simulated waveforms of the hybrid PV/wind system with phase-shifted PWM operating under the conditions of $m_{pv} = m_{wind}$, $I_{pv} = I_{wind}$, $f_{line} = 50$ Hz and $f_{sw} = 20$ kHz (top to bottom) i_1, i_2, i_{dc}, i_{inv}, v_{ac}, and i_{ac}.

(d) The waveform of the grid current i_{ac} is close to sinusoidal with low THD. The low amount of harmonic distortion is due to the elimination of high-order harmonic contents by the filtering effect of CL low-pass filter.

Figure 16 shows the simulated waveforms for the proposed CSI, operating at higher switching frequency. It can be observed that the proposed converter can produce a smooth AC current at the utility grid with low harmonic components. The waveforms of the proposed grid-connected CSI for hybrid PV/wind system with phase-shifted multicarrier modulation are shown in Figure 17. It can be noted that the inverter output current waveform i_{inv} is formed with five current levels.

In higher power applications, the increasing of output power rating of a hybrid PV/wind power generation system is required. It can be achieved by connecting more PV/wind

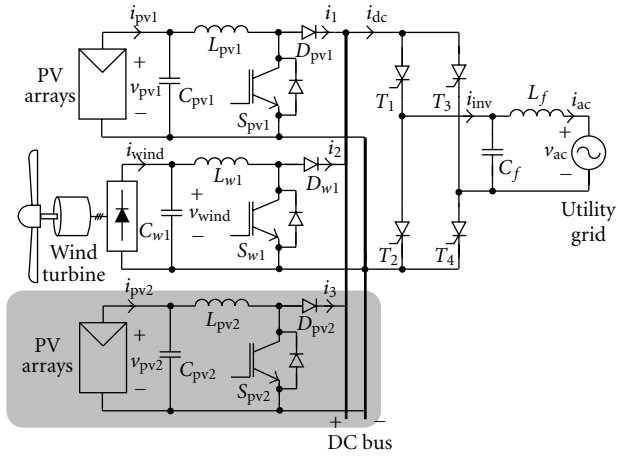

Figure 18: Extension energy sources for increasing the output power of the proposed hybrid PV/wind system.

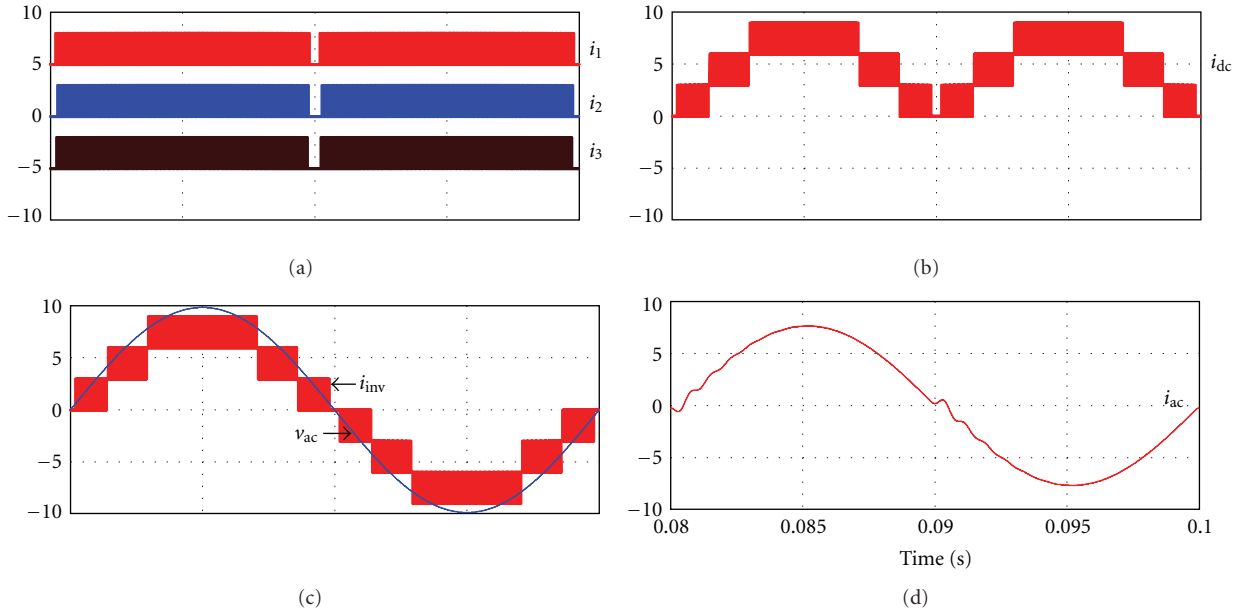

Figure 19: Simulated waveforms of the multimodules hybrid PV/wind system with phase-shifted PWM operating under the conditions of $m_{pv1} = m_{wind} = m_{pv2}$, $I_{pv1} = I_{wind} = I_{pv2}$, $f_{line} = 50$ Hz and $f_{sw} = 20$ kHz (top to bottom) i_1, i_2, i_3, i_{dc}, i_{inv}, v_{ac}, and i_{ac}.

modules in parallel with the other modules through their own DC-DC chopper to a common DC-bus. The configuration of multimodules PV/wind system with all modules connected in parallel is shown in Figure 18. The waveforms of the converter can be shown in Figure 19.

5. Conclusion

A grid-connected inverter for hybrid PV/wind power generation system was proposed. The proposed inverter was based on the current source inverter (CSI) topology. A number of issues were investigated, including the simple current sharing technique, the inverter configuration, operating principle, PWM strategy technique, PWM current analysis, and design consideration. The emphasis of this paper was on the new power converter scheme, where the operating analysis was discussed in details. The proficiency of the proposed inverter was accessed through the computer simulation under the different operation conditions. The performance of the proposed CSI was confirmed by the simulation results.

Acknowledgments

This work is supported in part by Thailand Research Fund (TRF) through the Royal Golden Jubilee Ph.D. program under Grant no. PHD/0166/2550, by the French Government's contribution to the RGJ-Ph.D program, and by the Energy Policy and Planning Office (EPPO), Ministry of Energy, Thailand. This work is also supported by National Research University (NRU) Project from Office of the Higher Education Commission of Thailand.

References

[1] Y. M. Chen, Y. C. Liu, S. C. Hung, and C. S. Cheng, "Multi-input inverter for grid-connected hybrid PV/wind power system," *IEEE Transactions on Power Electronics*, vol. 22, no. 3, pp. 1070–1077, 2007.

[2] C. Liu, K. T. Chau, and X. Zhang, "An efficient wind-photovoltaic hybrid generation system using doubly excited permanent-magnet brushless machine," *IEEE Transactions on Industrial Electronics*, vol. 57, no. 3, pp. 831–839, 2010.

[3] P. G. Barbosa, H. A. C. Braga, M. C. B. Rodrigues, and E. C. Teixeira, "Boost current multilevel inverter and Its application on single-phase grid-connected photovoltaic systems," *IEEE Transactions on Power Electronics*, vol. 21, no. 4, pp. 1116–1124, 2006.

[4] Y. Chen and K. Smedley, "Three-phase boost-type grid-connected inverter," *IEEE Transactions on Power Electronics*, vol. 23, no. 5, pp. 2301–2309, 2008.

[5] N. Vázquez, H. López, C. Hernández, E. Vázquez, R. Osorio, and J. Arau, "A different multilevel current-source inverter," *IEEE Transactions on Industrial Electronics*, vol. 57, no. 8, pp. 2623–2632, 2010.

[6] R. T. H. Li, H. S. H. Chung, W. H. Lau, and B. Zhou, "Use of hybrid PWM and passive resonant snubber for a grid-connected CSI," *IEEE Transactions on Power Electronics*, vol. 25, no. 2, pp. 298–309, 2010.

[7] B. M. T. Ho and H. S. H. Chung, "An integrated inverter with maximum power tracking for grid-connected PV systems," *IEEE Transactions on Power Electronics*, vol. 20, no. 4, pp. 953–962, 2005.

[8] G. Ertasgin, D. M. Whaley, N. Ertugrul, and W. L. Soong, "Implementation and performance evaluation of a low-cost current-source grid-connected inverter for PV applications," in *Proceedings of the IEEE International Conference on Sustainable Energy Technologies (ICSET '08)*, pp. 939–944, November 2008.

[9] M. Kazerani, Z. C. Zhang, and B. T. Ooi, "Linearly controllable boost voltages from tri-level PWM current-source inverter," *IEEE Transactions on Industrial Electronics*, vol. 42, no. 1, pp. 72–77, 1995.

[10] B. Bouneb, D. M. Grant, A. Cruden, and J. R. McDonald, "Grid connected inverter suitable for economic residential fuel cell operation," in *Proceedings of the European Conference on Power Electronics and Applications*, p. 10, September 2005.

Hindawi Publishing Corporation
International Journal of Photoenergy
Volume 2012, Article ID 613969, 4 pages
doi:10.1155/2012/613969

Research Article

Photoanode of Dye-Sensitized Solar Cells Based on a ZnO/TiO_2 Composite Film

Lu-Ting Yan, Fang-Lue Wu, Lan Peng, Li-Juan Zhang, Pu-Jun Li, Sui-Yang Dou, and Tian-Xiang Li

School of Science, Beijing Jiaotong University, Beijing 100044, China

Correspondence should be addressed to Lu-Ting Yan, ltyan@bjtu.edu.cn

Received 6 April 2012; Accepted 12 July 2012

Academic Editor: G. N. Tiwari

A photoanode of dye-sensitized solar cells based on a ZnO/TiO_2 composite film was fabricated on a transparent conductive glass substrate using different techniques including electrophoretic deposition, screen printing, and colloidal spray coating. The ZnOs used in the composite film were ZnO tetrapods prepared via thermal evaporation and ZnO nanorods obtained via hydrothermal growth. The structural and morphological characterizations of the thin composite films were carried out using scanning electron microscope (SEM). The best power conversion was 1.87%, which corresponds to the laminated TiO_2/ZnO/TiO_2 structure prepared via screen printing.

1. Introduction

Dye-sensitized solar cells (DSSCs) have attracted increasing attention due to their high efficiency for energy conversion and low production cost compared with silicon solar cells [1, 2]. Photoanodes are important components of DSSC because of their functions in supporting dye molecules and transferring electrons. A high electron transport rate is required to reduce electron-hole recombination rate and enhance conversion efficiency. ZnO is one of the semiconductor materials containing abundant nanostructure morphologies and having high electron mobility (about 10^{-1}–10^{-3} $cm^2\,V^{-1}\,s^{-1}$ in ZnO nano-particle film and $>100\,cm^2\,V^{-1}\,s^{-1}$ in bulk ZnO). Recently, significant efforts have been given to the ZnO photoanode in place of the porous TiO_2 photoanode, in the hope of further enhancing the performance of solar cells by improving electron gathering and transporting efficiency and inhibiting charge recombination at the same time [3–6]. However, the instability of ZnO in acid dyes and its low electron injection efficiency from Ru-based dyes resulted in a low conversion efficiency of DSSC based on a pure ZnO photoanode [7]. Therefore, photoanodes built by two or more materials have attracted new attention due to the obvious advantages of combining different materials, that is, the high electron transport rate of ZnO and the high electron injection efficiency of TiO_2 from Ru-based dyes.

In this paper, a hybrid photoanode composed of ZnO and TiO_2 was fabricated on a SnO_2: F (FTO) transparent conductive glass substrate using different techniques including electrophoretic deposition, screen printing, and colloidal spray coating. Two kinds of ZnO, namely, ZnO tetrapods and ZnO nanorods, were adopted in this study. The structural and morphological characterizations of the composite thin films were carried out using scanning electron microscope (SEM). The current density-voltage (I-V) curve, under AM 1.5 illumination with a $100\,mW/cm^2$ light intensity, was measured and analyzed.

2. Experimental

2.1. ZnO Tetrapods and Nanorods Synthesis. ZnO tetrapods were prepared via the thermal evaporation method from our previous report [8]. ZnO nanorods were synthesized on the FTO glass substrates, with predeposited ZnO seed particles via the hydrothermal growth route. The ZnO seed layer was

prepared through combining a sol-gel process and a spin-coating technique, following the steps reported in [9].

2.2. Screen Printing. Approximately, 2.0 g of TiO_2 and 2.0 g of ZnO tetrapods were dispersed into two mixtures, each containing 0.4 g PEG-20000, 10 mL terpineol, 0.4 g ethyl cellulose, and 0.4 mL acetylacetone, and ground for 2 h, respectively.

A TiO_2 layer was screen printed on the faced-up conductive surface and then annealed at 450°C for 0.5 h. The procedure was repeated for the ZnO mixture. Lastly, another TiO_2 layer was screen printed and annealed under the same conditions. An alternative method for this process would be to spin coat one layer of TiO_2 sol first, and then screen printing the ZnO/TiO_2 layers to get the composite thin films.

2.3. Colloidal Spray Coating. The slurry used in colloidal spray coating is same with that used in screen printing. FTO glasses were vertically fixed on the walls with paper tape, and the spray gun is 30 cm away from the glasses. A ZnO layer was first spray coated on the FTO glasses followed by another TiO_2 layer. Afterward, the composite ZnO/TiO_2 layers were annealed at 450°C for 0.5 h.

2.4. Electrophoretic Deposition. The preparation of ZnO tetrapods/TiO_2 thin films through electrophoresis involves the following steps: (1) the mixture of 0.1000 g ZnO tetrapods and 0.0010 g TiO_2 were dispersed into the mixed solvent composed of 75 mL of ethanol and 25 mL of water under ultrasonic dispersion for 10 min; (2) two clean FTO glass substrates were used as positive and negative electrodes with a 1.5 cm space between the two electrode surfaces; (3) the electrophoresis voltage was set to 60 V; (4) the sample was annealed at 150°C for 20 min after electrophoresis; (5) steps 1–4 were repeated to obtain three ZnO tetrapods/TiO_2 layers; (6) finally, the composite films were annealed at 450°C for 0.5 h.

2.5. ZnO Nanorods/TiO_2 Composite Film. TiO_2 sol was first prepared using 16 mL of tetrabutyltitanate, 10 mL of ethylene glycol monomethylether, 40 mL of ethanol, and 0.0240 g of PEG, which were mixed and stirred at 60°C.

Subsequently, the FTO glass with ZnO nanorods was soaked in the solution for about 0.5 h and then annealed at 450°C for 0.5 h.

2.6. DSSC Assembly. The prepared ZnO/TiO_2 hybrid photoanodes were immersed in a N3 ethanol solution for 5 h to absorb the dye and then washed with ethanol several times. A Pt-coated FTO glass was used as a counterelectrode. The electrolyte was then dropped into it, and a sandwich type of solar cell was fabricated and employed to measure the photo-to-electric conversion efficiency.

2.7. Characterizations. The morphology of the ZnO/TiO_2 composite photoanodes was measured using SEM (Hitachi S-4800). The *I-V* characteristics of the solar cells were measured using a Keithley 2410 source meter under 1-sun illumination (AM 1.5, 100 mW/cm^2) from a solar simulator.

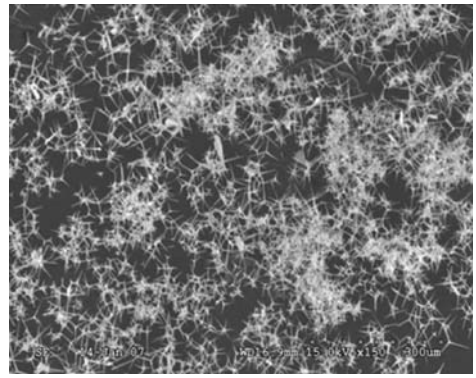

Figure 1: SEM image of the ZnO tetrapods.

3. Results and Discussion

3.1. Morphology of ZnO and ZnO/TiO_2 Composite Film. Figure 1 shows the SEM image of the ZnO tetrapods obtained via the thermal evaporation method, which is the easiest way to prepare ZnO tetrapods. Zinc powder was placed directly into the reactor for thermal evaporation and oxidation. No catalyst is needed in this process, and the reaction atmosphere needs not be controlled in the reactor as well. In addition, the ZnO tetrapods prepared using thermal evaporation exhibited perfect morphology with high crystal quality.

Figure 2 shows the SEM image of ZnO nanorods obtained via hydrothermal growth. The ZnO nanorods showed perfect hexagonal shapes with good orientations.

Figure 3 shows the cross-sectional and top-view images of the ZnO tetrapods/TiO_2 photo-anode fabricated via screen printing. The image shows that the ZnO tetrapods/TiO_2 composite film exhibits a uniform porous structure, which can greatly increase the surface area and improve dye absorption.

Figure 4 shows the SEM image of the composite film fabricated through colloidal spray coating. The film also has a porous structure. However, this porous structure is not uniform compared with the film prepared via screen printing. Figure 5 presents the morphology of the electrophoretic deposited ZnO tetrapods/TiO_2 composite film, which also shows a porous structure.

Figure 6 shows the morphology of ZnO nanorods/TiO_2 composite film, and the TiO_2 nanoparticles show a dense packing that is unfavorable to dye absorption.

3.2. DSSC Performance. Figure 7 shows the *I-V* characteristics of DSSC under AM 1.5 illumination with a 100 mW/cm^2 light density. The short-circuit current density (JSC), open-circuit voltage (VOC), fill factor (FF), and energy conversion (η) derived from the *I-V* curve are listed in Table 1. The DSSC based on the screen printing laminated TiO_2/ZnO tetrapods/TiO_2 photoanode has the highest efficiency of

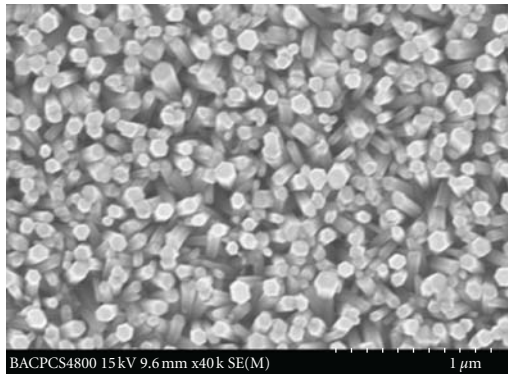

Figure 2: SEM top-view image of the ZnO nanorods.

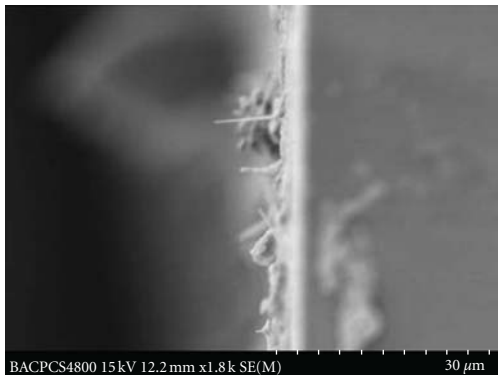

(a)

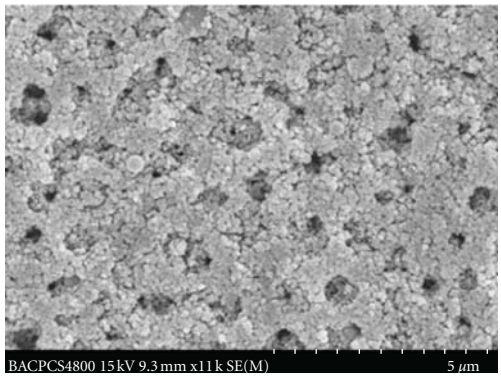

(b)

Figure 3: SEM cross-sectional (a) and top-view image (b) of ZnO tetrapods/TiO_2 photoanode fabricated via screen printing.

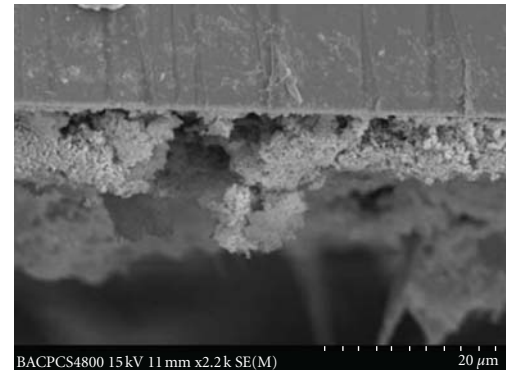

(a)

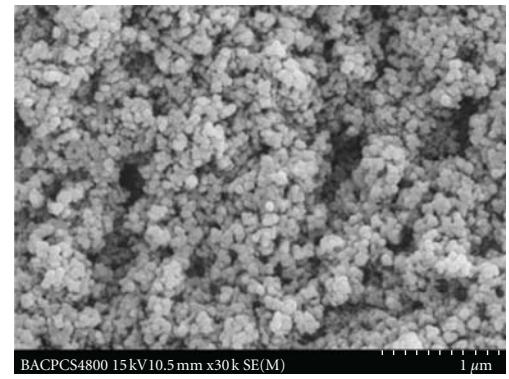

(b)

Figure 4: SEM cross-sectional (a) and top-view image (b) of ZnO tetrapods/TiO_2 photoanode fabricated through colloidal spray coating.

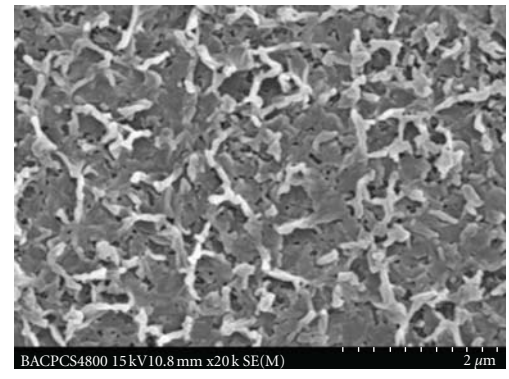

Figure 5: SEM image of ZnO tetrapods/TiO_2 photoanode fabricated via electrophoretic deposition.

1.87%, which is attributed to its uniform porous structure. On the other hand, the colloidal spray coated ZnO tetrapods/TiO_2 composite film has a nonuniform porous structure; thus, the efficiency of DSSC based on it decreased to 0.34%. The ZnO nanorod/TiO_2 has a densely packed structure and is unfavorable for dye absorption, causing its efficiency to decrease to 0.24%. The DSSC based on the electrophoretic deposited ZnO tetrapods/TiO_2 composite photoanode has the lowest efficiency of 0.1%, which may be due to the microlevel size of the ZnO tetrapods. This condition is unfavorable to electrophoretic deposition, resulting in a poor quality composite film. Another reason may be that the best ratio of ZnO to TiO_2 and the optimal electrophoresis parameters remain unknown. On account of the high electron transport efficiency and a variety of morphology structures of ZnO, ZnO/TiO_2 composite photoanodes still prove to be very good prospects in improving the photoelectric conversion efficiency of DSSCs.

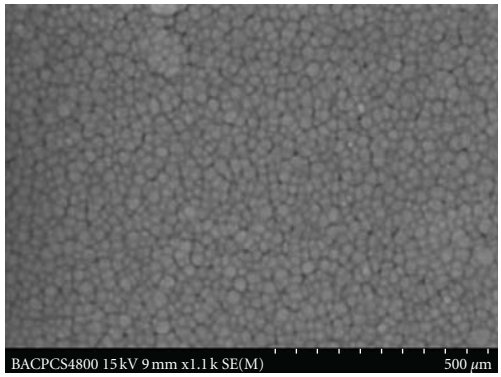

Figure 6: SEM image of ZnO nanorods/TiO_2 photoanode.

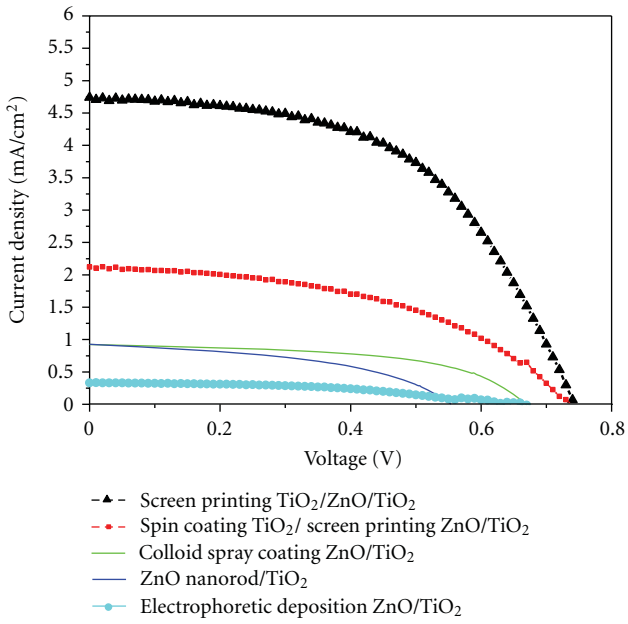

Figure 7: IV curve of DSSC based on ZnO/TiO_2 composite film.

4. Conclusions

Hybrid ZnO/TiO_2 photoanodes were prepared using electrophoresis deposition, screen printing, and colloidal spray coating to utilize the high electron transport rate of ZnO and the high electron injection efficiency and stability of TiO_2 materials. DSSCs based on these hybrid photoanodes were assembled. DSSC based on screen printing has the highest power conversion of 1.87%, whereas DSSC based on electrophoresis deposition has the lowest power conversion of 0.10%. Meanwhile, the large-sized ZnO tetrapods from thermal evaporation are not suitable for electrophoresis deposition and yielded a poor quality electrophoresis film. Thus, smaller-sized ZnO tetrapods from microemulsion and organic pyrolysis methods will be used for future electrophoresis deposition processes.

Table 1: Photovoltaic performance of DSSC based on ZnO/TiO_2 composite film.

Samples	Jsc (mA/cm^2)	Voc (V)	FF	Eff (%)
1	4.74	0.74	0.53	1.87
2	2.12	0.74	0.47	0.73
3	0.92	0.67	0.55	0.34
4	0.93	0.55	0.46	0.24
5	0.34	0.67	0.43	0.10

Acknowledgments

The work was supported by National Natural Science Foundation of China (60907014) and School Foundation of Beijing Jiaotong University (2009JBZ019-2), (2009JBM110).

References

[1] B. O'regan and M. Grätzel, "A low-cost, high-efficiency solar cell based on dye-sensitized colloidal TiO_2 films," *Nature*, vol. 353, no. 6346, pp. 737–740, 1991.

[2] M. Grätzel, "Conversion of sunlight to electric power by nanocrystalline dye-sensitized solar cells," *Journal of Photochemistry and Photobiology A*, vol. 164, no. 1–3, pp. 3–14, 2004.

[3] M. Law, L. E. Greene, J. C. Johnson, R. Saykally, and P. D. Yang, "Nanowire dye-sensitized solar cells," *Nature Materials*, vol. 4, no. 6, pp. 455–459, 2005.

[4] A. B. F. Martinson, J. W. Elam, J. T. Hupp, and M. J. Pellin, "ZnO nanotube based dye-sensitized solar cells," *Nano Letters*, vol. 7, no. 8, pp. 2183–2187, 2007.

[5] L. E. Greene, B. D. Yuhas, M. Law, D. Zitoun, and P. D. Yang, "Solution-grown zinc oxide nanowires," *Inorganic Chemistry*, vol. 45, no. 19, pp. 7535–7543, 2006.

[6] W. Chen, H. Zhang, I. M. Hsing, and S. Yang, "A new photoanode architecture of dye sensitized solar cell based on ZnO nanotetrapods with no need for calcination," *Electrochemistry Communications*, vol. 11, no. 5, pp. 1057–1060, 2009.

[7] Q. Zhang, C. S. Dandeneau, X. Zhou, and C. Cao, "ZnO nanostructures for dye-sensitized solar cells," *Advanced Materials*, vol. 21, no. 41, pp. 4087–4108, 2009.

[8] W. Peng, Y. Luting, W. Hongpeng, Z. Chunyan, and S. Wenjie, "Effect of process parameters on the preparation T-ZnOw," *Journal of Materials Science & Engineering*, vol. 27, no. 1, pp. 75–77, 2009.

[9] M. Ohyama, H. Kozuka, and T. Yoko, "Sol-gel preparation of ZnO films with extremely preferred orientation along (002) plane from zinc acetate solution," *Thin Solid Films*, vol. 306, no. 1, pp. 78–85, 1997.

Hindawi Publishing Corporation
International Journal of Photoenergy
Volume 2012, Article ID 869753, 8 pages
doi:10.1155/2012/869753

Review Article

Concentrating PV/T Hybrid System for Simultaneous Electricity and Usable Heat Generation: A Review

Longzhou Zhang, Dengwei Jing, Liang Zhao, Jinjia Wei, and Liejin Guo

International Research Center for Renewable Energy, State Key Laboratory of Multiphase Flow in Power Engineering, Xi'an Jiaotong University, Xi'an 710049, China

Correspondence should be addressed to Dengwei Jing, dwjing@mail.xjtu.edu.cn

Received 18 April 2012; Revised 14 June 2012; Accepted 22 July 2012

Academic Editor: Christophe Menezo

Photovoltaic (PV) power generation is one of the attractive choices for efficient utilization of solar energy. Considering that the efficiency and cost of PV cells cannot be significantly improved in near future, a relatively cheap concentrator to replace part of the expensive solar cells could be used. The photovoltaic thermal hybrid system (PV/T), combining active cooling with thermal electricity and providing both electricity and usable heat, can enhance the total efficiency of the system with reduced cell area. The effect of nonuniform light distribution and the heat dissipation on the performance of concentrating PV/T was discussed. Total utilization of solar light by spectral beam splitting technology was also introduced. In the last part, we proposed an integrated compound parabolic collector (CPC) plate with low precision solar tracking, ensuring effective collection of solar light with a significantly lowered cost. With the combination of beam splitting of solar spectrum, use of film solar cell, and active liquid cooling, efficient and full spectrum conversion of solar light to electricity and heat, in a low cost way, might be realized. The paper may offer a general guide to those who are interested in the development of low cost concentrating PV/T hybrid system.

1. Introduction

Solar energy is the richest renewable energy on Earth. It is pollutant-free, widely scattered, and inexhaustible. However, solar energy is of low density, dispersed, unstable, and discontinuous. Currently, methods for solar energy conversion mainly include solar hydrogen production, solar thermal power generation, and photovoltaic (PV) power generation. Compared with solar thermal power generation, PV power generation can realize direct photoelectrical conversion, leaving out the intermediate energy conversion step. Thus, its generating efficiency is not restrained by the Carnot cycle. Moreover, because of its less demand for solar radiation intensity, PV power generation has more extensive applicability and is the best choice for the distributed energy supply, such as in a small-scale households [1, 2]. Two urgent problems need to be addressed in solar PV application, that is, the high cost of PV power generation and the relatively low photoelectric conversion efficiency. Currently, the industrial production of crystalline silicon solar cell conversion efficiency is approximately 16% to 17%, the highest being only about 22%.

Under the circumstances in which the efficiency and cost of PV cells cannot be significantly improved in a short period, the following two approaches can be adopted to promote the large-scale commercialization of the technology. (1) The highly efficient and low-cost concentration technology should be developed. In this case, the unit area incident light intensity of the PV cell should be improved to reduce the cell area required for the given generated power. A relatively cheap concentrator as a replacement for the part of an expensive solar cell could be used. (2) When sunlight reaches the PV cell, incident photon energy should be converted into electric energy only. When the incident photon energy is more than the band gap of the semiconducting material, the extra energy not only cannot be converted into electric energy but into wasted heat, which severely affects the photoelectric conversion efficiency [3]. Experimental and theoretical researches on these two crucial issues have been conducted.

2. Traditional Concentrating PV System

The concentrator is an important component for concentrating PV systems. It is classified according to optical principle, concentrator types, and geometric concentration ratio. The line focus solar concentrator includes the lens, parabolic trough, and line focusing parabolic collector. The point focusing concentrator is called the axial concentrator. The concentrator lens or reflectors of this type of concentrator are on the same optical axis of the solar cell [4]. According to the geometric concentration ratio, the concentrator can be divided into a low-concentration system and a high-concentration system with a solar tracking. Although the concentration ratio of the low-concentration system is not high, the scattered radiation can be used without a solar tracking and be applied in the area with inadequate direct radiation. Generally, if the concentration ratio is more than 10, the system can only use direct sunlight. As a result, the tracking system must be adopted.

Since the mid-1970s, with a concentration ratio of 50 and efficiency of 12.7%, the first concentrating PV system was developed in Sandia National Laboratories in US. This technology has rapidly developed. In its earlier stage, the Fresnel lens was superior in property to other light concentrating devices. The passive cooling was also feasible with the high-concentration ratio, and the application of the diamond plate and copper heat sink promoted the development of the technology. The schematic diagram of the PV concentrator Fresnel lens is shown in Figure 1.

The solar PV power generation has benefited from the improvement of the Fresnel lens. For instance, the 20 kW point focusing Fresnel lens array was developed by Amonix and SunPower after 15 years of continuous research [5]. Ryu et al. [6] designed the modularized and microfaceted Fresnel lens with a moderate concentration ratio, bringing about efficient superposition and finally uniform distribution of incident solar flux. They also formulated a mathematical model to solve the distribution of the energy flux on PV panel and the collecting efficiency. The calculation indicates that the nonuniformity of energy distribution remains within 20%. Under the condition of the lower-middle concentration ratios (50 times), the radiation transmittance is more than 70%. Andreev et al. [7] designed the full-glass high-concentration ratio PV modular with second-concentration lens of small aperture between the Fresnel lens and cells, which further improve the light concentration. The concentrating ratio of the concentrator system reaches 1000, and the size of PV is only 1.2 mm. It is convenient to scaleup the module and improve its weathering resistance. Rosell et al. [8] designed a line focused PV system with Fresnel lens. It was found that heat conduction between solar cells and heat absorber is crucial to the energy efficiency of the whole system. Recently, Wu et al. [9] conducted extensive indoor experimental investigation on the heat loss from a point focus Fresnel lens PV concentrator with a concentration ratio of 100× under a range of simulated solar radiation intensities between 200 and 1000 W/m^2, different ambient air temperatures, and natural and forced convection. It was found that the solar cell temperature

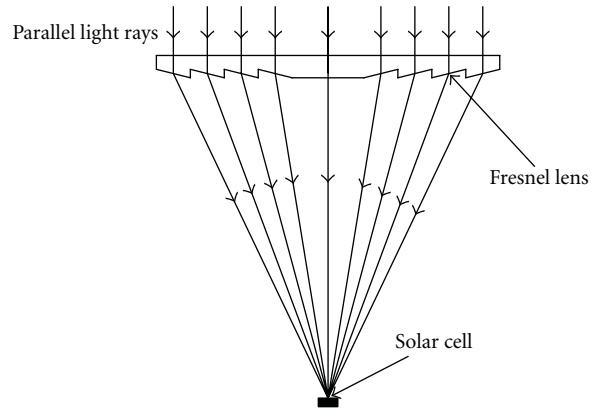

Figure 1: Schematic illustration of PV concentrator Fresnel lens [5].

increased proportionally with the increase in simulated solar radiation for all experimental tests, indicating that conductive and convective heat transfer were significantly larger than the long wave radiative heat transfer within and from the system.

The Fresnel lens belongs to the refractive concentrator, leading to a small light aperture and hence a small battery plate area. The reflecting concentrator can overcome this weakness. The point focused rotating parabolic concentrators and the line focused trough-type concentrators PV systems are mostly employed in the reflective PV concentrator. A representative 10 m^2 trough concentrator PV with geometric concentration ratio of 30.8 is shown in the left part of Figure 2 [10].

The trough-type PV system caused the solar cell to be between the sun and the reflecting surface. The solar cell is always below the reflective parabolic focal line where the rays are inevitably sheltered, thus leading to optical nonuniform flux distribution. In recent years, the butterfly-shaped PV concentrator has been developed. A row of plane mirrors is installed at its bottom. A solar cell module is fixed on its top, reducing the shelter of sunlight by the PV devices to a certain extent. Xu et al. [11] developed a butterfly-shaped PV concentrator, as shown by the right part of Figure 2. The sunlight reflected through the mirror plane uniformly reaches the solar cell array of the corresponding side, with its concentrations varying between 2 and 12 times.

A multidisc parabolic concentrator PV with a dual-axis tracking system was developed by NREL of US. This disc-type concentrator system includes 16 reflecting surfaces, with each surface containing 76 reflecting blocks. The mirror area of the system covers 113 m^2 with a highly precise tracking system and a concentration ratio of 250 [12]. The well-known Spanish solar energy research institution PSA developed a multidisc PV concentrator demonstration system with a concentration ratio of 2000. It includes the heliostat, optical grating, multidisc concentrator, and PV board and can simultaneously test the PV response to the direct solar radiation and thermal flux distribution [13].

In terms of the low concentration PV system, Solanki et al. [14] integrated the monocrystalline silicon solar cell into the V-type reflection trough made of aluminum foil,

(a) (b)

Figure 2: Representative trough (left hand) [10] and butterfly-shaped (right hand) concentration PV system [11].

which not only plays the role of reflection and concentration but also contributes to the heat dissipating capacity. However, its concentration ratio is only 2. The working temperature of the system is approximately the same as the one required for the nonconcentration condition. As a result, the efficient control of the temperature and the increase in the current density improve the output of the open circuit voltage. However, this type of concentrator not only has a low concentration ratio but also nonuniform radiation distribution and severe loss of reflection. In the different types of concentrating PV systems mentioned above, with the exception of the low-concentration V-type reflecting trough, the Fresnel lens, trough-type concentrator, butterfly-shaped PV concentrator, and multidisc parabolical mirror concentrator systems all need high-precision single-axis or dual-axis tracking, which uses only direct solar radiation and diffuse reflections (generally occupying 30% of the solar spectrum) which are unavailable for such tracking system.

Compound parabolic collector (CPC) is a nonimaging collector designed according to the marginal optical principle. Theoretically, all the incoming light with incident angle smaller than the maximum half acceptance angle (θ) could be line focused on the absorber. Both direct and diffuse portion of the solar radiation could be utilized. The performance of CPC is very close to that of the ideal concentrator. If the CPC concentrator adopts the stationary installation, the largest acceptance angle would be 30°. In this case, the concentration ratio would be less than 2 [15]. If the installation is in the east-west direction, and the tilt angle is adjustable, the largest acceptance angle would be less than 30°, with the concentration ratio as high as approximately 4 [16]. Nilsson et al. [17] designed a compound PV system with an asymmetric CPC and conducted investigation on the output performance of the system in different seasons and sunlight with MINSUN program. The research indicates that the total annual reflecting power of CPC with the reflective materials of anodic aluminum oxide and steel aluminum, respectively, is very close. When the PV panel faces the CPC light aperture, the output of the electric power per unit area is 205 Kwh/(m^2 cell area), and the output of the thermal energy in the cooling system is 145 kWh/m^2. Hatwaambo et al. [18] conducted research on the concentration PV system based on a single CPC and investigated the influence of the light incident angle and the tilt of CPC angle on the output performance of PV. Radiation flux distribution on PV surface was simulated by ray tracing. The theoretical model was validated by experimental measurement.

3. Cooling of Concentrating PV System

For different types of concentration PV at a fixed temperature, the general tendency of the change in the solar cell efficiency corresponds to the change in the concentration ratio. The cell efficiency increases with the increase in the concentration ratio at the low-concentration ratio and decreases with the increase in the concentration ratio at the high-concentration ratio. Under the condition of the given output power, the tandem-type cell may increase the voltage output and reduce the ohmic loss. However, the nonuniformity of light intensity distribution and the poor heat dissipation leads to overheat of the cell panel, affecting the current output of the whole cell array. This is the called "the current matching problem." The effective PV cell cooling or the appropriate design of the concentrator may lessen the consumption of the parasitic power [19].

Hein et al. [21] demonstrated that the distribution of light intensity produced by the parabolic trough concentrator is similar to a Gaussian curve. Compared to uniform illumination, both the open-circuit voltage and efficiency of the concentrator PV cell would decrease. The decrease could be aggravated when the peak intensity of light distribution is increased. This decrease may lead to a serious nonuniform flux distribution. Currently, tandem-type module was adopted by most polycrystalline silicon solar cells and the current output of each cell module is equal in this case. For such type of module, the low light intensity in some areas (corresponding to the smaller light current) greatly limits the general current output of the whole PV system. Therefore, in case one or more cells are shaded, for example, like in Figure 3(a), module performance will be limited by the output of these cells. For the thin film module in Figure 3(b) however, all cells span across the full length of the module. The current generation will therefore be equally affected for each cell, and the power output is only reduced in proportion to the shaded area [20].

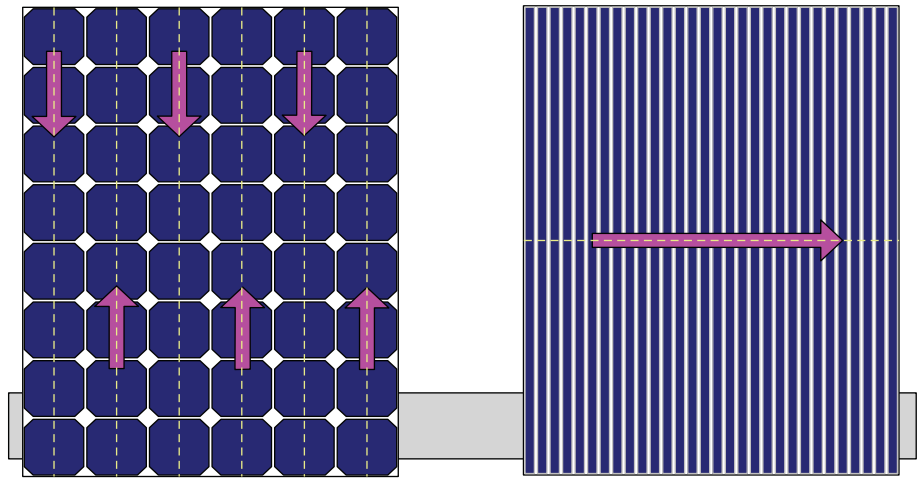

(a) (b)

Figure 3: Schematic drawing of a conventional c-Si module (a) and a thin film module (b) under nonuniform illumination. For each module, the order in which the cells are series connected is indicated with a dashed line [20].

Under the high concentration ratios, for instance, the multidisc concentrator with 150 concentration ratios, the PV system has a severe cooling problem. Such PV system requires active cooling and a lower thermal resistance [22–24]. To some extent, nonuniform flux distribution even exists in the CPC. For the CPC with a concentration ratio of 3 to 5, the concentration ratio in some points may reach 50. The nonuniform distribution of light intensity and poor heat dissipating may cause temperature gradient, especially in the high-concentrating PV. Recent research shows that the "Thomson effect" produced by the interaction between the temperature gradient and the electrical current may either improve or lower the power output of the cell [25], that is, when the current passes through the conductor with the temperature gradient, heat exchanges could take place absorbing or dissipating heat. Therefore, in the process of numerical simulation, the Thomson effect has to be considered.

As regards the cooling of the PV cell panel, except for the usual air or water cooling measures, techniques such as heat tube cooling, jet flow, microchannel cooling, and liquid immersion cooling has been investigated [26–28]. The liquid immersion cooling may effectively eradicate the contact thermal resistance caused by the traditional PV back cooling, thus improving cell efficiency. However, the study reveals that despite the quite uniform distribution of the temperature in the system, the long time immersion in the deionized water may also lower the I-V output performance of PV.

4. The Photovoltaic Thermal Hybrid System (PV/T)

The cooling modes mentioned above not only have a poor heat dissipating effect, but they also generate waste heat. The photovoltaic thermal hybrid system (PV/T) combining active cooling with thermal electricity provides both electricity and usable heat which can enhance total efficiency of the system. The area covered required for PV/T is also reduced compared to traditional PV. These factors are especially beneficial to the distributed energy supply.

For the nonconcentration, plate PV/T system as developed by Sandnes and Rekstad [29], the silicon PV cell is attached to the flat plate surface that is covered with the glass. For such system, the experiment was conducted mainly at a low water temperature. Saitoh et al. [30] developed a PV/T collector by attaching the silicon PV cell to the aluminum plate, whose back is made of copper tubing. The thermal output performance of the system was tested using salt water as working medium. Zakharchenko et al. [31] proposed a PV/T collector with its surface covered with a black PVC absorber, and the collector itself can combine with different PV cells. They found that when the area of the PV cell is smaller than that of the collector plate, and that the cell is located at the cooling water inlet, a better cooling effect and higher thermal efficiency could be achieved. Theoretically, the total energy efficiency of the PV/T system may reach 60%–80% [32]. Dupeyrat et al. proposed a real size PV/T module tested at Fraunhofer solar test facilities. The PV/T module showed a total efficiency of above 87% (79% thermal efficiency plus 8.7% electrical efficiency, based on the absorber area) [33]. An experimental flat plate PV/T collector was built by the same group using the single package lamination method, focusing on an improved heat transfer between PV cells and cooling fluid and on improved optical performance. The thermal efficiency at zero reduced temperature was measured at 79% under PV operation with a corresponding electrical efficiency of 8.8%, leading to a high overall efficiency of almost 88% [34].

Kostic et al. [35] studied the effect of reflectivity on the energy efficiency of a plate-type PV/T and optimized the installing position and tilt angle. The study shows that the reflection coefficient of the plate-type receiver made of aluminum plate and that of aluminum foil is almost the same.

However, the reflecting surface made of aluminum foil enhanced the concentration intensity, thus improving the total thermoelectricity conversion efficiency.

The PV/T system with the parabolic trough concentrator (concentration is 37 times, and the peak light intensity in some areas is 100 times) was developed by Coventry [36]. It has thermal efficiency of 58%, electrical efficiency of 11%, and total energy conversion efficiency of 69%. Wang et al. [37] constructed a trough-concentrating solar PV/T. Under the 10 times solar concentration, the monocrystalline silicon solar power could be increased by 5.05 times. Sun and Shi [38] analyzed the thermoelectric properties of the PV/T system with a parabolic solar concentrator and radiating fin. They established a one-dimensional steady-state mathematical model of the heat transfer process inside the PV/T. They also conducted a numerical simulation of the heat transfer process and analyzed the air mass flow, incident light intensity, concentration ratio, ambient temperature, height of the upper channel, and effect of the fin parameters on air temperature, cell plate temperature, and thermal efficiency of the system.

Studies on the system with a low concentration of CPC-based PV/T have also been conducted. However, most of them have fixed CPCs or CPCs that could only be quarterly adjusted. These PV/T systems adopt simple air cooling or water cooling. For instance, Garg and Adhikari [39] studied a PV/T with CPC as the concentrator and air as the cooling medium. The parametric analysis showed that with the increase in the length of the collector, the amount of air flow or the surface covering ratio of the collector would greatly enhance the heat and electricity output properties, whereas the increase in the width of the air flow channel is not beneficial. Othman et al. [40] designed a CPC-based double channel solar air collector installed with heat conducting fins. The air passes through the upper channel containing the glass plate and the PV panels. The PV plate is directly heated by the sun. Air coming out of the upper channel flows out from the channel at the bottom, where the heat exchange of air in the direction of the PV may be enforced, improving the efficiency of the system. The authors simultaneously analyzed the heat transfer efficiency of the system by adopting the one-dimensional steady-state model.

Brogren et al. [41] introduced a water-cooled PV-thermal hybrid system with low concentrating aluminium compound parabolic concentrators, as shown in Figure 4. The system was installed at 60.5°N 17.4°E of Sweden. The following are the system parameters: $C = 4$, the peak power output is 0.5 kW, the corresponding annual electric power output of the solar cell in the unit area is 250 kWh, and the thermal output is 800 kWh. The optical efficiency was calculated to be 0.71. The research also showed that the antireflection coating on the optimized glass plate and the improvement of the reflecting ratio of the reflecting material could improve the power output by approximately 20% [41]. It is worth noted here that most of CPC-based PV systems use very simple design either employing fixed installation or with periodical adjustment in a few months. The design will lead to significant variation under different solar azimuth (such as 9 a.m and 5 p.m. contrast), so the system output would show great fluctuation in one working day. Here, we propose a new concept of integrated flat CPC plate for effective solar collection. As shown in Figure 5, the integrated CPC plate could be adjusted in two axes manually or by electric machinery. Such low precision solar tracking ensure effective collection of solar light with a significantly lower cost compared to traditional high-precision solar tracking. However, the total reception of solar irradiation in one day could be significantly enhanced. In fact, our such design of integrated CPC plate has been successfully applied to the solar-to-hydrogen conversion and the technique is therefore believed to be also applicable to concentrating PV/T [42, 43].

Figure 4: A representative PV-CPC is installed in Sweden (60.58°N, 17.48°E). The cooling water is flowing (from west to east) in copper pipes integrated in the aluminum fin on the backside of the m-Si cells [38].

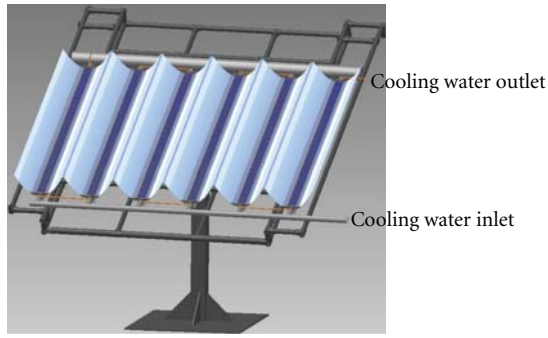

Figure 5: Our design of PV/T hybrid system composed of integrated CPC plate with low precision solar tracking.

5. Total Utilization of Solar Light by Spectral Beam Splitting Technology

The studies previously mentioned all aimed to improve the energy utilization efficiency of the whole system from the perspective of active and passive heat dissipation from the PV panel itself. In recent years, the concept of effective utilization of solar light by spectral beam splitting technology was proposed [44]. In contrast to the traditional solar PV utilization, this method achieves the photo-electricity and

thermal-electricity conversion by separately using the different parts of the solar spectrum. The thermal management problem in the traditional PV concentrator was effectively overcome by this method. Studies showed that the spectrum splitting PV/T hybrid system has several potential advantages over a PV-only system and it is especially suitable for working under high concentration conditions [45]. In such system, the thermal unit is no longer limited by the photoelectric unit, and the nanofluids directly absorbed solar radiation to achieve efficient photo-thermal conversion [46]. For instance, Jiang et al. [47] proposed such a PV/T design with a two-stage parabolic trough concentrator. A spectral splitting filter was added between the parabolic trough and the PV, filtering out the IR light. Based on the zero-dimensional optical model and the ray tracing method, the distribution of the energy flow was also analyzed.

Jiang et al. [48] achieved beam splitting with a 13-layer film and established a three-dimensional optical model by considering the solar angle. They studied the effect of the spectral beam splitting on the heat and electrical output properties of the semiparabolic trough concentrator in PV/T system. The spectral distribution in the system and the solar flux density distribution on the PV cell surface were investigated. Calculation showed that the optical efficiency of the system under the AM1.5 solar spectrum is 58.7%. The tilt angle of the cell should be optimized to achieve the uniform energy density for different concentrator apertures.

In terms of theoretical studies, Zhao et al. [49] conducted a numerical simulation of the absorption characteristics of the absorption medium, assuming the maximum passing through of the 200–800 nm and the maximum absorption of the 800–2000 nm solar spectrum. The simulation is based on the Lorentz-Drude model with damped oscillation. The derived expressions were validated by Kramers-Kronig conversion. The calculations indicated that the thermal unit could absorb 89% of the infrared and pass through 84% of visible light. If the upper flow rate is reduced, the outlet temperature may reach 74°C.

6. Conclusion and Perspective

To sum up, concentration PV can be classified into three categories in accordance with the comprehensive utilization of electricity or heat. (1) The temperature-control mode concentrating PV system with high concentration ratios (e.g., the immersion mode). It usually maintained a high electrical efficiency with low working temperature of below 50°C. It is unable to supply usable heat due to the small area of the cell unit. (2) The PV/T mode system, which uses PV as the major thermal supply, provides the usable heat at higher temperature such as 80°C. However, the power output of the PV will often be affected. (3) The full spectrum utilization of solar energy, that is, by spectral beam splitting technologies. It lowers the working temperature of PV, maintaining its high efficiency, and supplies the required thermal output due to its large PV surface area.

As described above, the current research on concentrating PV/T focuses mainly on the concentrators of Fresnel, trough-type, and butterfly-type, and so forth. The common weaknesses of these collectors are their high cost required by sun tracking. More importantly, these collectors cannot use the diffused solar light, which occupy a considerable part of the solar radiation and cover a large area of land. A few studies related to CPC concentrating PV/T system showed that CPC might be a good choice. However, most of these systems use very simple design of the CPC either employing fixed installation or with periodical adjustment in a few months. The design will lead to significant variation under different solar azimuth and therefore fluctuation in output. We proposed a PV system with integrated CPC plate as illustrated in Figure 5 to overcome these drawbacks. On the other hand, the maximal receiving and utilization of solar flux itself could be obtained by beam splitting of solar spectrum, such as by nanofluids. Combination of thin film solar cell to overcome nonuniform light distribution, active cooling for heat utilization and integrated CPC plate as solar collector, and efficient and full spectrum conversion of solar light to electricity and usable heat, in a low cost way, might be realized.

Acknowledgments

The authors gratefully acknowledge the financial support of the National Natural Science Foundation of China (no. 50821064, 20906074), National Basic Research Program of China (no. 2009CB220000) and 863 Program (no. 2012AA051501).

References

[1] V. Quaschning, "Technical and economical system comparison of photovoltaic and concentrating solar thermal power systems depending on annual global irradiation," *Solar Energy*, vol. 77, no. 2, pp. 171–178, 2004.

[2] H. A. Zondag, "Flat-plate PV-Thermal collectors and systems: a review," *Renewable & Sustainable Energy Reviews*, vol. 12, no. 4, pp. 891–959, 2008.

[3] L. T. Kostić, T. M. Pavlović, and Z. T. Pavlović, "Optimal design of orientation of PV/T collector with reflectors," *Applied Energy*, vol. 87, no. 10, pp. 3023–3029, 2010.

[4] G. Zubi, J. L. Bernal-Agustín, and G. V. Fracastoro, "High concentration photovoltaic systems applying III-V cells," *Renewable & Sustainable Energy Reviews*, vol. 13, no. 9, pp. 2645–2652, 2009.

[5] K. Ryu, J. G. Rhee, K. M. Park, and J. Kim, "Concept and design of modular Fresnel lenses for concentration solar PV system," *Solar Energy*, vol. 80, no. 12, pp. 1580–1587, 2006.

[6] V. Garboushian, D. Roubideaux, and S. W. Yoon, "Integrated high-concentration PV near-term alternative for low-cost large-scale solar electric power," *Solar Energy Materials & Solar Cells*, vol. 47, no. 1–4, pp. 315–323, 1997.

[7] V. M. Andreev, V. A. Grilikhes, V. P. Khvostikov et al., "Concentrator PV modules and solar cells for TPV systems," *Solar Energy Materials & Solar Cells*, vol. 84, no. 1–4, pp. 3–17, 2004.

[8] J. I. Rosell, X. Vallverdú, M. A. Lechón, and M. Ibáñez, "Design and simulation of a low concentrating photovoltaic/thermal system," *Energy Conversion & Management*, vol. 46, no. 18-19, pp. 3034–3046, 2005.

[9] Y. P. Wu, P. Eames, T. Mallick, and M. Sabry, "Experimental characterisation of a Fresnel lens photovoltaic concentrating system," *Solar Energy*, vol. 86, no. 1, pp. 430–440, 2012.

[10] M. Li, X. Ji, G. L. Li, Z. M. Yang, S. X. Wei, and L. L. Wang, "Performance investigation and optimization of the Trough Concentrating Photovoltaic/Thermal system," *Solar Energy*, vol. 85, no. 5, pp. 1028–1034, 2011.

[11] Z. L. Xu, J. D. Liu, P. F. Feng, D. P. Hou, J. Y. Zhang, and Y. M. Zhang, "Research on a butterfly concentrator for photovoltaic generation," *Acta Energiae Solaris Sinica*, vol. 28, no. 2, pp. 174–177, 2007.

[12] L. Zhu, R. F. Boehm, Y. P. Wang, C. Halford, and Y. Sun, "Water immersion cooling of PV cells in a high concentration system," *Solar Energy Materials & Solar Cells*, vol. 95, no. 2, pp. 538–545, 2011.

[13] J. Fernández-Reche, I. Cañadas, M. Sánchez et al., "PSA Solar furnace: a facility for testing PV cells under concentrated solar radiation," *Solar Energy Materials & Solar Cells*, vol. 90, no. 15, pp. 2480–2488, 2006.

[14] C. S. Solanki, C. S. Sangani, D. Gunashekar, and G. Antony, "Enhanced heat dissipation of V-trough PV modules for better performance," *Solar Energy Materials & Solar Cells*, vol. 92, no. 12, pp. 1634–1638, 2008.

[15] M. J. Carvalho, M. Collares-Pereira, J. M. Gordon, and A. Rabl, "Truncation of CPC solar collectors and its effect on energy collection," *Solar Energy*, vol. 35, no. 5, pp. 393–399, 1985.

[16] M. Brogren, M. Rönnelid, and B. Karlsson, "PV-thermal hybrid low concentrating CPC module," in *Proceedings of the 16th European Photovoltaic Solar Energy Conference and Exhibition*, pp. 1–5, Glasgow, UK, May 2000.

[17] J. Nilsson, H. Håkansson, and B. Karlsson, "Electrical and thermal characterization of a PV-CPC hybrid," *Solar Energy*, vol. 81, no. 7, pp. 917–928, 2007.

[18] S. Hatwaambo, H. Hakansson, J. Nilsson, and B. Karlsson, "Angular characterization of low concentrating PV-CPC using low-cost reflectors," *Solar Energy Materials and Solar Cells*, vol. 92, no. 11, pp. 1347–1351, 2008.

[19] T. T. Chow, "A review on photovoltaic/thermal hybrid solar technology," *Applied Energy*, vol. 87, no. 2, pp. 365–379, 2010.

[20] J. Wennerberg, J. Kessler, J. Hedström, L. Stolt, B. Karlsson, and M. Rönnelid, "Thin film PV modules for low-concentrating systems," *Solar Energy*, vol. 69, supplement 6, pp. 243–255, 2001.

[21] M. Hein, F. Dimroth, G. Siefer, and A. W. Bett, "Characterisation of a 300 × photovoltaic concentrator system with one-axis tracking," *Solar Energy Materials & Solar Cells*, vol. 75, no. 1-2, pp. 277–283, 2003.

[22] A. Royne, C. J. Dey, and D. R. Mills, "Cooling of photovoltaic cells under concentrated illumination: a critical review," *Solar Energy Materials & Solar Cells*, vol. 86, no. 4, pp. 451–483, 2005.

[23] H. Yusof, M. Othman, B. Yatim, K. Sopian, M. Nazari, and A. Bakar, "Performance analysis of a double-pass photovoltaic/thermal (PV/T) solar collector with CPC and fins," *Renewable Energy*, vol. 30, no. 13, pp. 2005–2017, 2005.

[24] H. Singh and P. C. Eames, "A review of natural convective heat transfer correlations in rectangular cross-section cavities and their potential applications to compound parabolic concentrating (CPC) solar collector cavities," *Applied Thermal Engineering*, vol. 31, no. 14-15, pp. 2186–2196, 2011.

[25] N. Ari and A. Kribus, "Impact of the Thomson effect on concentrating photovoltaic cells," *Solar Energy Materials & Solar Cells*, vol. 94, no. 8, pp. 1421–1425, 2010.

[26] M. Beccali, P. Finocchiaro, and B. Nocke, "Energy and economic assessment of desiccant cooling systems coupled with single glazed air and hybrid PV/thermal solar collectors for applications in hot and humid climate," *Solar Energy*, vol. 83, no. 10, pp. 1828–1846, 2009.

[27] L. Zhu, R. F. Boehm, Y. Wang, C. Halford, and Y. Sun, "Water immersion cooling of PV cells in a high concentration system," *Solar Energy Materials & Solar Cells*, vol. 95, no. 2, pp. 538–545, 2011.

[28] A. Royne and C. J. Dey, "Design of a jet impingement cooling device for densely packed PV cells under high concentration," *Solar Energy*, vol. 81, no. 8, pp. 1014–1024, 2007.

[29] B. Sandnes and J. Rekstad, "A photovoltaic/thermal (PV/T) collector with a polymer absorber plate. Experimental study and analytical model," *Solar Energy*, vol. 72, no. 1, pp. 63–73, 2002.

[30] H. Saitoh, Y. Hamada, H. Kubota et al., "Field experiments and analyses on a hybrid solar collector," *Applied Thermal Engineering*, vol. 23, no. 16, pp. 2089–2105, 2003.

[31] R. Zakharchenko, L. Licea-Jiménez, S. A. Pérez-García et al., "Photovoltaic solar panel for a hybrid PV/thermal system," *Solar Energy Materials & Solar Cells*, vol. 82, no. 1-2, pp. 253–261, 2004.

[32] M. A. Hasan and K. Sumathy, "Photovoltaic thermal module concepts and their performance analysis: a review," *Renewable & Sustainable Energy Reviews*, vol. 14, no. 7, pp. 1845–1859, 2010.

[33] P. Dupeyrat, C. Ménézo, H. Wirth, and M. Rommel, "Improvement of PV module optical properties for PV-thermal hybrid collector application," *Solar Energy Materials & Solar Cells*, vol. 95, no. 8, pp. 2028–2036, 2011.

[34] P. Dupeyrat, C. Ménézo, M. Rommel, and H. M. Henning, "Efficient single glazed flat plate photovoltaic-thermal hybrid collector for domestic hot water system," *Solar Energy*, vol. 85, no. 7, pp. 1457–1468, 2011.

[35] L. T. Kostic, T. M. Pavlovic, and Z. T. Pavlovic, "Influence of reflectance from flat aluminum concentrators on energy efficiency of PV/Thermal collector," *Applied Energy*, vol. 87, no. 2, pp. 410–416, 2010.

[36] J. S. Coventry, "Performance of a concentrating photovoltaic/thermal solar collector," *Solar Energy*, vol. 78, no. 2, pp. 211–222, 2005.

[37] L. L. Wang, M. Li, Z. Q. Yang et al., "The combined heat and power cycle with concentrating trough solar power," *Acta Energiae Solaris Sinica*, vol. 30, no. 8, pp. 1054–1057, 2009.

[38] J. Sun and M. H. Shi, "Performance analysis of a solar photovoltaic/thermal system with compound parabolic concentrator," *Acta Energiae Solaris Sinica*, vol. 30, no. 11, pp. 1513–1518, 2009.

[39] H. P. Garg and R. S. Adhikari, "Performance analysis of a hybrid photovoltaic/thermal (PV/T) collector with integrated CPC troughs," *International Journal of Energy Research*, vol. 23, no. 15, pp. 1295–1304, 1999.

[40] M. Y. H. Othman, B. Yatim, K. Sopian, and M. N. Abu Bakar, "Performance analysis of a double-pass photovoltaic/thermal (PV/T) solar collector with CPC and fins," *Renewable Energy*, vol. 30, no. 13, pp. 2005–2017, 2005.

[41] M. Brogren, P. Nostell, and B. Karlsson, "Optical efficiency of a PV-thermal hybrid CPC module for high latitudes," *Solar Energy*, vol. 69, supplement 6, pp. 173–185, 2000.

[42] D. W. Jing, X. H. Zhang, C. J. Xing, X. M. Zhang, and L. J. Guo, "Photocatalytic hydrogen production under direct solar light in a CPC based solar reactor: Reactor design and preliminary

results," *Energy Conversion & Management*, vol. 50, no. 12, pp. 2919–2926, 2009.

[43] L. J. Guo, "Advances in solar hydrogen technologies," in *Solar & Alternative Energy*, Proceedings of SPIE, April 2011.

[44] A. G. Imenes and D. R. Mills, "Spectral beam splitting technology for increased conversion efficiency in solar concentrating systems: a review," *Solar Energy Materials and Solar Cells*, vol. 84, no. 1–4, pp. 19–69, 2004.

[45] B. Fisher and J. Biddle, "Luminescent spectral splitting: efficient spatial division of solar spectrum at low concentration," *Solar Energy Materials & Solar Cells*, vol. 95, no. 7, pp. 1741–1755, 2011.

[46] M. A. Hamdy and S. H. El-Hefnawi, "Effect of spectrally selective liquid absorption-filters on silicon solar-cells," *Applied Energy*, vol. 35, no. 3, pp. 177–188, 1990.

[47] S. L. Jiang, P. Hu, S. P. Mo, and Z. H. Chen, "Optical modeling for a two-stage parabolic trough concentrating photovoltaic/thermal system using spectral beam splitting technology," *Solar Energy Materials & Solar Cells*, vol. 94, no. 10, pp. 1686–1696s, 2010.

[48] S. L. Jiang, Z. S. Chen, P. Hu, and S. P. Mo, "Performance analysis of semi-parabolic trough concentrating spectral beam splitting PV system," *Journal of Engineering Thermophysics*, vol. 30, no. 3, pp. 365–369, 2009.

[49] J. F. Zhao, Y. C. Song, W. H. Lam et al., "Solar radiation transfer and performance analysis of an optimum photovoltaic/thermal system," *Energy Conversion & Management*, vol. 52, no. 2, pp. 1343–1353, 2011.

Hindawi Publishing Corporation
International Journal of Photoenergy
Volume 2012, Article ID 312168, 6 pages
doi:10.1155/2012/312168

Research Article

The Experimental Performance of an Unglazed PVT Collector with Two Different Absorber Types

Jin-Hee Kim[1] and Jun-Tae Kim[2]

[1] *Green Home Energy Technology Research Center, Kongju National University, 275 Budae-Dong, Cheonan, Chungnam 330-717, Republic of Korea*
[2] *Department of Architectural Engineering, Kongju National University, 275 Budae-Dong, Cheonan, Chungnam 330-717, Republic of Korea*

Correspondence should be addressed to Jun-Tae Kim, jtkim@kongju.ac.kr

Received 6 April 2012; Revised 12 June 2012; Accepted 28 June 2012

Academic Editor: Tin-Tai Chow

Photovoltaic-thermal collectors combine photovoltaic modules and solar thermal collectors, forming a single device that produces electricity and heat simultaneously. There are two types of liquid-type PVT collectors, depending on the existence or absence of a glass cover over the PV module. The glass-covered (glazed) PVT collector produces relatively more thermal energy but has a lower electrical yield, whereas the uncovered (unglazed) PVT collector has a relatively low thermal energy and somewhat higher electrical performance. The thermal and electrical performance of liquid-type PVT collectors is related not only to the collector design, such as whether a glass cover is used, but also to the absorber design, that is, whether the absorber is for the sheet-and-tube type or the fully wetted type. The design of the absorber, as it comes into contact with the PV modules and the liquid tubes, is regarded as important, as it is related to the heat transfer from the PV modules to the liquid in the tubes. In this paper, the experimental performance of two liquid-type PVT collectors, a sheet-and-tube type and a fully wetted type, was analyzed.

1. Introduction

The photovoltaic/thermal (PVT) concept offers an opportunity to increase the overall efficiency of a PV module through the use of the waste heat generated in the module in a BIPV system. It is well known that PVT systems enhance the PV efficiency through a cooling effect. Moreover, this can be achieved by circulating a relatively cold fluid, water, or air on the underside of the PV module.

PVT collectors combine a photovoltaic module and a solar thermal collector, forming a single device that converts solar energy into electricity and heat at the same time [1]. The heat from PV modules can be removed in order to improve their electrical performance; this heat can be converted into useful thermal energy. As a result, PVT collectors can generate more solar energy per unit surface area than can side-by-side photovoltaic modules and solar thermal collectors [2].

In general, regarding liquid-type PVT collectors, two types can be distinguished. The first is the glazed PVT collector (Figure 1), which has the advantage of heat production, and the second is the unglazed PVT collector (Figure 2), which produces relatively less thermal energy but shows better electrical performance than the former type.

Glazed PVT collectors are very similar in appearance to flat-plate solar thermal collectors, consisting of a PV-covered absorber in an insulated collector box with a glass cover. This glass-covered insulation leads to high thermal efficiency with some reduction of electrical efficiency due to solar radiation reflection and the increase in the PV module temperature caused by the glass cover. Unglazed PVT collectors are more similar to regular PV panels. They consist of a PV-covered absorber with no additional glass cover. The configuration without a glass cover results in lower thermal efficiency compared to the glazed PVT collector. On the other hand, the electrical efficiency of an unglazed PVT collector is higher

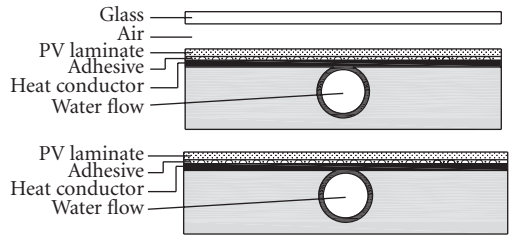

Figure 1: Sectional view of a glazed (above) and unglazed (below) PVT collector.

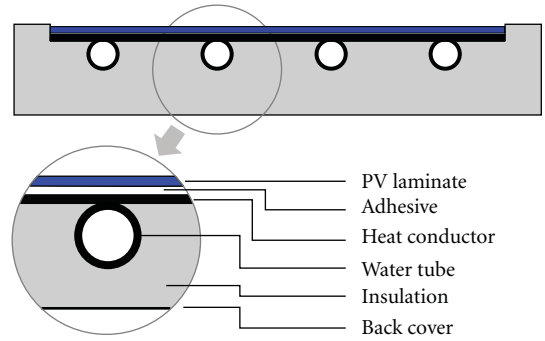

Figure 2: Sectional view of the sheet-and-tube PVT collector.

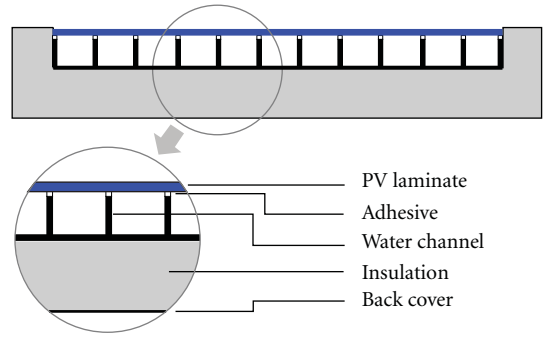

Figure 3: Sectional view of fully wetted PVT collector.

than that of a glazed PVT collector and is even higher than that of regular PV panels due to the PV cooling effect [3].

The thermal and electrical performance of liquid-type PVT collectors is also related to the absorber design. The absorber, which comes into contact with the PV modules and the liquid tubes, is regarded as important, as it is related to the heat transfer from the PV modules to the thermal medium. Two types of the PVT collectors can be distinguished according to absorber attached to the PV module, that is, whether it is a sheet-and-tube absorber (Figure 2) or the fully wetted absorber (Figure 3). It is believed that the latter has better thermal performance, as it increases the heat transfer surfaces.

In a study focused on an absorber design of liquid-type PVT collector, Bergene and Løvvik [4] thoroughly analyzed the electrical and thermal efficiencies of a liquid-type PVT system and the energy conversion between different factors. Sopian et al. [5] compared the performances of single-pass and double-pass combined PVT collectors with steady-state models. They concluded that the double-pass PVT collector had better performance due to the cooling effect of solar cell. Another study [6] introduced a dynamic model for analyzing performances of sheet-and-tube PVT collector. It analyzed the heat transfer between the encapsulated solar cell and the absorber plate; it also analyzed the heat transfer between the absorber plate and the water tube.

Various types of liquid PVT collectors have also been suggested, such as a channel-type PVT collector [7], a PVT collector with polymer square tube absorbers [8], and thermosyphon PVT collectors [9–11].

Chow et al. [12–14] designed the aluminum-alloy flat box absorber with rectangular shape for PVT collectors and tested their performance. Ibrahim et al. [15] studied the performance simulation of PVT collectors with different absorber collectors design, such as rectangular and round tubes. This study involved new design configurations of absorber collectors such as parallel, direct, spiral, oscillatory, serpentine, and web flow, which were modelled and compared. They concluded that the best design configuration is the spiral flow design. In another study [16], the collector was constructed with commercial PV modules attached on a corrugated polycarbonate absorber plate with square-shape box channels.

Various designs of liquid type PVT systems have since been proposed, and the theoretical and experimental performances of PVT systems have been evaluated.

The aim of this study is to compare the electrical and thermal performance of the sheet-and-tube and the fully wetted PVT collectors, both categorized as unglazed. In this paper, two different types of liquid-type PVT collectors were created, and their thermal and electrical performances were measured outdoors. The results were then compared. In addition, the electrical performance of the PV module alone, identical to the modules used for the PVT collectors, was compared to the performance of the fully wetted PVT collector.

2. PVT Collector Design

Liquid-type unglazed PVT collectors with the two types of absorbers, that is, the sheet-and-tube type and the fully wetted type of absorber, were designed and made for this study. The sheet-and-tube absorber is widely used in solar thermal collectors. Regarding the fully wetted absorber, the rectangular shape of the water flow channel can reduce the thermal resistance between the PV module and the collector fluid [17]. The fully wetted absorber has no absorber sheet, as the PV module forms one side of the channel.

The PVT collectors consist of PV modules in combination with water heat extraction units made of aluminum in both cases. Also, the PVT collectors consist of a PV-covered absorber with no additional glass cover. They are both thermally protected with 50 mm of glass-wool insulation.

Table 1: PV module specifications.

Cell type	Monocrystalline silicon
Maximum power	240 W
Maximum voltage	29.93 V
Maximum current	8.15 A
Shot current	8.56 A
Open voltage	37.55 V
Size	1656 ∗ 997 ∗ 50 mm

For the sheet-and-tube absorber PVT collector, the aluminum sheet-and-tube absorber was attached to the back side of the PV module using a thermal conduction adhesive. The PV modules used for the collectors were 240 W_p mono-Si PV modules which show an electrical efficiency rating of 16.5% under standard test conditions (STCs). The specifications are shown in Table 1.

The configuration of the fully wetted PVT collector was identical to that of the sheet-and-tube PVT collector except for the absorber design.

3. Experiment

The two different PVT collector types were tested at a solar radiation level that exceeded W/m^2 and at a liquid flow rate of 0.02 kg/s m^2, based on ASHRAE Standard 93 [18] and the PVT performance measurement guidelines of the ECN [19]. The electrical and thermal performance measurements were carried out under a quasi-stationary condition in an outdoor environment at the same time (Figure 4). In addition, a conventional PV module of the type used in PVT collectors was tested under the same outdoor conditions.

Several experimental devices were installed to measure the data related to the thermal and electrical performance of the PVT collector.

The PVT collector was tested at steady-state conditions to determine their electrical and thermal performance for various inlet operating temperature. Inlet and outlet temperature of PVT collector were monitored and measured using an RTD-type thermocouple with a measurement error of ±0.1% at 0°C. The inlet temperature of PVT collector was controlled by set temperature equipment and the inlet temperature remained constant, while an outlet temperature varied. Also, the ambient temperature was measured by a T-type thermocouple with measurement error of ±0.2°C. Antifreezing liquid was supplied to the PVT collector at an uniform flow rate of 0.02 kg/sm^2 from a pump. The mass flow rate at inlet pipe of the PVT collector was measured by an electronic flow meter. The normal quantity of solar radiation on the PVT collector surface was measured by Epply pyranometer installed parallel to the collector plane.

Electrical loading resistors and a power meter were installed in order to measure the electrical performance of the PVT. All of data related to the thermal and electrical performance of the PVT collector were monitored and recorded at 10 s intervals through a data acquisition system.

(a)

(b)

Figure 4: View of two types of PVT collector (a) in the experiment and the measuring equipment (b).

4. Results and Discussion

With the results of the outdoor test of the PVT collectors, the thermal and electrical performances were analyzed.

4.1. Thermal Performance. The thermal efficiency is determined as a function of the solar radiation (G), the input fluid temperature (T_i), and the ambient temperature (T_a). The steady-state efficiency is calculated by the following equation:

$$\eta_{\text{th}} = \frac{\dot{m}C_p(T_o - T_i)}{A_{\text{pvt}}G}, \tag{1}$$

where η_{th} is the thermal efficiency [—]; A_{pvt} is the collector area [m^2]; T_o is the collector outlet temperature [°C]; $T_i$is the collector inlet temperature [°C]; $\dot{m}$ is the mass flow rate [kg/s]; C_p is the specific heat [J/kg K]; G is the irradiance on the collector surface [W/m^2].

The thermal efficiency of the PVT collectors was conventionally calculated as a function of the ratio $\Delta T/G$, where $\Delta T = T_m - T_a$.

Here, T_m and T_a are the PVT collector's mean fluid temperature and the ambient temperature, respectively, and

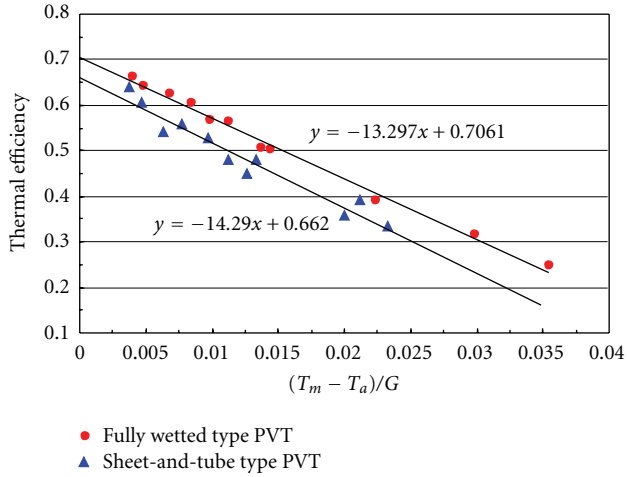

FIGURE 5: Thermal efficiency of the fully wetted and sheet-and-tube PVT collectors.

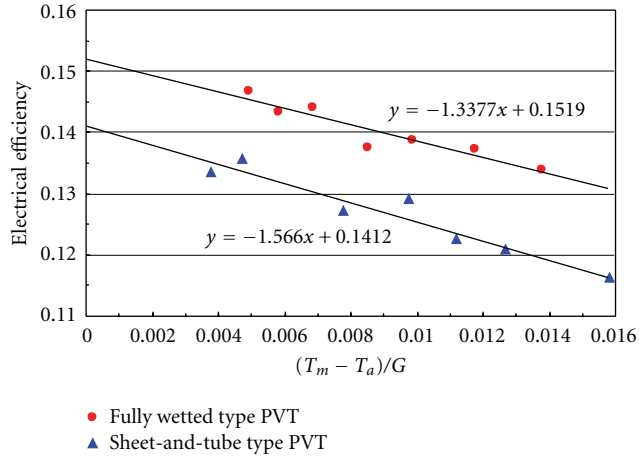

FIGURE 6: Electrical efficiency of the fully wetted and sheet-and-tube PVT collectors.

G is the solar radiation on the collector surface. Hence, ΔT denotes the measurement of the temperature difference between the collector and its surroundings relative to the solar radiation. The thermal efficiency, η_{th}, is expressed as

$$\eta_{\text{th}} = \eta_o - \alpha_1 \left(\frac{\Delta T}{G} \right), \tag{2}$$

where η_0 is the thermal efficiency at zero reduced temperature and α_1 is the heat loss coefficient.

With the measurement results of the unglazed PVT collectors with the two absorber types, the thermal performance is shown in Figure 5. The thermal efficiencies of the sheet-and-tube and the fully wetted PVT collector can be expressed with the following relational expressions: $\eta_{\text{th}} = 0.66 - 14.29(\Delta T/G)$ and $\eta_{\text{th}} = 0.70 - 13.29(\Delta T/G)$, respectively. Thus, the thermal efficiencies (η_o) at zero reduced temperature are 0.66 and 0.70, respectively, showing that the efficiency of the fully wetted PVT collector is about 4% higher than that of the sheet-and-tube PVT collector. Also, the heat loss coefficients (α_1) are $-14.29\ \text{W/m}^2{}^\circ\text{C}$ and $-13.29\ \text{W/m}^2{}^\circ\text{C}$, respectively; the fully wetted PVT collector had better thermal performance than the sheet-and-tube PVT collector, but their heat losses were similar.

Therefore, the thermal performance difference according to the absorber type was found to be relatively small. The average thermal efficiency of the sheet-and-tube type and the fully wetted type of PVT collector is about 48% and 51%, respectively, under the same outdoor condition.

4.2. Electrical Performance. The electrical efficiency depends mainly on the incoming solar radiation and the PV module temperature. It is calculated with the following equation:

$$\eta_{\text{el}} = \frac{I_m V_m}{A_{\text{pvt}} G}. \tag{3}$$

Here, I_m and V_m are the current and the voltage of the PV module operating under a maximum power.

The electrical efficiencies of the PVT collectors under the outdoor condition are shown in Figure 6. The performance of the sheet-and-tube and fully wetted PVT collectors

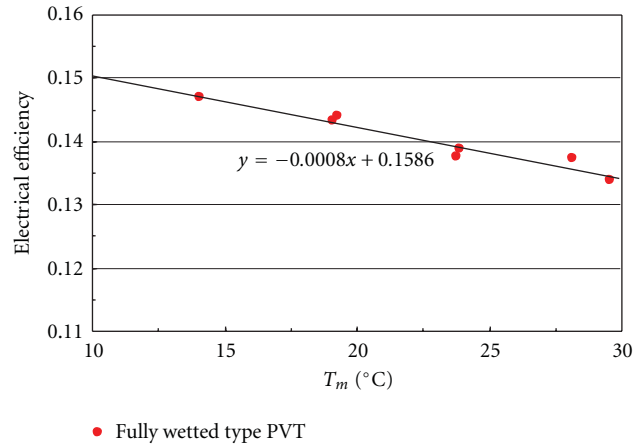

FIGURE 7: Electrical efficiency of the fully wetted PVT collector as a function of the mean fluid temperature.

can be expressed with the following relational expressions: $\eta_{\text{el}} = 0.14 - 1.56(\Delta T/G)$ and $\eta_{\text{el}} = 0.15 - 1.33(\Delta T/G)$, respectively. Thus, the electrical efficiencies (η_o) at zero reduced temperature are 0.14 and 0.15, respectively, and the electricity loss coefficients are -1.56 and -1.33, respectively. These results show that the electrical efficiency of the fully wetted PVT collector is approximately 8% higher compared to the sheet-and-tube PVT collector. This difference appears to be significant, as it reflects a difference of about 1% regarding the overall electrical efficiency of the PV module. On the other hand, the average electrical efficiencies of the sheet-and-tube and the fully wetted PVT collectors were found to be approximately 12.6% and 14.0%, respectively.

It was found that the fully wetted PVT collector had better electricity performance as well as better thermal performance.

The PV module temperature of PVT collectors is closely related to the cooling effect by the fluid that circulates the collectors. The electrical performance levels can be analyzed by means of the fluid temperature. Figures 7 and 8 show

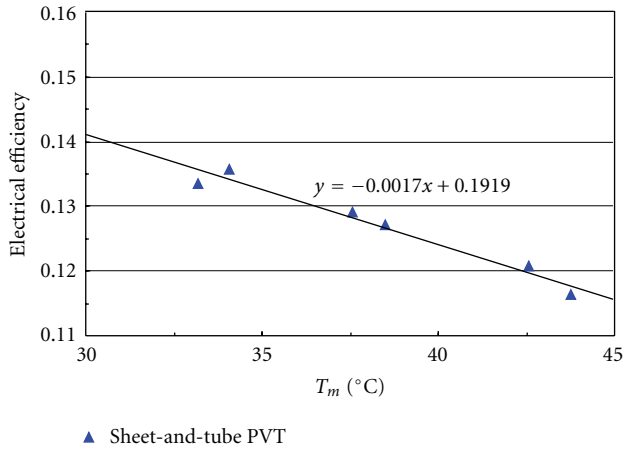

Figure 8: Electrical efficiency of the sheet-and-tube PVT collector as a function of the mean fluid temperature.

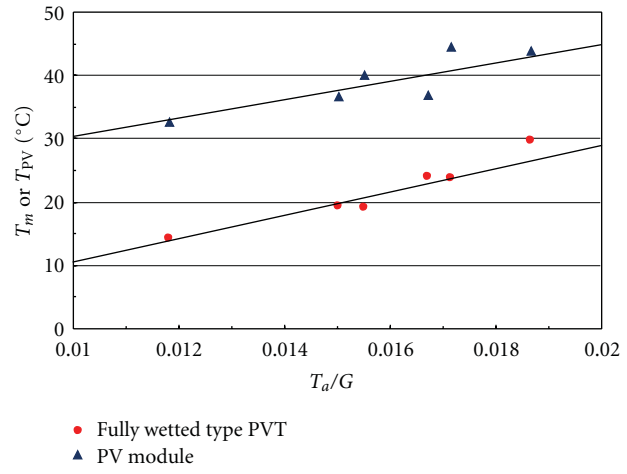

Figure 9: Mean temperature of the fully wetted PVT collector and PV temperature of as a function of the ambient temperature and solar radiation.

the electrical efficiency of a PVT collector as the function of the mean fluid temperature.

For the sheet-and-tube and fully wetted PVT collectors, the electrical efficiency decreased according to an increase of the mean fluid temperature in both cases. These results indicate that the fluid temperature of the PVT collector affected the PV module temperature, which in turn influences the PV performance.

To analyze the effect of the fully wetted absorber for a PVT collector, the electrical performances levels of the fully wetted PVT collector and a PV module alone were analyzed. They were compared as a function of the ambient temperature and the solar radiation (Figure 9).

There will be some thermal resistance between the fluid and the PV module in a liquid-type PVT collector, which may have an influence on the heat transfer between the two elements, thus determining their temperature and in turn the PV electrical performance. For example, for the sheet-and-tube absorber, nonoptimized adhesive contact between the

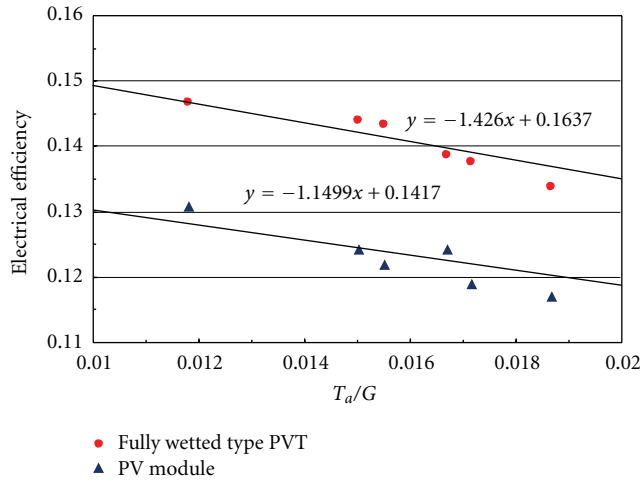

Figure 10: Electrical Efficiency of the fully wetted type of PVT collector and a PV module of as a function of the ambient temperature and solar radiation.

PV and the metal absorber will result in a higher temperature difference between these two components. This indicates that the heat from the PV module may be transferred less to the liquid. However, for the fully wetted absorber, the temperature difference between the two parts may be lower, as there will be good heat transfer through the contact area of entire PV module. Therefore, the mean fluid temperature of the fully wetted PVT collector would be well close to the PV module temperature under the effective convective heat transfer condition.

The mean fluid temperature of the fully wetted PVT collector rises according to an increase in the T_a/G coefficient, as does the temperature of the PV module alone. Under the same T_a/G coefficient condition, the PV module presents a higher PV temperature as compared to the mean fluid temperature of the fully wetted type PVT collector. Therefore, the fully wetted PVT collector can maintain a lower PV temperature due to the fluid coming into the collector. As a result, it can be said that the PV temperature of the PVT collector is lower than that of the PV module alone due to the cooling effect of the liquid.

The electrical efficiency levels of the fully wetted PVT collector and the PV module as a function of the T_a/G coefficients are shown in Figure 10. In both cases, the electrical efficiency decreased according to the increase in the T_a/G coefficient. The electrical efficiency of the fully wetted PVT collector is nearly 2% higher than that of the PV module alone. These results indicate that this type of PVT collector has better electrical performance than the PV module alone.

5. Conclusion

This paper analyzed the experimental energy performance of two different unglazed liquid PVT collectors: one with a sheet-and-tube type of absorber and the other with a fully wetted absorber type of absorber.

The results show that at zero reduced temperature, the thermal and electrical efficiency levels of the sheet-and-tube PVT collector are 66% and 14%, respectively, while those of the fully wetted PVT collector are 70% and 15%, respectively. Therefore, the fully wetted PVT collector had better thermal and electrical performance than the sheet-and-tube PVT collector.

The overall energy performance of the collectors can be compared by combining the values of the average thermal and electrical efficiency. The fully wetted PVT collector presents a value of 65% and the sheet-and-tube PVT collector gives a value of 60.6%. Although the overall performance of the fully wetted collector is 5.6% higher than that of the sheet-and-tube collector, it cannot be concluded that the former is superior to the latter due to the fact that the fully wetted absorber may require a more difficult bonding technique than the sheet-and-tube absorber.

Also, it is clear that the electrical performance of PVT collectors depends on the cooling effect of the PV module by the fluid. In particular, it was found that the fully wetted PVT collector could maintain the electrical performance by similar level to the electrical efficiency in STC. Additionally, the electrical efficiency of the fully wetted PVT collector was, on average, approximately 2% higher than that of the PV module alone. These results show that unglazed PVT collectors provide better electrical performance than a PV module alone.

Acknowledgments

This work was supported by the Priority Research Centers Program through the National Research Foundation of Korea (NRF) funded by the Ministry of Education, Science and Technology (no. 2009-0093825) and by a Grant from the Human Resources Development Project of the Korea Institute of Energy Technology Evaluation & Planning (no. 20114010 203040) funded by the Ministry of Knowledge Economy.

References

[1] J. H. Kim and J. T. Kim, "An experimental study of a water type glazed PV/thermal combined collector module," *Journal of Korean Air-Conditioning and Refrigeration*, vol. 20, no. 4, pp. 260–265, 2008.

[2] J. H. Kim, J. T. Kim et al., "The comparison of the electrical and thermal performance of glazed and unglazed PVT collectors," in *The Proceedings of the 8th EuroSun Conference*, Graz, Austria, August 2010.

[3] J. H. Kim, J. G. Kang, and J. T. Kim, "Experimental performance comparison of water type glazed and unglazed PV-thermal combined collectors," *Journal of Korean Institute of Ecological Architecture and Environment*, vol. 9, no. 4, pp. 37–42, 2009.

[4] T. Bergene and O. M. Løvvik, "Model calculations on a flat-plate solar heat collector with integrated solar cells," *Solar Energy*, vol. 55, no. 6, pp. 453–462, 1995.

[5] K. Sopian, K. S. Yigit, H. T. Liu, S. Kakaç, and T. N. Veziroglu, "Performance analysis of photovoltaic thermal air heaters," *Energy Conversion and Management*, vol. 37, no. 11, pp. 1657–1670, 1996.

[6] T. T. Chow, "Performance analysis of photovoltaic-thermal collector by explicit dynamic model," *Solar Energy*, vol. 75, no. 2, pp. 143–152, 2003.

[7] H. A. Zondag, D. W. de Vries, W. G. J. van Helden, R. J. C. van Zolingen, and A. A. van Steenhoven, "The yield of different combined PV-thermal collector designs," *Solar Energy*, vol. 74, no. 3, pp. 253–269, 2003.

[8] B. Sandnes and J. Rekstad, "A photovoltaic/thermal (PV/T) collector with a polymer absorber plate. Experimental study and analytical model," *Solar Energy*, vol. 72, no. 1, pp. 63–73, 2002.

[9] H. P. Garg, R. K. Agarwal, and J. C. Joshi, "Experimental study on a hybrid photovoltaic-thermal solar water heater and its performance predictions," *Energy Conversion and Management*, vol. 35, no. 7, pp. 621–633, 1994.

[10] T. T. Chow, A. L. S. Chan, K. F. Fong, W. C. Lo, and C. L. Song, "Energy performance of a solar hybrid collector system in a multistory apartment building," *Proceedings of the Institution of Mechanical Engineers A*, vol. 219, no. 1, pp. 1–11, 2005.

[11] T. T. Chow, W. He, J. Ji, and A. L. S. Chan, "Performance evaluation of photovoltaic-thermosyphon system for subtropical climate application," *Solar Energy*, vol. 81, no. 1, pp. 123–130, 2007.

[12] T. T. Chow, W. He, and J. Ji, "Hybrid photovoltaic-thermosyphon water heating system for residential application," *Solar Energy*, vol. 80, no. 3, pp. 298–306, 2006.

[13] T. T. Chow, J. Ji, and W. He, "Photovoltaic-thermal collector system for domestic application," *Solar Energy Engineering*, vol. 129, no. 2, pp. 205–209, 2007.

[14] J. Ji, J. P. Lu, T. T. Chow, W. He, and G. Pei, "A sensitivity study of a hybrid photovoltaic/thermal water-heating system with natural circulation," *Applied Energy*, vol. 84, no. 2, pp. 222–237, 2007.

[15] A. Ibrahim, M. Y. Othman, M. H. Ruslan et al., "Performance of photovoltaic thermal collector (PVT) with different absorbers design," *WSEAS Transactions on Environment and Development*, vol. 5, no. 3, pp. 321–330, 2009.

[16] B. J. Huang, T. H. Lin, W. C. Hung, and F. S. Sun, "Performance evaluation of solar photovoltaic/thermal systems," *Solar Energy*, vol. 70, no. 5, pp. 443–448, 2001.

[17] P. Affolter, W. Eisenmann, H. Fechner et al., *PVT Roadmap: An European Guide For the Development And Market Introduction of PV-Thermal Technology*, ECN, 2006.

[18] American Society of Heating, *Refrigerating and Air Conditioning Engineers (ASHRAE), Standard 93–2010—Methods of Testing To Determine the Thermal Performance of Solar Collectors*, ASHRAE Inc, Atlanta, Ga, USA, 1991.

[19] H. Zondag, N. Van der Borg, and W. Eisenmann, *D8-6: PVT Performance Measurement Guidelines: Guidelines For Performance Measurements of Liquid-Cooled Non-ConCentrating PVT Collectors Using C-Si Cells*, ECN & ISFH: Emmerthal, Petten, Netherlands, 2005.

Hindawi Publishing Corporation
International Journal of Photoenergy
Volume 2012, Article ID 265838, 13 pages
doi:10.1155/2012/265838

Research Article

Analysis of a Hybrid PV/Thermal Solar-Assisted Heat Pump System for Sports Center Water Heating Application

Y. Bai,[1] T. T. Chow,[1] C. Ménézo,[2,3] and P. Dupeyrat[4]

[1] *BEETRU-BST, City University of Hong Kong, Kowloon, Hong Kong*
[2] *CETHIL UMR 5008, CNRS/INSA/UCB-Lyon 1, 69621 Lyon, France*
[3] *LOCIE, FRE CNRS 3220, Université de Savoie, Savoie Technolac, 73370 Le Bourget-du-lac, France*
[4] *Département EnerBaT, EDF R&D, 77818 Moret sur Loing, France*

Correspondence should be addressed to Y. Bai, yubai3@cityu.edu.hk

Received 6 May 2012; Accepted 13 June 2012

Academic Editor: G. N. Tiwari

The application of solar energy provides an alternative way to replace the primary source of energy, especially for large-scale installations. Heat pump technology is also an effective means to reduce the consumption of fossil fuels. This paper presents a practical case study of combined hybrid PV/T solar assisted heat pump (SAHP) system for sports center hot water production. The initial design procedure was first presented. The entire system was then modeled with the TRNSYS 16 computation environment and the energy performance was evaluated based on year round simulation results. The results show that the system COP can reach 4.1 under the subtropical climate of Hong Kong, and as compared to the conventional heating system, a high fractional factor of energy saving at 67% can be obtained. The energy performances of the same system under different climatic conditions, that include three other cities in France, were analyzed and compared. Economic implications were also considered in this study.

1. Introduction

There are various applications of solar energy for medium-grade heating, including water heating, space heating, distillation, and the like. The utilization of solar energy for hot water production is one most popular application. However, large rooftop or other space in buildings is needed for installing enough solar collector arrays to satisfy the full services requirements in the large-scale and/or multiple-demand cases. From this point of view, the combined solar-assisted heat-pump system appears a suitable alternative, which not only saves building space but also reduces the reliance on utilities electricity supply. The combined system is then able to work more efficiently.

Unlike the conventional solar thermal collectors, the hybrid photovoltaic/thermal (PV/T) collectors make possible higher energy outputs per unit surface area because the absorbed solar radiation is converted into electricity and usable heat simultaneously. The studies on this topic were initiated in the 1970s and since then many innovative systems have been introduced. Several recent technical reviews [1–3] cover the latest developments of PV/T collector designs and their performances in terms of electrical/thermal outputs as well as application potentials. The increased attention and research outputs in this area indicate that hybrid PV/T technologies present many attractive features for wide applications and industrialization opportunities for large scale production. Specifically in the research area of hot water co-generation, a series of experimental and numerical studies have been undertaken on the stand-alone and building-integrated photovoltaic/water-heating (PV/W) systems for warm climate application [4–6]. The year round thermal and cell conversion efficiencies were found 37.5% and 9.4% respectively for the case of BiPV/W application in Hong Kong. The overall heat transmission through the PVW wall was reduced to 38% of the normal building façade. Santbergen et al. [7] took a detailed analysis of the energy yield of solar domestic hot water systems with covered sheet-and-tube PV/T collectors. A detailed quantitative analysis of all loss mechanisms inherent to the PV/T collectors was performed on top of those related to PV modules and conventional thermal collectors. The annual electrical

efficiencies of the PV/T systems they investigated were found lower than the plain PV systems (up to 14% relatively) and the annual thermal efficiencies were also lower than the conventional thermal collector systems (up to 19% relatively). With the aim to improve the overall system performance, many parametric studies have been done [8–11]. Charalambous et al. [8] carried out an optimization study based on the "low-flow" concepts, of which the advantages include improved system performance, smaller pump, reduced size and thickness of tubing and insulation, less construction work and time for the optimum absorber configuration, and thus also cost saving. The optimized flow rate for the header and riser in serpentine PV/T collectors is determined, respectively, by using the EES code. A similar study was taken by Cristofari et al. [9] on copolymer PV/T collectors.

To improve the global system efficiency in large-scale installations of hybrid PV/T technology, the combined use with other efficient energy systems (such as heat pump systems) can be promising.

A number of research investigations have been conducted in the design, modeling, and testing of solar-assisted heat pump systems. Ozgener and Hepbasli [12, 13] reviewed the reported works on energy and exergy analysis of SAHP systems. Bridgeman and Harrison [14] conducted a preliminary experimental evaluation of indirect SAHP system for domestic hot water applications; tests were conducted with a range of evaporator supply temperatures and the results indicated that the COP can span from 2.8 to 3.3, depending on the evaporator and condenser temperatures. Dikici et al. [15] performed an energy-exergy analysis of solar-assisted heat pump system for space heating in a test room of 60 m^2. The system COP was determined as 3.08 while the exergy loss of the solar collector was found to be 1.92 kW. The authors concluded that the COP increased when the exergy loss of evaporator decreased. Through system simulation Li and Yang [16] studied a parallel SAHP system for supplying hot water to a hypothetical residential building; the author concluded that the solar collector area affects the optimum flow rate significantly. Wang et al. [17] developed a novel indirect-expansion solar-assisted multifunctional heat pump (IX-SAMHP). The proposed system not only works in operation modes included in the two household appliances, but also operates in four new energy-saving operation modes for space cooling, space heating, and water heating. The experimental results indicated that the IX-SAMHP on cloudy days can produce hot water with considerable reduction in electricity consumption than a solar water heater and in cold winter can operate in much higher COP (3.5–4.2) than a domestic heat pump. Sterling and Collins [18] carried out a feasibility analysis of an indirect SAHP system for domestic water heating as compared to: (i) a traditional solar domestic hot water system and (ii) an electric domestic hot water system. It was found that the electrical consumption and operating cost were most favorable with the indirect SAHP system.

From our literature review, we found that the experimental and theoretical analysis of hybrid SAHP system for large-scale water heating application is very limited. In this study, an indirect hybrid PV/T solar-assisted heat pump system has been investigated from the initial design phase to the detailed analysis of the annual performance through numerical simulation. The cost investment on the proposed system was also estimated.

2. System Description

A hypothetical sports center was taken as a reference case. A perspective view of the building is shown in Figure 1. The floor area of the sports center is 3200 m^2, corresponding to 80 m (L) by 40 m (W). The provisions include an indoor swimming pool, one general-games sport hall, several general minigames rooms, one gym, and the relevant services spaces like changing rooms, canteen, lobby, and office. The central plant room is located at the ground level. In this case study, the designed energy system was used for hot water production to cater for bathing and hand washing in the changing rooms.

A simplified schematic diagram of the proposed PVT-SAHP system is presented in Figure 2. The solar heat source is for water preheating. An indirect solar water heating mode was chosen in this case. The solar preheating system mainly consists of an array of hybrid PV/T collectors, a plate heat exchanger, and solar storage tanks. On the hot side of the heat exchanger, the fluid in the thermal collector circulates according to the temperature differential between the collector outlet T_1 and the bottom of the storage tank T_7, which was monitored by an on-off differential controller R_1. Upper and lower dead bands were set at 10°C and 2°C, respectively. On the cold side of the exchanger, cold water is taken from the bottom of the tank and delivered to the heat exchanger connected to the collector where it gains solar energy and returns to the tank at a higher temperature. The water circulation is controlled by the on-off differential controller R_2 according to the tem differential between the entrance of the heat exchanger on the hot side T_2 and the bottom of the tank T_7. The dead bands values are the same as in R_1. The feed water stream is divided into two parts. On part enters from the bottom of the solar tank, and another part is mixed with the water exiting from the heat pump system. The proportion is controlled by a temperature-controlled liquid flow diverter according to the designed load water temperature. After preheating by the solar collector system and the small back-up electric heater in the tank, water then passes through the heat pump for reheating as the temperature is still not reaching the desired delivery water temperature. The internal heater in the solar tank is activated only during the winter season. The external auxiliary heater is functioned to keep the desired pool water temperature, of which the set point temperature should be higher than the required delivery temperature in order to cover the heat losses in the pipe distribution system.

3. Design of Solar Water Preheating System

3.1. Calculation of the Daily Heating Demand of the Sports Center. According to the practical design guides of sports

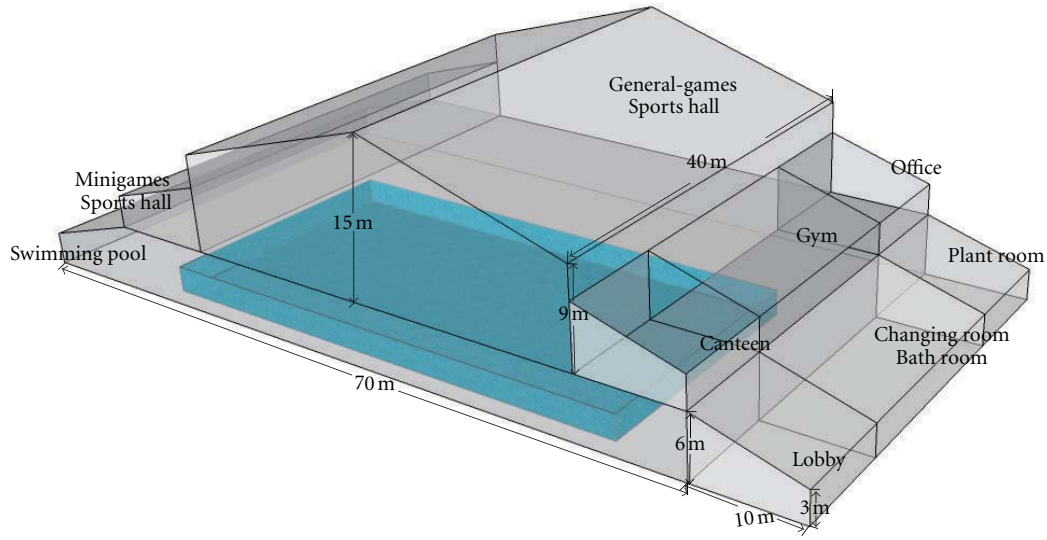

Figure 1: Prospective view of the sports center model.

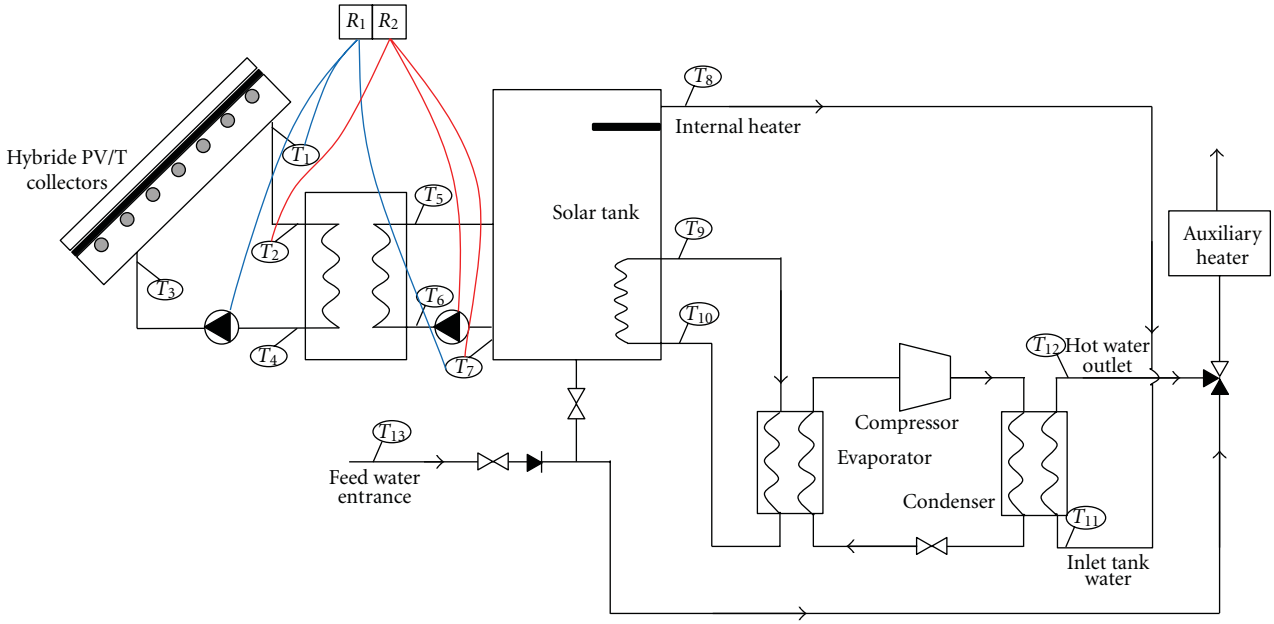

Figure 2: Schematic overview of the indirect PV/T solar-assisted heat pump system.

center hot water heating, the water load can be determined according to: (i) the daily average hot water consumption per person or (ii) the hourly water consumption per shower faucet and lavabo.

In our study, the hot water load is calculated by using the daily water load Q_h, which depends on the number of showers faucets and lavabos in the provision, hence

$$\dot{m}_{\text{dis}} = \sum q_h n_0 b, \tag{1}$$

where q_h is the hourly water consumption of shower faucets and lavabos, in kg/h; n_0 is the number of the shower faucets and lavabos, b is the simultaneous using factor of the shower facets and lavabos within one hour, which is usually taken as 100% for the sports center cases.

The hot water demand is then calculated by:

$$\dot{m}_h = k_r \dot{m}_{\text{dis}}, \tag{2}$$

where k_r is the hot water mixing factor. This is determined according to the designed hot water temperature at the outlet of the heat pump system and the delivery temperature, as shown (3) that follows:

$$k_r = \frac{T_{\text{dis}} - T_{\text{fw}}}{T_h - T_{\text{fw}}}, \tag{3}$$

where T_{dis} is the delivery water temperature after mixing, in °C; T_h is the hot water temperature at the outlet of the tank, in °C; T_{fw} is the feed water temperature, in °C.

The required heating load is then calculated on the basis of:

$$Q_h = \dot{m}_h C_p (T_h - T_{fw}). \quad (4)$$

3.2. Estimation of the Required Solar Collector Area. The required thermal collector area is dependent on several factors including the daily water heating load of the sports center, the collector characteristics, and the climatic conditions. The area of solar collector is determined by the following relation in the direct heating mode:

$$A_{cd} = \frac{24 Q_f}{[J_T \eta_{cd}(1 - \eta_L)]}, \quad (5)$$

where A_c is the total collector area when the indirect heating mode is used, in m^2; J_T is the average daily solar radiation level, in $kJ/m^2 \cdot d$; η_L the heat loss coefficient of the hydraulic piping system, normally between 0.2 and 0.3 for the well-insulated case; η_{cd} is the collector efficiency determined by practical test, in general this value varies between 0.25 and 0.5.

For the indirect heating mode, as in this study, the required collector area is determined on considering the heat exchanger characteristics, as shown in (6):

$$A_c = A_{cd}\left(1 + \frac{\delta A_{cd}}{K_{hx} A_{hx}}\right), \quad (6)$$

where A_{cd} is the total collector area when the direct heating mode is used, in m^2; A_{hx} is the heat exchanger surface area, in m^2; f is the general solar fraction according to the different climatic zone; δ is the collector heat loss coefficient, in $W/(m^2 \cdot K)$; K_{hx} is the heat transfer coefficient of the heat exchanger, in $W/(m^2 \cdot K)$.

In this case study, arbitrarily $\eta_L = 0.2$ and $\eta_{cd} = 0.4$.

3.3. Modeling of the Heat Pump System. In the heat pump unit, the heating capacity of the condenser can be calculated by

$$Q_{cond} = m_{rf}(h_{out} - h_{in}), \quad (7)$$

where m_{rf} is mass flow rate of the refrigerant (R410A), kg/s; h_{out} and h_{in} are the specific enthalpy of R410A at the inlet and outlet of the condenser, kJ/kg.

The heat transfer to water is determined by the following relation:

$$Q_{dhw} = m_{dhw} C_p (T_{dhw\_in} - T_{dhw\_out}), \quad (8)$$

where m_{dhw} is mass flow rate of hot water, kg/s; T_{dhw_in} and T_{dhw_out} are the inlet and outlet hot water temperatures, °C.

The power consumption of the heat pump unit is the total energy consumed by the compressor, water pumps, and the controller, in kWh.

$$Q_{hp} = \sum_{\tau=0}^{t} \left(P_{comp} + P_{controller} + P_{pump}\right), \quad (9)$$

where P_{comp}, $P_{controller}$, and P_{pump} represent the power of the compressor, the controller, and the water pumps, respectively, in kW.

The coefficient of performance of the overall heating system can be defined as

$$COP_{sys} = \frac{Q_{dhw}}{Q_{hp}}. \quad (10)$$

4. System Simulation

The entire system simulation was carried out based on the initial design parameters under the TRNSYS transient simulation environment [19]. This computer program is popularly used by the international scientific community in the energy and thermal engineering field. It is based on interconnecting elementary modules called TYPE, which are either components of the studied system such as storage tanks or particular functions such as the weather data reader which allows connecting the selected area weather database to the system.

The numerical model of each component used in this study was either available in the existing library or developed as a new component. The hybrid PV/T collector model was developed based on a prototype from the collaborative research of the Fraunhofer Institute for Solar Energy Systems (Fraunhofer ISE) and the National Institute of Applied Science in Lyon, France (INSA Lyon) and with the support of EDF R&D. In this prototype, the physical configurations of the absorber, that include the water channels and the solar cells, are shown in Figure 3. Four strings of eight pseudosquare sc-Si PV cells were connected in series and laminated with encapsulant and a polymer film onto the surface of a flat *Rollbond* [20] aluminum heat exchanger with an electric insulating coating. In spite of slightly lower thermal properties than copper, the lower price of aluminum enables a higher plate thickness to be considered (1 mm instead of 0.2 mm) in order to provide a better stiffness to the solar cells in the absence of glazing [21, 22]. The absorber was inserted into a collector frame. The collector front cover was a 4 mm AR glass with a transmission above 0.93 and the distance between the glass cover and the absorber was 20 mm. Thermal insulation material was then applied on the back side of the absorber. The main design data of this prototype is given in Table 1.

The simulation model is based on a nodal approach originally developed by Fraisse et al. [24, 25] and later modified by Dupeyrat et al. [26] according to the actual physical arrangements. 12 temperature nodes have been considered for the different interfaces from the cover to the backside of the collector including the collector fluid temperature. The nodal temperatures then can be obtained by solving the group of equations derived from the energy balance of each interface. This "TYPE" is different from the other models of solar thermal collectors in TRNSYS because it takes into account several important dynamic properties such as:

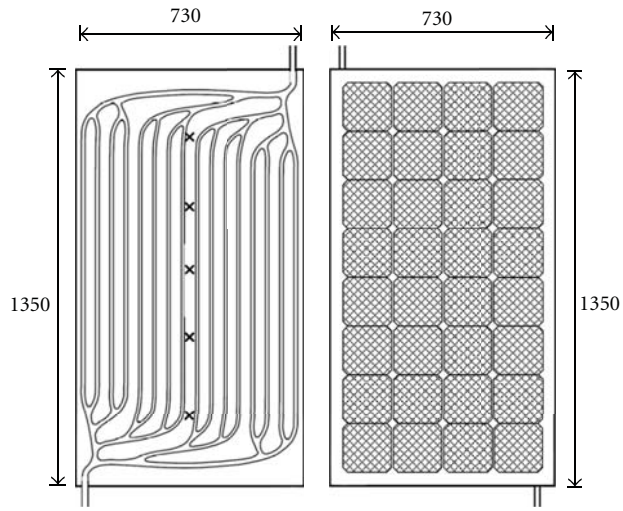

Figure 3: Description of the PV-T absorber plate rear side (a) and front side (b) [23].

Table 1: Key parameters of the PVT collector unit.

Front glazing	
Thickness of glass	0.004 m
Emissivity of glass	0.9
Thermal capacity	840 kJ/(kg·K)
Density	2500 kg/m^3
Depth of air gap underneath	0.02 mm
PV cell	
Length of the PV cell	0.156 m
Width of the PV cell	0.156 m
Thickness	0.0002 m
Thermal conductivity	148 W/(m·K)
Emissivity	0.91
Absorptivity	0.93
Reference electrical efficiency of the sc-Si module	14%
Packing factor	0.79
Thermal absorber	
Length of the module	1.350 m
Width of the module	0.73 m
Thermal capacity	910 kJ/(kg·K)
Density	2700 kg/m^3
Absorptivity	0.94
Number of tubes	16
Thickness of insulation layer	0.05 m
Insulation thermal conductivity	0.04 W/(m·K)

(i) the long-wave radiation exchange between the cover and the environment (exchanges between the ground and sky are separated),

(ii) the thermophysical characteristics of the collector (instead of the empirical correlation obtained from experiments).

For the evaluation of the convective exchange in the sealed-air channel between the PV cell layer and the cover, the air properties are determined as a function of the air temperature (instead of using constant values). The coefficients of correlation are obtained from the experimental results.

(i) Energy balance of the cover

$$C_C \frac{T_{CF} - T_{CI}}{\Delta t} = K_1(T_{AF} - T_{CF}) + K_{C1}(T_{\text{amb}} - T_{CF}) + K_{R1}(T_s - T_{CF}) + B_c \text{GA}_C, \tag{11}$$

with:

$$C_C = \rho_C \cdot e_C \cdot A_C \cdot Cp_C,$$
$$K_1 = A_C(h_{ci} + h_{ri}),$$
$$K_{C1} = A_C(h_c + h_{ri}),$$
$$K_{R1} = A_C h_{rs}, \tag{12}$$

T_{CI} and T_{CF} are the cover temperatures at the beginning and the end of every time step, K; ρ_C is the cover density, kg/m^3; e_C is the thickness of the cover, m; Cp_C is the specific heat of the cover, kJ/(kg·K); h_{ci} is the convective heat transfer coefficient between the absorber and the cover, W/(m^2 · K); h_{ri} is the radiative heat transfer coefficient between the absorber and the cover, W/(m^2 · K); h_c is the convective heat transfer coefficient between the cover and ambience, W/(m^2·K); h_{rs} is the radiative heat transfer coefficient between the cover and the sky, W/(m^2 · K).

(ii) Energy balance of the absorber

$$\text{C}_A \frac{T_{AF} - T_{AI}}{\Delta t} = K_1(T_{CF} - T_{AF}) + K_2(T_{\text{bs}} - T_{AF}) + K_3\left(T_f - T_{AF}\right) + \text{BGA}_C \tag{13}$$

with:

$$C_A = \rho_A \cdot e_A \cdot A_C \cdot Cp_A + \rho_T \cdot Cp_T \cdot \frac{\pi}{4} \cdot \left[(D_T + 2 \cdot e_T)^2 - {D_T}^2\right] \cdot L_T \cdot N_T. \quad (14)$$

The heating capacity of the absorber including the tubes can be written as

$$K_2 = \frac{A_C}{e_{\text{ins}}/\lambda_{\text{ins}} + 1/h_{\text{bs}}}, \qquad K_3 = h_0 \pi D_T L_T N_T, \quad (15)$$

where, T_{AI} and T_{AF} are the absorber temperatures at the beginning and the end of the time step respectively, K; B is the optical factor of the absorber; ρ_A is the absorber density, kg/m^3; e_A is the thickness of the absorber, m; Cp_A is the specific heat of the absorber, kJ/(kg·K); ρ_T is the tube density, kg/m^3; e_T is the thickness of the tube, m; Cp_T is the specific heat of the tube, kJ/(kg·K); D_T is the diameter of the tubes, m; L_T is the length of the tubes, m; N_T is the number of tubes; e_{ins} is the thickness of the insulation, m; λ_{ins} is the thermal conductivity of the insulation, W/(m·K); T_{bs} is the collector backside temperature, °C; h_0 is the convective heat transfer coefficient of the fluid, W/(m^2·K).

(iii) Energy balance of the fluid

$$C_f \frac{T_{fF} - T_{fI}}{\Delta t} = K_4\left(T_{if} - T_{fF}\right) + K_3\left(T_{AF} - T_{fF}\right), \quad (16)$$

where,

$$C_f = \rho_f \cdot Cp_f \cdot \frac{\pi {D_T}^2}{4} \cdot L_T \cdot N_T, \qquad K_4 = \frac{\dot{m}_f \cdot Cp_f}{(1/(1 - e^{-\alpha L_T}) - 1/\alpha L_{\text{T}})}, \qquad \alpha = \frac{h_0 \pi D_T}{\left(\dot{m}_f \cdot Cp_f \cdot N_T\right)}. \quad (17)$$

T_{fI} and T_{fF} are the fluid temperatures at the beginning and the end of the time step, K; ρ_f is the fluid density, kg/m; Cp_f is the specific heat of the cover, kJ/kg·K); $\dot{m}_f$ is the fluid mass flow rate, kg/s.

The electrical efficiency is determined as follows:

$$\text{Eff}_{\text{PV}} = \text{Eff}_{\text{PV\_ref}} \cdot \left(1 + \beta_r (T_{\text{PV}} - T_{\text{PV}_{\text{ref}}})\right) \cdot \gamma \cdot \tau_1, \quad (18)$$

where γ is the PV cell packing factor, τ_1 is the transmittance of the covers, $\text{Eff}_{\text{PV\_ref}}$ is the reference cell efficiency at the reference operating temperature $T_{\text{PV\_ref}} = 298.15$ K; T_{PV} is the PV cell surface temperature, K; β_r is the temperature coefficient, %/K.

At every time step, the exchange coefficients are to be calculated by using the initial temperatures of the nodes. The three differential equations, namely, (11), (13), and (16), which are defined according to the energy balance of every nodes, are solved numerically.

Table 2: Simulation parameters of sanitary equipment and required temperature.

Mass flow rate per shower equipment	300 L/h
Mass flow rate per lavabo	30 L/h
Number of the shower equipment	150
Number of the lavabo	80
Bathing water temperature	35°C

Table 3: Simulation parameters of the solar water preheating system.

Collectors area	600 m^2
Number of collectors in series	10
Number of the array group in parallel	12
Mass flow rate	40 L/h·m^2
Auxiliary heater power	5 kW
Tank model with internal coil exchanger	Horizontal cylinder tank
Orientation/tilt angle	South-facing/23°

Table 4: Water source heat pump unit characteristics under the standard condition.

Type of refrigerant	R410A
Heat capacity	14.61 kW (40°C/45°C hot water, constant flow)
C.O.P	4.9
Cooling capacity	10.37 (12°C/7°C chilled water, constant flow)
E.E.R	4.5

The storage tank (Type 60) was modeled as a component of the vertical stratified cylindrical tank including internal heat exchanger. The thermal stratification can be modeled by assuming that the tank consists of N ($N \leqslant 100$) fully mixed equal volume segments. The degree of stratification is determined by the value of N. If N is equal to 1, the storage tank is modeled as a fully mixed tank and no stratification effects are possible.

Listed in Tables 2, 3 and 4 are the system parameters and input data considered in the simulation process.

5. Results and Discussion

Both the system energy and exergy performance were determined. The year round simulation results were obtained using the typical meteorological year (TMY) hourly weather data of Hong Kong. The simulation time step was 12 minutes.

5.1. Energy Evaluation Criteria. The rate of useful thermal energy produced from the PV/T collector can be evaluated as:

$$Q_u = \dot{m}_f C_p (T_{oc} - T_{ic}). \quad (19)$$

The electrical energy generated in kWh is given by:

$$E_{\text{elect}} = \text{Eff}_{\text{PV}} \cdot Ac \cdot G. \quad (20)$$

Annual thermal equivalent of electrical energy produced can be evaluated by using:

$$Q_{\text{elecannual}} = \frac{E_{\text{elecannual}}}{0.38}. \tag{21}$$

An efficiency of 0.38 was arbitrarily used for the conversion of thermal energy into electrical energy for thermal power plants.

The overall annual thermal output can be evaluated by:

$$Q_t = Q_{\text{elecannual}} + Q_{\text{uannual}}. \tag{22}$$

Collector thermal efficiency, which is the ratio of the useful energy gain Q_u to the absorbed solar energy by the collectors, can be evaluated using (23), in that

$$\text{Eff}_{\text{thermal}} = \frac{Q_u}{(A_C G)}. \tag{23}$$

The fraction of energy saving is another evaluation criterion to estimate the system performance as compared to the conventional system by using the primary source energy. It can be determined by:

$$Q_{\text{sav}} = Q_{\text{convention}} - Q_{\text{aux}}, \tag{24}$$

where, Q_{aux} is the sum of the auxiliary consumption including the energy consumption of the auxiliary heater, the components (compressor, pumps, and, etc.) in the heat pump system:

$$F_{\text{sav}} = \frac{Q_{\text{sav}}}{Q_{\text{convention}}}. \tag{25}$$

5.2. Energy Evaluation Criteria. The exergy output is critical to define the real performance of PV/T system [25–27]. This can be calculated from the expression given by Fraisse et al. [28], as follows:

$$Q_{\text{exth}} = \sum_{k=1}^{12}\sum_{j=1}^{N}\sum_{i=1}^{n}\dot{Q}_u\left(1 - \frac{T_a}{T_{\text{sun}}}\right), \tag{26}$$

where T_a is the ambient temperature in Kevin, and T_{sun} is temperature of the sun (5777 K).

As the electrical output of a PV/W collector is a form of exergy, the total annual exergy output of the collector can be obtained by

$$Q_{\text{exann}} = E_{\text{elect}} + Q_{\text{exth}}. \tag{27}$$

The exergy from the solar radiation can be given by:

$$Q_{\text{exsolar}} = GA\left(1 - \frac{T_a}{T_{\text{sun}}}\right). \tag{28}$$

The exergy efficiency of the collector then can be calculated by

$$\text{Eff}_{\text{excol}} = \frac{Q_{\text{exann}}}{Q_{\text{exsolar}}}. \tag{29}$$

The exergy efficiency of the overall system is then given as:

$$\text{Eff}_{\text{exsys}} = \frac{\dot{m}_m C_p (T_{\text{dis}} - T_{\text{fw}}) - T_a \dot{m}_m \ln(T_{\text{dis}}/T_{\text{fw}}) + E_{\text{elect}}}{Q_{\text{exsolar}} + Q_{\text{aux}}}. \tag{30}$$

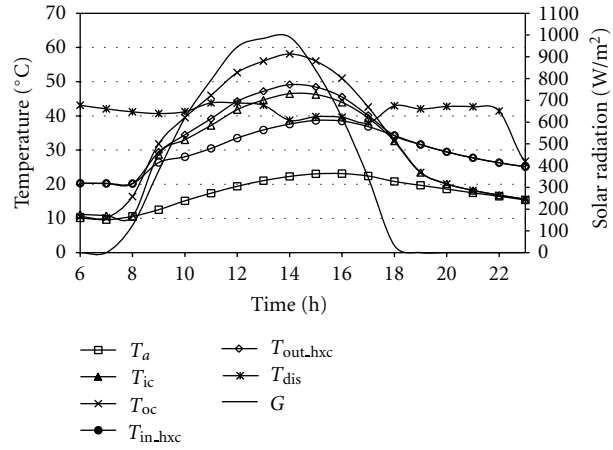

Figure 4: Daily variation of temperatures and the incident solar radiation, mi February.

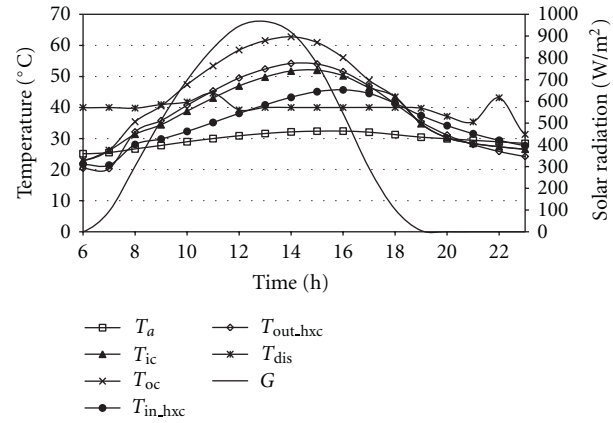

Figure 5: Daily variation of temperatures and the incident solar radiation, mi August.

5.3. Daily and Monthly System Energy and Exergy Performance in Hong Kong. Figures 4-5 show the variations of the collector inlet and outlet water temperatures (hot side of the heat exchanger), cold side inlet, and outlet temperatures of the heat exchanger connected to tank, delivery water temperature, and the outdoor air temperature of two typical sunny days, one in winter (mid February) and the other in summer (mid August) of Hong Kong. The mass flow rates in the solar loop and in the heat exchanger-tank loop are 2400 l/h and 2000 l/h, respectively. The fluid circulation on both sides is regulated by the corresponding temperature differential controller. During the system operating period, the temperature difference between the inlet and outlet of the solar collectors can be close to 10°C when there is water flow in the solar loop. As expected, the temperature of load water T_{dis} could be maintained around 40°C, which is slight higher than the expected pool water temperature on considering the heat losses in pipe distribution. The collector temperature is found higher in summer than in winter for the same solar radiation level.

Table 5: Annual energy and exergy assessment of the designed system under different climates.

City	Solar radiation (kWh)	Collector useful thermal energy (kWh)	Collector electrical output (kWh)	Overall thermal output (kWh)	Exergy output (kWh)	Auxiliary energy consumption (kWh)
Hong Kong	8.74E + 05	4.31E + 05	9.00E + 04	1.21E + 06	1.29E + 05	4.19E + 05
Paris	6.74E + 05	2.93E + 05	7.24E + 04	1.63E + 06	1.29E + 05	6.26E + 05
Lyon	7.82E + 05	3.46E + 05	8.28E + 04	1.76E + 06	1.89E + 05	5.29E + 05
Nice	9.78E + 05	4.71E + 05	1.02E + 05	1.79E + 06	1.83E + 05	4.67E + 05

Table 6: Annual efficiencies of the designed system.

City	Col. electrical efficiency (%)	Col. thermal efficiency (%)	Col. overall efficiency (%)	Exergy efficiency (%)	C.O.P of HP system (%)	Fraction of energy saving (%)
Hong Kong	10.29	49.24	76.32	10.06	4.11	66.55
Paris	10.75	43.45	71.73	9.85	4.34	67.98
Lyon	10.59	44.29	72.16	9.13	4.52	71.05
Nice	10.42	48.11	75.54	11.93	4.34	75.63

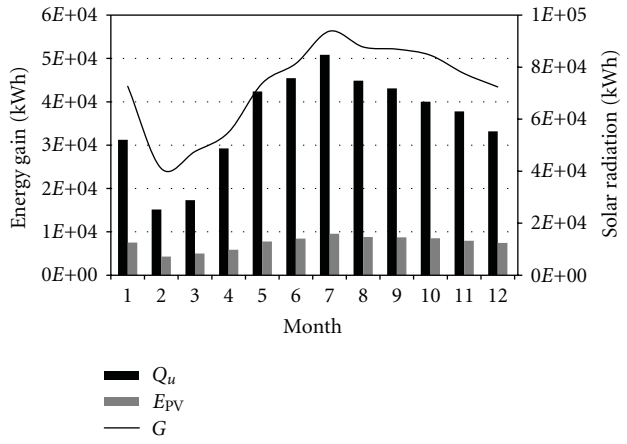

Figure 6: Monthly thermal and electrical energy gain of arrays of solar collectors and the incident solar radiation.

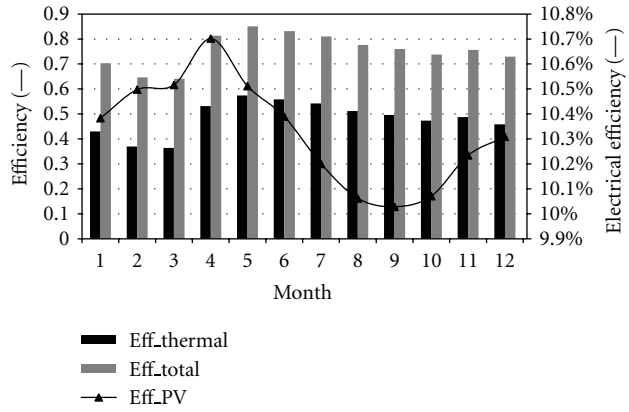

Figure 7: Monthly collector efficiencies.

The monthly energy gain of the hybrid collectors is shown in Figure 6. Q_u represents the useful thermal output of the collectors. E_{pv} represents the electricity generation from the collectors. It can be observed that the variation of the heat gain of the solar collectors agrees well with the incident solar radiation. The heat gain is low during the first quarter of the year as the solar radiation level is also relatively low in this period. The highest useful heat gain of 5.08E + 04 kWh and the electricity generation of 9.57E + 03 kWh as well are obtained in July. As shown in Figure 7, the collector thermal efficiency varies between 0.37 and 0.57 over the year. But the PV electrical efficiency is relatively constant (fluctuating between 10.1% and 10.7%). The year round thermal and electrical efficiencies are 49.3% and 10.3%, respectively. The combined energy efficiency is then 76.3%, with 0.38 as the conversion factor.

Figure 8 shows the solar energy delivered to the tank Q_{hxc} and the total energy auxiliary energy consumption of the system (auxiliary heater, heat pump components). It can be observed that the transferred solar energy via the heat exchanger is slightly lower than the useful thermal energy collected in the collector. This is because of the heat losses induced by the heat exchanger. The overall auxiliary energy consumption is more important for the winter season. This is when the small internal auxiliary heater is activated to keep the desired water temperature before the reheating by the heat pump system. Compared to the conventional electrical heating system, the monthly fraction of energy saving was around 65% over the winter period. This fraction became higher in the warm season and was around 90%.

The monthly thermal performance of the heat pump series and the system COP are given in Figure 9. Q_{hw} represents the heat transfer to hot water; Q_{hp} is the sum of the energy consumption of the compressor and the controller in the heat pump system. The energy consumption of the heat pump system is more important for the winter season when the water temperature exiting the storage tank is relatively low. More reheat energy is needed to push up to the desired delivery temperature. The system COP in the warm season is relatively low. This is so especially during the last three

Table 7: Investment of the designed system.

System configuration				
Component	Hong Kong	Paris	Lyon	Nice
Collector area (m^2)	600	600	600	600
Heat pump heating capacity (kW)	175	270	240	220
Power of auxiliary heater unit (kW)	15	15	50	50
Storage tank (m^3)	60	60	60	60
Cost (HK$)				
Solar collectors	5.10E + 06	6.00E + 06	6.00E + 06	6.00E + 06
Water tank	4.02E + 05	2.40E + 06	2.40E + 06	2.40E + 06
Auxiliary heater	5.94E + 03	1.05E + 04	1.05E + 04	1.05E + 04
Heat pump systems	2.78E + 05	3.20E + 06	2.56E + 06	2.40E + 06
Accessories	5.38E + 05	9.20E + 05	8.56E + 05	8.40E + 05
Transportation	2.18E + 04	2.24E + 05	1.98E + 05	1.92E + 05
Cost of Balance of system plus site installation and testing	1.50E + 04	4.60E + 05	4.28E + 05	4.20E + 05
Total investment	6.36E + 06	1.32E + 07	1.25E + 07	1.23E + 07
Tax reduction and governmental subvention (percentage of total investment)	NA	**13**%	**13**%	**13**%
Energy saving (kWh)	6.72E + 05	1.19E + 06	1.12E + 06	1.16E + 06
Payback period	**10.52**	8.82	8.83	**8.40**

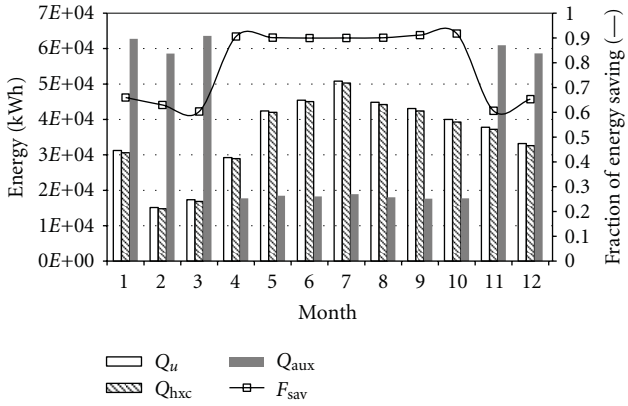

Figure 8: Monthly system auxiliary energy consumption and the energy saving.

summer months when the temperature of heat source turns high, and this affects the heat pump performance.

5.4. Comparison of Annual Energy and Exergy Performance under Different Climates. The annual energy and exergy performance of the designed system were evaluated under different climates, that is, in Hong Kong under subtropical climate and in three other cities of France. There are three climate zones in France, namely, Oceanic, Continental, and Mediterranean. The three cities Paris, Lyon and Nice, each could represent the typical climatic condition of each zone, were indicated on the map in Figure 10. The selected four cities can represent also most of the similar region climate of the world. The numerical computation of the annual performance was performed based on the hourly TMY weather data of individual cities. All cities were assumed to have the same load profile as in Hong Kong and thereby creating a common basis for comparison. The feed water temperature was determined according to the fresh water temperature and the return load water temperature as shown in Figure 11.

Table 5 lists the estimation of annual energy and exergy performance in the four cities. Regarding the total incident solar radiation, Nice has the highest level of solar radiation which yields also the highest outputs (useful thermal energy at 4.71E + 05 kWh and electricity at 1.02E + 05 kWh). Paris has the least energy gains as the solar radiation level and ambient temperature in this zone are relatively low. Consequently, more auxiliary energy was consumed in Paris. In terms of the system thermal output that affected by the freshwater temperature, Hong Kong has the lowest thermal output, at 1.21E + 06 kWh. Concerning the exergy output, Hong Kong and Paris are positioned at the same low level, whereas Lyon has the best exergy performance of 1.89E + 05 kWh.

The annual system efficiencies are given in Table 6. The electrical efficiency for these four cities vary slightly between 10.29% and 10.75%. The collector thermal efficiency and the overall efficiency are relatively low for Paris and Lyon and are around 5% lower than Hong Kong—the city with the highest collector overall efficiency. Concerning the performance of the heat pump series, the system COP remains almost the same for all the cities, and the fraction of energy saving is all around 78%. Overall speaking, the system performs less desirable in exergy efficiency, at around 10% for all climatic conditions.

6. Economic Analysis

The investment on a combined solar-assisted heat pump system includes the material and labour costs of the solar

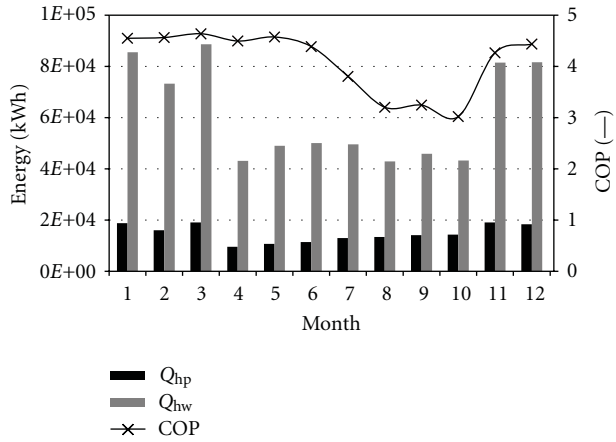

Figure 9: Monthly water source heat pump energy consumption and the system COP.

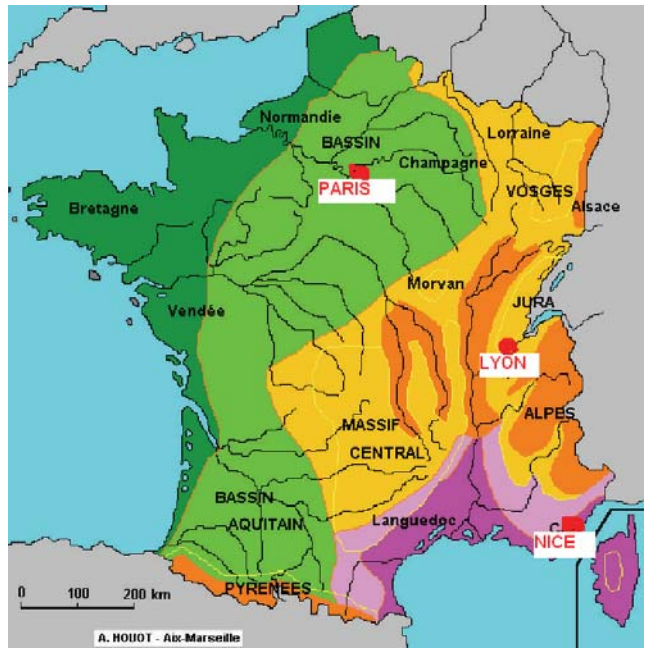

Figure 10: Climatic zones in France.

collectors, thermal storage tank, heat pump series, accessories (such as heat exchanger, pumps, controller, valves and, etc.) and the relevant system test and transportation. By making reference to the expenses of other similar SAHP systems in Hong Kong and in France, the costs of the entire system were evaluated and shown in Table 7. The most important investment item lies in the solar collectors. In France, according to the low carbon promotion policy, every installation of photovoltaic system could benefit by 11% tax credit [29] based on the total system investment. In addition, there exist some kinds of local subvention depending on the region and relevant department. In this case study, we took on average 2% of the total investment as the sum of the subvention. The average cost per kWh of electricity in Hong Kong is 1 HK$ and this is 0.1074 € (equivalent 1.1 HK$) [30] in France. The cost payback period was then estimated for each city. The results are listed in Table 7. Hong Kong has the longest payback period of 10.52 years even though the cost of material is less expensive compared to the other French cities. So far in Hong Kong, there is no subvention formulated

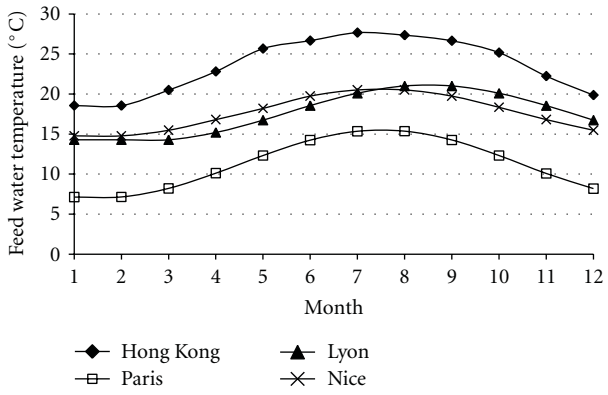

Figure 11: Feed water temperature of different cities.

for the solar thermal or electrical installations. The payback periods for the French cities are all around 9 years. In Nice, the city which possesses the richest annual solar radiation, this could be shortened to 8.4 years. However, the French government lowers the tax reduction for photovoltaic system year by year (25% for 2010, 22% for 2011 and 11% for 2012). The payback period will be probably longer in future, if the technical advancements are not to be considered.

7. Conclusions

This study was intended to investigate the potential application of the hybrid PV/T solar-assisted heat pump system for indoor sports centre water heating under the subtropical climatic condition of Hong Kong, as well as the multiple climates in France. An initial design procedure was first presented, and the energy performance was evaluated through the use of the TRNSYS transient simulation tool. The numerical results showed that the designed system can well satisfy the system energy demands. The hot water supply temperature can be reheated to 40°C during the operating period. The mean heating COP of the SAHP system is found to be 4.3. The overall efficiency of PV/T collectors can reach 76% in Hong Kong. The global fractional energy saving factor can achieve a maximum of 75% in Nice. The payback period of 10.52 years for Hong Kong is comparatively long. The stake of the further research led on this topic should be on the improvement of system exergy efficiency by optimizing the system configuration and parametric studies. The system life cycle assessment should also be in place to assess the environmental impacts.

Nomenclature

A_c: Area of hybrid PV/T collector in indirect heating mode (m^2)
A_{cd}: Area of hybrid PV/T collector in direct heating mode (m^2)
B: B is the optical factor of the absorber (—)
C_p: Specific heat of water (kJ/kg·K)
e: Thickness (m)
E_{elect}: Electrical energy generated from the collector (kWh)
$Eff_{thermal}$: Thermal efficiency of collector (—)
Eff_{PV}: Electrical efficiency of collector (—)
F_{hx}: Heat exchanger surface area (m^2)
G: Total incident solar radiation (kWh)
K_{hx}: Heat transfer coefficient of the heat exchanger ($W/m^2 \cdot K$)
J_T: Average daily solar radiation level ($kJ/m^2 \cdot day$)
h_c: Convective heat transfer coefficient between the cover and ambience ($W/m^2 \cdot K$)
h_0: Convective heat transfer coefficient of the fluid, ($W/m^2 \cdot K$)
h_{ri}: Radiative heat transfer coefficient between the absorber and the cover ($W/m^2 \cdot K$)
h_{rs}: Radiative heat transfer coefficient between the cover and the sky ($W/m^2 \cdot K$)
k_r: Hot water mixing factor
$\dot{m}_f$: Collector fluid mass-flow rate (kg/s)
$\dot{m}_h$: Mass-flow rate of hot water from the tank (kg/h)
$\dot{m}_{dis}$: Mass-flow rate of load water (kg/h)
i: Segment in the tank (—)
Q_{aux}: Total auxiliary energy consumption (kWh)
$Q_{elecannual}$: Annual thermal equivalent of electrical energy (kWh)
Q_h: Required heat load (kJ/h)
$Q_{uannual}$: Annual useful thermal energy of collector (kWh)
Q_u: Instant useful thermal energy of the solar collector (kJ/h)
T_a: Outdoor air temperature (°C)
T_{CI}: Collector cover temperature at the beginning of every time step (K)
T_{CF}: Collector cover temperature at the end of every time step (K)
T_{dis}: Load water temperature (°C)
T_{fI}: Collector fluid temperature at the end of every time step (K)
T_{fF}: Collector fluid temperature at the end of every time step (K)
T_{fw}: Feed water temperature (°C)
T_h: Hot water temperature (°C)
T_{PV}: PV cell surface temperature (°C)
T_{PV_ref}: PV reference operating temperature
T_{sun}: Sun temperature (K)
$UA_{flue,i}$: Heat transfer capacity of the fluid in the i segment (kJ/h·K)
Δx: Distance between the segments (m)
Δt: Time step for the system simulation (min).

Greek Symbols

β: Collector slope (°)
β_r: PV temperature coefficient (%/K)
γ: PV cell covering factor (−)
δ: Collector heat loss coefficient ($W/m^2 \cdot K$)

λ: Fluid thermal conductivity (W/m·K)
τ_1: Transmittance of the cover
ρ: Density (kg/m^3)
η_{cd}: Collector efficiency determined by the practical testing (−)
η_L: Heat loss coefficient of the hydraulic piping system (−).

Acknowledgment

The research work described in this paper was fully supported by the grants from the Research Grants Council of the Hong Kong Special Administrative Region, China [Project nos. City U 112009 and 112508].

References

[1] M. A. Hasan and K. Sumathy, "Photovoltaic thermal module concepts and their performance analysis: a review," *Renewable and Sustainable Energy Reviews*, vol. 14, no. 7, pp. 1845–1859, 2010.

[2] T. T. Chow, "A review on photovoltaic/thermal hybrid solar technology," *Applied Energy*, vol. 87, no. 2, pp. 365–379, 2010.

[3] T. T. Chow, W. He, and J. Ji, "An experimental study of facade-integrated photovoltaic/water-heating system," *Applied Thermal Engineering*, vol. 27, no. 1, pp. 37–45, 2007.

[4] T. T. Chow, W. He, and J. Ji, "An experimental study of façade-integrated photovoltaic/water-heating system," *Applied Thermal Engineering*, vol. 27, no. 1, pp. 37–45, 2007.

[5] T. T. Chow, W. He, A. L. S. Chan, K. F. Fong, Z. Lin, and J. Ji, "Computer modeling and experimental validation of a building-integrated photovoltaic and water heating system," *Applied Thermal Engineering*, vol. 28, no. 11-12, pp. 1356–1364, 2008.

[6] T. T. Chow, A. L. S. Chan, K. F. Fong, Z. Lin, W. He, and J. Ji, "Annual performance of building-integrated photovoltaic/water-heating system for warm climate application," *Applied Energy*, vol. 86, no. 5, pp. 689–696, 2009.

[7] R. Santbergen, C. C. M. Rindt, H. A. Zondag, and R. J. C. van Zolingen, "Detailed analysis of the energy yield of systems with covered sheet-and-tube PVT collectors," *Solar Energy*, vol. 84, no. 5, pp. 867–878, 2010.

[8] P. G. Charalambous, S. A. Kalogirou, G. G. Maidment, and K. Yiakoumetti, "Optimization of the photovoltaic thermal (PV/T) collector absorber," *Solar Energy*, vol. 85, no. 5, pp. 871–880, 2011.

[9] C. Cristofari, G. Notton, and J. L. Canaletti, "Thermal behavior of a copolymer PV/Th solar system in low flow rate conditions," *Solar Energy*, vol. 83, no. 8, pp. 1123–1138, 2009.

[10] A. Tiwari and M. S. Sodha, "Parametric study of various configurations of hybrid PV/thermal air collector: experimental validation of theoretical model," *Solar Energy Materials and Solar Cells*, vol. 91, no. 1, pp. 17–28, 2007.

[11] O. Zogou and H. Stapountzis, "Flow and heat transfer inside a PV/T collector for building application," *Applied energy*, vol. 91, no. 1, pp. 103–115, 2012.

[12] O. Ozgener and A. Hepbasli, "A review on the energy and exergy analysis of solar assisted heat pump systems," *Renewable and Sustainable Energy Reviews*, vol. 11, no. 3, pp. 482–496, 2007.

[13] A. Hepbasli and Y. Kalinci, "A review of heat pump water heating systems," *Renewable and Sustainable Energy Reviews*, vol. 13, no. 6-7, pp. 1211–1229, 2009.

[14] A. Bridgeeman and S. Harrison, "Preliminary experimental evaluation of indirect solar assisted heat pump systems," in *Proceedings of the 3rd Canadian Solar Building Conference*, Fredericton, NB, Canada, August 2008.

[15] A. Dikici and A. Akbulut, "Performance characteristics and energy-exergy analysis of solar-assisted heat pump system," *Building and Environment*, vol. 43, no. 11, pp. 1961–1972, 2008.

[16] H. Li and H. Yang, "Study on performance of solar assisted air source heat pump systems for hot water production in Hong Kong," *Applied Energy*, vol. 87, no. 9, pp. 2818–2825, 2010.

[17] Q. Wang, Y. Q. Liu, G. F. Liang, J. R. Li, S. F. Sun, and G. M. Chen, "Development and experimental validation of a novel indirect-expansion solar-assisted multifunctional heat pump," *Energy and Buildings*, vol. 43, no. 2-3, pp. 300–304, 2011.

[18] S. J. Sterling and M. R. Collins, "Feasibility analysis of an indirect heat pump assisted solar domestic hot water system," *Applied Energy*, vol. 93, pp. 11–17, 2011.

[19] TRNSYS, *A Transient Simulation Program*, Solar Energy Laboratory, University of Wisconsin, Maidison, Wis, USA, 2003.

[20] Bionicol 2010, Bionicol-Development of a bionic solar collector with aluminum *Rollbond* absorber-Project status after second year, http://www.bionicol.eu/, 2011.

[21] P. Dupeyrat, C. Ménézo, M. Rommel, and H. M. Henning, "Efficient single glazed flat plate photovoltaic-thermal hybrid collector for domestic hot water system," *Solar Energy*, vol. 85, no. 7, pp. 1457–1468, 2011.

[22] P. Dupeyrat, C. Ménézo, H. Wirth, and M. Rommel, "Improvement of PV module optical properties for PV-thermal hybrid collector application," *Solar Energy Materials and Solar Cells*, vol. 95, no. 8, pp. 2028–2036, 2011.

[23] P. Dupeyrat, *Experimental development and simulation investigation of a photovoltaic-thermal hybrid solar collector [Ph.D. thesis]*, National Institute of Applied Science, Lyon, France, 2011.

[24] C. Plantier, *Etude numérique et expérimentale d'un prototype de chauffe-eau solaire équipé d'un stockage à changement de phase [Ph.D. thesis]*, University of Savoie, Savoy, France, 2005.

[25] G. Fraisse, C. Ménézo, and K. Johannes, "Energy performance of water hybrid PV/T collectors applied to combisystems of Direct Solar Floor type," *Solar Energy*, vol. 81, no. 11, pp. 1426–1438, 2007.

[26] P. Dupeyrat, Y. Bai, C. Menezo et al., "Performances énergétiques de capteurs solaires hybrides PV-T pour la production d'eau chaude sanitaire," in *Proceedings of the Annual conference of Societe France de Thermique (SFT)*, Perpignan, France, 2011.

[27] V. Raman, G. N. Tiwari, and H. D. Pandey, "Life cycle cost analysis of a hybrid photovoltaic-thermal water and air collector: a comparison study based on energy and exergy," *International Journal of Low Carbon Technologies*, vol. 3, no. 3, pp. 173–190, 2008.

[28] G. Fraisse, Y. Bai, N. Le Pierrès, and T. Letz, "Comparative study of various optimization criteria for SDHWS and a suggestion for a new global evaluation," *Solar Energy*, vol. 83, no. 2, pp. 232–245, 2009.

[29] A. S. Joshi, I. Dincer, and B. V. Reddy, "Analysis of energy and exergy efficiencies for hybrid PV/T systems," *International Journal of Low-Carbon Technologies*, vol. 6, no. 1, Article ID ctq045, pp. 64–69, 2011.

[30] M. Bosonac, B. Sorensen, I. Katic, H. Sorensen, B. Nielsen, and J. Badran, "Photovoltaic/thermal solar collector and their potential in Denmark," Final Report. EEP project 1713/00-0014, 2003.

Hindawi Publishing Corporation
International Journal of Photoenergy
Volume 2012, Article ID 686393, 8 pages
doi:10.1155/2012/686393

Research Article

Simulation Study of Building Integrated Solar Liquid PV-T Collectors

Tomas Matuska

Faculty of Mechanical Engineering, Czech Technical University in Prague, Technicka 4, 166 07 Prague, Czech Republic

Correspondence should be addressed to Tomas Matuska, tomas.matuska@fs.cvut.cz

Received 7 April 2012; Accepted 26 May 2012

Academic Editor: T. T. Chow

Influence of building integration of polycrystalline PV modules on their performance and potential for use of active liquid cooling by use of BIPV-T collectors has been investigated by simulation analysis with a detailed model. Integration of PV modules into building envelope could reduce the annual production of electricity by a rate above 5% and negatively influence lifetime due to thermal stresses induced by high operation temperatures above 100°C in the case of warm climate and above 90°C in moderate climate. Two configurations of unglazed PV-T collectors (low-tech, high-tech) and their ability to eliminate overheating of BIPV module have been discussed. Simulation study on combined heat and electricity production from given BIPV-T collectors has been presented for three typical applications (5°C: primary circuits of heat pumps; 15°C: cold water preheating; 25°C: pool water preheating). Thermal output of unglazed BIPV-T collectors is up to 10 times higher than electricity. Electricity production could be up to 25% higher than BIPV (without cooling) for warm climate and up to 15% in moderate climate.

1. Introduction

Utilization of solar energy being a scarce energy source needs a large area of south-facing collecting surfaces. Rational use of building envelopes for the collection of solar energy and its conversion to required energy carrier results into integration of active solar devices into the building envelope structure and leads to multifunctional or hybrid solar collector configurations combining several purposes (heat and electricity generation, daylighting, and air-liquid) in a single unit [1]. The integration of solar collectors into building envelope instead of separate installation represents a transition from the concept of envelope considered as an energy loss to envelope being an energy source—energy active envelope—which actually means a way to solar active buildings. As photovoltaic modules are getting more and more common in sustainable buildings in order to compensate the electricity consumption by electricity production on site, the combination of photovoltaic and solar thermal technology in hybrid PV-T collectors could represent a step further with combined heat and power production (solar cogeneration).

Standard commercial PV modules cannot convert more than 15% of incident solar radiation to electricity, the rest of energy is converted to waste heat which increases temperature of PV cell. The rise of PV cell temperature affects negatively the efficiency of photovoltaic solar/electricity conversion. Aesthetically preferred building envelope integrated PV (BIPV) installations could show significantly higher operation temperatures than separate standalone PV modules due to limited natural cooling by wind. Introduction of active cooling of BIPV modules results in hybrid photovoltaic-thermal collectors (PV-T collectors) which can provide low-temperature heat and electricity, while heat production is usually several times higher than electricity.

There are generally three reasons to use PV-T collectors instead of PV collectors in building envelope integrated applications:

(i) overheating protection-reduction and elimination of excessive thermal load of PV cells lamination (EVA foil) and protection from accelerated degradation;

(ii) increase of electricity production by keeping the PV cell at considerably lower operation temperatures during a whole year;

(iii) higher specific energy gain from 1 m^2 of building envelope compared to separate installation of PV

and PT collectors, if low potential heat is usable in technical system of the building.

Hybrid PV-T collectors can be generally realised in several principal alternatives: glazed or unglazed, flatplate or concentrating and with different heat removal liquids (air, liquid). Review of recent extensive research on different construction types of PV-T technology can be found in [2–5]. Hybrid PV-T air collectors with natural cooling do not allow an effective removal of the heat from PV cell. On the other hand, forced air circulation consumes auxiliary electricity which can generally negate the higher electricity gain achieved by cooling if not properly designed. PV-T air systems have also a limited potential for building integration due to large air duct systems and low usability of ambient warm air for cooling in summer season [6].

Contrary to PV modules cooled by air, PV-T liquid collector concept seems to be more suitable for BIPV applications if combined with efficient use of low temperature heat, for example, for cold water preheating, swimming pool heating circuits, or primary circuits of heat pumps. Several studies have been led on combination of unglazed PV-T collectors with heat pumps [7, 8] or floor heating [9]. Unglazed PV-T liquid collectors are suitable to applications with priority of electricity generation and waste heat removed from cells is a byproduct at low temperature level with worse usability than in standard solar thermal collectors. While glazed PV-T collectors allow higher operation temperature levels and better usability of generated heat, on the other side they face, lower production of valuable electricity, and the problems with too high stagnation temperatures for PV cells (even above 120°C) still remain unsolved [10]. Unglazed solar PV-T collectors represent a robust and simple construction. They have been already introduced into the market in a number of products recently, also in concepts ready for building integration. However, price of PV-T collectors especially those with high quality of heat removal (high-tech) is relatively high, often more than double or triple when compared with PV modules alone. Therefore, there are attempts to reduce cost-benefit ratio through the development of low-tech configurations based on standard PV modules but with generally lower thermal performance due to heat removal restrictions resulting from simplifications of design [11]. Several studies are available on building integrated PV-T solar collectors [12–14] used as multifunctional components for built environment.

This work is focused on building integrated solar liquid PV-T collectors and several analyses are presented. First, the operation conditions of both building integrated PV modules and separately installed PV modules are simulated in two different European climates (warm, moderate). Performance figures of both installations are compared and reasons for BIPV cooling are revealed. Further, thermal performance of two different configurations of unglazed PV-T collectors representing high-tech and low-tech alternatives is analysed in detail both for building envelope integrated and separate installations. Heat transfer rate and efficiency of PV cell cooling expressed by efficiency factor F' and its influence on operation temperature of PV cell are discussed. Finally, performance figures of combined heat and electricity generation by unglazed BIPV-T collectors (high-tech, low-tech) are presented for three temperature levels representing the low temperature applications.

2. Modelling of (BI)PV and (BI)PV-T Collectors

There is a number of mathematical models developed for solar liquid PV-T collectors [15–17]. A detailed mathematical model of unglazed solar flat-plate hybrid PV-T liquid collector (PVT-NEZ) has been developed recently [18] and validated with experimental investigations [19]. Model is based on principle theory for energy balance of solar thermal collectors [20] expanded for photovoltaic conversion [21]. Calculation approach of PVT-NEZ model uses external energy balance of PV-T absorber (heat transfer from PV-T absorber surface to ambient) and internal energy balance of PV-T absorber (electric yield, heat transfer from PV-T absorber surface to liquid), see Figure 1. Both balances are solved in iteration loops to find temperature of PV-T absorber (PV cell) and relevant heat transfer coefficients. Both external and internal energy balances of absorber are mutually dependent and superior loop transfers the results of external balance to internal balance (collector heat loss) and results of internal balance to external balance (mean absorber temperature). Detailed description of mathematical model can be found in literature [18].

Input parameters of the model are thermal, optical, electrical, and geometrical properties of individual parts of PV-T collector (e.g., PV reference electric efficiency, temperature coefficient; material and geometry for heat exchanger, thermal insulation layer if applied), climate conditions (solar irradiance, ambient temperature and humidity, wind velocity, and sky temperature), and operation conditions (temperature of liquid entering collector, mass flow rate). Main output parameters of the model are usable electric and thermal power, output temperature of liquid, and temperature of absorber surface (PV cell). Building envelope integrated installations are modelled with added adjacent envelope insulation layer of given heat resistance at the back side of PV or PV-T collector with constant temperature behind considered (as interior temperature), see Figure 1(b).

Mathematical model PVT-NEZ of unglazed solar flat-plate PV-T liquid collector allows to analyze and to optimize the collector construction based on detailed design parameters and operation/climate conditions. Moreover, mathematical model could be used as a universal tool; the electric and thermal output and efficiency can be evaluated for various PV-T collector configurations as well as only thermal output for strictly thermal unglazed collector (efficiency $\eta_{el,r} = 0$) or strictly electric output of PV module (liquid mass flow set to 0 kg/s) with temperature and solar irradiance effects on its performance. The model could be used for theoretical analyses or as a base for validation of real product models from experimental data.

To simulate the annual energy output of solar PV modules and PV-T collectors, simulation tool coupling the detailed mathematical model PVT-NEZ and hourly climate

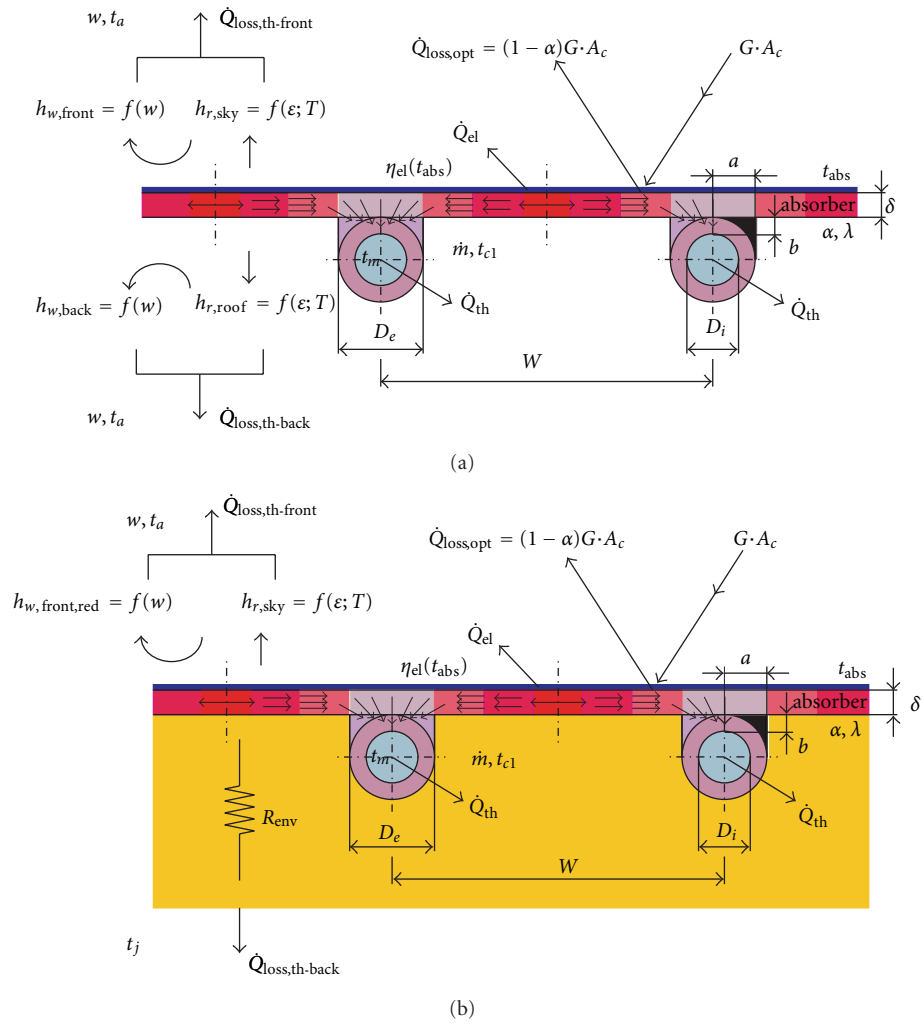

Figure 1: Scheme of unglazed PVT-NEZ model (separate and building envelope integrated installation).

data processor which supplies boundary conditions for the model in each simulation step has been developed. Incidence-angle-dependent optical properties of PV-T collectors (IAM characteristics) have been considered. Performance of unglazed solar collectors is strongly influenced by wind and sky radiation conditions due to direct influence on U-value and indirectly also on collector efficiency factor F'. Detailed modelling of these relationships with iteration external/internal balance loop in PVT-NEZ model for each calculation time step has provided more precise results for annual energy outputs than simplified models related to reduced number of influence factors.

Hourly data processor uses climate databases from Meteonorm [22] with meteorological elements: solar irradiation, ambient temperature, wind velocity, and relative humidity. Additional parameters are operation conditions given by mass flow and temperature of cooling liquid entering the PV-T collector. These parameters were maintained constant throughout the simulations. Positive hourly outputs have been summed up, negative set to zero. When negative thermal output was determined, the electric output was taken without cooling effect to take into account the real operation (system pump is off).

3. Overheating of BIPV Collectors

General experience from applications of building integrated of PV modules is the operation at elevated temperatures due to limited heat transfer from PV to ambient. In the extreme climate conditions (clear hot day with no wind), the operation temperatures can overcome the safe limit value 80°C. Figure 2 shows the electric efficiency of polycrystalline PV module in standalone and building integrated application at different solar irradiance and wind velocity levels for ambient temperature 25°C. Standard polycrystalline module has been considered with efficiency 14.2% (at STC) and temperature coefficient 0.45%/K. Thermal resistance of adjacent envelope is 6 m^2K/W. It is apparent that the integration of PV module into building envelope brings a significant thermal stress for PV cells, temperatures of PV cells excess 80°C at no wind conditions and can induce the degradation or

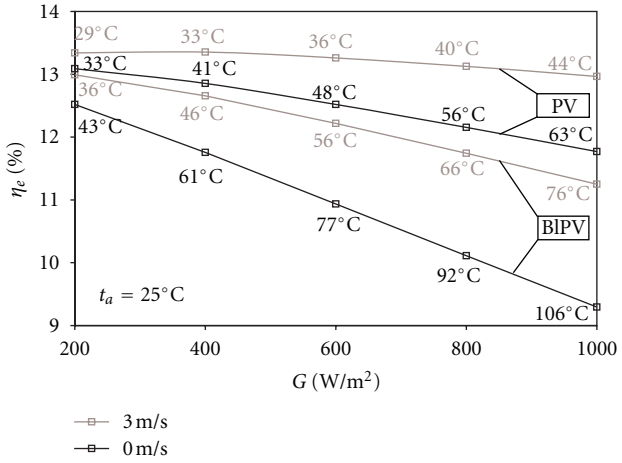

Figure 2: Efficiency and temperature of PV modules (separate and building envelope integrated installation).

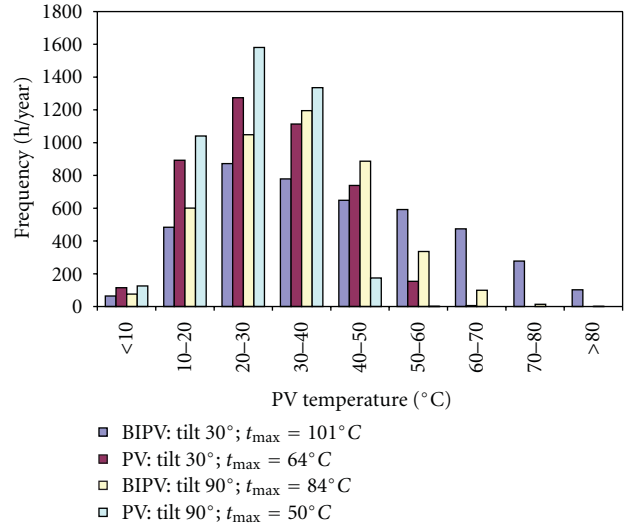

Figure 3: Operation temperature of PV module in separate installation (PV) and building envelope integrated installation (BIPV) for warm Athens (Greece) climate.

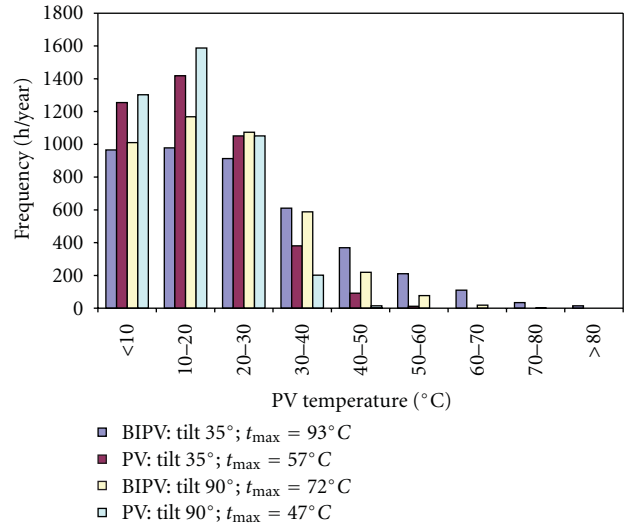

Figure 4: Operation temperature of PV module in separate installation (PV) and building envelope integrated installation (BIPV) for moderate Prague (Czech Republic) climate.

even destruction of PV cells at such an extreme climate conditions.

Figure 2 shows also a characteristic decrease of PV module efficiency with higher level of irradiance due to direct influence on PV temperature rise at a given wind velocity. Generally, polycrystalline PV module efficiency rises with solar irradiance if temperature of PV cell is kept low. This could be seen for high wind velocity (3 m/s) and separate installation of PV module. Increase of efficiency due to higher solar irradiance above 400 W/m^2 has been compensated by the decrease due to PV cell temperature rise. For other curves, it is not apparent due to prevailing temperature effect.

Presented examples do not provide information on annual PV operation figures in a real climate. Simulation analysis of PV module operation in separate (PV) and building envelope integrated (BIPV) installation has been performed for two different climates (warm-Athens/GR, moderate-Prague/CZ). Two alternatives of the collector tilt have been considered: optimum tilt for a given climate (Athens 30°, Prague 35°) and facade (90°). Orientation of collectors is south for all cases. Figures 3 and 4 show the histograms of PV module operation temperature. Impact of building integration and associated overheating of PV module on its electric performance in real operation conditions is given by the frequency of occurrence of high irradiation level and reduced wind cooling combination. The histograms show the increase of extreme temperatures frequency (above 80°C) especially for roof installations in warm climate (Athens). Facade BIPV application is not concerned by excessive temperatures for both considered climates.

Separate roof and facade installations of PV modules do not bring extreme temperatures and stress for PV cells. Operation temperatures of PV modules could be maintained bellow 60°C in both climates. PV module integration into the roof increases the frequency of high-temperature occurrence above 60°C. Especially in warm climate, the frequency of temperatures above 80°C becomes significant. Moderate climate shows low frequency of extreme temperatures; however maximum temperature 93°C indicates possible problems (tension in PV cell, cracking, delamination of foils, etc.). PV module integration into the facade does not show real problems to safe operation of PV for considered climates.

Shift of operation temperature to higher levels due to integration brings also the decrease of annual electric performance of building envelope integrated modules. Table 1 compares the annual electricity production by a given PV module per m^2 for investigated installation (roof BIPV and PV, facade BIPV and PV) and indicates the loss of the electricity yield by building integration.

Table 1: Yield reduction due to envelope integration of PV module.

Climate	Roof		Facade	
	BIPV	PV	BIPV	PV
Athens	192 kWh/(m²·a)	210 kWh/(m²·a)	121 kWh/(m²·a)	128 kWh/(m²·a)
	−9%		−6%	
Prague	129 kWh/(m²·a)	138 kWh/(m²·a)	89 kWh/(m²·a)	93 kWh/(m²·a)
	−7%		−5%	

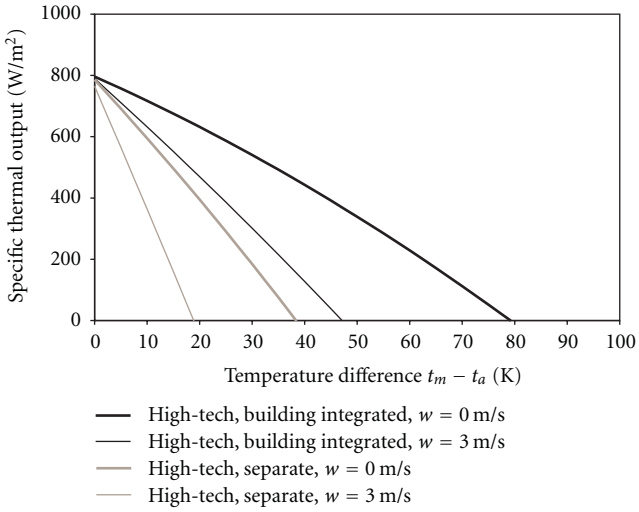

Figure 5: Thermal output characteristics for high-tech PV-T collector at different configurations and conditions.

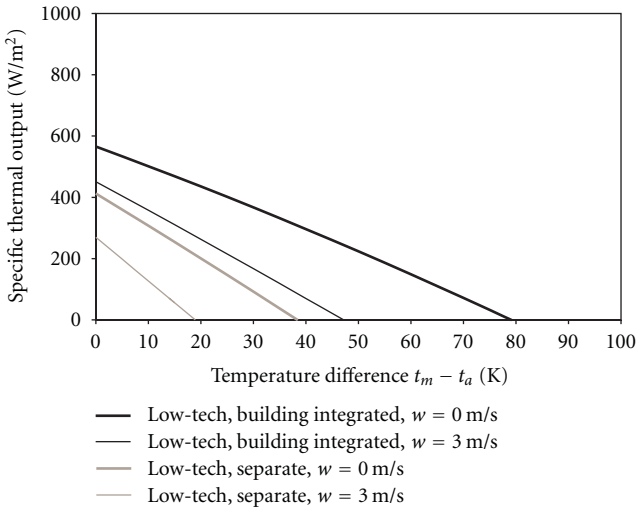

Figure 6: Thermal output characteristics for low-tech PV-T collector at different configurations and conditions.

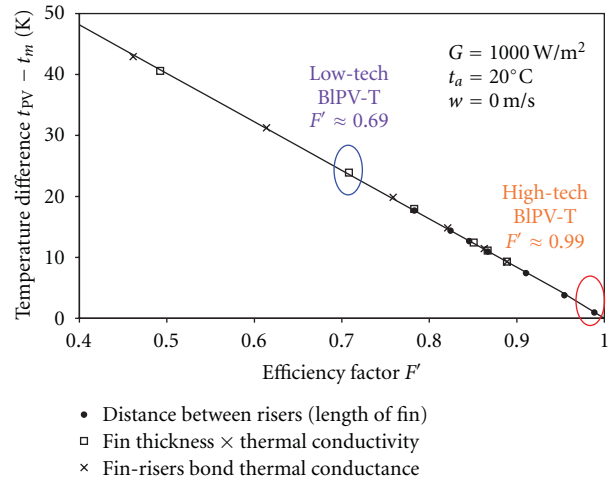

Figure 7: Relation between PV-liquid temperature difference and efficiency factor for BIPV-T collectors.

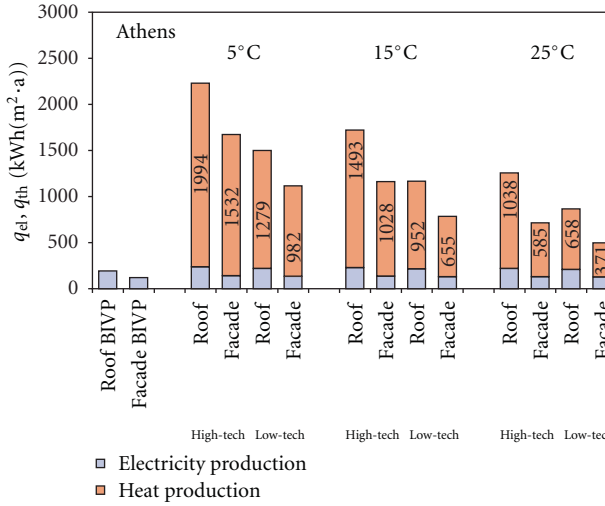

Figure 8: Energy production from roof and facade BIPV-T collectors in warm climate (Athens).

Loss in energy production of PV module by building integration for the considered climates is quite similar. BIPV in warm climate with higher irradiance levels lose 9% in roof installations and 6% in facade installations; relevant figures for moderate climate are 7% and 5% of loss.

The need for protection of PV modules against extreme operation temperatures as well as the need to keep the electricity production at sufficient level results in efforts to cool the PV modules and to develop the different BIPV-T collector configurations.

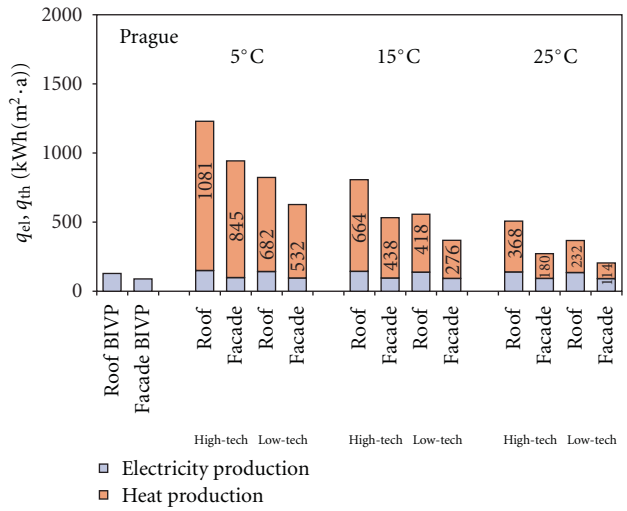

Figure 9: Energy production from roof and facade BIPV-T collectors in moderate climate (Prague).

4. Thermal Performance of BIPV-T Collectors

Generally, electrical and thermal outputs of PV-T collectors are mutually dependent. Higher electricity output through higher photovoltaic conversion efficiency results in lower thermal output of the collector, that is, lower level of waste heat removed from PV module. However, considering a given photovoltaic conversion efficiency of PV cell, the thermal performance of PV-T collector can be regarded as an indicator of overall quality defined by ability to cool down the PV module. Efficiency of PV module cooling depends on heat transfer from PV cell to liquid. "Heat transfer path" in liquid PV-T collectors is basically given by two components of heat exchanger participating in heat transfer: cooling fin system in contact with PV cell/module and thermal bond between piping with heat transfer liquid and cooling fins. Basic scheme has been already illustrated in Figure 1. The heat transfer between inner pipe wall and liquid by forced convection has very limited influence in usual configurations (fin-pipe system, antifreeze mixture).

Figure 5 shows thermal characteristic of "high-tech" PV-T collector with high conductance between PV cell and liquid due to advanced design of heat exchanger in configuration with and without building envelope integration. High-tech collector shows a high specific thermal output at zero difference between the mean liquid temperature and ambient temperature practically in all cases. However, thermal output characteristics differ significantly by heat loss rate at elevated temperature differences between liquid and ambient. The situation is a bit different in the case of "low-tech" PV-T collector (see Figure 6) with bad thermal contact between PV and liquid and simplifications in heat exchanger design to save material and ease production (see Table 2). Characteristics differ significantly in specific thermal output at zero temperature difference while rate of thermal output decrease by heat loss is similar. This is caused by strong impact of heat loss on efficiency factor F' of the collector

Table 2: Design parameters of considered PV-T collector (high-tech, low-tech) characteristics.

PV cell parameters		
Temperature coefficient	$\beta = 0.45\,\%/K$	
Reference efficiency	$\eta_{el,r} = 14.2\%$	
Reference temperature	$t_r = 25°C$	
Heat removal part	High-tech	Low-tech
Pipes diameter	$D_e/D_i = 10/8$ mm	
Pipes distance/fin length W	10 mm	100 mm
Cooling fin thickness d	2 mm	0.2 mm
Cooling fin conductivity λ	350 W/mK	250 W/mK
Bond conductance C_b	200 W/m·K	5 W/m·K
Mass flow rate of liquid	0.02 kg/s·m^2	

Table 3: Selected parameters and results for F' and temperature difference between PV and liquid.

W (mm)	$d \times \lambda$ (W/K)	C_b (W/mK)	F' (−)	$t_{PV} - t_m$ (K)
10	**0.7**	**200**	**0.99**	**0.9**
80	0.7	200	0.91	7.4
160	0.7	200	0.82	14.4
100	0.1	200	0.87	11.1
100	0.01	200	0.71	23.9
100	0.002	200	0.49	40.6
100	0.7	25	0.86	11.4
100	0.7	5	0.76	19.9
100	0.7	2	0.61	31.3
100	**0.05**	**5**	**0.69**	**24.4**

(mainly the heat exchanger cooling PV cells in the function of absorber) when F' value becomes very low. Therefore, building envelope integration of low-tech PV-T collector significantly increases the effectiveness of heat removal from PV even for very small liquid temperature difference from ambient compared to high-tech PV-T collector. In other words, while building integration brings negligible effect to high-tech PV-T collector for low operation temperatures, it brings a large improvement to low-tech PV-T collectors.

Relationship between the PV-liquid temperature difference and efficiency factor F' for BIPV-T collectors has been shown in Figure 7. The relationship has approximately a linear character. Low values of efficiency factor F' are generally caused by low conductance of the bond between risers and cooling fin/plate, low fin thermal conductivity and thickness product or large length of cooling fin. Individual points in Figure 7 represent practically possible values of the parameters or their combinations in usual range (bond conductance from 2 to 200 W/mK, conductivity-thickness product from 0.002 to 0.07 W/K, and cooling fin length from 10 to 200 mm). For given boundary conditions, efficiency factor values have been highlighted for investigated building integrated high-tech and low-tech PV-T configurations. Because of poor heat transfer between PV cell and heat removal liquid in the low-tech BIPV-T collector, the large

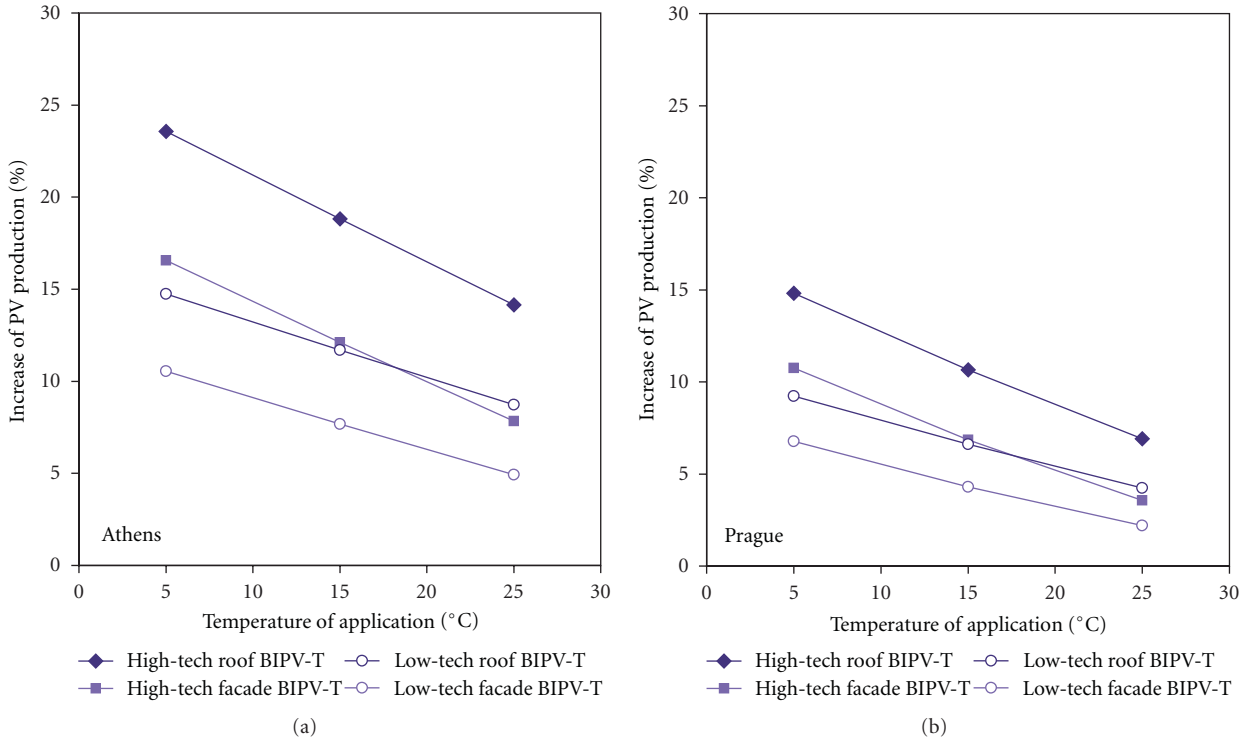

Figure 10: Increase of electricity production from BIPV modules by use of BIPV-T collectors.

temperature difference between PV cell and liquid is established. The question is how it could affect the ability of such configuration to sufficiently cool the PV cells and avoid overheating in real operation for a given climate.

Table 3 shows the selected points from graph in Figure 7 representing different geometry and physical parameters of PV-T collector configurations. Rows for investigated low-tech and high-tech PV-T collector configurations are highlighted.

5. Combined Heat and Electricity Production

Energy (electricity, heat) production for two unglazed BIPV-T collectors with different heat removal quality has been simulated. Mathematical models of BIPV-T collectors discussed above have been used to investigate whole year performance in two different climates (Athens, Prague) and for three temperature levels representing the typical applications of low potential heat utilization: primary circuits of heat pumps (5°C), cold water preheating (15°C), and pool water preheating (25°C). The temperatures were considered as temperatures of liquid entering the PV-T collector and were kept constant throughout the year in time periods when cooling of PV could bring a heat gain.

Figures 8 and 9 show the results for warm and moderate climate conditions. It is apparent that heat production is up to ten times higher than electricity production from BIPV-T collectors. Part of the thermal output is a heat gain from ambient environment especially for applications with low operation temperatures. Low-tech BIPV-T collector achieves only around 65% of high-tech thermal output regardless of application temperature and climate. Electricity production from low-tech and high-tech BIPV-T collectors differs in range of several percents for applications with higher temperatures (25°C) and up to 7% for applications with very low temperatures (5°C).

Improvement in electricity production by use of BIPV-T collectors instead of BIPV modules without cooling has been shown in Figure 10 for warm climate (a) and moderate climate (b). High-tech BIPV-T collectors show high improvement in electric performance up to 25% in annual electric yield for warm climate and 15% for moderate climate for roof installations while relevant figures for low-tech BIPV-T are 15% and 9%. Despite that the low-tech BIPV-T collectors achieve lower improvement in electric yields when compared with ideal high-tech configuration, the figures are still encouraging for their application due to low production costs. Facade BIPV-T collectors show generally lower improvement in electric performance than roof installations, relatively about 30 to 50% when compared to roof percent figures (see Figure 10).

6. Conclusions

Drawbacks associated with integration of PV modules into building envelopes (roofs, facades) have been outlined. Reduction of electricity production above 5% has been shown both for warm and moderate climate compared to separate installation. Moreover, extreme temperatures of PV cells leading to degradation problems could appear at

considerable frequency for roof BIPV especially in warm climate, but temperatures above 80°C are present even in the moderate climate. Facade integration doesn't show real problems to safe operation of PV for considered climates.

Knowledge of the BIPV figures results in application of PV-T collectors for installations with high degree of integration into building construction (facade or roof claddings). Expensive high-tech and low cost low-tech configurations have been discussed to reveal differences in thermal performance of both as an indicator of overall PV-T performance. Main factors defining the quality of PV-T thermal performance are cooling fin quality (conductivity, thickness, and length) and bond conductance between riser pipe and cooling fin. Building integration brings a large improvement especially to low-tech PV-T collectors. While high-tech BIPV-T collector configuration shows negligible temperature difference between PV and liquid at nominal conditions (efficiency factor $F' = 0.99$), low-tech BIPV-T configuration results in large temperature difference around 25 K due to worse heat removal from PV cell ($F' = 0.69$).

A simulation study has been performed for these two configurations to show the potential energy production in different climates and applications. There is a huge potential for roof applications of BIPV-T collectors instead of BIPV with 15% to 25% increase of electricity production in warm climate (Athens) and 8% to 15% increase in moderate climate (Prague). Associated heat production is from several times to 10 times higher than electricity production. High values are valid for low application temperatures (5°C) where a large portion of ambient heat is also used. Low-tech BIPV-T collectors could contribute with reduced performance level but still with considerable improvement when compared to BIPV modules without cooling.

References

[1] T. Matuska, "Advanced solar collectors for building integration," in *Proceedings of the World Renewable Energy Congress (WREC-X)*, pp. 1547–1552, Glasgow, UK, 2008.

[2] P. G. Charalambous, G. G. Maidment, S. A. Kalogirou, and K. Yiakoumetti, "Photovoltaic thermal (PV/T) collectors: a review," *Applied Thermal Engineering*, vol. 27, no. 2-3, pp. 275–286, 2007.

[3] H. A. Zondag, "Flat-plate PV-Thermal collectors and systems: a review," *Renewable and Sustainable Energy Reviews*, vol. 12, no. 4, pp. 891–959, 2008.

[4] T. T. Chow, "A review on photovoltaic/thermal hybrid solar technology," *Applied Energy*, vol. 87, no. 2, pp. 365–379, 2010.

[5] A. Ibrahim, M. Y. Othman, M. H. Ruslan, S. Mat, and K. Sopian, "Recent advances in flat plate photovoltaic/thermal (PV/T) solar collectors," *Renewable and Sustainable Energy Reviews*, vol. 15, no. 1, pp. 352–365, 2011.

[6] Y. Tripanagnostopoulos, "Aspects and improvements of hybrid photovoltaic/thermal solar energy systems," *Solar Energy*, vol. 81, no. 9, pp. 1117–1131, 2007.

[7] M. Bakker, H. A. Zondag, M. J. Elswijk, K. J. Strootman, and M. J. M. Jong, "Performance and costs of a roof-sized PV/thermal array combined with a ground coupled heat pump," *Solar Energy*, vol. 78, no. 2, pp. 331–339, 2005.

[8] E. Bertram, M. Stegmann, J. Scheuren, C. Rosinski, and K. Kundmüller, "Unglazed photovoltaic thermal collectors in heat pump systems," in *Proceedings of the Eurosun 2010*, Graz, Austria, 2010.

[9] G. Fraisse, C. Ménézo, and K. Johannes, "Energy performance of water hybrid PV/T collectors applied to combisystems of direct solar floor type," *Solar Energy*, vol. 81, no. 11, pp. 1426–1438, 2007.

[10] P. Dupeyrat, C. Ménézo, M. Rommel, and H. M. Henning, "Efficient single glazed flat plate photovoltaic-thermal hybrid collector for domestic hot water system," *Solar Energy*, vol. 85, no. 7, pp. 1457–1468, 2011.

[11] H. A. Zondag, D. W. de Vries, W. G. J. van Helden, R. J. C. van Zolingen, and A. A. van Steenhoven, "The yield of different combined PV-thermal collector designs," *Solar Energy*, vol. 74, no. 3, pp. 253–269, 2003.

[12] T. T. Chow, J. W. Hand, and P. A. Strachan, "Building-integrated photovoltaic and thermal applications in a subtropical hotel building," *Applied Thermal Engineering*, vol. 23, no. 16, pp. 2035–2049, 2003.

[13] T. T. Chow, W. He, and J. Ji, "An experimental study of façade-integrated photovoltaic/water-heating system," *Applied Thermal Engineering*, vol. 27, no. 1, pp. 37–45, 2007.

[14] T. N. Anderson, M. Duke, G. L. Morrison, and J. K. Carson, "Performance of a building integrated photovoltaic/thermal (BIPVT) solar collector," *Solar Energy*, vol. 83, no. 4, pp. 445–455, 2009.

[15] T. Bergene and O. M. Løvvik, "Model calculations on a flat-plate solar heat collector with integrated solar cells," *Solar Energy*, vol. 55, no. 6, pp. 453–462, 1995.

[16] H. A. Zondag, D. W. de Vries, W. G. J. van Helden, R. J. C. van Zolingen, and A. A. van Steenhoven, "The thermal and electrical yield of a PV-thermal collector," *Solar Energy*, vol. 72, no. 2, pp. 113–128, 2002.

[17] T. T. Chow, "Performance analysis of photovoltaic-thermal collector by explicit dynamic model," *Solar Energy*, vol. 75, no. 2, pp. 143–152, 2003.

[18] T. Matuska, "Theoretical analysis of solar unglazed hybrid photovoltaic-thermal liquid collector," in *Proceedings of the Eurosun 2010*, Graz, Austria, 2010.

[19] T. Matuska and L. Buchta, "Experimental investigation of solar PV-T/liquid collector," in *Proceedings of the ISES Solar World Congress 2011*, Kassel, Germany, 2011.

[20] H. C. Hottel and A. Whillier, "Evaluation of flat-plate solar collector performance," in *Transactions of the Conference on Use of Solar Energy*, vol. 2, pp. 74–78, University of Arizona Press, 1958.

[21] L. W. Florschuetz, "Extension of the Hottel-Whillier model to the analysis of combined photovoltaic/thermal flat plate collectors," *Solar Energy*, vol. 22, no. 4, pp. 361–366, 1979.

[22] "Climate databases from Meteonorm 5.1," Meteotest, 2004.

Hindawi Publishing Corporation
International Journal of Photoenergy
Volume 2012, Article ID 760791, 8 pages
doi:10.1155/2012/760791

Research Article

Grid-Connection Half-Bridge PV Inverter System for Power Flow Controlling and Active Power Filtering

Chih-Lung Shen and Jye-Chau Su

Department of Electronic Engineering, National Kaohsiung First University of Science and Technology, Nanzih, 1, University Road, Yuanchau, Kaohsiung 824, Taiwan

Correspondence should be addressed to Chih-Lung Shen, clshen@ccms.nkfust.edu.tw

Received 19 March 2012; Accepted 11 May 2012

Academic Editor: G. N. Tiwari

A half-bridge photovoltaic (PV) system is proposed, which can not only deal with bidirectional power flowing but also improve power quality. According to varying insolation, the system conditions real power for dc and ac loads to accommodate different amounts of PV power. Furthermore, the system eliminates current harmonics and improves power factor simultaneously. As compared with conventional PV inverter, the total number of active switches and current sensors can be reduced so that its cost is lower significantly. For current command determination, a linear-approximation method (LAM) is applied to avoid the complicated calculation and achieve the maximum power point tracking (MPPT) feature. For current controlling, a direct-source-current-shaping (DSCS) algorithm is presented to shape the waveform of line current. Simulation results and practical measurements also demonstrate the feasibility of the proposed half-bridge PV system.

1. Introduction

Solar energy is clean, pollution-free, and inexhaustible, so developing solar energy power system can solve the energy crisis of exhausting in fossil fuel. Recently, photovoltaic arrays are widely used for power supply [1–14]. PV systems can be briefly classified into stand-alone and grid-connection types. Owing to more flexibility in power conditioning, the study on the grid-connection type stimulates many interests. Figure 1 shows the configuration of a conventional grid-connection PV system, which consists of multiple stages, leading to low efficiency, large volume, and high cost. To improve part of the disadvantages, some researchers have designed two-stage configurations, as shown in Figure 2. For further efficiency improvement and cost reduction, single-stage PV system has been developed [15–18], of which block diagram is shown in Figure 3. Even though the structure of a single-stage PV system is simpler than that of a two-stage one, a couple of active switches, current sensors, and corresponding drivers are still needed in the power stage.

In this paper a half-bridge single-stage PV system is proposed to reduce the total number of active switches and current sensors. As a result, the proposed PV inverter system is compact and cost can be reduced significantly. Furthermore, the proposed system can not only process real power bidirectionally but also improve power factor and eliminate harmonic currents. To draw maximum power from PV arrays, a linear-approximation method (LAM) is developed to complete the maximum power point tracking (MPPT). Based on the LAM, a reference dc-link voltage is chosen. With an outer-voltage controller, source current commands are determined, which avoids optimal current determination from complicated calculations. A direct-source-current-shaping (DSCS) algorithm is applied to perform wave shaping for bidirection power flow controlling and power factor improvement. A prototype is established, simulated, tested, and measured. The simulation results and experimental measurements have verified the feasibility of the proposed PV system.

2. Configuration of the PV System

Figure 4 illustrates the configuration of the PV power system, which consists of a dc-bus filter, a half-bridge inverter,

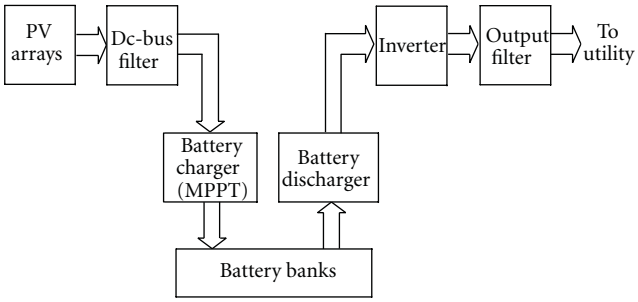

Figure 1: A block diagram of a conventional grid-connection PV system.

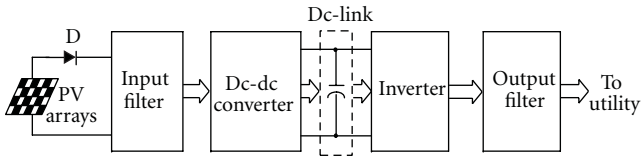

Figure 2: Illustration for a two-stage grid-connection PV system.

an output filter, and a system controller. The half-bridge inverter, which contains two active switches and two dc-voltage-divided capacitors, can process real power bidirectionally. That is, the inverter either transfers PV power to ac side or draws power from utility for dc loads. In addition, the inverter performs current harmonics eliminating and power factor correcting to improve power quality. The dc-bus filter suppresses dc-link voltage fluctuations and filters out ac components on the dc side for accurate MPPT, while the output filter serves as an interface between the inverter and the utility to prevent inrush current from occurring. According to dc-link, reference, and line voltages, the system controller implemented in a DSP chip calculates current commands and then determines appropriate switch signals to perform wave shaping. A conceptual block diagram of the system controller is shown in Figure 5.

3. Operation Principle of the PV System

To understand the operation principle of the PV system, power flow controlling is discussed. The PV system processes real power, reactive power, and distortion power simultaneously. Figure 6 is the power tetrahedron diagram, which shows the relationship among these types of power. In Figure 6, the S stands for apparent power and is expressed as

$$S = \sqrt{(\overline{p})^2 + (\overline{q})^2 + \left(h_{pw}\right)^2}, \tag{1}$$

where $\overline{p}$, $\overline{q}$, and h_{pw} denote real power, reactive power, and distortion power, respectively. According to different insolation, the PV system can deal with power bidirectionally. Based on $\overline{p}$-$\overline{q}$-h_{pw} coordinate frame, Figure 7 shows a trajectory to indicate operation points varying with insolation. From point a to point b, during the interval of high insolation the PV system generates solar power to supply dc loads and ac loads and inject real power into utility. In addition, the half-bridge inverter processes reactive power and distortion power for ac loads so as to improve power factor. A corresponding power flow is illustrated in Figure 8. From point b to point c, during the interval of medium insolation the system supplies power for dc loads and part of real power for ac loads and the insufficient draws from utility. Figure 9 is the related power flow. From point c to point d, during the interval of low insolation the PV arrays cannot feed total amount of dc demanded power so that the inverter transforms ac power to dc one for dc loads and deals with reactive power and distortion power for ac loads simultaneously. The corresponding power flow is shown in Figure 10. At point d, during the interval of no insolation the inverter processes real power for dc loads and deals with reactive power and distortion power for ac loads. Figure 11 shows the power flow direction.

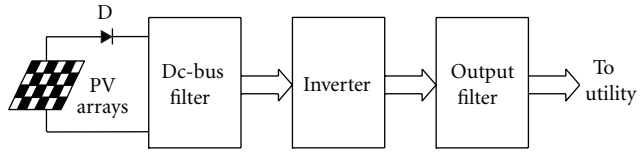

Figure 3: A block diagram to represent a single-stage grid-connection PV system.

4. Derivation of Current Commands

In the PV system, once a current command is determined, the output current of the half-bridge inverter will trace the waveform of the reference current to perform power flow controlling and power quality improvement. In the following, an optimal current command is derived.

According to the current and voltage definitions shown in Figure 4, the line voltage $v_s(t)$ and nonlinear load current $i_L(t)$ are expressed as

$$\begin{aligned} v_s(t) &= \sqrt{2}V_{\text{rms}}\sin(\omega t - \phi), \\ i_L(t) &= \sum_{n=1}^{\infty}\sqrt{2}I_n\sin(n\omega t - \theta_n), \end{aligned} \tag{2}$$

respectively. Then, the load instantaneous real power ($p_L(t)$) and instantaneous reactive power ($q_L(t)$) can be calculated as follows:

$$\begin{aligned} p_L(t) &= v_s(t)i_L(t) \\ &= V_{\text{rms}}I_1\cos(\phi - \theta_1) - V_{\text{rms}}I_1\cos(2\omega t + \phi + \theta_1) \\ &\quad + \sum_{n=2}^{\infty} 2V_{\text{rms}}I_n\sin(n\omega t + \theta_n)\sin(\omega t + \phi) \\ &= \overline{p}_L + \widetilde{p}_L, \end{aligned} \tag{3}$$

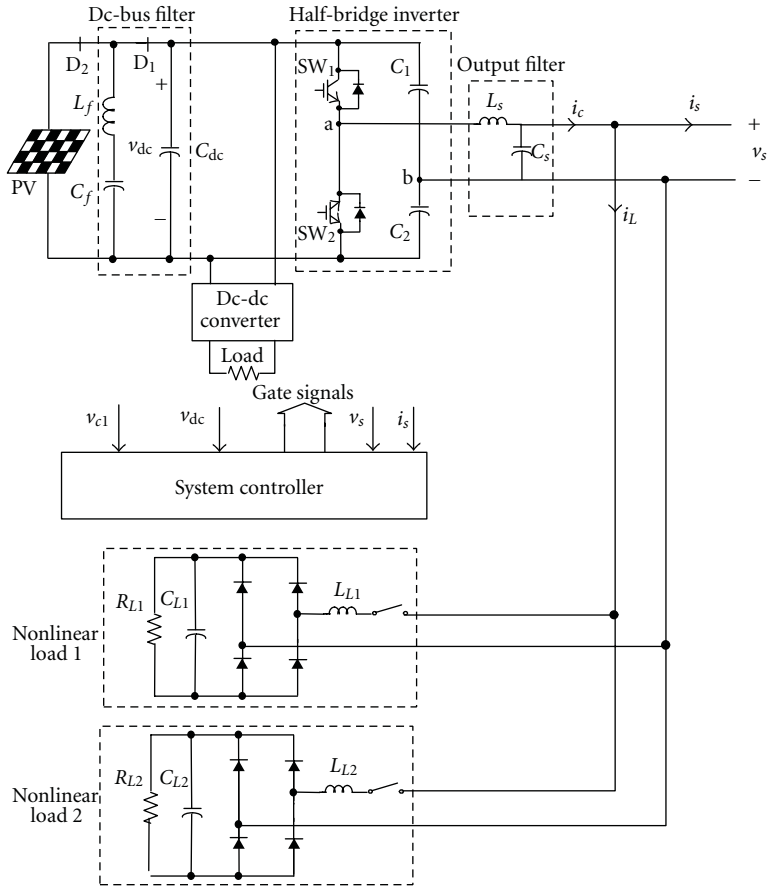

Figure 4: Configuration of the PV inverter system.

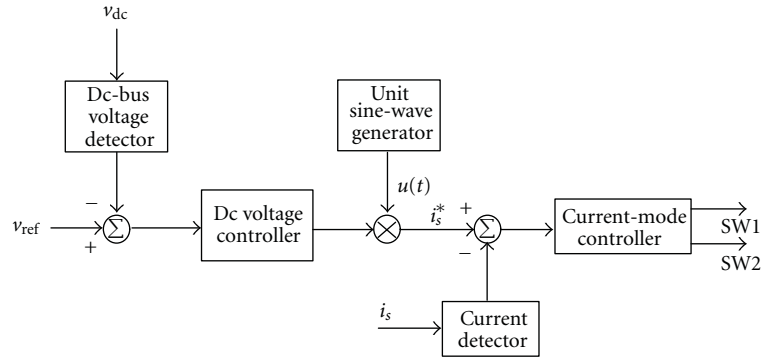

Figure 5: A block diagram of the system controller.

where

$$\begin{aligned}\overline{P}_L &= V_{\text{rms}} I_1 \cos(\phi - \theta_1),\\ \widetilde{p}_L &= V_{\text{rms}} I_1 \cos(2\omega t + \phi + \theta_1)\\ &\quad + \sum_{n=2}^{\infty} 2V_{\text{rms}} I_n \sin(n\omega t + \theta_n)\sin(\omega t + \phi).\end{aligned} \tag{4}$$

Notation $\overline{p}_L$ represents the constant part and $\widetilde{p}_L$ denotes the variant component. The instantaneous reactive power can be obtained by multiplying the nonlinear load current with a 90°-shifted voltage as follows:

$$\begin{aligned}q_L(t) &= v_s'(t) i_L(t)\\ &= V_{\text{rms}} I_1 \sin(\phi - \theta_1) - V_{\text{rms}} I_1 \sin(2\omega t + \phi + \theta_1)\\ &\quad - \sum_{n=2}^{\infty} 2V_{\text{rms}} I_n \sin(n\omega t + \theta_n)\cos(\omega t + \phi)\\ &= \overline{q}_L + \widetilde{q}_L,\end{aligned} \tag{5}$$

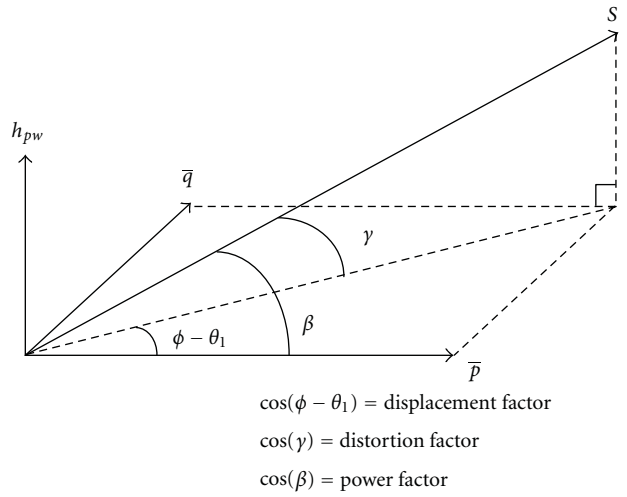

Figure 6: Power tetrahedron diagram.

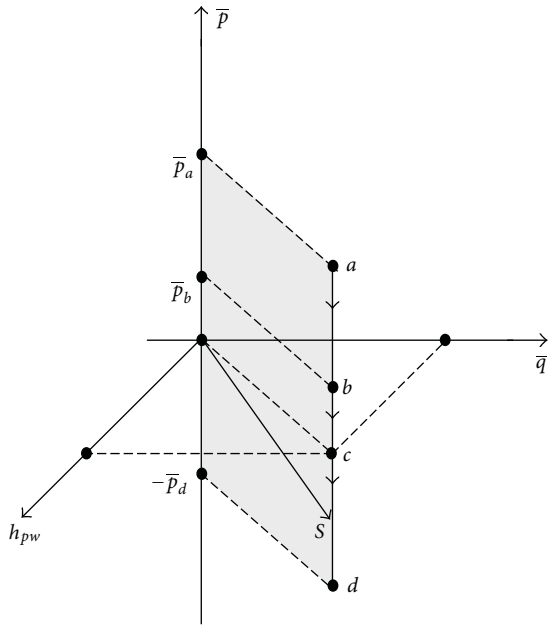

Figure 7: A trajectory to indicate operation points varying with insolation.

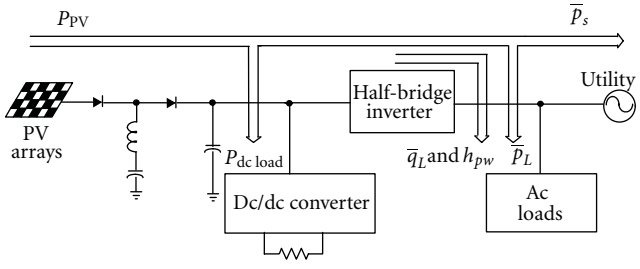

Figure 8: Illustration of power flow during the interval of high insolation.

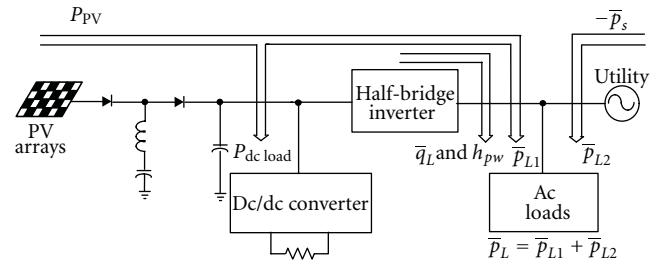

Figure 9: Illustration of power flow during the interval of medium insolation.

where $v_s'(t)$ is the line voltage shifted by 90°, $\widetilde{q}_L$ is the constant part, and $\widetilde{q}_L$ is the variant component of instantaneous reactive power. Apparent power is determined by

$$S = V_{\text{rms}}\sqrt{\sum_{n=1}^{\infty} I_n^2}$$

$$= \sqrt{\left[V_{\text{rms}} I_1 \cos(\phi - \theta_1)\right]^2 + \left[V_{\text{rms}} I_1 \sin(\phi - \theta_1)\right]^2 + \sum_{n=2}^{\infty} V_{\text{rms}}^2 I_n^2}, \tag{6}$$

in which the first, second, and third terms are the square of real, reactive, and distortion powers, respectively. The reactive and distortion powers of a nonlinear load will be supplied by the PV system. As a result, a compensated line current, of which amplitude depends on PV power, is purely sinusoidal and in phase with line voltage. It can be determined by

$$i_s^* = \frac{\sqrt{2}\left(p_{\text{MPPT}} - \overline{p}_L(t)\right)}{V_{\text{rms}}} \sin(\omega t - \phi). \tag{7}$$

In addition, a corresponding inverter output current is expressed as

$$i_c^* = \frac{\sqrt{2}\left(p_{\text{MPPT}} - \overline{p}_L(t)\right)}{V_{\text{rms}}} \sin(\omega t - \phi) + i_L, \tag{8}$$

where p_{MPPT} is the maximum power drawn from the PV arrays and can be represented as

$$p_{\text{MPPT}} = \left(v_{\text{PV}}(t) \cdot i_{\text{PV}}(t)\right)_{\max}. \tag{9}$$

In (7) and (8), the difference between p_{MPPT} and $\overline{p}_L(t)$ decides the amplitudes of current commands, which can be also obtained from the comparison of the dc-link voltage with a reference voltage. The linear-approximation method (LAM) to achieve the maximum power point tracking (MPPT) is illustrated in Figures 12 and 13, from which it can be found that the trajectories of maximum power point varying with irradiation and temperature are linear. Once the reference voltage corresponding to a maximum power point is determined, maximum power drawing from PV arrays can be readily achieved. In Figure 12, maximum power of the PV arrays is proportional to output voltage with the increasing

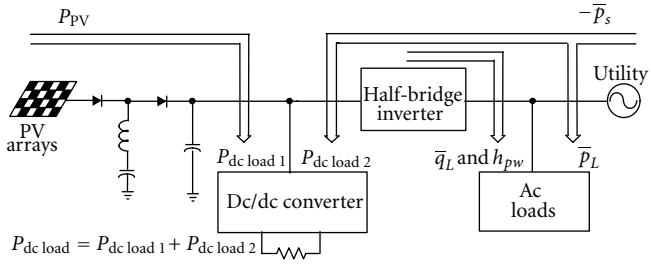

Figure 10: Illustration of power flow during the interval of low insolation.

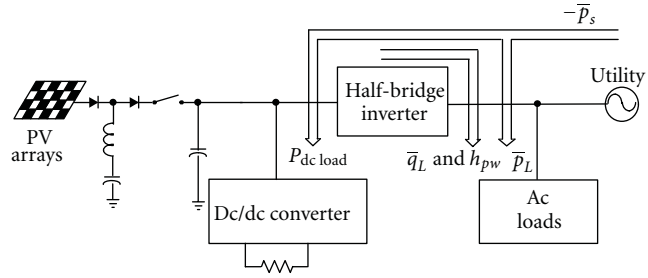

Figure 11: Illustration of power flow during the interval of no insolation.

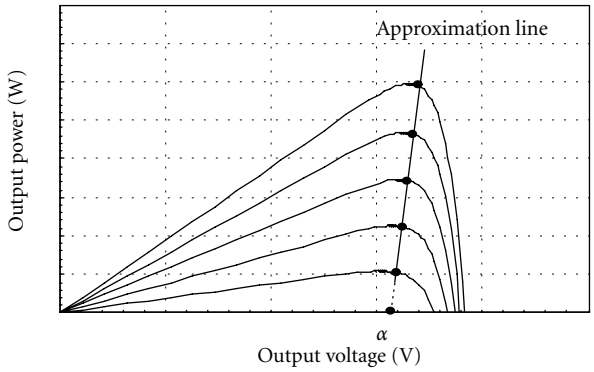

Figure 12: Illustration of the trajectory of maximum power point varying with insolation while PV temperature is invariant.

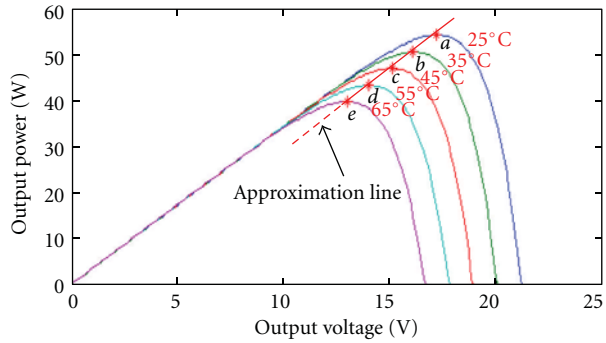

Figure 13: Illustration of the trajectory of maximum power point varying with temperature while insolation is constant.

of insolation, while temperature is constant. In this paper, insolation is detected by a photodiode converting luminance into current and then measured by a resistor. According to Figure 12, the MPPT voltage v'_{ref} is determined as

$$v'_{ref} = \frac{k}{m} i_p + \alpha, \tag{10}$$

where m represents the slope of the approximation line, α stands for the crossover point with output-voltage axis, i_p is the output current of a photodiode, and k is a coefficient determined by the ratio of luminance to photodiode current. In Figure 13, a maximum power point also varies with temperature such that v'_{ref} should be modified. As illustrated in Figure 14, a maximum power voltage drops linearly with

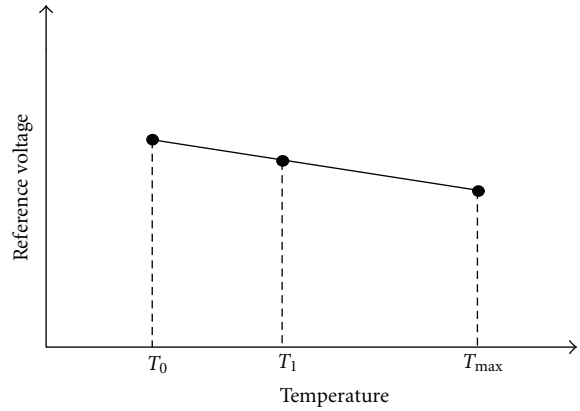

Figure 14: Illustration of the relationship between reference voltage and temperature.

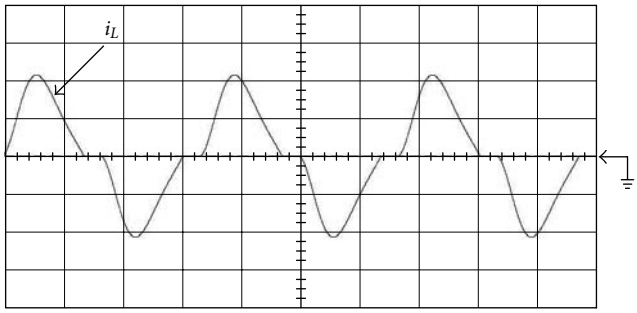

(i_L: 5 A/div, time: 5 ms/div)

Figure 15: Load current while nonlinear loads are connected to utility.

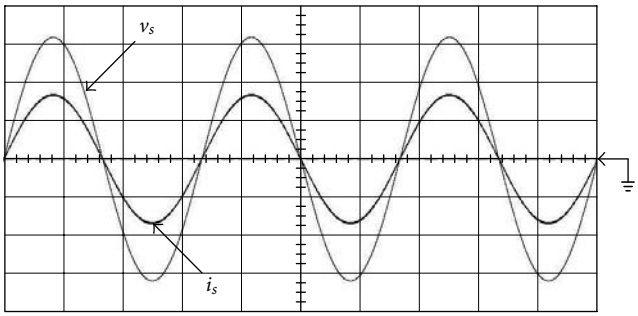

(v_s: 50 V/div, i_s: 5 A/div, time: 5 ms/div)

Figure 16: Filtered line current and line voltage during the interval of high insolation.

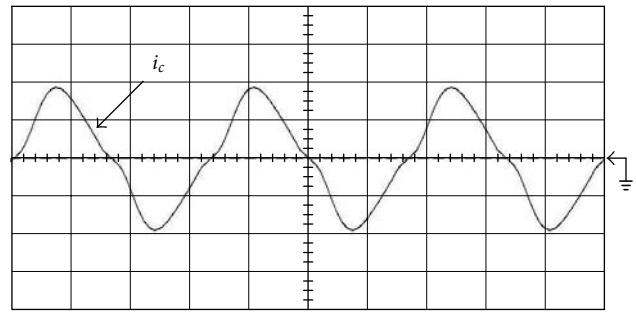

(i_c: 10 A/div, time: 5 ms/div)

Figure 17: The corresponding inverter current during the interval of high insolation.

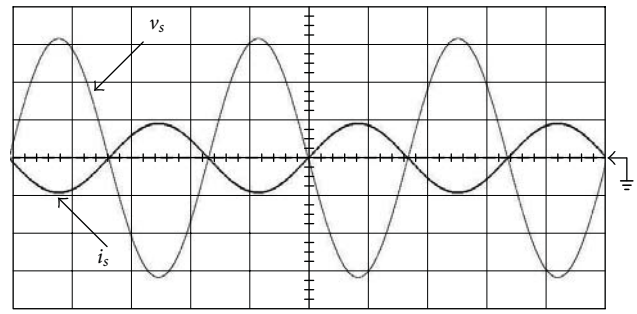

(v_s: 50 A/div, i_s: 5 A/div, time: 5 ms/div)

Figure 18: Filtered line current and line voltage during the interval of medium insolation.

the increasing of temperature under constant insolation. As a result, a reference voltage v_{ref} can be found by

$$v_{\text{ref}} = \varsigma v'_{\text{ref}} + \beta, \tag{11}$$

where ζ is temperature compensation coefficient and notation β is a constant value.

5. Simulated and Experimental Results

An example of 110 V 60 Hz half-bridge PV system is designed, simulated, and implemented, of which operation range of input voltage is from 395 to 420 V. Component values and important parameters are determined as

power switches: IGBT, TOSHIBA GT25Q101, 1200 V/25 A,

PV arrays: SHARP NT-KR5EX (12 pieces in series),

$f_s = 20$ kHz,

$C_1 = C_2 = C_{\text{dc}} = 940\,\mu$F, $C_f = 880\,\mu$F,

$L_s = 4$ mH, $L_f = 2$ mH,

v_{ref}: from 395 V to 420 V,

PV power: from 200 W to 1.8 kW.

Nonlinear loads are connected to utility, of which power dissipation is 650 W. Figure 15 shows the waveform of the load current. During the interval of high insolation, PV arrays generate 1.8 kW. In addition, a reference dc-link voltage v_{ref} is 420 V based on the LAM for MPPT. The simulated line current and the corresponding inverter current are shown in Figures 16 and 17, respectively. In this period, PV system supplies total amount of demanded power for dc and ac loads and injects real power into utility. Simultaneously, PV system compensates reactive power and distortion power for nonlinear loads to improve power factor. From Figure 16, it can be observed that line current is sinusoidal and in phase with line voltage. That is, high power factor is achieved and PV power can be injected into utility. During the interval of medium insolation, output power of the PV arrays is 800 W and reference voltage v_{ref} is 404 V. PV system provides total amount of power for dc load and part of real power for nonlinear loads. The simulated line current is shown in Figure 18, while Figure 19 is the corresponding inverter current. From Figure 18, it can be found that the line current is purely sinusoidal and 180° out of phase to line voltage. That is, insufficient power for ac load is fed from utility and power factor correction is performed by the half-bridge inverter simultaneously. During the interval of low insolation, PV power is 200 W and a reference dc-link voltage is 395 V. Figure 20 shows the simulated line current, and Figure 21 is the corresponding inverter current. Once

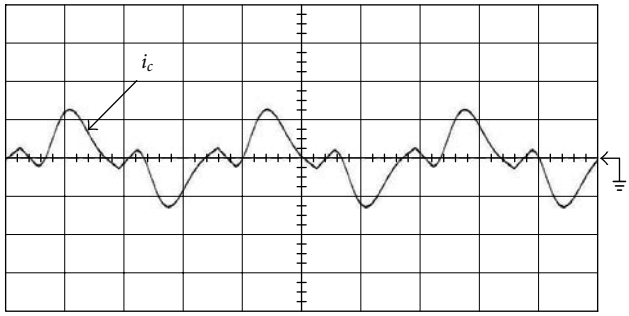

(i_c: 5 A/div, time: 5 ms/div)

Figure 19: The corresponding inverter current during the interval of medium insolation.

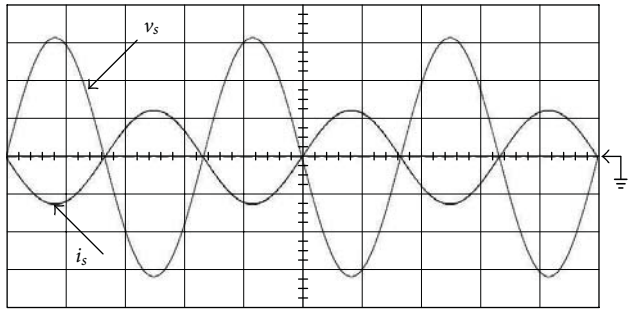

(v_s: 50 V/div, i_s: 10 A/div, time: 5 ms/div)

Figure 20: Filtered line current and line voltage during the interval of low insolation.

there is no insolation, the reference voltage is 395 V and the half-bridge inverter provides reactive power and distortion power for nonlinear loads and draws real power from utility for dc loads. The line current and inverter current are shown in Figures 22 and 23, in turn. Figures 24 and 25 present the practical measurements of line currents during the intervals of high insolation and medium insolation, respectively. In the case of no insolation, the filtered line current and line voltage are shown in Figure 26. During the interval of no insolation the PV system is totally in charge of active power filtering. The amplitude of the filtered line current is greater than that in medium insolation. That is, the utility provides more active power to the load.

6. Conclusions

A half-bridge PV inverter capable of dealing with power flow bidirectionally is presented in this paper. As compared with full-bridge one, the total number of active switches is reduced by half so that the system configuration is simplified and its cost is lowered significantly. The LAM is applied to obtain an optimal reference voltage for the determination of a current command and to achieve MPPT feature, which avoids sophisticated calculation. The DSCS algorithm is

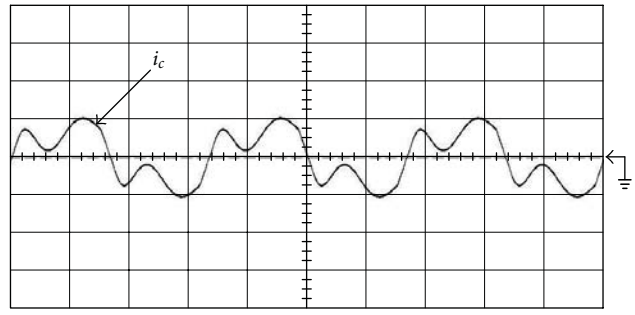

(i_c: 5 A/div, time: 5 ms/div)

Figure 21: The corresponding inverter current during the interval of low insolation.

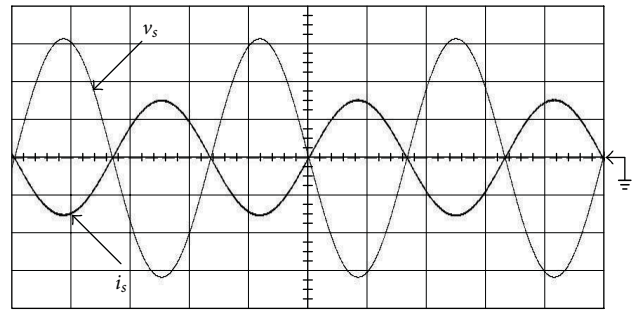

(v_s: 50 V/div, i_s: 10 A/div, time: 5 ms/div)

Figure 22: Filtered line current and line voltage during the interval of no insolation.

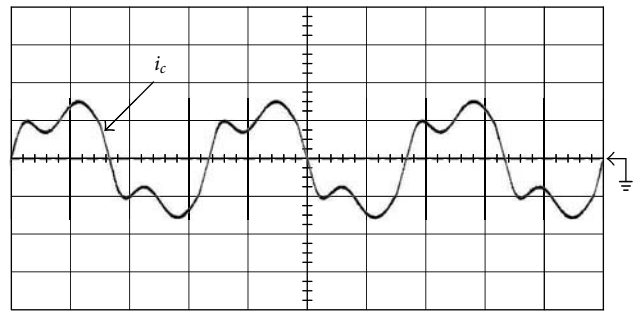

(i_c: 5 A/div, time: 5 ms/div)

Figure 23: The corresponding inverter current during the interval of no insolation.

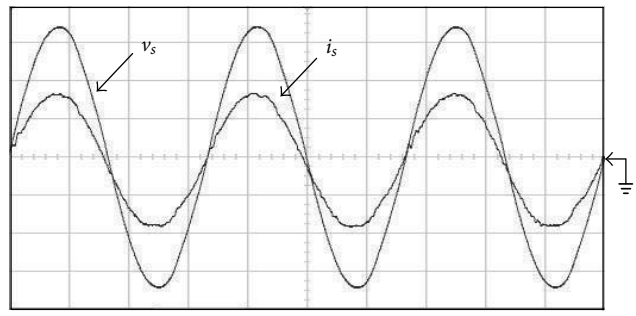

(v_s: 50 V/div, i_s: 5 A/div, time: 5 ms/div)

Figure 24: Experimental result: the filtered line current and line voltage during the interval of high insolation.

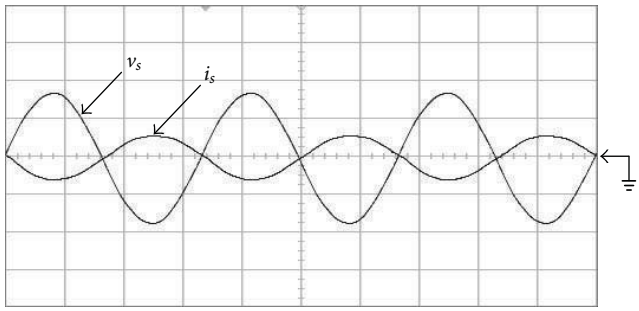

(v_s: 100 V/div, i_s: 10 A/div, time: 5 ms/div)

Figure 25: Experimental result: the filtered line current and line voltage during the interval of medium insolation.

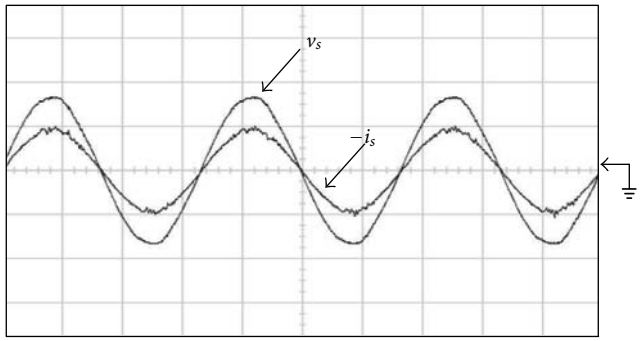

(v_s: 100 V/div, i_s: 10 A/div, time: 5 ms/div)

Figure 26: Experimental result: the line voltage and the filtered line current during the interval of no insolation.

embedded to perform wave shaping for line current so as to achieve power quality improvement directly. Simulation results and practical measurements have demonstrated the feasibility of the PV inverter system.

References

[1] L. Asiminoaei, R. Teodorescu, F. Blaabjerg, and U. Borup, "A digital controlled PV-inverter with grid impedance estimation for ENS detection," *IEEE Transactions on Power Electronics*, vol. 20, no. 6, pp. 1480–1490, 2005.

[2] T.-F. Wu, C.-L. Shen, C.-H. Chang, and J. Chiu, "1ϕ3 W grid-connection PV power inverter with partial active power filter," *IEEE Transactions on Aerospace and Electronic Systems*, vol. 39, no. 2, pp. 635–646, 2003.

[3] S. A. Daniel and N. AmmasaiGounden, "A novel hybrid isolated generating system based on PV fed inverter-assisted wind-driven induction generators," *IEEE Transactions on Energy Conversion*, vol. 19, no. 2, pp. 416–422, 2004.

[4] H. Koizumi, T. Mizuno, T. Kaito et al., "A novel microcontroller for grid-connected photovoltaic systems," *IEEE Transactions on Industrial Electronics*, vol. 53, no. 6, pp. 1889–1897, 2006.

[5] T.-F. Wu, H.-S. Nien, C.-L. Shen, and T.-M. Chen, "A single-phase inverter system for PV power injection and active power filtering with nonlinear inductor consideration," *IEEE Transactions on Industry Applications*, vol. 41, no. 4, pp. 1075–1083, 2005.

[6] P. P. Barker and J. M. Bing, "Advances in solar photovoltaic technology: an applications perspective," in *Proceedings of the IEEE Power Engineering Society General Meeting*, pp. 1955–1960, June 2005.

[7] B. M. T. Ho and H. S. H. Chung, "An integrated inverter with maximum power tracking for grid-connected PV systems," *IEEE Transactions on Power Electronics*, vol. 20, no. 4, pp. 953–962, 2005.

[8] P. G. Barbosa, H. A. C. Braga, M. C. B. Rodrigues, and E. C. Teixeira, "Boost current multilevel inverter and Its application on single-phase grid-connected photovoltaic systems," *IEEE Transactions on Power Electronics*, vol. 21, no. 4, pp. 1116–1124, 2006.

[9] J. J. Negroni, C. Meza, D. Biel, and F. Guinjoan, "Control of a Buck inverter for grid-connected PV systems: a digital and sliding mode control approach," in *Proceedings of the IEEE International Symposium on Industrial Electronics (ISIE '05)*, pp. 739–744, June 2005.

[10] C. Rodriguez and G. A. J. Amaratunga, "Dynamic maximum power injection control of AC photovoltaic modules using current-mode control," *IEE Proceedings of Electric Power Applications*, vol. 153, no. 1, pp. 83–87, 2006.

[11] A. Kotsopoulos, P. J. M. Heskes, and M. J. Jansen, "Zero-crossing distortion in grid-connected PV inverters," *IEEE Transactions on Industrial Electronics*, vol. 52, no. 2, pp. 558–565, 2005.

[12] N. Kasa, T. Iida, and L. Chen, "Flyback inverter controlled by sensorless current MPPT for photovoltaic power system," *IEEE Transactions on Industrial Electronics*, vol. 52, no. 4, pp. 1145–1152, 2005.

[13] N. Femia, D. Granozio, G. Petrone, G. Spagnuolo, and M. Vitelli, "Optimized one-cycle control in photovoltaic grid connected applications," *IEEE Transactions on Aerospace and Electronic Systems*, vol. 42, no. 3, pp. 954–971, 2006.

[14] A. O. Zué and A. Chandra, "Simulation and stability analysis of a 100 kW grid connected LCL photovoltaic inverter for industry," in *Proceedings of the IEEE Power Engineering Society General Meeting (PES '06)*, June 2006.

[15] T.-F. Wu, C.-L. Shen, H.-S. Nein, and G.-F. Li, "A 1ϕ3 W inverter with grid connection and active power filtering based on nonlinear programming and fast-zero-phase detection algorithm," *IEEE Transactions on Power Electronics*, vol. 20, no. 1, pp. 218–226, 2005.

[16] Y. Chen and K. M. Smedley, "A cost-effective single-stage inverter with maximum power point tracking," *IEEE Transactions on Power Electronics*, vol. 19, no. 5, pp. 1289–1294, 2004.

[17] K. S. Phani Kiranmai and M. Veerachary, "A single-stage power conversion system for the PV MPPT application," in *Proceedings of the IEEE International Conference on Industrial Technology (ICIT '06)*, pp. 2125–2130, December 2006.

[18] R. González, J. López, P. Sanchis, and L. Marroyo, "Transformerless inverter for single-phase photovoltaic systems," *IEEE Transactions on Power Electronics*, vol. 22, no. 2, pp. 693–697, 2007.